Modelling Denitrification In Soil

A thesis submitted to the School of Mathematics of the University of East Anglia in partial fulfilment of the requirements for the degree of Doctor of Philosophy

By Christopher Richard Bocking

June 2013

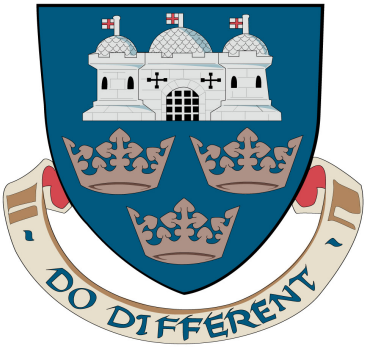

Abstract

Denitrification is a process used by many bacterial species to support anaerobic respiration, where, faced with a lack of oxygen, energy is instead created from available nitrates. Arable soils with high nitrogen content, and commonly-used fertilisers, encourage this process. Unfortunately, the ultimate impact on the environment is negative since nitrous oxide gas, which emerges as a bi-product, escapes into the atmosphere where it presents a 300-fold greater danger for global warming than carbon dioxide. The aim of this thesis is find a way to estimate the level of nitrous oxide which may escape into the atmosphere from denitrifying soil.

Traditionally, the chain of chemical reactions followed in the denitrification process is modelled using Michaelis-Menten kinetics. We begin this thesis by reviewing existing work, discussing some of its limitations and proposing various alterations.

Later, we present a preliminary model of the oxygen distribution within a soil with the aim of identifying anaerobic micro-sites where bacteria can denitrify. Our first models consist of a solitary circle of oxygen-absorbing soil residing beneath ground level in an environment saturated with oxygen. We show that normal respiration occurs inside the circle except within a core anaerobic region where denitrification occurs.

We extend the oxygen distribution model by generalising to multiple oxygen-absorbing regions. The model is then considered from two viewpoints. We either think of the model as an aggregated soil where each circle represents an individual aggregate surrounded by air. Or we think of the model as a solid non-aggregated soil, where each circle represents a high respiration area. For both of these viewpoints results are found for realistic parameters and levels of denitrification within the soil can be estimated.

Acknowledgements

I would like to thank my supervisors who have always been both encouraging and helpful. I would especially like to thank Mark Blyth for his patience, guidance, and support throughout the course of my PhD.

I would also like to thank all of the friends I've made in my seven years at UEA for making my time so enjoyable. Particularly my colleagues in MTH and CMP, and those who have put up with living with me!

Contents

Abstract iii

Acknowledgements iv

1 Introduction 1
- 1.1 Denitrification . . . 1
- 1.2 Nitrous Oxide . . . 2
- 1.3 The Nitrous Oxide Focus Group . . . 3
- 1.4 Processes To Be Investigated . . . 3
- 1.5 Modelling Chemical Reactions . . . 4
- 1.6 Oxygen Distribution . . . 6
  - 1.6.1 A Single Area Of Respiration . . . 7
  - 1.6.2 Multiple Areas Of Respiration . . . 10
- 1.7 The Boundary Element Method . . . 11
- 1.8 The Modified Schwarz Problem . . . 15
  - 1.8.1 An Invalid Problem . . . 18
  - 1.8.2 Numerical Verification . . . 19
  - 1.8.3 Avoiding Branch Cuts . . . 20

2 The Metabolic Pathway 21
- 2.1 Michaelis-Menten Kinetics . . . 21
- 2.2 Modelling Using A Matched Asymptotic Expansion . . . 23
  - 2.2.1 Inner Time-scale . . . 23
  - 2.2.2 Outer Time-scale . . . 25
  - 2.2.3 Matching The Two Time-scales . . . 27
  - 2.2.4 Composite Solution . . . 29
- 2.3 Adding A Feed Term . . . 30
- 2.4 Previous Models . . . 34
- 2.5 Conservation Of Mass . . . 36
- 2.6 A Model With An Inhibitor . . . 38
- 2.7 Comparison With Experimental Results . . . 40

3 One Dimensional Oxygen Distribution Models **42**
3.1 Absorption-Diffusion Equation . . . 42
3.2 Proportional Absorption . . . 45
3.3 Time Dependent Point Sink Model . . . 48
3.4 Proportional Absorption At A Point . . . 50
3.5 Point Absorption With A Switch . . . 54
3.6 Multiple Points Of Absorption . . . 55

4 Two Dimensional Oxygen Distribution Models **57**
4.1 Soil With No Absorption . . . 57
4.2 A Conformal Mapping Model . . . 58
4.3 A Model With Multiple Point Sinks . . . 61
4.3.1 Neumann Boundary Condition . . . 61
4.3.2 Dirichlet Boundary Condition . . . 64
4.4 Further Development Of A Two-Dimensional Model . . . 66
4.5 The Anaerobic Core Model . . . 73
4.5.1 Concentric Circles Model, with Proportional Absorption . . . 73
4.5.2 Line Boundary Model, with Proportional Absorption . . . 77
4.5.3 Concentric Circles Model, with Constant Absorption . . . 79
4.5.4 Line Boundary Model, with Constant Absorption . . . 82
4.6 An Asymptotic Expansion Method . . . 86
4.6.1 Concentric Circles Model, with Constant Absorption . . . 86
4.6.2 Concentric Circles Model, with Proportional Absorption . . . 90
4.6.3 Line Boundary Model, with Constant Absorption . . . 92
4.6.4 Line Boundary Model, with Proportional Absorption . . . 101
4.6.5 Asymptotic Method Summary . . . 106

5 Multiple Areas Of Oxygen-Absorbing Soil **108**
5.1 Extending The Boundary Element Method . . . 108
5.1.1 Anaerobic Cores Excluded . . . 109
5.1.2 Anaerobic Cores Included . . . 110
5.2 Extending the Asymptotic Method . . . 112
5.3 An Infinite Array of Soil Aggregates . . . 118
5.4 Summary of Models Created . . . 122

6 Oxygen Distribution Model Results **123**
6.1 Aggregated Soil . . . 124
6.1.1 Single Aggregate Result . . . 124
6.1.2 Multiple Aggregate Result . . . 127
6.2 Non-aggregated soil . . . 132
6.2.1 A Single Region of Oxygen Absorption . . . 132
6.2.2 Two Regions of Oxygen Absorption . . . 135

7 Conclusions **136**
7.1 Concluding Remarks 136
7.2 Further Work 136

List of figures

1.1 The Nitrogen Cycle [1] 1
1.2 Schematic illustration of the nitrogen cycle, from [39]. 2
1.3 Nitrous Oxide emissions by source, 1990-2007, [34] 3
1.4 Spherical soil aggregate with an anaerobic core. 6
1.5 A single area of respiring bacteria within soil, B, beneath an air/soil boundary A absorbing oxygen to create an anaerobic core C. 8
1.6 A circular boundary B is split into N straight elements 13
1.7 An example of an invalid problem when solving using the Crowdy method on a annulus of unit outer radius, and inner radius r_I. 19
1.8 The quadruply connected circular domain from the numerical verification section of Crowdy's paper [11]. The interior circular discs have radius 0.1 and centres at 0.5, $-0.1 + 0.35i$ and $-0.4i$. The cross marks the point at which we shall choose to take α in order to verify the method. 20
2.1 Concentrations of substrate and complex for the two time-scales, given by (2.2.47), (2.2.48) and (2.2.49). For $S(0) = 50$, $E(0) = 1$, $k_1 = 2$, $k_2 = 1$, $k_{-1} = 0.1$. 30
2.2 Non-dimensionalised substrate-enzyme reaction model. A numerical solution has been found using a Runge-Kutta method, and compared to the solution found using matched asymptotic expansions (MAE). For $S(0) = 50$, $E(0) = 1$, $k_1 = 2$, $k_2 = 1$, $k_{-1} = 0.1$. Note that $\epsilon = 0.02$ and that smaller ϵ will give better agreement between the methods. 31
2.3 Non-dimensionalised substrate-enzyme reaction with feed term model. Numerical solution found using a Runge-Kutta method, compared to solution found using matched asymptotic expansions. For $S(0) = 50$, $E(0) = 1$, $k_1 = 2$, $k_2 = 1$, $k_{-1} = 0.1$, $F = 0.4$. Note that $\epsilon = 0.02$ and that smaller ϵ will give better agreement between the methods. 34
2.4 Substrate and product given by (2.3.6) found using Runge-Kutta, for various feed rates. 35
2.5 Numerical solution of (2.4.2) found using Runge-Kutta, with $K_{m_1} = 1$, $K_{m_2} = K_{m_3} = K_{m_4} = 2$ and $V_{max_1} = 2$, $V_{max_2} = 4$, $V_{max_3} = 8$, $V_{max_4} = 6$, as in [6] 36

2.6 Solutions found using Runge-Kutta of:
a) (2.5.2) with $k_i = 1$ for $i = 1..8$ and $k_{-1} = k_{-3} = k_{-5} = k_{-7} = 0.1$
b) (2.6.2) with $k_i = 1$ for $i = 1..8$, $k_9 = 5$, and $k_{-1} = k_{-3} = k_{-5} = k_{-7} = k_{-9} = 0.1$ 38
2.7 An example of experimental data collected at UEA [18]. 40
3.1 Concentration of oxygen given by (3.1.11) for various t. $\lambda^2 = 0.1, D = 1, \kappa = 0.5$ 44
3.2 Contour used to integrate (3.2.6), $\Gamma = B + C + U + C_\epsilon + L$ 46
3.3 Oxygen concentration modelled by (3.2.1) solved using a finite difference method (in blue) and a Laplace transform method (in red). Using parameters: $\mu = 1, D = 1, \lambda^2 = 1, \kappa = 0.5$ 48
3.4 Concentration of oxygen with a point of constant absorption, given by (3.3.11) and (3.3.12), with conditions (3.3.2). $x_a = 1$, $\lambda^2 = 1$, $D = 1$, $\kappa = 0.1$ 51
3.5 Concentration of oxygen with a point of proportional absorption, given by (3.4.1), with conditions (3.4.2). $x_a = 1$, $\lambda^2 = 1$, $D = 1$, $\kappa = 0.1$. Found by the Finite Difference Method 53
3.6 An example of a 1D oxygen distribution model with multiple points of absorption and switches. a) Constant absorption, b) Proportional absorption. $\hat{\varphi} = 0.2$, $\kappa = 0.1$, $D = 1$. $x_{a,1} = 1$, $x_{a,2} = 3$, $x_{a,3} = 5$, $x_{a,4} = 7$, $x_{a,5} = 10$. $\lambda_1^2 = 0.25$, $\lambda_2^2 = 0.5$, $\lambda_3^2 = 0.5$, $\lambda_4^2 = 0.25$, $\lambda_5^2 = 0.5$ 56
4.1 The zero absorption model 58
4.2 The oxygen distribution model used in the conformal mapping method . . 59
4.3 The domain shown in Figure 4.2 after it has been mapped 60
4.4 A contour plot of the concentration of oxygen, modelled using (4.2.11), with $r_B = 1$, $c = -2$, $\mu_1 = 1$, $\mu_2 = 0.5$ 61
4.5 Position of soil particles modelled as point sinks, with strength m. 62
4.6 Concentration of oxygen using the array of point sinks model, with Neumann boundary condition. $a = b = 2$ and $m = \frac{a}{2\pi}$. Note that the oxygen concentration is not constant on the air/soil boundary at $y = 0$. 64
4.7 Concentration of oxygen using the array of point sinks model, with Dirichlet boundary condition. $a = b = 2$ and $m = \frac{a}{2\pi}$. Note that the oxygen concentration is constant on the air/soil boundary at $y = 0$. 65
4.8 The 2D non-symmetric oxygen distribution model with proportional absorption 66
4.9 Oxygen concentration on the boundary, B. Found using the boundary element method. B was split into 45 straight elements. $r_B = 1$, $c = -2$, $\mu = 1$ $D_1 = D_2 = 1$, $\lambda = 2$ 70
4.10 Oxygen concentration found throughout the domain using the boundary values found previously and shown in Figure 4.9. $r_B = 1$, $c = -2$, $\mu = 1$ $D_1 = D_2 = 1$, $\lambda = 2$ 71

4.11 Showing that the minimum value of oxygen concentration does not coincide with the centre of region 2. The second graph is a plot of the difference between the depth of the point of minimum oxygen concentration and the centre of region 2. $r_B = 1, \mu = 1$ $D_1 = D_2 = 1, \lambda = 2$ 72
4.12 The Concentric Circle Anaerobic Core Model 73
4.13 Oxygen concentration, φ, throughout the domain of the concentric circles model with proportional absorption. With $r_B = 1, \lambda = 2, D_1 = D_2 = 1$ and a threshold value of $T = 0.5$, it was found that $r_C = 0.67$. 76
4.14 The Anaerobic Core Model with Proportional Absorption 77
4.15 Oxygen concentration found using the proportional absorption anaerobic core model. $r_B = 1, \lambda = 2, D_1 = D_2 = 1, T = 0.2, \mu = 1$ 78
4.16 Oxygen concentration, φ, throughout the domain of the concentric circle model with constant absorption. With $r_B = 1, \lambda = 2, D_1 = D_2 = 1$ and a threshold value of $T = 0.5$, it was found that $r_C = 0.82$. 82
4.17 Oxygen concentration found using the constant absorption anaerobic core model. $r_B = 1$, $\lambda = 2$, $D_1 = D_2 = 1$, $T = 0.2$, $\mu = 1$ 84
4.18 Comparing anaerobic core sizes created by the different oxygen-absorption definitions, for $T = 0.2, \lambda = 2, \mu = 1, D_1 = D_2 = 1$. 85
4.19 The concentric circle constant absorption model 87
4.20 The concentric circle constant absorption $O(1)$ problem. Left: Region 1. Right: Region 2. 89
4.21 The concentric circle constant absorption $O(\epsilon)$ problem. Left: Region 1. Right: Region 2. 89
4.22 The concentric circle proportional absorption model 90
4.23 Comparing oxygen distribution throughout the concentric circles models. $D_1 = 100$, $D_2 = 1$, $\lambda = 2$ and the threshold, $T = 0.5$ 92
4.24 The line boundary constant absorption model 93
4.25 The line boundary constant absorption $O(1)$ problem. Left: Outer problem. Right: Inner problem. 94
4.26 The line boundary constant absorption $O(\epsilon)$ problem. Left: Region 1. Right: Region 2. 95
4.27 The bipolar coordinate system, as defined by (4.6.44), for circles of constant η where $0 \leq \xi < 2\pi$ 96
4.28 The individual parts of the constant absorption asymptotic solution, where $\epsilon = 0.01$, $c = -3$, $m = 2$, $r_B = 1$, and $T = 0.5$. Top: $O(1)$, contours at gaps of 0.1. Bottom: $O(\epsilon)$, contours at gaps of 0.5. 100
4.29 The line boundary proportional absorption model 101
4.30 The individual parts of the proportional absorption asymptotic solution, where $\epsilon = 0.01$, $c = -3$, $m = 2$, $r_B = 1$, and $T = 0.5$. Top: $O(1)$, contours at gaps of 0.1. Bottom: $O(\epsilon)$, contours at gaps of 0.5. 104

4.31 Oxygen concentration for the line boundary model when $x = 0$, found using the asymptotic approximation with terms up to $O(\epsilon)$ included. Showing a comparison between proportional absorption and constant absorption of oxygen within the aggregate. Where $\epsilon = 0.01$, $c = -3$, $m = 2$ and $r_B = 1$, $T = 0.5$. 105
5.1 A model with two circular regions of oxygen absorbing soil, below an air/soil boundary at $y = 0$ 109
5.2 The outer region, $O(\epsilon)$ problem 112
5.3 The outer region $O(\epsilon)$ problem using method of images, in the complex z-plane 113
5.4 The outer region $O(\epsilon)$ problem in the ζ-plane 114
5.5 A contour plot of φ_1 from the outer region $O(\epsilon)$ problem. which shows the oxygen concentration decreasing around the soil aggregates but returning to the background level with increased depth. Each contour represents a level step of 1, decreasing towards a minimum in the area between the aggregates. $r_B = 1$, $m = 2$, $\epsilon = 0.01$, $T = 0.5$ 118
5.6 A contour plot of φ_1 from the outer region $O(\epsilon)$ periodic problem, which shows the oxygen concentration decreasing as depth into the soil is increasing. Each contour represents a level step of 2. $r_B = 1$, $m = 2$, $\epsilon = 0.01$, $T = 0.5$, $L = 4$ 121
6.1 Oxygen concentration found using the non-dimensionalised line boundary model when $x = 0$. Found using the asymptotic approximation with terms up to $O(\epsilon)$ included. For an aggregate of depth $H = 2.5$ with $\alpha = 14.5$, $\delta = 0.53 \times 10^{-5}$, $\tau = 0$. 125
6.2 The individual parts of the single aggregate asymptotic solution. Top: $O(1)$, contours at gaps of 0.25. Bottom: $O(\epsilon)$, contours at gaps of 2. For an aggregate of depth $H = 2.5$ with $\alpha = 14.5$, $\delta = 0.53 \times 10^{-5}$, $\tau = 0$. 126
6.3 The individual parts of the periodic asymptotic solution, where there are two vertically aligned aggregates in each period. The aggregates are of depth $H_1 = 1.1$ and $H_1 = 3.2$ with $\alpha = 14.5$, $\delta = 0.53 \times 10^{-5}$, $\tau = 0$. Top: $O(1)$, contours at gaps of 0.25. Bottom: $O(\epsilon)$, contours at gaps of 50. . . . 129
6.4 Showing the anaerobic cores (dotted lines) of the periodic model, found using the full boundary element method with the same parameter values as above. 130
6.5 A plot of the areas of the anaerobic cores from the aggregated soil model for varying D_1. Keeping all the other parameter values the same as in previous results. 130
6.6 A plot of the area of the anaerobic cores from the aggregated soil model for increasing aggregate radius, r_B. With other parameter values kept constant, $\alpha = 14.5$, $\delta = 0.53 \times 10^{-5}$, $\tau = 0$. 131

6.7 A contour plot showing oxygen distribution in a non-aggregated soil, where an area of high microbial activity at depth $H = 4$ has decreased the surrounding oxygen levels. The contour step size is 0.2. The dotted line represents the outside of the patch. $\alpha = 0.91$, $\delta = 1$, $\tau = 0$. 133
6.8 Anaerobic core area, as a percentage of the area of the high respiration patch, plotted against increasing depth. 133
6.9 Comparing anaerobic cores for increasing depth, produced with a single circular high respiration patch within a non-aggregated soil. The most central dotted line represents the core when H=4, then moving outwards, H=8,12,16. $\alpha = 0.91$, $\delta = 1$, $\tau = 0$. 134
6.10 Comparing anaerobic cores, for a horizontal alignment of two high microbial activity patches. 135
6.11 Comparing anaerobic cores, for a vertical alignment of two high microbial activity patches. The parameter values have been kept the same, $\alpha = 0.91$, $\delta = 1$, $\tau = 0$. 135

Chapter 1

Introduction

1.1 Denitrification

Denitrification is a process used by many bacterial species to support anaerobic respiration, where, faced with a lack of oxygen, energy is created by using available nitrates. Soils with a high nitrogen content, as used in arable farming, encourage this process. During denitrification water-soluble nitrates are converted into the gaseous products, nitric oxide (NO), nitrous oxide (N_2O) and dinitrogen (N_2). The denitrifying bacteria protect themselves from the endogenous cytotoxic NO by converting it into N_2O, which is then released into the atmosphere [39]. The basic denitrification chemical pathway is as follows,

$$\text{Nitrate} \rightarrow \text{Nitrite} \rightarrow \text{Nitric Oxide} \rightarrow \text{Nitrous Oxide} \rightarrow \text{Dinitrogen} \tag{1.1.1}$$

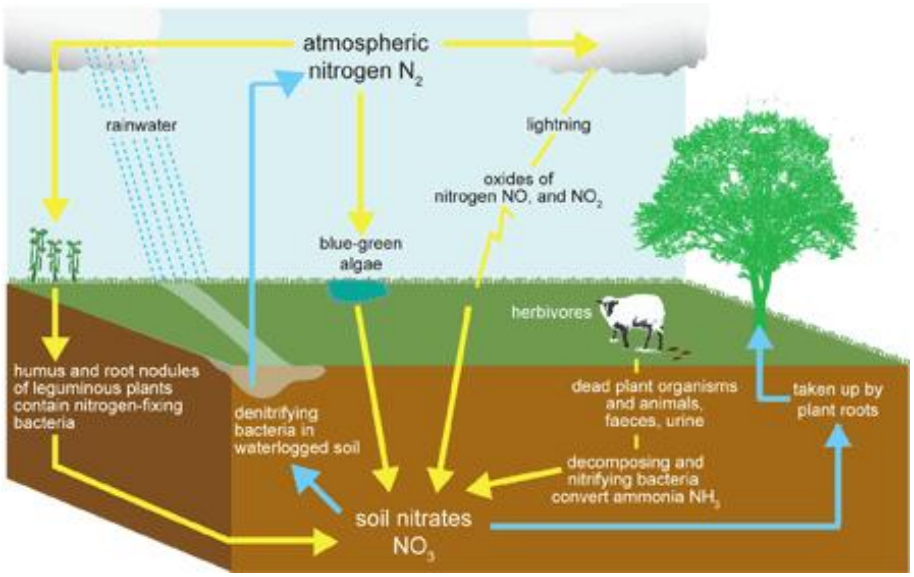

Figure 1.1: The Nitrogen Cycle [1]

Denitrification is one of the main pathways in the nitrogen cycle, whereby nitrogen (N) goes through a variety of redox reactions, as illustrated in Figures 1.1 and 1.2. Nitrogen is found in all organisms with an average content of up to 6.25% of their dry mass. It also

accounts for around 78% of our atmosphere [39].

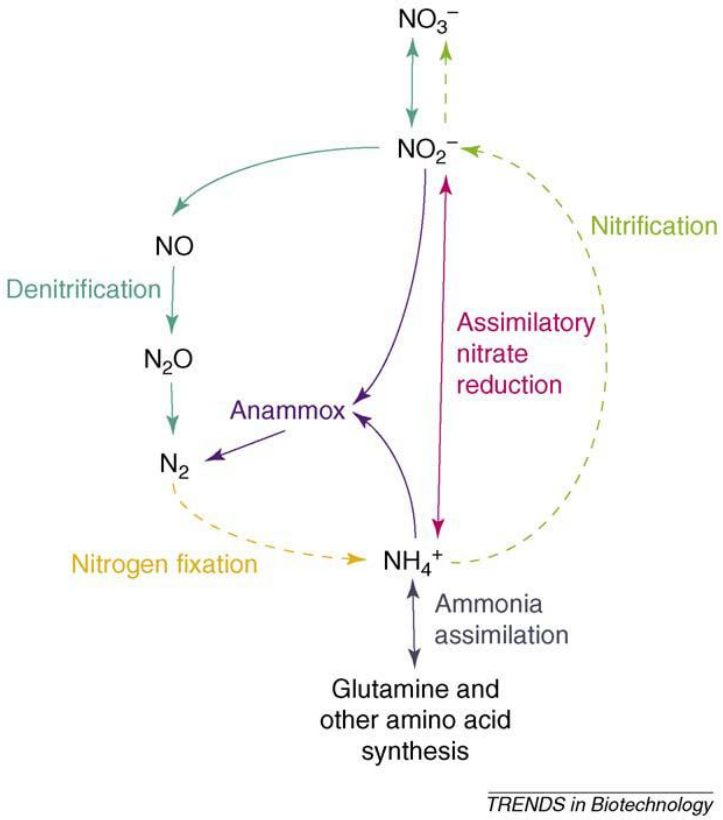

Figure 1.2: Schematic illustration of the nitrogen cycle, from [39].

There are three big issues surrounding denitrification. In farming denitrification is a major problem because it decreases the effectiveness of fertilisers due to the removal of NO_3^-. In waste water treatment the removal of NO_3^- is vital as NO_3^- leakage can lead to eutrophication. And finally, the gaseous product nitrous oxide created during denitrification, is a potent greenhouse gas.

1.2 Nitrous Oxide

Nitrous oxide is one of the four green house gases specifically mentioned in the Kyoto Protocol. According to Montzka and Fraser in [30] nitrous oxide has a global warming potential of 278 times that of carbon dioxide in the next 20 years and 300 times more in the next 100 years. They also say that nitrous oxide has an atmospheric lifetime of 114 years. In the Department for Energy and Climate Change's latest report [34] it is stated that weighted by global warming potential, nitrous oxide emissions accounted for about 5% of the U.K.'s man-made greenhouse gas emissions in 2007. The 2007 paper from the Intergovernmental Panel on Climate Change [19] reported that the concentration of nitrous oxide in the atmosphere continued to rise by approximately 0.26% per year and reached 319 parts per billion in 2005. However, in [34], it is claimed nitrous oxide emissions in the UK fell by 47% between 1990 and 2007 with the largest reductions due to a decrease of

emissions from adipic acid production between 1998 and 1999. This leaves agriculture as the main source, accounting for over two thirds of emissions. Although nitrous oxide is produced naturally in soil several factors are significantly increasing this figure. The main cause is the use of nitrogenous fertilisers (first used in the 1900s) where nitrogen is directly added to the soils to increase crop growth [39]. It is thought that by studying the factors involved in nitrous oxide production and by mathematically modelling denitrification it may be possible to develop techniques to limit emissions in the future.

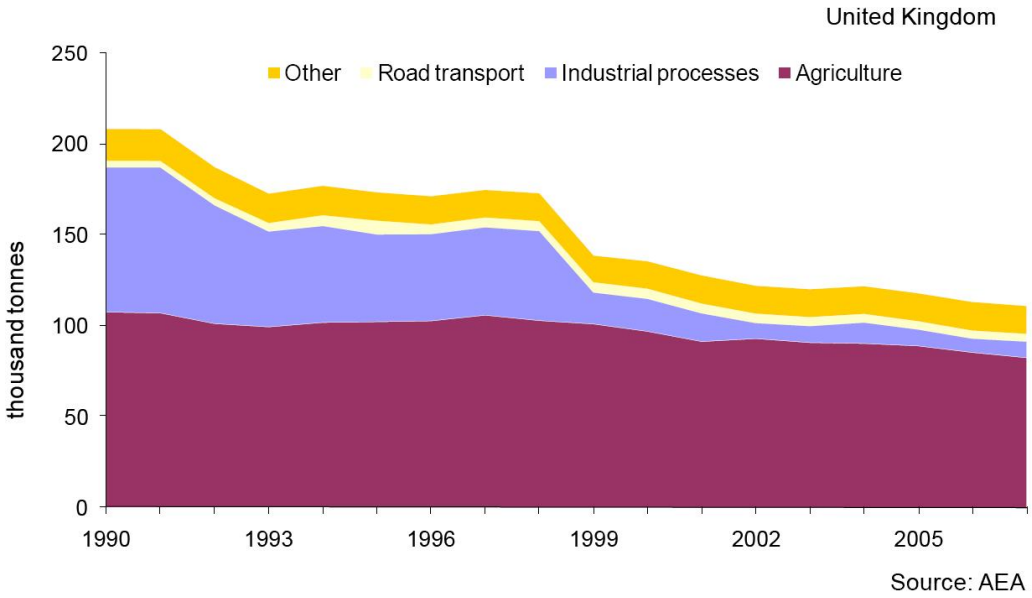

Figure 1.3: Nitrous Oxide emissions by source, 1990-2007, [34]

1.3 The Nitrous Oxide Focus Group

The Nitrous Oxide Focus Group (`http://www.nitrousoxide.org`) is a consortium based research initiative created to study nitrous oxide and develop techniques to mitigate its climate changing effects. Led by Professor David Richardson of the University of East Anglia, the group's main aim is to develop a computational model of denitrification.

Some of the earlier work carried out for this thesis has been used by the group as the basis of further investigation into modelling denitrification reactions rates when affected by levels of copper, as reported in the recently accepted paper by Woolfenden, Gates, Bocking, Blyth, Richardson and Moulton [45].

1.4 Processes To Be Investigated

The rate of bacterial denitrification in soil and the amount of nitrous oxide released because of it, is affected by several elements. Factors such as soil temperature, soil saturation levels, and availability of nitrates and oxygen, all affect the rate at which bacteria in the soil denitrify. In this thesis, in a bid to estimate the level of nitrous oxide which may escape

into the atmosphere, we shall model mathematically two of the main processes that are involved in bacterial denitrification.

Firstly, we investigate the chemical reactions that are occurring within the bacteria and make up the denitrification chemical pathway. Traditionally, the chain of chemical reactions has been modelled using Michaelis-Menten kinetics, as in [6]. In this thesis we review this existing work and discuss some of its limitations and propose various alterations.

Secondly, as we know that denitrification only takes place when bacteria are faced with a lack of oxygen, we model oxygen distribution within a soil. This model shall aim to identify anaerobic micro-sites within the soil where denitrification can take place. We shall develop this model firstly in one-dimensional domains, and then build to a more realistic two-dimensional approach. The most realistic models consist of circles of soil residing beneath ground level in an environment saturated with oxygen. We then consider the models from two separate but similar viewpoints. Either we model an aggregated soil, where each individual circle of soil represents a single soil aggregate surrounded by air. Or we model a non-aggregated soil, where everywhere below ground level is considered to be solid soil and the circular region is an area of high microbial activity, with much higher respiration levels than in the soil surrounding it.

From either of these viewpoints, there shall be an area within the circles where oxygen levels are depleted sufficiently through respiration that the bacteria within the soil will choose instead to denitrify. It is then our aim to calculate the size and shape of this denitrification region. From this the amount of nitrous oxide being generated within the soil can be estimated.

Through consideration of these two processes we can put together an overall idea of what is happening within a soil. We can predict the areas where denitrification would take place, and then the rate at which the resulting chemical reactions would occur.

1.5 Modelling Chemical Reactions

Modelling chemical reactions mathematically can be difficult as there is no one perfect rule relating the stoichiometric equation of a reaction - such as the generic version (1.5.1) - to its rate. Whilst there are assumptions that can be made, the only way to be sure is to observe the rates experimentally. At the University of East Anglia, denitrification rates have been measured in the bacteria *Paracoccus denitrificans*. The experiments consisted of mixing a solution which included certain levels of nitrate and the bacteria within a device known as a chemostat. The chemostats regulate the temperature and stirring of the solution and can then be used to measure the levels of the chemical products created. When we consider our theoretical models of denitrification rates, we bear these results in mind, and aim to create a model that resembles their findings. In this thesis our chemical reaction models show the overall behaviour of the reactions. In the recently accepted paper [45], models based on those in this thesis are fitted with realistic parameters and shown to predict denitrification levels.

$$aA + bB \xrightarrow{k} pP + qQ \tag{1.5.1}$$

The rate of a reaction is defined as the rate of change of the concentration of reactants or products involved. In [33], Nicholas defines the rate of the reaction, (1.5.1), to be,

$$R = -\frac{d[A]}{dt} = -\frac{a}{b}\frac{d[B]}{dt} = \frac{a}{p}\frac{d[P]}{dt} = \frac{a}{q}\frac{d[Q]}{dt}, \tag{1.5.2}$$

where the square brackets indicate to take the concentration of their argument. Alternatively the reaction rate can be defined as,

$$R = -\frac{1}{a}\frac{d[A]}{dt} = -\frac{1}{b}\frac{d[B]}{dt} = \frac{1}{p}\frac{d[P]}{dt} = \frac{1}{q}\frac{d[Q]}{dt}, \tag{1.5.3}$$

as in [22], [5], which is the definition we shall use throughout this thesis.

Most texts, such as [33] and [5], agree that for reactions that can be written in the form of (1.5.1), it is usually true that,

$$R = k[A]^x[B]^y, \tag{1.5.4}$$

where x and y are constants. Therefore, the rate of a reaction is proportional to the product of the concentrations of the reactants involved, raised to some power. This appears to make a lot of sense when thinking about collisions between particles. The reactants can only combine when they collide, and the probability of this happening would be higher for higher concentrations. The powers x and y, are not necessarily integers, but Nicholas [33] suggests that usually $0 < x, y < 3$. Throughout the literature it is thought that the exact rate equation, including the values of x and y, can only be confirmed experimentally.

In mathematical biology textbooks, such as [40], [41], [8] and [31], a widely used approximation to calculate reaction rates is the law of mass action. This law suggests how to determine the rate of a reaction from its stoichiometric equation. This definition would mean that for (1.5.1),

$$R = k[A]^a[B]^b. \tag{1.5.5}$$

This approximation is generally considered to be accurate for elementary reactions [5], and is widely used when considering enzyme kinetics. Throughout our work will consider our overall reaction in a form broken down into a chain of assumed elementary reactions so that the law of mass action remains valid.

When modelling chemical reactions that include an enzyme we can use Michaelis-Menten kinetics, as described in [8]. This method uses the above law of mass action to model the rate of the reactions involved. It also uses an approximation known as the quasi-steady-state hypothesis, which simplifies the rate equations significantly. Michaelis-Menten kinetics are explained at the beginning of the relevant chapter in this thesis, and are then used as a base for moving on to more complex models of the whole denitrification chemical pathway.

1.6 Oxygen Distribution

Denitrification only occurs in soil that has a limited supply of oxygen. It is therefore important to model the distribution of oxygen throughout the soil. As discussed by [26], [42], and [43] (among others) anaerobic micro-sites are created when plants and micro-organisms within the soil consume oxygen quicker than it can diffuse back into the soil from the atmosphere. The micro-organisms, such as the bacteria *Paracoccus denitrificans*, absorb oxygen during respiration and denitrify when the oxygen concentration is low. In the review paper [43], models of the various biological processes within soil that can contribute to greenhouse gas emissions are discussed. The rates of these processes are greatly affected by temperature, pH and soil moisture content. For example, an increase in temperature increases the rate at which the bacteria in the soil respire. The increased respiration rate means an increase in oxygen absorption, and therefore, a larger anaerobic volume of soil is created.

One of the simplest models of anaerobic micro-sites within soil is where oxygen distribution is modelled throughout a spherical soil aggregate, as shown in Figure 1.4. This aggregate is made of solid soil and is assumed to contain an even distribution of organisms with the potential to denitrify.

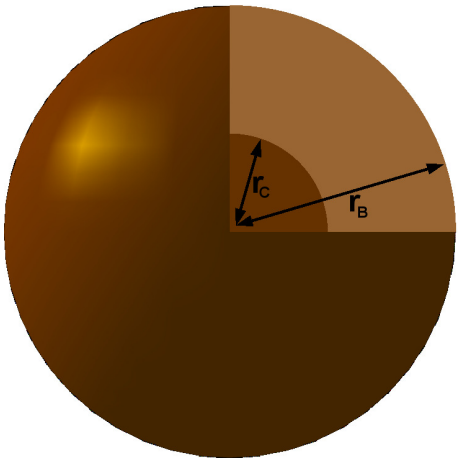

Figure 1.4: Spherical soil aggregate with an anaerobic core.

In [21], Greenwood uses such a model with a constant rate of oxygen absorption, λ, throughout the area of soil that is respiring. When the oxygen concentration is depleted to a critical threshold value, T, anaerobic conditions are reached and the micro-organisms within the soil switch from respiration to denitrification and oxygen absorption stops. As reported in [21], whilst this threshold value varies between micro-organisms, it is always very small and it could be acceptable to estimate this value as being equal to zero. This type of model is also used in tumour modelling when predicting the size of a necrotic core created when nutrients cannot reach the centre of a tumour, as in [8]. Within the soil aggregate, but outside of the anaerobic core, Poisson's equation with only radial variation

is used as the governing diffusion equation,

$$\frac{D}{r^2}\frac{\partial}{\partial r}\left(r^2\frac{\partial\varphi}{\partial r}\right) = \lambda^2, \tag{1.6.1}$$

with boundary conditions,

$$\varphi(r_B) = \mu \tag{1.6.2}$$

$$\varphi(r_C) = T \tag{1.6.3}$$

$$\frac{\partial\varphi(r_C)}{\partial r} = 0. \tag{1.6.4}$$

This model could be used to find the radius, r_C, of the anaerobic area at the centre of the soil aggregate, when the constant oxygen concentration on the outer boundary and the absorption rate within the respiring volume are both known.

An alternative model of oxygen distribution that appears throughout the literature, is that of a one-dimensional domain with constant oxygen absorption throughout the soil, as in [24], [35] and [37]. These models have the advantage of including a boundary at zero depth where the soil is exposed to the air and the oxygen concentration can be approximated as being constant. These models also usually include a no-flux boundary condition to represent an impermeable layer of rock, at either finite or infinite depth.

We aim to construct a model of oxygen diffusion that includes elements of both of these types of models. We wish to create a model where the oxygen concentration does not have to be constant on the edge of the aggregate and the anaerobic core need not be central or circular.

The composition of the area around the soil aggregate can be thought of in two ways: either the region may be viewed as being simply filled with air (or water in a saturated soil); or alternatively it may be thought of as comprising of further soil but in which there is negligible oxygen absorption. The latter may then be viewed as a model of soil in which there is a considerably higher rate of oxygen absorption in some parts than in others, for example a soil containing decomposing leaves. This idea of a non-aggregated soil with "hot-spots" of microbial activity is mentioned in [32].

The most realistic of the oxygen distribution models created in this thesis and some of the results found using them have been outlined in the paper by Bocking and Blyth [7] which is currently in preparation.

1.6.1 A Single Area Of Respiration

In this thesis we firstly develop a model of soil with a single area of oxygen-absorbing respiration activity. The final model we are aiming for is as described here, and throughout the following chapters we bear in mind that this is what we are building towards.

In this two-dimensional model, a single circular area of oxygen absorbing soil is positioned at a distance below ground level, as shown in Figure 1.5. The model consists of three boundaries A, B and C, with oxygen diffusing throughout, and being absorbed

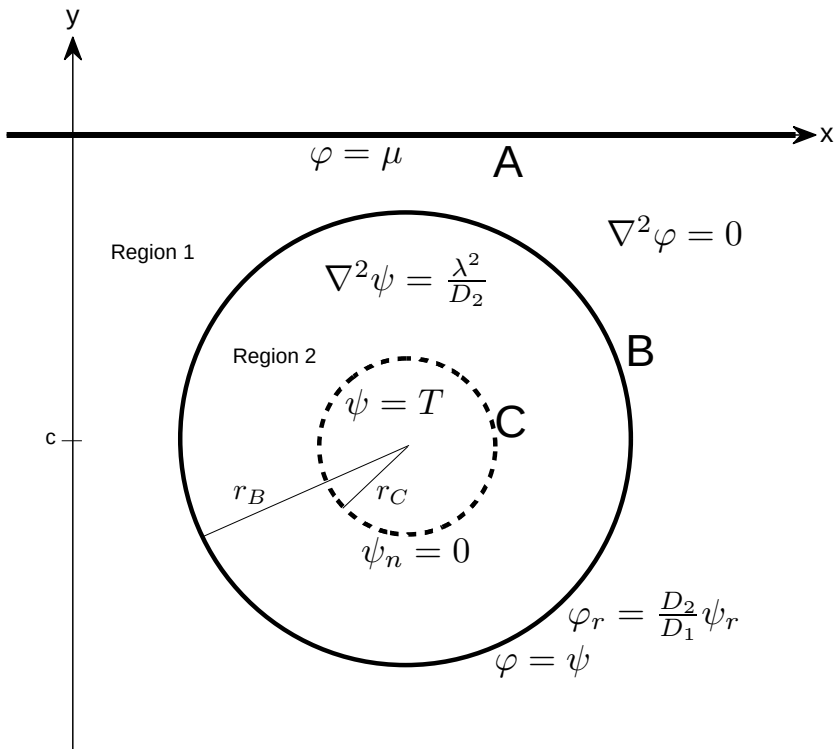

Figure 1.5: A single area of respiring bacteria within soil, *B*, beneath an air/soil boundary *A* absorbing oxygen to create an anaerobic core *C*.

between *B* and *C*.

Boundary *B* is the edge of a single circle of oxygen absorbing soil, with radius r_B and centred at $y = c$. Within *B* but outside *C*, which we shall henceforth refer to as region 2, oxygen is absorbed at a constant rate λ^2. The absorption from this soil aggregate will decrease the concentration of oxygen both inside and outside *B*. Oxygen concentration in region 2, is given by ψ, which is governed by,

$$D_2\nabla^2\psi = \lambda^2 \tag{1.6.5}$$

where D_2 is the diffusivity constant inside the aggregate. This formulation is equivalent to that seen in the previously mentioned tumour model.

Boundary *A*, at $y = 0$, represents the top of the soil or ground level, where the oxygen concentration can be assumed to be a constant, μ. Whilst it may seem like we are incorrectly placing a lid on the soil we note that a boundary condition where oxygen concentration simply tends to constant above the soil is probably less realistic, as this would affect the concentration of oxygen above the ground which is known to be constant. Another point of note is that we shall always be modelling the soil as having a flat top. Later when we consider an aggregated soil this may seem wrong as the top of the soil could be thought of as the top of the aggregates. However, the area around the aggregates may be filled with water and therefore a flat boundary at $y = 0$ still seems realistic. There is also a possibility that there may be a small boundary layer between the soil and the air. However, we assume that the potential affects of this will be insignificant enough to be ignored, and no such

boundary layer has been found to be present in any of the models in the literature.

Between boundaries A and B, which we shall henceforth refer to as region 1, oxygen concentration is given by φ, and diffuses according to Laplace's equation,

$$D_1 \nabla^2 \varphi = 0 \tag{1.6.6}$$

On the boundary B we therefore have the conditions,

$$\begin{aligned} \varphi(r_B, \theta) &= \psi(r_B, \theta) \\ D_1 \varphi_r(r_B, \theta) &= D_2 \psi_r(r_B, \theta). \end{aligned} \tag{1.6.7}$$

The third boundary, C, is the edge of the anaerobic core of the soil aggregate. This boundary has unknown size and shape, and it is our aim to determine this. As mentioned above, it is created when the oxygen concentration drops to the threshold value, T, and the bacteria inside C start denitrifying. There will be no absorption of oxygen inside C and no flux of oxygen into C. Due to the effects of boundary A on the soil aggregate it is probable that the anaerobic core will be positioned lower in the aggregate as the oxygen concentration will be higher on the top edge of the aggregate. Therefore when considering the radius from the centre of the aggregate to the edge of the anaerobic core, r_C, we note that this is a function of θ. The boundary conditions on C can be written,

$$\begin{aligned} \psi(r_C) &= T \\ \mathbf{n} \cdot \nabla \psi(r_C) &= 0 \\ r_C &= r_C(\theta). \end{aligned} \tag{1.6.8}$$

Our model also includes the condition that

$$\lim_{y \to -\infty} \frac{\partial \varphi}{\partial y} = 0, \tag{1.6.9}$$

which can be interpreted as the effect of an impermeable layer of rock under the soil at large depth.

As mentioned earlier, we can consider this model in two ways. Firstly, we can think of an aggregated soil, in which the soil aggregate B is surrounded by air (or water if the soil is saturated, as it would be after heavy rainfall). This model shall be developed to include an infinite array of soil aggregates positioned to represent a cross section of soil. Alternatively, we can consider a non-aggregated soil, where below $y = 0$ is solid soil. In this version of the model the region inside B represents an area of much higher microbial activity than in the soil around it. This area could be created by, for example, decaying organic matter. We then consider the region outside B to have negligible oxygen absorption. The diffusivity of oxygen in air is much faster than it is in soil, therefore, the main difference between the two versions of the model is the diffusivity ratio between the two regions.

It is possible to non-dimensionalise using the region 2 radius, r_B, as the reference length and the ground oxygen level, μ, as the reference concentration. Accordingly we

obtain the dimensionless problem in region 1,

$$\nabla^2\varphi = 0, \tag{1.6.10}$$

with $\varphi = 1$ on A, the continuity conditions on B,

$$\varphi = \psi, \qquad \mathbf{n}\cdot\nabla\varphi = \delta\,\mathbf{n}\cdot\nabla\psi, \tag{1.6.11}$$

where $\mathbf{n}$ is the unit normal pointing out of the aggregate, and the condition that $\phi_y \to 0$ as $y \to -\infty$. In region 2, we have the dimensionless problem

$$\nabla^2\psi = \alpha, \tag{1.6.12}$$

with

$$\psi = \tau, \qquad \mathbf{n}\cdot\nabla\psi = 0 \tag{1.6.13}$$

on C, where $\mathbf{n}$ is the unit normal to C pointing outwards. The pertinent dimensionless parameters are

$$\alpha = \frac{r_B^2\lambda^2}{\mu D_2}, \qquad \delta = \frac{D_2}{D_1}, \qquad \tau = \frac{T}{\mu}, \qquad H = \frac{-c}{r_B}, \tag{1.6.14}$$

where the last parameter provides a measure of how far the aggregate is beneath ground level. On biological grounds, since denitrification only takes place when the oxygen level falls below a critical value which is much lower than that prevailing in the ambient environment, we can assume that $\tau < 1$. When we consider the aggregated soil case the parameter δ would be small, as the rate of diffusion inside the soil aggregate is much slower than in the surround. For the non-aggregated soil case we shall set $\delta = 1$, as both regions will consist of solid soil.

Note that whilst developing the model in the following chapters we use the full problem rather than the non-dimensionalised version, and only return to the non-dimensionalised version once we have decided upon our final model.

1.6.2 Multiple Areas Of Respiration

For aggregated soil we shall eventually expand the model to include an infinite array of soil aggregates, surrounded by either air or water. This will give a representation of a cross section of an aggregated soil, in which we will be able to observe decreasing oxygen levels for increasing depth. Within each individual aggregate there will be an aerobic area absorbing oxygen and an anaerobic area where denitrification takes place, which should increase in size for aggregates deeper in the soil.

For the non-aggregated soil with high microbial activity patches, an infinite array seems less appropriate. We shall, however, observe the results of including multiple patches as the multiple areas of oxygen absorption will affect the size of the anaerobic cores.

1.7 The Boundary Element Method

In this thesis the boundary element method will be used to find solutions to Laplace's or Poisson's equation when only information on the domain boundaries are known. The solutions are found from integral equations which are relatively straight forward to solve numerically. Outlined below is a description of how the method is derived, similar to that found in [36], and an introduction to how the method will be used in later chapters.

We aim to find a solution to Laplace's equation,

$$\nabla^2\varphi = 0 \tag{1.7.1}$$

inside a domain D, with boundary D'. We derive the relevant boundary integral equation from Green's second identity,

$$G\nabla^2\varphi - \varphi\nabla^2 G = \nabla.(G\nabla\varphi - \varphi\nabla G), \tag{1.7.2}$$

where $G(\mathbf{x}, \mathbf{x_0})$ is a Green's function which satisfies

$$\nabla^2 G + \delta(\mathbf{x} - \mathbf{x_0}) = 0, \tag{1.7.3}$$

where δ is the standard Dirac delta function. Depending on the problem we are solving and the boundary conditions involved, the choice of Green's function will vary. However, it will always be a solution of (1.7.3), or a very similar equivalent if we are solving for other diffusion equations. We note that we have now defined $\mathbf{x_0}$ to be a singular point within A. We then integrate (1.7.2) over the domain A, and by using the divergence theorem arrive at,

$$\iint_D G\nabla^2\varphi - \varphi\nabla^2 G dA = -\int_{D'} G\mathbf{n}\cdot\nabla\varphi dl + \int_{D'}\varphi\mathbf{n}\cdot\nabla G dl. \tag{1.7.4}$$

Here, and in all other boundary integral equations in this thesis, $\mathbf{n}$ is defined to be the unit normal on the boundary pointing into the domain. Note that in the divergence theorem $\mathbf{n}$ is defined in the opposite direction, hence the change of minus sign in (1.7.4). As φ satisfies (1.7.1) and G satisfies (1.7.3), we can substitute these into (1.7.4) so that,

$$\varphi(\mathbf{x_0}) = -\int_{D'} G(\mathbf{x}, \mathbf{x_0})\mathbf{n}\cdot\nabla\varphi(\mathbf{x}) dl(\mathbf{x}) + \int_{D'}\varphi(\mathbf{x})\mathbf{n}\cdot\nabla G(\mathbf{x}, \mathbf{x_0}) dl(\mathbf{x}). \tag{1.7.5}$$

From this boundary integral equation we can compute values of $\varphi(\mathbf{x_0})$ for any interior point $\mathbf{x_0}$ when only the boundary values of φ and $\mathbf{n}\cdot\nabla\varphi$ are known. This is the most important property of the boundary element method and is the reason why it is so useful for solving the problems in this thesis.

However, it is possible to go one step further as solutions can also be found when only one of φ and $\mathbf{n}\cdot\nabla\varphi$ are known on the boundary. For this we are required to take $\mathbf{x_0}$ to be positioned on the boundary D'. As $\mathbf{x_0}$ approaches D' from inside D and crosses the boundary the two integrals in (1.7.5) behave differently. The first integral, known as the single layer potential, is continuous as $\mathbf{x_0}$ crosses D'. The second integral in (1.7.5), known

as the double layer potential, has a discontinuity as $\mathbf{x_0}$ crosses D' and jumps in value. In order to calculate the value of this jump we first note that,

$$\int_{D'} \mathbf{n} \cdot \nabla G(\mathbf{x}, \mathbf{x_0}) dl = -\iint_D \nabla^2 G(\mathbf{x}, \mathbf{x_0}) dA = \begin{cases} 1, & \text{if } \mathbf{x_0} \text{ inside } D' \\ 0, & \text{if } \mathbf{x_0} \text{ outside } D' \end{cases} \tag{1.7.6}$$

and that,

$$\int_{D'}^{PV} \mathbf{n} \cdot \nabla G(\mathbf{x}, \mathbf{x_0}) dl = \frac{1}{2}, \text{ if } \mathbf{x_0} \text{ on } D', \tag{1.7.7}$$

where the superscript PV indicates to take the principal value of the integral.

Care must be taken when integrating around the boundary as there will come a point where $\mathbf{x} = \mathbf{x_0}$, therefore we write,

$$\begin{aligned} \lim_{\mathbf{x_0} \to D'} \int_{D'} \varphi(\mathbf{x}) \mathbf{n} \cdot \nabla G(\mathbf{x}, \mathbf{x_0}) dl &= \lim_{\mathbf{x_0} \to D'} \int_{D'} \left[\varphi(\mathbf{x}) - \varphi(\mathbf{x_0})\right] \mathbf{n} \cdot \nabla G(\mathbf{x}, \mathbf{x_0}) dl \\ &\quad + \lim_{\mathbf{x_0} \to D'} \int_{D'} \varphi(\mathbf{x_0}) \mathbf{n} \cdot \nabla G(\mathbf{x}, \mathbf{x_0}) dl. \end{aligned} \tag{1.7.8}$$

The second integral on the right hand side of (1.7.8) can be rewritten using the identities (1.7.6) and (1.7.7), as $\varphi(\mathbf{x_0})$ is a constant for each choice of $\mathbf{x_0}$. We can write,

$$\lim_{\mathbf{x_0} \to D'} \int_{D'} \varphi(\mathbf{x_0}) \mathbf{n} \cdot \nabla G(\mathbf{x}, \mathbf{x_0}) dl = \varphi(\mathbf{x_0}) \int_{D'}^{PV} \mathbf{n} \cdot \nabla G(\mathbf{x}, \mathbf{x_0}) dl + \frac{1}{2} \varphi(\mathbf{x_0}), \tag{1.7.9}$$

where $\mathbf{x_0}$ approaches D' from the inside, and on the right hand side of (1.7.9) $\mathbf{x_0}$ is positioned on D'.

In the first integral on the right hand side of (1.7.8) although the Green's function becomes singular when $\mathbf{x} = \mathbf{x_0}$, it will be pre-multiplied by zero. This allows us to integrate using the principal value in order to find a finite value. Therefore we can write,

$$\begin{aligned} \lim_{\mathbf{x_0} \to B} \int_B \varphi(\mathbf{x}) \mathbf{n} \cdot \nabla G(\mathbf{x}, \mathbf{x_0}) dl &= \int_B^{PV} \left[\varphi(\mathbf{x}) - \varphi(\mathbf{x_0})\right] \mathbf{n} \cdot \nabla G(\mathbf{x}, \mathbf{x_0}) dl \\ &\quad + \varphi(\mathbf{x_0}) \int_B^{PV} \mathbf{n} \cdot \nabla G(\mathbf{x}, \mathbf{x_0}) dl + \frac{1}{2} \varphi(\mathbf{x_0}), \end{aligned} \tag{1.7.10}$$

which simplifies to,

$$\lim_{\mathbf{x_0} \to B} \int_B \varphi(\mathbf{x}) \mathbf{n} \cdot \nabla G(\mathbf{x}, \mathbf{x_0}) dl = \int_B^{PV} \varphi(\mathbf{x}) \mathbf{n} \cdot \nabla G(\mathbf{x}, \mathbf{x_0}) dl + \frac{1}{2} \varphi(\mathbf{x_0}).$$

Putting this back together with the single layer potential, our boundary integral equation for $\mathbf{x_0}$ on B is,

$$\varphi(\mathbf{x_0}) = -2 \int_B G(\mathbf{x}, \mathbf{x_0}) \mathbf{n} \cdot \nabla \varphi(\mathbf{x}) dl + 2 \int_B^{PV} \varphi(\mathbf{x}) \mathbf{n} \cdot \nabla G(\mathbf{x}, \mathbf{x_0}) dl. \tag{1.7.11}$$

Using this boundary integral equation if we know the values of φ or $\mathbf{n} \cdot \nabla \varphi$ on B we can solve to find $\mathbf{n} \cdot \nabla \varphi$ or φ on B respectively. Once both are known we can then use (1.7.5) to

solve for any $\mathbf{x_0}$ in A.

The integrals in (1.7.5) and (1.7.11) will be computed in this thesis by discretizing the domain boundaries into N straight elements, as shown for an example circular domain in Figure 1.6. Along each element it is assumed φ and $\mathbf{n} \cdot \nabla\varphi$ are constant. This method of discretizing the boundary into straight elements allows solutions to be found for domains with any boundary shape without the problem becoming more complex.

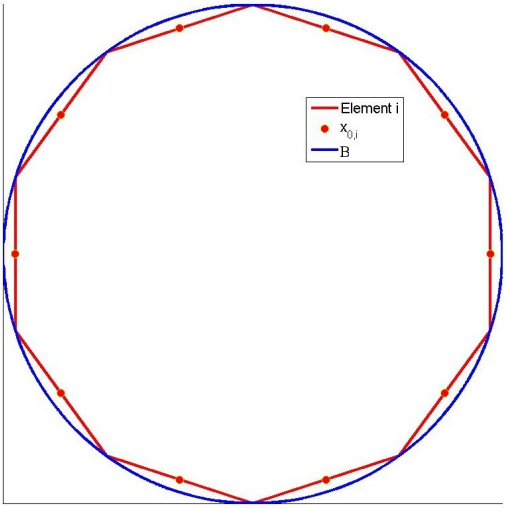

Figure 1.6: A circular boundary B is split into N straight elements

In order to find either φ or $\mathbf{n} \cdot \nabla\varphi$ on the boundary, we construct a system of N boundary integral equations by choosing $\mathbf{x_0}$ to be positioned at the midpoint of each element. We then impose (1.7.11) at each of these $\mathbf{x_0}$ so that we have N linear algebraic equations with N unknowns. This system can then be solved using methods such as Gaussian elimination.

For each of the N integral equations in our system the individual integrals must be evaluated along each of the N elements. This means that for each integral there will be one singular element where $\mathbf{x_0}$ is currently positioned.

Integration along each of the non-singular boundary elements can be done using the following Gauss-Legendre quadrature, as described in [36]. We define,

$$h_s = \frac{1}{2}\sqrt{(x_{i+1} - x_i)^2 + (y_{i+1} - y_i)^2} \tag{1.7.12}$$

$$dl = \sqrt{dx^2 + dy^2} = h_s ds \tag{1.7.13}$$

where x_i and y_i are the element end points. This is so that integration can be carried out using

$$\int_{-1}^{1} f(s)ds \approx \sum_{n=1}^{N_Q} f(s_n)\omega_n, \tag{1.7.14}$$

where the s_n are defined by the Gauss-Legendre quadrature, and create the base points via,

$$\begin{aligned} x_{i,n} &= \frac{1}{2}(x_{i+1} + x_i) + \frac{1}{2}(x_{i+1} - x_i)s_n \\ y_{i,n} &= \frac{1}{2}(y_{i+1} + y_i) + \frac{1}{2}(y_{i+1} - y_i)s_n, \end{aligned} \tag{1.7.15}$$

and the ω_n are the associated weightings. N_Q represents the total number of base points requested and better accuracy can be achieved by taking larger values of N_Q. For the calculations in this thesis $N_Q = 6$ throughout, as this was deemed to be a good compromise between the accuracy of the result and the computation time required.

For the singular elements, i.e. when $\mathbf{x_0}$ lies on that element, we separate out the singularity so that we can integrate analytically. What this actually requires us to do will depend on our choice of Green's function. This will be described later in the thesis, and is explained in detail by Pozrikidis, in [36].

In order to actually compute the solutions we can rewrite (1.7.11) as,

$$\frac{1}{2}\varphi(\mathbf{x_0}) = \sum_{i=1}^{N} \alpha_i(\mathbf{x_0})\,(\mathbf{n}\cdot\nabla\varphi)_i + \sum_{i=1}^{N} \beta_i(\mathbf{x_0})\varphi_i, \tag{1.7.16}$$

where we have defined,

$$\begin{aligned} \alpha_i(\mathbf{x_0}) &= -\int_{l_i}^{l_{i+1}} G(\mathbf{x}(l), \mathbf{x_0})dl \\ \beta_i(\mathbf{x_0}) &= \int_{l_i}^{l_{i+1}} \mathbf{n}\cdot\nabla G(\mathbf{x}(l), \mathbf{x_0})dl, \end{aligned} \tag{1.7.17}$$

which are the integrals of the Green's function and its normal derivative on each boundary element. Note that the $\mathbf{x}(l)$ in the integrals follow the path of each straight boundary element and that the range l_i to l_{i+1} means to integrate along the length of each element. As mentioned above each of the individual φ_i and $(\mathbf{n}\cdot\nabla\varphi)_i$ are now assumed constant on each boundary element. By imposing (1.7.16) N times, once for each of the $\mathbf{x_0}$, positioned on the element midpoints, we will arrive at a solvable boundary integral system. We re-write the N equations created in a matrix form as,

$$\frac{1}{2}\mathbf{I_N}\mathbf{F} = \mathbf{A}\mathbf{F}' + \mathbf{B}\mathbf{F}, \tag{1.7.18}$$

where we have defined,

$$\mathbf{F} = \begin{pmatrix} \varphi_1 \\ \vdots \\ \varphi_N \end{pmatrix}, \quad \mathbf{F}' = \begin{pmatrix} (\mathbf{n}\cdot\nabla\varphi)_1 \\ \vdots \\ (\mathbf{n}\cdot\nabla\varphi)_N \end{pmatrix}, \tag{1.7.19}$$

$$\mathbf{A} = \begin{pmatrix} \alpha_1(\mathbf{x_{0,1}}) & \cdots & \alpha_N(\mathbf{x_{0,1}}) \\ \vdots & \vdots & \vdots \\ \alpha_1(\mathbf{x_{0,N}}) & \cdots & \alpha_N(\mathbf{x_{0,N}}) \end{pmatrix}, \quad \mathbf{B} = \begin{pmatrix} \beta_1(\mathbf{x_{0,1}}) & \cdots & \beta_N(\mathbf{x_{0,1}}) \\ \vdots & \vdots & \vdots \\ \beta_1(\mathbf{x_{0,N}}) & \cdots & \beta_N(\mathbf{x_{0,N}}) \end{pmatrix}, \tag{1.7.20}$$

and $\mathbf{I}_N$ is the N by N identity matrix. We can then rearrange (1.7.18) to,

$$\mathbf{AF'} = \left(\mathbf{B} - \frac{1}{2}\mathbf{I_N}\right)\mathbf{F}, \tag{1.7.21}$$

which can clearly be solved to find either $\mathbf{F}$ or $\mathbf{F'}$ and therefore the individual φ_i or $(\mathbf{n}\cdot\nabla\varphi)_i$.

Once the boundary values have been found, we can substitute them into a discretized version of (1.7.5) in order to find φ at any $\mathbf{x_0}$. The discretized equation will be of the form,

$$\varphi(\mathbf{x_0}) = \sum_{i=1}^{N} \alpha_i(\mathbf{x_0})\,(\mathbf{n}\cdot\nabla\varphi)_i + \sum_{i=1}^{N} \beta_i(\mathbf{x_0})\varphi_i. \tag{1.7.22}$$

1.8 The Modified Schwarz Problem

In Crowdy's paper, [11], an integral formula for the solution of the modified Schwarz problem in a multiply connected circular domain is presented. Later we shall use this formula to solve part of an asymptotic expansion problem in an oxygen distribution model. What follows here is a brief outline of the derivation of the generic integral equation, as in [11].

We define a multiply-connected domain, D, in the complex z-plane to consist of the unit-circle, C_0, with M non-intersecting smaller circles, C_k ($k = 1, ..., M$), cut out from the inside of C_0. We then refer to the whole boundary as δD. Inside this domain, we define a new real function, ϕ, such that,

$$\phi(z, \bar{z}) = \mathrm{Re}[f_s(z)], \tag{1.8.1}$$

where, $f_s(z)$, is some analytic and single-valued function in D. This therefore means that ϕ is harmonic and also single-valued in D. The function ϕ can then be used to represent oxygen concentration later in the thesis for a problem similar to the one described in the earlier section. However, using this method we must first find the complex solution $f_s(z)$ before finding the real part $\phi(z, \bar{z})$. We also note that as $f_s(z)$ is single-valued,

$$\oint_{C_k} \frac{\partial}{\partial s}\left[\mathrm{Im}(f_s)\right] ds = \oint_{C_k} \frac{\partial \phi}{\partial n} ds = 0, \tag{1.8.2}$$

where $\frac{\partial}{\partial n}$ means to take the normal derivative to the circle C_k. From (1.8.2), we know that for each of the inner circles the total flow in is equal to the total flow out.

As with the boundary element method, we begin by only knowing the values of ϕ on the boundary δD and then use an integral equation to find the values of $f_s(\alpha)$ for α throughout D. To find this integral equation we begin by using Green's second identity to

write,

$$\iint_D (\phi \nabla^2 G - G\nabla^2 \phi) dA = \oint_{\delta D} \left(\phi \frac{\partial G}{\partial n} - G \frac{\partial \phi}{\partial n} \right) ds, \tag{1.8.3}$$

where G is a Green's function defined in [11] as,

$$G(z;\alpha) = \mathrm{Im}\left[\tilde{G}(z;\alpha)\right], \tag{1.8.4}$$

$$\tilde{G}(z;\alpha) = \frac{i}{2\pi} \log\left(\frac{\omega(z,\alpha)}{|\alpha|\omega(z,\bar{\alpha}^{-1})} \right), \tag{1.8.5}$$

in which $\omega(z,\alpha)$ is the Shottky-Klein prime function, which we calculate using code provided on-line as described in [12]. This Green's function has the properties that,

$$\begin{aligned} \nabla^2 G(z,\alpha) &= \delta(z-\alpha) \\ G &= 0 \qquad \text{on } C_0, \\ G &= \gamma_k(\alpha) \qquad \text{on } C_k,\ k = 1, ..., M, \end{aligned} \tag{1.8.6}$$

where the $\gamma_k(\alpha)$ were found using the condition,

$$\oint_{C_k} \frac{\partial G}{\partial n} ds = 0. \tag{1.8.7}$$

Using the properties of G (1.8.6), condition (1.8.2), and the fact that ϕ is harmonic in D, we can reduce (1.8.3) to,

$$\phi(\alpha,\bar{\alpha}) = \oint_{\delta D} \phi \frac{\partial G}{\partial n} ds. \tag{1.8.8}$$

This equation is the basis of the final integral equation we are looking for. In order to progress further we consider the Wirtinger derivative, which is defined as,

$$\frac{\partial G}{\partial z} = \frac{1}{2}\left(\frac{\partial G}{\partial x} - i \frac{\partial G}{\partial y} \right). \tag{1.8.9}$$

By multiplying the Wirtinger derivative (1.8.9) by,

$$-i\frac{dz}{ds} = \frac{dy}{ds} - i\frac{dx}{ds}, \tag{1.8.10}$$

we can show that,

$$2\left(\frac{\partial G}{\partial z}\right)\left(-i\frac{dz}{ds}\right) = \frac{\partial G}{\partial x}\frac{dy}{ds} - \frac{\partial G}{\partial y}\frac{dx}{ds} - i\frac{\partial G}{\partial x}\frac{dx}{ds} - i\frac{\partial G}{\partial y}\frac{dy}{ds}. \tag{1.8.11}$$

We also notice that,

$$\frac{\partial G}{\partial n} = n \cdot \nabla G = \frac{\partial G}{\partial x}\frac{dy}{ds} - \frac{\partial G}{\partial y}\frac{dx}{ds}. \tag{1.8.12}$$

Remembering that G is real, by substituting (1.8.12) into (1.8.11), we can show that,

$$\frac{\partial G}{\partial n} ds = \mathrm{Im}\left[2\frac{\partial G}{\partial z} dz \right]. \tag{1.8.13}$$

We can use the Cauchy-Riemann equations to show that,

$$\frac{d\tilde{G}}{dz} = \frac{\partial G}{\partial y} + i\frac{\partial G}{\partial x}. \tag{1.8.14}$$

We can then combine this with the Wirtinger derivative (1.8.9), so that,

$$\frac{d\tilde{G}}{dz} - 2i\frac{\partial G}{\partial z} = 0. \tag{1.8.15}$$

Rearranging (1.8.15) and substituting into (1.8.13), leads to,

$$\frac{\partial G}{\partial n} ds = \mathrm{Re}\left[-d\tilde{G}(z;\alpha)\right] \tag{1.8.16}$$

We now substitute (1.8.5) and (1.8.16) into (1.8.8), which can then be rearranged to,

$$\phi(\alpha,\bar{\alpha}) = \mathrm{Re}\left[\frac{1}{2\pi i}\oint_{\delta D} \phi\left(d\log\omega(z,\alpha) + d\log\bar{\omega}(\bar{z},\alpha^{-1})\right)\right]. \tag{1.8.17}$$

We can now recast the integral equation into a form ready for later use by defining the Möbius map,

$$\theta_k(z) = \delta_k + \frac{q_k^2 z}{1-\bar{\delta_k} z}. \tag{1.8.18}$$

The parameters δ_k and q_k are from describing each of the circles, C_k, using

$$|z-\delta_k|^2 = (z-\delta_k)(\bar{z}-\bar{\delta_k}) = q_k^2, \tag{1.8.19}$$

which means that,

$$\bar{z} = \bar{\delta_k} + \frac{q_k^2}{z-\delta_k}. \tag{1.8.20}$$

We can also write that,

$$\bar{\theta_k}(z) = \bar{\delta_k} + \frac{q_k^2 z}{1-\delta_k z}. \tag{1.8.21}$$

So for the inner circles, C_k, we write,

$$\bar{z} = \bar{\theta_k}\left(z^{-1}\right) \tag{1.8.22}$$

For the outer circle, C_0 as it has unit radius and is centred at the origin (1.8.19) becomes,

$$|z| = z\bar{z} = 1 \tag{1.8.23}$$

therefore,

$$\bar{z} = z^{-1}. \tag{1.8.24}$$

So separating the boundary into the individual circles for integration and using the above

allows us to write the final form of our integral equation,

$$\begin{aligned} f_s(\alpha) &= \frac{1}{2\pi i}\oint_{C_0}\phi\left[d\log\omega(z,\alpha)+d\log\bar{\omega}(z^{-1},\alpha^{-1})\right] \\ &\quad -\sum_{k=1}^{M}\frac{1}{2\pi i}\oint_{C_k}\phi\left[d\log\omega(z,\alpha)+d\log\bar{\omega}(\bar{\theta}_k(z^{-1}),\alpha^{-1})\right] \\ &\quad +iC \end{aligned} \tag{1.8.25}$$

where $f_s(\alpha)$ is single valued and ϕ is the real part of $f_s(\alpha)$ and C is an arbitrary real constant. The minus sign in (1.8.25) arises from the definition of the normal vectors in (1.8.3), which in Green's identity should always been pointing outwards. We have defined them as to be always pointing into the domain D, which means on the outer circle they will point in the opposite direction to the rest.

As shown in [11], the method above and the resulting integral equation solution, simplifies for simply and doubly connected domains to the Poisson integral formula and Villat formula respectively. In this thesis we will use the Villat formula as it was used in [13] as one way of finding oxygen concentration around a single circle of respiring soil. This model can be re-described using the method of images which will then present us with a doubly connected domain. This domain can then be mapped to an annulus where the outer circle has radius one and the inner circle has radius ρ. For the area remaining inside the annulus, a solution can be calculated using the Villat formula as will be described later.

1.8.1 An Invalid Problem

The simplest example of solving Laplace's equation, $\nabla^2\phi = 0$, in two dimensions inside an annulus would probably be when the boundary values are both constant. For this example we set an annulus to have outer radius equal to 1, and inner radius, r_I. The boundary conditions are then $\phi(1) = A$, $\phi(r_I) = B$, as shown in Figure 1.7.

Unfortunately, this example does not work with the current method as the problem in this instance is not valid. The solution found analytically would give

$$\phi = \frac{B-A}{\log r_I}\log r + A. \tag{1.8.26}$$

This would correspond to the problem in the complex plane of finding $\psi(z)$, such that $\mathrm{Re}(\psi) = \phi$ on the boundaries. The solution to this problem is,

$$\psi(z) = \frac{B-A}{\log r_I}\log z + A = \frac{B-A}{\log r_I}\log r + A + i\theta\frac{B-A}{\log r_I}. \tag{1.8.27}$$

The problem then stems from the $\log(z)$ term in (1.8.27). As $r = (x^2+y^2)^{\frac{1}{2}}$ and $\theta = \arctan(y/x)$ we can write,

$$\log z = u + iv \tag{1.8.28}$$

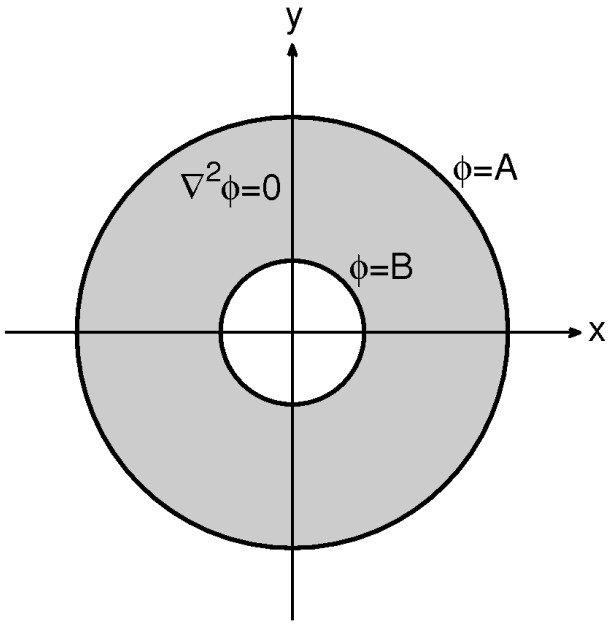

Figure 1.7: An example of an invalid problem when solving using the Crowdy method on a annulus of unit outer radius, and inner radius r_1.

where

$$\begin{aligned} u &= \frac{1}{2}\log(x^2+y^2), \\ v &= \arctan\left(\frac{y}{x}\right). \end{aligned} \tag{1.8.29}$$

We can then see that the Cauchy-Riemann equations hold except for when $x = y = 0$, therefore, $\log z$ is analytic as long as $z \neq 0$, which is fine as this is not within our domain. However, ψ is not single-valued, due to the final term of (1.8.27). This is then an unacceptable result, as in the formulation of the integral equations it was demanded that both $f_s(z)$ and $\phi(z)$ must be single-valued throughout D.

1.8.2 Numerical Verification

In [11], Crowdy verifies the method above numerically for the quadruply connected circular domain shown in Figure 1.8. This domain has been created so that by choosing interior discs of increasing radius the accuracy of the method can be evaluated for boundaries of decreasing distance apart. It has also been created such that it is devoid of any geometrical symmetries.

Using the above domain, the test function will be

$$f_s = z, \tag{1.8.30}$$

which is clearly both analytic and single valued.

In order to find the solution we follow the method in [11] as closely as possible, using Crowdy's code available on-line to compute the value of the Shottky-Klein prime function

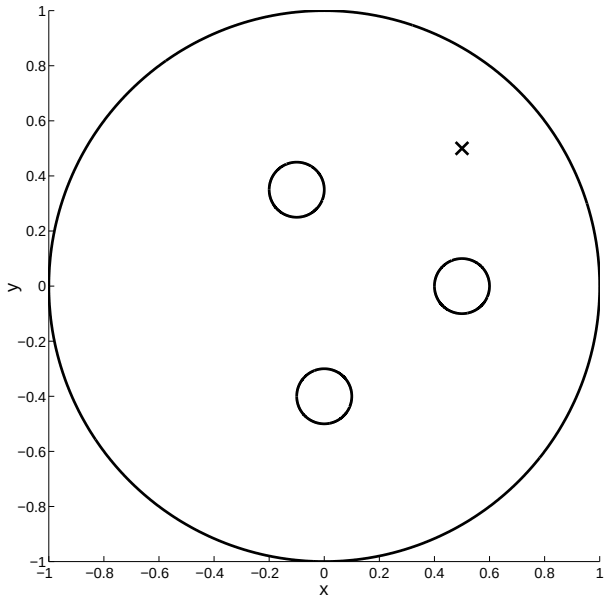

Figure 1.8: The quadruply connected circular domain from the numerical verification section of Crowdy's paper [11]. The interior circular discs have radius 0.1 and centres at 0.5, $-0.1 + 0.35i$ and $-0.4i$. The cross marks the point at which we shall choose to take α in order to verify the method.

when needed. We have found that whilst the method has worked, we have been unable to reproduce the levels of accuracy reported within the paper [11]. This is most likely due to the fact that Crowdy's on-line code does not apply when the evaluation point lies on the boundary [Crowdy, Private Communication]. This method however, remains very powerful and has considerable advantages over using numerical methods such as the boundary element method. The advantages for our particular problem will be discussed in detail in the relevant section later in the thesis.

1.8.3 Avoiding Branch Cuts

Later in this thesis when we introduce models with multiple soil aggregates, we will need the full version of the integral equation (1.8.25). Whilst the integrals are simple to compute numerically due to their compactness, we must consider one difficulty with care. The integrals contain logarithms that could include branch cuts. This is because whilst

$$z = re^{i\theta} = re^{i(\theta \pm 2\pi)}, \tag{1.8.31}$$

is single valued, when taking logs,

$$\log(z) = \log(re^{i\theta}) = \log(r) + i(\theta \pm 2\pi), \tag{1.8.32}$$

which is multivalued. We will eliminate these in our numerical integration methods by adding or subtracting 2π to θ as necessary in order to ensure $\log \omega$ and $\log \bar{\omega}$ are always continuous.

Chapter 2

The Metabolic Pathway

In this chapter we investigate methods of modelling chemical reactions that can then be used to model the whole denitrification chemical pathway. In the previous work of Betlach and Tiedje [6], which is widely referred to in the literature, the denitrification pathway is modelled using Michaelis-Menten kinetics as described below. However, they seem to have missed out some important details in their model, and below we shall investigate these in order to suggest some improvements.

One important consideration when modelling chemical reactions is that of a separate time-scale at the beginning of the reaction when the reaction rates are much quicker. The work below investigates this inner time-scale which is ignored in models which use the Michaelis-Menten techniques. These results are important as they show that the behaviour of the chemicals at the beginning of the reactions is much different to later in the reactions. This could mean that if the Michaelis-Menten method is used to model a reaction a change in the initial conditions may be required.

2.1 Michaelis-Menten Kinetics

The simplest way of modelling the reactions in the metabolic pathway of bacterial denitrification is to use Michaelis-Menten kinetics, as in [6]. As described below, this method uses standard approximations to produce a model where the only remaining unknown parameters are two constants for each reaction in the chain. The first of these constants will be V_{max}, which represents the maximum rate of the reaction. The second is the Michaelis constant, K_m, which can be shown to be equal to the substrate concentration when the reaction rate is half of V_{max}. Both of these constants can be measured experimentally.

We begin with the generic enzyme-substrate reaction,

$$\text{Substrate} + \text{Enzyme} \underset{k_{-1}}{\overset{k_1}{\rightleftarrows}} \text{Complex} \underset{k_{-2}}{\overset{k_2}{\rightleftarrows}} \text{Product} + \text{Enzyme}. \tag{2.1.1}$$

The back reaction rate, k_{-2}, is known to be very small and thus it is acceptable to set it equal to zero from here on. We model the rate of change of the concentrations of the chemicals in (2.1.1) via the law of mass action, as described in the introduction, which

gives the following four ordinary differential equations,

$$\frac{dS}{dt} = k_{-1}C - k_1 S E \tag{2.1.2}$$
$$\frac{dE}{dt} = (k_{-1} + k_2)C - k_1 S E \tag{2.1.3}$$
$$\frac{dC}{dt} = k_1 S E - (k_2 + k_{-1})C \tag{2.1.4}$$
$$\frac{dP}{dt} = k_2 C, \tag{2.1.5}$$

where $S(t), E(t), C(t)$ and $P(t)$ represent the concentrations of the substrate, enzyme, complex, and product respectively. The initial concentrations are denoted as,

$$S(0) = S_0, \quad E(0) = E_0, \quad C(0) = C_0, \quad P(0) = P_0. \tag{2.1.6}$$

The initial conditions are then given by,

$$S_0 \gg E_0 \neq 0, \quad C_0 = P_0 = 0, \tag{2.1.7}$$

which reflects the fact that only a relatively small concentration of enzyme is required to catalyse the reaction, and that the reaction begins with no complex or product present. Now using the quasi-steady-state hypothesis we make the approximation $\frac{dC}{dt} \approx 0$, so that (2.1.4) becomes

$$k_1 S E - (k_2 + k_{-1})C = 0. \tag{2.1.8}$$

From inspection $\frac{d(C+E)}{dt} = 0$, so we can deduce $\frac{dE}{dt} = 0$, and then $E = E_0 - C$. Using all of this leads to

$$C = \frac{S E_0}{K_m + S}, \tag{2.1.9}$$

where we have set $K_m = \frac{k_{-1}+k_2}{k_1}$, the Michaelis constant. We can then also show that

$$\frac{dS}{dt} = \frac{-V_{max} S}{K_m + S}, \tag{2.1.10}$$

where $V_{max} = k_2 E_0$ which is the maximum velocity of the reaction, reached when the substrate concentration is large. The above also leads to

$$\frac{dP}{dt} = \frac{V_{max} S}{K_m + S}. \tag{2.1.11}$$

By integrating (2.1.10) using separation of variables and the initial conditions, we can find a solution analytically,

$$t = \frac{K_m}{V_{max}} \ln\left(\frac{S_0}{S}\right) + \frac{1}{V_{max}}(S_0 - S). \tag{2.1.12}$$

At this stage we notice that the initial conditions do not appear to hold in (2.1.9). At

$t = 0$, we have

$$C_0 = \frac{S_0 E_0}{K_m + S_0} \neq 0. \tag{2.1.13}$$

This is because the reaction happens on two different time-scales; the main reaction that we see in the long term, and a very short time-scale at the beginning of the reaction as the concentration of complex increases rapidly away from zero. So near $t = 0$ our quasi-steady-state hypothesis breaks down.

2.2 Modelling Using A Matched Asymptotic Expansion

In order to create a model of the reaction (2.1.1) that is valid for all time, we must split the problem into two parts, with an inner and an outer time-scale. This method is described in [8] and [31], and we reproduce similar work here. First, we non-dimensionalise the system (2.1.2) to (2.1.5) by defining,

$$s = \frac{S}{S_0}, \quad c = \frac{C}{E_0}, \quad e = \frac{E}{E_0}, \quad p = \frac{P}{S_0}, \quad \tau = k_1 E_0 t, \quad \kappa_e = \frac{k_{-1}}{k_1 S_0}, \quad \kappa_m = \frac{k_{-1} + k_2}{k_1 S_0}, \tag{2.2.1}$$

which gives the system

$$\begin{aligned} \frac{ds}{d\tau} &= \kappa_e c - se \\ \epsilon\frac{de}{d\tau} &= \kappa_m c - se \\ \epsilon\frac{dc}{d\tau} &= se - \kappa_m c \\ \frac{dp}{d\tau} &= (\kappa_m - \kappa_e)c, \end{aligned} \tag{2.2.2}$$

where $\epsilon = \frac{E_0}{S_0} \ll 1$, as we expect there to be much more substrate than enzyme. This system represents the outer time-scale, which we work with later.

2.2.1 Inner Time-scale

For the inner time-scale we define $T = \frac{\tau}{\epsilon}$. The dependant variables are $\hat{s}(T) = s(\tau)$, $\hat{e}(T) = e(\tau)$, $\hat{c}(T) = c(\tau)$ and $\hat{p}(T) = p(\tau)$. By doing this we magnify the region close to $\tau = 0$. Our equations for substrate and complex become

$$\begin{aligned} \frac{d\hat{s}}{dT} &= \epsilon(\kappa_e \hat{c} - \hat{s}\hat{e}) \\ \frac{d\hat{e}}{dT} &= \kappa_m \hat{c} - \hat{s}\hat{e} \\ \frac{d\hat{c}}{dT} &= \hat{s}\hat{e} - \kappa_m \hat{c} \\ \frac{d\hat{p}}{dT} &= \epsilon(\kappa_m - \kappa_e)c. \end{aligned} \tag{2.2.3}$$

Also required are the initial conditions $\hat{s}(0) = 1$, $\hat{e}(0) = 1$, and $\hat{c}(0) = \hat{p}(0) = 0$. From inspection it is clear that

$$\frac{d\hat{e}}{dT} = -\frac{d\hat{c}}{dT} \tag{2.2.4}$$

$$\frac{d\hat{p}}{dT} = -\frac{d\hat{s}}{dT} - \epsilon\frac{d\hat{c}}{dT}. \tag{2.2.5}$$

By integrating (2.2.4) and applying the relevant initial conditions we find $\hat{e} = 1 - \hat{c}$, and from (2.2.5) we find $\hat{p} = 1 - \hat{s} - \epsilon\hat{c}$.

Using the same method as in [28], we expand $\hat{s}$ and $\hat{c}$ as power series in ϵ,

$$\begin{aligned} \hat{s}(T) &= \hat{s}_0(T) + \epsilon\hat{s}_1(T) + O(\epsilon^2) \\ \hat{c}(T) &= \hat{c}_0(T) + \epsilon\hat{c}_1(T) + O(\epsilon^2). \end{aligned} \tag{2.2.6}$$

Substituting these into (2.2.3) and taking only the leading order terms gives

$$\frac{d\hat{s}_0}{dT} = 0 \tag{2.2.7}$$

$$\frac{d\hat{c}_0}{dT} = \hat{s}_0(1 - \hat{c}_0) - \kappa_m\hat{c}_0. \tag{2.2.8}$$

We know $\hat{s}(0) = 1$, so we must have $\hat{s}_0 = 1$, then by substituting this into (2.2.8) we can integrate and use $\hat{c}(0) = 0$ to show

$$\hat{s}_0 = 1, \qquad \hat{c}_0 = \frac{1 - e^{-T(1+\kappa_m)}}{1 + \kappa_m}. \tag{2.2.9}$$

Now considering the $O(\epsilon)$ terms of (2.2.3),

$$\frac{d\hat{s}_1}{dT} = (\kappa_e + \hat{s}_0)\hat{c}_0 - \hat{s}_0 \tag{2.2.10}$$

$$\frac{d\hat{c}_1}{dT} = \hat{s}_1(1 - \hat{c}_0) - (\hat{s}_0 + \kappa_m)\hat{c}_1. \tag{2.2.11}$$

We can also see that the relevant initial conditions are $\hat{s}_1(0) = 0$ and $\hat{c}_1(0) = 0$. By substituting the previous expressions for $\hat{s}_0$ and $\hat{c}_0$ into (2.2.10) we can integrate in a straight forward way and apply the initial condition to show that,

$$\hat{s}_1 = \left(\frac{\kappa_e - \kappa_m}{1 + \kappa_m}\right)T + \frac{\kappa_e + 1}{(1 + \kappa_m)^2}e^{-(1+\kappa_m)T} - \frac{\kappa_e + 1}{(1 + \kappa_m)^2}. \tag{2.2.12}$$

We then substitute this expression for s_1 into (2.2.11), along with the expressions for $\hat{s}_0$ and $\hat{c}_0$, which can then be integrated using an integrating factor. After some manipulation

we can then show that,

$$\begin{aligned}\hat{c}_1 &= \frac{\kappa_m^2 - 2\kappa_e\kappa_m - \kappa_m - (\kappa_e+1)e^{-2(1+\kappa_m)T}}{(1+\kappa_m)^4} + \frac{(\kappa_e + 1 - \kappa_m^2 + 2\kappa_e\kappa_m + \kappa_m)}{(1+\kappa_m)^4}e^{-(1+\kappa_m)T} \\ &+ \left[\frac{\kappa_e\kappa_m + \kappa_m - \kappa_e - 1}{(1+\kappa_m)^3}e^{-(1+\kappa_m)T} + \frac{\kappa_e\kappa_m - \kappa_m^2}{(1+\kappa_m)^3}\right]T \\ &+ \frac{\kappa_e - \kappa_m}{2(1+\kappa_m)^2}e^{-(1+\kappa_m)T}T^2. \end{aligned} \tag{2.2.13}$$

We now have a complete solution for the inner time-scale.

2.2.2 Outer Time-scale

Now working with the outer time-scale, i.e. the longer one where the initial conditions will not hold, from (2.2.2) we have the concentrations given by,

$$\begin{aligned}\frac{ds}{d\tau} &= \kappa_e c - s(1-c) \\ \epsilon\frac{de}{d\tau} &= \kappa_m c - s(1-c) \\ \epsilon\frac{dc}{d\tau} &= s(1-c) - \kappa_m c \\ \frac{dp}{d\tau} &= (\kappa_m - \kappa_e)c. \end{aligned} \tag{2.2.14}$$

We expand s and c as power series in ϵ

$$\begin{aligned}s(\tau) &= s_0(\tau) + \epsilon s_1(\tau) + O(\epsilon^2) \\ c(\tau) &= c_0(\tau) + \epsilon c_1(\tau) + O(\epsilon^2), \end{aligned} \tag{2.2.15}$$

then substituting these into (2.2.14) gives

$$\begin{aligned}\frac{ds_0}{d\tau} + \epsilon\frac{ds_1}{d\tau} &= (\kappa_e c_0 - s_0 + s_0 c_0) + \epsilon(\kappa_e c_1 + s_0 c_1 - s_1 + s_1 c_0) + O(\epsilon^2) \\ \epsilon\frac{dc_0}{d\tau} &= (s_0 - s_0 c_0 - \kappa_m c_0) + \epsilon(s_1 - s_0 c_0 - \kappa_m c_1) + O(\epsilon^2). \end{aligned} \tag{2.2.16}$$

By considering only the leading order terms of (2.2.16) we arrive at

$$\frac{ds_0}{d\tau} = \kappa_e c_0 - s_0 + s_0 c_0 \tag{2.2.17}$$

$$0 = s_0 - s_0 c_0 - \kappa_m c_0. \tag{2.2.18}$$

By rearranging (2.2.18) to find an expression for c_0 and then substituting this into (2.2.17) we get

$$\frac{ds_0}{d\tau} = \frac{(\kappa_e - \kappa_m)s_0}{\kappa_m + s_0}, \qquad c_0 = \frac{s_0}{\kappa_m + s_0}. \tag{2.2.19}$$

By integrating the first of these with respect to τ, we arrive at an equation which we can use to find s_0.

$$\kappa_m \ln s_0 + s_0 = (\kappa_e - \kappa_m)\tau + A \tag{2.2.20}$$

We note that this equation looks similar to the dimensional solution (2.1.12) found earlier.

We now consider only the $O(\epsilon)$ terms in (2.2.16) to find s_1 and c_1,

$$\frac{ds_1}{d\tau} = \kappa_e c_1 + s_0 c_1 - s_1(1 - c_0) \tag{2.2.21}$$

$$\frac{dc_0}{d\tau} = -s_0 c_1 + s_1(1 - c_0) - \kappa_m c_1. \tag{2.2.22}$$

We can use our previous expression for c_0 (2.2.19) to write

$$\frac{dc_0}{d\tau} = \frac{\kappa_m \dot{s}_0}{(\kappa_m + s_0)^2}, \tag{2.2.23}$$

so that (2.2.22) can be rearranged to

$$c_1 = \frac{s_1(1 - c_0)}{(\kappa_m + s_0)} - \frac{\kappa_m \dot{s}_0}{(\kappa_m + s_0)^3}. \tag{2.2.24}$$

Substituting this expression into (2.2.21) gives

$$\frac{ds_1}{d\tau} = (\kappa_e + s_0)\left[\frac{s_1(1 - c_0)}{(\kappa_m + s_0)} - \frac{\kappa_m \dot{s}_0}{(\kappa_m + s_0)^3}\right] - s_1(1 - c_0), \tag{2.2.25}$$

which can be rearranged, using (2.2.19), to

$$\frac{ds_1}{d\tau} + \frac{\kappa_m(\kappa_m - \kappa_e)}{(\kappa_m + s_0)^2} s_1 = \frac{-\kappa_m \dot{s}_0(\kappa_e + s_0)}{(\kappa_m + s_0)^3}, \tag{2.2.26}$$

which can be solved using the integrating factor method. To find the integrating factor we must use (2.2.19) so that

$$\begin{aligned} \text{IF} &= \exp\left[-\kappa_m \int \frac{\dot{s}_0}{s_0(\kappa_m + s_0)} d\tau\right] \\ &= \frac{\kappa_m + s_0}{s_0}. \end{aligned} \tag{2.2.27}$$

So we now have

$$\begin{aligned} \frac{(\kappa_m + s_0)s_1}{s_0} &= -\kappa_m \int \frac{\dot{s}_0(\kappa_e + s_0)}{s_0(\kappa_m + s_0)^2} d\tau \\ &= -\frac{\kappa_e}{\kappa_m} \ln\left(\frac{s_0}{\kappa_m + s_0}\right) + \frac{\kappa_m - \kappa_e}{\kappa_m + s_0} + B, \end{aligned} \tag{2.2.28}$$

where B is a constant of integration.

From (2.2.14) we see that

$$\frac{de}{d\tau} = -\frac{dc}{d\tau} \tag{2.2.29}$$

$$\frac{dp}{d\tau} = -\frac{ds}{d\tau} + \epsilon\frac{ds}{d\tau} \tag{2.2.30}$$

so $e = C - c$, and $p = D - s - \epsilon c$ where C and D are constants of integration.

We now wish to apply the initial conditions to find first A and B and then C and D but it immediately becomes apparent that by satisfying one, the other will not hold. This shows that our outer solution breaks down as $t \to 0$ and we must use the method of matched asymptotic expansions. We wish to match the solutions for the two time-scales together so that they meet in the middle.

2.2.3 Matching The Two Time-scales

In order to compare the solutions for the two time-scales we introduce an intermediate time variable

$$\tau_i = \frac{\epsilon T}{\nu} = \frac{\tau}{\nu}, \tag{2.2.31}$$

where we define the function, ν, to have the properties,

$$\lim_{\epsilon\to 0} \nu(\epsilon) = 0, \quad \lim_{\epsilon\to 0} \frac{\nu(\epsilon)}{\epsilon} = \infty. \tag{2.2.32}$$

Substituting this new time variable, τ_i, into the inner time-scale solution for substrate gives,

$$\begin{aligned} \hat{s}\left(\frac{\tau_i\nu}{\epsilon}\right) &= \hat{s}_0\left(\frac{\tau_i\nu}{\epsilon}\right) + \epsilon\hat{s}_1\left(\frac{\tau_i\nu}{\epsilon}\right) \\ &= 1 + \left(\frac{\kappa_e - \kappa_m}{1+\kappa_m}\right)\tau_i\nu + \frac{\epsilon(\kappa_e+1)}{(1+\kappa_m)^2}e^{-(1+\kappa_m)\frac{\tau_i\nu}{\epsilon}} - \frac{\epsilon(\kappa_e+1)}{(1+\kappa_m)^2}. \end{aligned} \tag{2.2.33}$$

For the outer solution we also substitute in the new time variable, τ_i, so that,

$$s(\tau) = s(\tau_i\nu) = s_0(\tau_i\nu) + \epsilon s_1(\tau_i\nu). \tag{2.2.34}$$

We can now match the two time-scales together by comparing (2.2.33) and (2.2.34). Firstly, we match the $O(1)$ terms, which requires

$$\lim_{\epsilon\to 0}[s_0(\tau_i\nu)] = \lim_{\epsilon\to 0}\left[1 + \left(\frac{\kappa_e - \kappa_m}{1+\kappa_m}\right)\tau_i\nu\right]. \tag{2.2.35}$$

In order for (2.2.35) to hold, it must be true that,

$$s_0(0) = 1. \tag{2.2.36}$$

Enforcing the condition (2.2.36) on the expression for s_0 (2.2.20) allows us to find the value of the previously unknown constant of integration in the $O(1)$ solution, we find that $A = 1$.

Similarly matching the $O(\epsilon)$ terms in (2.2.33) and (2.2.34) gives the requirement that,

$$\lim_{\epsilon\to 0}[s_1(\tau_i\nu)] = \lim_{\epsilon\to 0}\left[\frac{\kappa_e+1}{(1+\kappa_m)^2}e^{-(1+\kappa_m)\frac{\tau_i\nu}{\epsilon}} - \frac{\kappa_e+1}{(1+\kappa_m)^2}\right]. \tag{2.2.37}$$

From this we can deduce the final condition needed for matching the two substrate solutions together,

$$s_1(0) = -\frac{\kappa_e+1}{(1+\kappa_m)^2}. \tag{2.2.38}$$

Substituting the two conditions (2.2.36) and (2.2.38) into (2.2.28) and rearranging slightly leads to,

$$\frac{\kappa_e}{\kappa_m(1+\kappa_m)}\ln(1+\kappa_m) + \frac{\kappa_m-\kappa_e}{(1+\kappa_m)^2} + \frac{B}{1+\kappa_m} = -\frac{\kappa_e+1}{(1+\kappa_m)^2}, \tag{2.2.39}$$

from which we can find the value of the other constant of integration in the substrate solution,

$$B = -1 - \frac{\kappa_e}{\kappa_m}\ln(1+\kappa_m). \tag{2.2.40}$$

We therefore now have a full solution for s_1 in terms of s_0,

$$s_1 = \frac{s_0}{s_0+\kappa_m}\left[\frac{\kappa_e}{\kappa_m}\ln\left(\frac{s_0+\kappa_m}{s_0(1+\kappa_m)}\right) - \frac{s_0+\kappa_e}{s_0+\kappa_m}\right]. \tag{2.2.41}$$

From (2.2.24) we can use (2.2.19) and then substitute (2.2.41) for a full solution for c_1 in terms of s_0,

$$c_1 = \frac{\kappa_m s_0}{(\kappa_m+s_0)^3}\left[\frac{\kappa_e}{\kappa_m}\ln\left(\frac{s_0+\kappa_m}{s_0(1+\kappa_m)}\right) + \frac{\kappa_m-2\kappa_e-s_0}{\kappa_m+s_0}\right]. \tag{2.2.42}$$

At this point we now have fully matched solutions for the substrate and complex in the two time-scales. It remains to find the values of the constants C and D in order to also match the solutions for the enzyme and product.

To match the inner and outer equations for the enzyme we require

$$\lim_{\epsilon\to 0} e(\tau_i\nu) = \lim_{\epsilon\to 0}\hat{e}\left(\frac{\tau_i\nu}{\epsilon}\right), \tag{2.2.43}$$

so we must have

$$C - \lim_{\epsilon\to 0} c(\tau_i\nu) = 1 - \lim_{\epsilon\to 0}\hat{c}\left(\frac{\tau_i\nu}{\epsilon}\right), \tag{2.2.44}$$

as we have already matched c with $\hat{c}$ this forces $C = 1$. For the product we require,

$$\lim_{\epsilon\to 0} p(\tau_i\nu) = \lim_{\epsilon\to 0}\hat{p}\left(\frac{\tau_i\nu}{\epsilon}\right), \tag{2.2.45}$$

so we must have

$$D - \lim_{\epsilon\to 0}[s(\tau_i\nu)+\epsilon c(\tau_i\nu)] = 1 - \lim_{\epsilon\to 0}\left[\hat{s}\left(\frac{\tau_i\nu}{\epsilon}\right) + \epsilon\hat{c}\left(\frac{\tau_i\nu}{\epsilon}\right)\right], \tag{2.2.46}$$

and as we have already matched c with $\hat{c}$ and s with $\hat{s}$ this forces $D = 1$. We now have complete solutions for the inner and outer time-scales for all four concentrations, to

summarise,

$$\kappa_m \ln s_0 + s_0 = (\kappa_e - \kappa_m)\tau + 1 \tag{2.2.47}$$

$$\begin{aligned}
s(\tau) &= s_0 + \frac{\epsilon s_0}{s_0 + \kappa_m}\left[\frac{\kappa_e}{\kappa_m}\ln\left(\frac{s_0 + \kappa_m}{s_0(1+\kappa_m)}\right) - \frac{s_0 + \kappa_e}{s_0 + \kappa_m}\right] \\
c(\tau) &= \frac{s_0}{\kappa_m + s_0} + \frac{\epsilon\kappa_m s_0}{(\kappa_m + s_0)^3}\left[\frac{\kappa_e}{\kappa_m}\ln\left(\frac{s_0 + \kappa_m}{s_0(1+\kappa_m)}\right) + \frac{\kappa_m - 2\kappa_e - s_0}{\kappa_m + s_0}\right] \\
e(\tau) &= 1 - c(\tau) \\
p(\tau) &= 1 - s(\tau) - \epsilon c(\tau)
\end{aligned} \tag{2.2.48}$$

$$\begin{aligned}
\hat{s}(T) &= 1 + \epsilon\left(\frac{\kappa_e - \kappa_m}{1+\kappa_m}\right)T + \epsilon\left(\frac{\kappa_e + 1}{(1+\kappa_m)^2}\right)e^{-(1+\kappa_m)T} - \epsilon\left(\frac{\kappa_e + 1}{(1+\kappa_m)^2}\right) \\
\hat{c}(T) &= \frac{1 - e^{-T(1+\kappa_m)}}{1+\kappa_m} \\
&+ \frac{\epsilon}{(1+\kappa_m)^4}\left[\kappa_m^2 - 2\kappa_e\kappa_m - \kappa_m - (\kappa_e + 1)e^{-2(1+\kappa_m)T}\right] \\
&+ \frac{\epsilon}{(1+\kappa_m)^4}(\kappa_e + 1 - \kappa_m^2 + 2\kappa_e\kappa_m + \kappa_m)e^{-(1+\kappa_m)T} \\
&+ \epsilon\left[\frac{\kappa_e\kappa_m + \kappa_m - \kappa_e - 1}{(1+\kappa_m)^3}e^{-(1+\kappa_m)T} + \frac{\kappa_e\kappa_m - \kappa_m^2}{(1+\kappa_m)^3}\right]T + \frac{\epsilon(\kappa_e - \kappa_m)}{2(1+\kappa_m)^2}e^{-(1+\kappa_m)T}T^2 \\
\hat{e}(T) &= 1 - \hat{c}(T) \\
\hat{p}(T) &= 1 - \hat{s}(T) - \epsilon\hat{c}(T)
\end{aligned} \tag{2.2.49}$$

Using an example set of parameters, the inner and outer time-scale solutions are both plotted in Figure 2.1. We can see from this figure the behaviour in the inner time-scale, i.e. the start of the chemical reaction, is much different to the behaviour during the rest of the reaction. Whilst the quasi-steady-state hypothesis is a good assumption for reactions that go on over a long period of time, we can see here that the behaviour during the first few moments of a reaction is significant, and from a mathematical point of view interesting to consider in our models.

2.2.4 Composite Solution

Using the solutions for the two separate time-scales we can construct a uniformly valid expansion. Using the method of additive composition, as described in [17], we write

$$\begin{aligned}
s_c &= \hat{s}(T) + s(\tau) - \lim_{\epsilon\to 0}\hat{s}(\tau) \\
e_c &= \hat{e}(T) + e(\tau) - \lim_{\epsilon\to 0}\hat{e}(\tau) \\
c_c &= \hat{c}(T) + c(\tau) - \lim_{\epsilon\to 0}\hat{c}(\tau) \\
p_c &= \hat{p}(T) + p(\tau) - \lim_{\epsilon\to 0}\hat{p}(\tau)
\end{aligned} \tag{2.2.50}$$

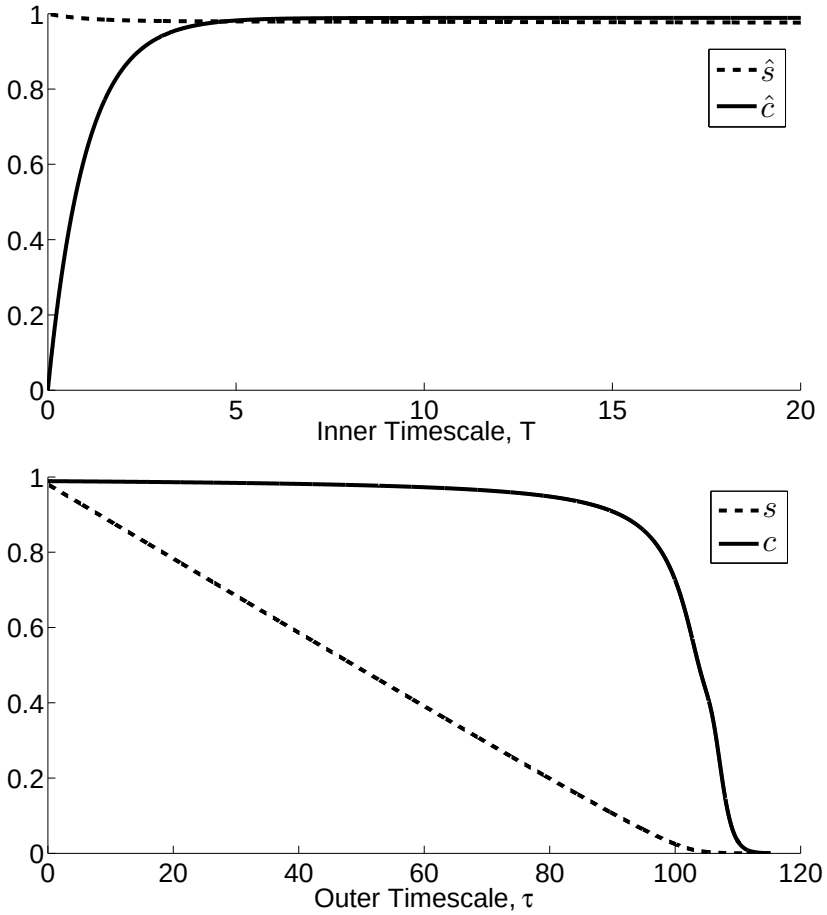

Figure 2.1: Concentrations of substrate and complex for the two time-scales, given by (2.2.47), (2.2.48) and (2.2.49). For $S(0) = 50$, $E(0) = 1$, $k_1 = 2$, $k_2 = 1$, $k_{-1} = 0.1$.

using two term expansions throughout.

$$\begin{aligned}
s_c &= \hat{s}(T) + s(\tau) - 1 - \frac{\kappa_e - \kappa_m}{1+\kappa_m}\tau + \frac{\epsilon(\kappa_e+1)}{(1+\kappa_m)^2} \\
e_c &= \hat{e}(T) + e(\tau) - 1 + \frac{1}{1+\kappa_m} + \frac{\kappa_e\kappa_m - \kappa_m^2}{(1+\kappa_m)^3}\tau + \frac{\epsilon(\kappa_m^2 - 2\kappa_e\kappa_m - \kappa_m)}{(1+\kappa_m)^4} \\
c_c &= \hat{c}(T) + c(\tau) - \frac{1}{1+\kappa_m} - \frac{\kappa_e\kappa_m - \kappa_m^2}{(1+\kappa_m)^3}\tau - \frac{\epsilon(\kappa_m^2 - 2\kappa_e\kappa_m - \kappa_m)}{(1+\kappa_m)^4} \\
p_c &= \hat{p}(T) + p(\tau) + \frac{\kappa_e - \kappa_m}{1+\kappa_m}\tau + \epsilon\left(\frac{1}{1+\kappa_m} + \frac{\kappa_e\kappa_m - \kappa_m^2}{(1+\kappa_m)^3}\tau - \frac{\kappa_e+1}{(1+\kappa_m)^2}\right) \quad (2.2.51)
\end{aligned}$$

These solutions can then be compared to numerical solutions of the non-dimensionalised system (2.2.2), as in Figure 2.2 below. We find that the matched asymptotic solution matches the numerical solution better for smaller values of ϵ, as would be expected.

2.3 Adding A Feed Term

We can modify our model to include a feed term i.e. a constant addition of the substrate. This is representative of what would occur during experiments when investigating bacterial

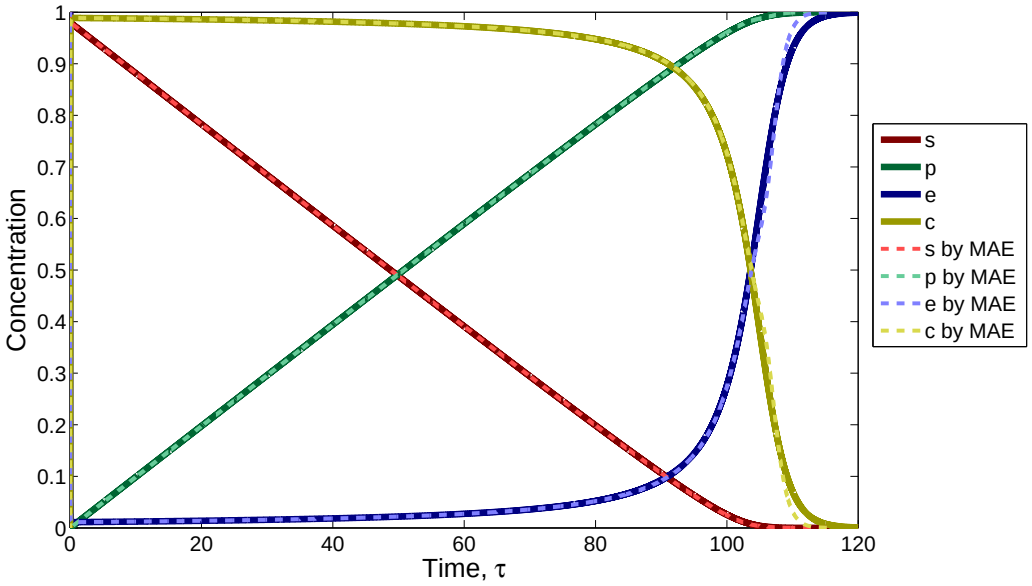

Figure 2.2: Non-dimensionalised substrate-enzyme reaction model. A numerical solution has been found using a Runge-Kutta method, and compared to the solution found using matched asymptotic expansions (MAE). For $S(0) = 50$, $E(0) = 1$, $k_1 = 2$, $k_2 = 1$, $k_{-1} = 0.1$. Note that $\epsilon = 0.02$ and that smaller ϵ will give better agreement between the methods.

denitrification within a chemostat. The bacteria would be continuously fed with a solution containing NO_3 in order to monitor the rate of the reaction at steady state. This work is also relevant to later work when we extend the model to include products further down the reaction pathway. In the original system we adjust the equation for substrate (2.1.2) to include the feed term, F, so that

$$\begin{aligned}
\frac{dS}{dt} &= k_{-1}C - k_1 S E + F \\
\frac{dE}{dt} &= (k_{-1} + k_2)C - k_1 S E \\
\frac{dC}{dt} &= k_1 S E - (k_2 + k_{-1})C \\
\frac{dP}{dt} &= k_2 C.
\end{aligned} \tag{2.3.1}$$

We then non-dimensionalise as above and set $f = \frac{F}{k_1 S_0 E_0}$. For the inner time-scale we now have

$$\begin{aligned}
\frac{d\hat{s}}{dT} &= \epsilon(\kappa_e \hat{c} - \hat{s}\hat{e}) + \epsilon f \\
\frac{d\hat{e}}{dT} &= \kappa_m \hat{c} - \hat{s}\hat{e} \\
\frac{d\hat{c}}{dT} &= \hat{s}\hat{e} - \kappa_m \hat{c} \\
\frac{d\hat{p}}{dT} &= \epsilon(\kappa_m - \kappa_e)c.
\end{aligned} \tag{2.3.2}$$

From inspection we can see that

$$\begin{aligned} \hat{e} &= 1 - \hat{c} \\ \hat{p} &= 1 - \hat{s} - \epsilon\hat{c} + \epsilon f T \end{aligned} \tag{2.3.3}$$

If f is a constant we can use a power series in ϵ, as above, and work in exactly the same way to show that

$$\hat{s} = 1 + \epsilon\left[\left(f + \frac{\kappa_e - \kappa_m}{1+\kappa_m}\right)T + \frac{\kappa_e + 1}{(1+\kappa_m)^2}e^{-(1+\kappa_m)T} - \frac{\kappa_e + 1}{(1+\kappa_m)^2}\right] \tag{2.3.4}$$

$$\begin{aligned} \hat{c} &= \frac{1 - e^{-(1+\kappa_m)T}}{1+\kappa_m} + \epsilon\frac{(1+\kappa_m)f + \kappa_e - \kappa_m}{2(1+\kappa_m)^2}e^{-(1+\kappa_m)T}T^2 \\ &\quad + \epsilon\left[\frac{\kappa_e\kappa_m + \kappa_m - \kappa_e - 1}{(1+\kappa_m)^3}e^{-(1+\kappa_m)T} + \frac{(1+\kappa_m)f + \kappa_e\kappa_m - \kappa_m^2}{(1+\kappa_m)^3}\right]T \\ &\quad + \epsilon\frac{\kappa_m^2 - 2\kappa_e\kappa_m - \kappa_m - (1+\kappa_m)f - (\kappa_e+1)e^{-2(1+\kappa_m)T}}{(1+\kappa_m)^4} \\ &\quad + \epsilon\frac{((1+\kappa_m)f + \kappa_e + 1 - \kappa_m^2 + 2\kappa_e\kappa_m + \kappa_m)e^{-(1+\kappa_m)T}}{(1+\kappa_m)^4} \end{aligned} \tag{2.3.5}$$

The system for the outer time-scale is

$$\begin{aligned} \frac{ds}{d\tau} &= \kappa_e c - se + f \\ \epsilon\frac{de}{d\tau} &= \kappa_m c - se \\ \epsilon\frac{dc}{d\tau} &= se - \kappa_m c \\ \frac{dp}{d\tau} &= (\kappa_m - \kappa_e)c. \end{aligned} \tag{2.3.6}$$

From inspection and by matching we find

$$\begin{aligned} e &= 1 - c \\ p &= 1 - s - \epsilon c + f\tau \end{aligned} \tag{2.3.7}$$

As above, after expanding s and c, we find

$$c_0 = \frac{s_0}{\kappa_m + s_0}. \tag{2.3.8}$$

The condition for matching is still $s_0(0) = 1$ so

$$\tau = \frac{s_0 - 1}{(\kappa_e - \kappa_m + f)} + \left[\frac{\kappa_m(\kappa_e - \kappa_m)}{(\kappa_e - \kappa_m + f)^2}\right]\ln\left[\frac{(\kappa_e - \kappa_m + f)s_0 + f\kappa_m}{(\kappa_e - \kappa_m + f + f\kappa_m)}\right]. \tag{2.3.9}$$

For the s_1 term we once again arrive at (2.2.26), which we again solve using an integrating

factor. From (2.3.6), we use (2.3.8) to show

$$\frac{ds_0}{d\tau} = \frac{(\kappa_e - \kappa_m + f)s_0 + f\kappa_m}{\kappa_m + s_0}. \tag{2.3.10}$$

Then the integrating factor can be manipulated into a form that can be integrated via partial fractions.

$$\begin{aligned} \text{IF} &= \exp\left[\kappa_m(\kappa_m - \kappa_e)\int \frac{\dot{s_0}}{(\kappa_e - \kappa_m)(\kappa_m + s_0)s_0 + f(\kappa_m + s_0)^2}d\tau\right] \\ &= \frac{\kappa_m + s_0}{(\kappa_e - \kappa_m + f)s_0 + f\kappa_m} \end{aligned} \tag{2.3.11}$$

Using this integrating factor (2.2.26) becomes

$$\frac{(\kappa_m + s_0)s_1}{(\kappa_e - \kappa_m + f)s_0 + f\kappa_m} = \int \frac{-\kappa_m(\kappa_e + s_0)}{(\kappa_m + s_0)^2[(\kappa_e - \kappa_m + f)s_0 + f\kappa_m]}d\tau. \tag{2.3.12}$$

After some manipulation and use of partial fractions once again we arrive at our final equation for s_1 in terms of s_0,

$$\begin{aligned} \frac{(\kappa_m + s_0)s_1}{(\kappa_e - \kappa_m + f)s_0 + f\kappa_m} &= \frac{\kappa_e + f}{\kappa_m(\kappa_m - \kappa_e)}\ln\left(\frac{(\kappa_m + 1)[(\kappa_m - \kappa_e - f)s_0 - f\kappa_m]}{(\kappa_m + s_0)(\kappa_m - \kappa_e - f - f\kappa_m)}\right) \\ &\quad + \frac{f + fs_0 - s_0 - \kappa_e}{(\kappa_m + s_0)(\kappa_e - \kappa_m + f + f\kappa_m)} \end{aligned} \tag{2.3.13}$$

To find c_1 we again use (2.2.24) but this time with (2.3.10) so that

$$c_1 = \frac{\kappa_m s_1}{(\kappa_m + s_0)^2} - \frac{\kappa_m(\kappa_e - \kappa_m + f)s_0 + f\kappa_m^2}{(\kappa_m + s_0)^4}. \tag{2.3.14}$$

We can now construct composite solutions as before which are given by

$$\begin{aligned} s_c &= \hat{s}(T) + s(\tau) \\ &\quad -1 - \left(f + \frac{\kappa_e - \kappa_m}{1 + \kappa_m}\right)\tau + \frac{\epsilon(\kappa_e + 1)}{(1 + \kappa_m)^2} \\ e_c &= \hat{e}(T) + e(\tau) \\ &\quad -1 + \frac{1}{1 + \kappa_m} + \frac{(1 + \kappa_m)f + \kappa_e\kappa_m - \kappa_m^2}{(1 + \kappa_m)^3}\tau + \frac{\epsilon(\kappa_m^2 - 2\kappa_e\kappa_m - \kappa_m - (1 + \kappa_m)f)}{(1 + \kappa_m)^4} \\ c_c &= \hat{c}(T) + c(\tau) \\ &\quad -\frac{1}{1 + \kappa_m} - \frac{(1 + \kappa_m)f + \kappa_e\kappa_m - \kappa_m^2}{(1 + \kappa_m)^3}\tau - \frac{\epsilon(\kappa_m^2 - 2\kappa_e\kappa_m - \kappa_m - (1 + \kappa_m)f)}{(1 + \kappa_m)^4} \\ p_c &= \hat{p}(T) + p(\tau) \\ &\quad + \frac{\kappa_e - \kappa_m}{1 + \kappa_m}\tau - \epsilon\frac{\kappa_e + 1}{(1 + \kappa_m)^2} + \frac{\epsilon}{1 + \kappa_m} + \epsilon\frac{(1 + \kappa_m)f + \kappa_e\kappa_m - \kappa_m^2}{(1 + \kappa_m)^3}\tau \end{aligned} \tag{2.3.15}$$

These solutions can then be compared to numerical solutions of the non-dimensionalised system (2.3.6), as in Figure 2.3 below.

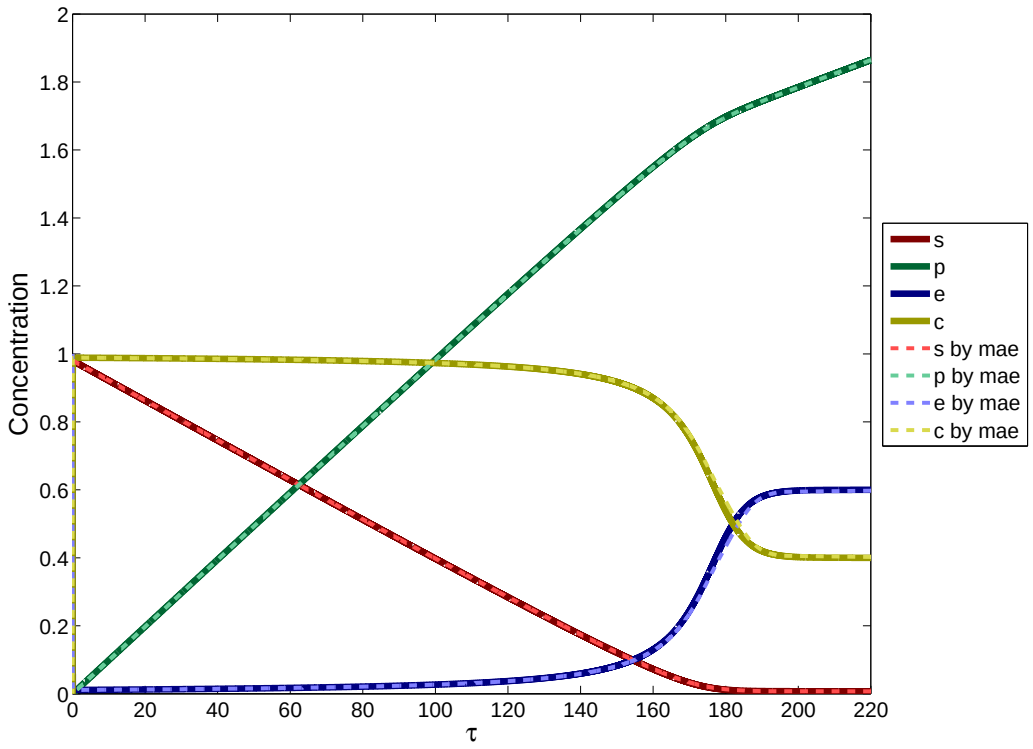

Figure 2.3: Non-dimensionalised substrate-enzyme reaction with feed term model. Numerical solution found using a Runge-Kutta method, compared to solution found using matched asymptotic expansions. For $S(0) = 50$, $E(0) = 1$, $k_1 = 2$, $k_2 = 1$, $k_{-1} = 0.1$, $F = 0.4$. Note that $\epsilon = 0.02$ and that smaller ϵ will give better agreement between the methods.

2.4 Previous Models

Betlach and Tiedje used Michaelis-Menten kinetics in [6] to model the whole denitrification pathway, $NO_3^- \rightarrow NO_2^- \rightarrow NO \rightarrow N_2O \rightarrow N_2$. The following work is very similar. We consider,

$$S + E \underset{k_{-1}}{\overset{k_1}{\rightleftarrows}} C_1 \overset{k_2}{\rightarrow} P_1 + E \underset{k_{-3}}{\overset{k_3}{\rightleftarrows}} C_2 \overset{k_4}{\rightarrow} P_2 + E \underset{k_{-5}}{\overset{k_5}{\rightleftarrows}} C_3 \overset{k_6}{\rightarrow} P_3 + E \underset{k_{-7}}{\overset{k_7}{\rightleftarrows}} C_4 \overset{k_8}{\rightarrow} P_4 + E, \quad (2.4.1)$$

where S represents nitrate and each P_i represents one of the products of denitrification; nitrite, nitric oxide, nitrous oxide and dinitrogen respectively. Using the same technique as above we arrive at a system of five ordinary differential equations in five variables which

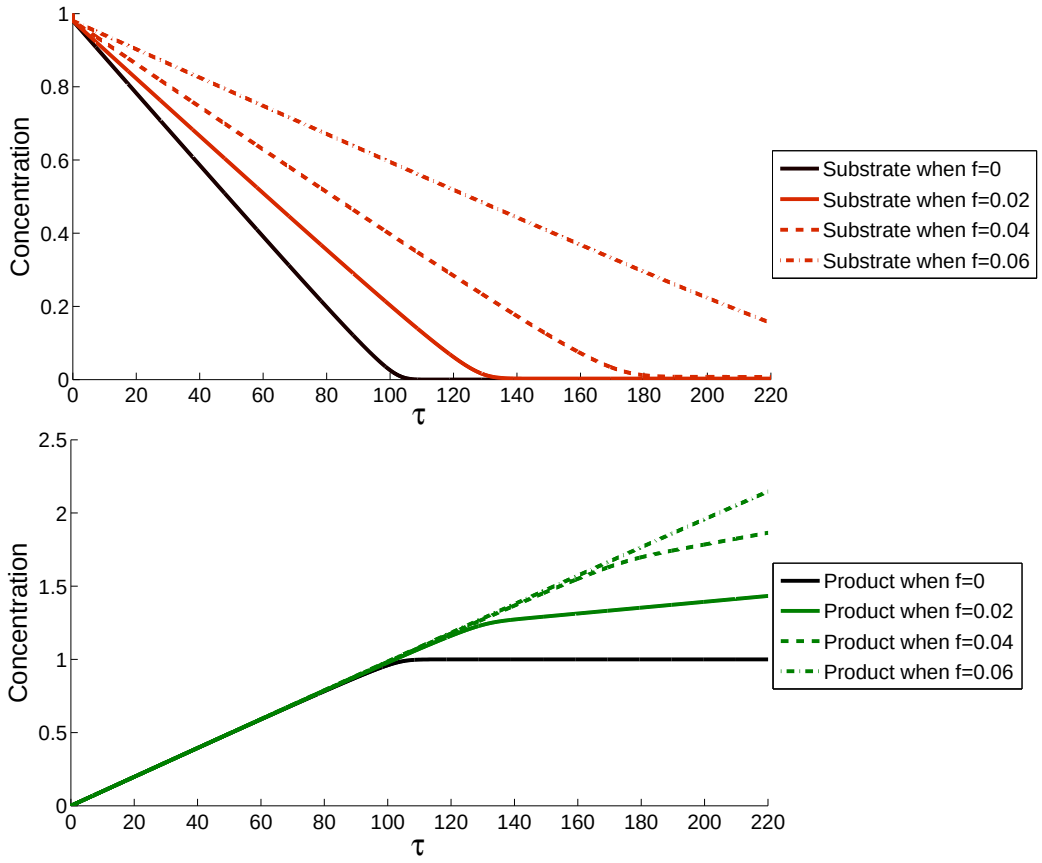

Figure 2.4: Substrate and product given by (2.3.6) found using Runge-Kutta, for various feed rates.

we can solve numerically via methods such as Runge-Kutta.

$$\begin{aligned}
\frac{dS}{dt} &= \frac{-V_{max_1}S}{K_{m_1}+S} \\
\frac{dP_1}{dt} &= \frac{V_{max_1}S}{K_{m_1}+S} - \frac{V_{max_2}P_1}{K_{m_2}+P_1} \\
\frac{dP_2}{dt} &= \frac{V_{max_2}P_1}{K_{m_2}+P_1} - \frac{V_{max_3}P_2}{K_{m_3}+P_2} \\
\frac{dP_3}{dt} &= \frac{V_{max_3}P_2}{K_{m_3}+P_2} - \frac{V_{max_4}P_3}{K_{m_4}+P_3} \\
\frac{dP_4}{dt} &= \frac{V_{max_4}P_3}{K_{m_4}+P_3};
\end{aligned} \tag{2.4.2}$$

The only unknowns in this model are the individual values of K_{m_i} and V_{max_i} for each reaction. It should be possible to find these experimentally. In Betlach and Tiedje's paper [6] values were chosen as in Figure 2.5, below.

There are obvious flaws with this model, not least, the assumption that each product consists of only one chemical. This means that everything you put in at the start of the experiment eventually becomes dinitrogen. We can see that this is not the case by deriving

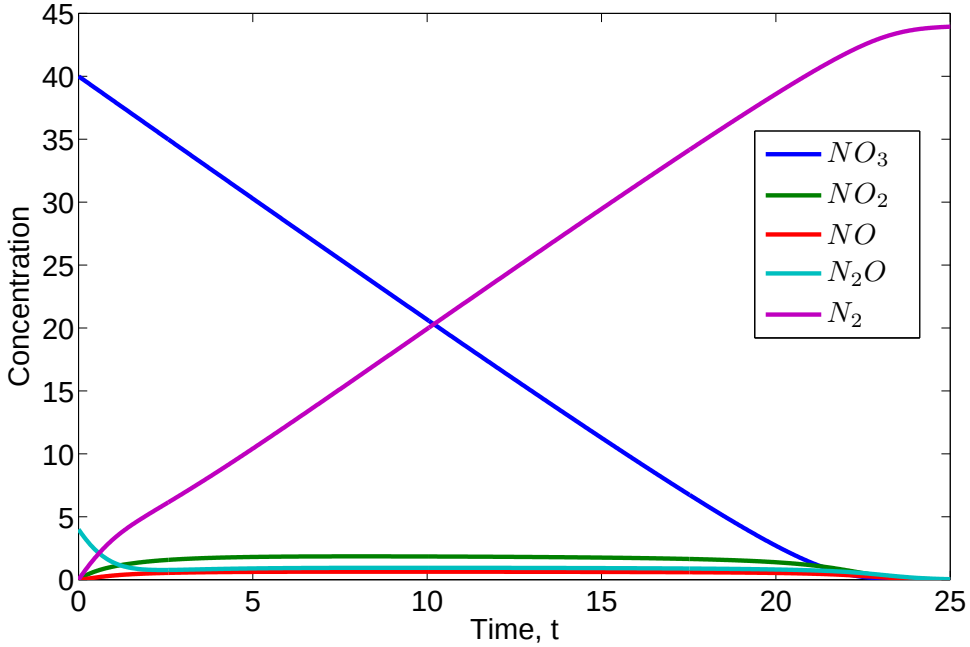

Figure 2.5: Numerical solution of (2.4.2) found using Runge-Kutta, with $K_{m_1} = 1$, $K_{m_2} = K_{m_3} = K_{m_4} = 2$ and $V_{max_1} = 2$, $V_{max_2} = 4$, $V_{max_3} = 8$, $V_{max_4} = 6$, as in [6]

the full reaction, using [39]. We arrive at,

$$\begin{aligned} \mathrm{NO_3^-} + 2\,\mathrm{H^+} + 2\,\mathrm{e^-} &\rightarrow \mathrm{NO_2^-} + \mathrm{H_2O} \\ \mathrm{NO_2^-} + 2\,\mathrm{H^+} + \mathrm{e^-} &\rightarrow \mathrm{NO} + \mathrm{H_2O} \\ 2\,\mathrm{NO} + 2\,\mathrm{H^+} + 2\,\mathrm{e^-} &\rightarrow \mathrm{N_2O} + \mathrm{H_2O} \\ \mathrm{N_2O} + 2\,\mathrm{H^+} + 2\,\mathrm{e^-} &\rightarrow \mathrm{N_2} + \mathrm{H_2O}. \end{aligned} \tag{2.4.3}$$

Considering the stoichiometry, it is clear that the reduction of two nitric oxide molecules only produces one molecule of nitrous oxide, which not only means we have half the amount of nitrous oxide produced, but also half the dinitrogen. This detail seems to have been missed by Betlach and Tiedje in their paper [6], but we shall include it in our following calculations.

2.5 Conservation Of Mass

Bearing in mind the model described above we attempt to create an improved version. We wish to construct a model that is biologically accurate whilst using the normal mathematical approximations. We shall once again use the principles of the law of mass action, but make sure to correctly consider the stoichiometry of our reactions. This means that a simple conservation of mass law will be created, whereby the conserved quantity is the amount of

nitrogen in the system. We inspect the whole denitrification chemical pathway,

$$\begin{aligned}
\mathrm{NO_3^-} + \mathrm{E_1} &\underset{k_{-1}}{\overset{k_1}{\rightleftarrows}} \mathrm{C_1} \overset{k_2}{\rightarrow} \mathrm{NO_2^-} + \mathrm{E_1} \\
\mathrm{NO_2^-} + \mathrm{E_2} &\underset{k_{-3}}{\overset{k_3}{\rightleftarrows}} \mathrm{C_2} \overset{k_4}{\rightarrow} \mathrm{NO} + \mathrm{E_2} \\
2\,\mathrm{NO} + \mathrm{E_3} &\underset{k_{-5}}{\overset{k_5}{\rightleftarrows}} \mathrm{C_3} \overset{k_6}{\rightarrow} \mathrm{N_2O} + \mathrm{E_3} \\
\mathrm{N_2O} + \mathrm{E_4} &\underset{k_{-7}}{\overset{k_7}{\rightleftarrows}} \mathrm{C_4} \overset{k_8}{\rightarrow} \mathrm{N_2} + \mathrm{E_4},
\end{aligned} \tag{2.5.1}$$

and use the definition (1.5.3) to define the rate of each reaction. We then apply the law of mass action to write out a set of differential equations, noting that $e_i + c_i = \text{const.} = e_i(0)$ still holds. We arrive at,

$$\begin{aligned}
\frac{dn_1}{dt} &= -k_1 n_1(e_1(0) - c_1) + k_{-1}c_1 \\
\frac{dn_2}{dt} &= -k_3 n_2(e_2(0) - c_2) + k_{-3}c_2 + k_2 c_1 \\
\frac{dn_3}{dt} &= -2k_5 n_3^2(e_3(0) - c_3) + 2k_{-5}c_3 + k_4 c_2 \\
\frac{dn_4}{dt} &= -k_7 n_4(e_4(0) - c_4) + k_{-7}c_4 + k_6 c_3 \\
\frac{dn_5}{dt} &= k_8 c_4 \\
\frac{dc_1}{dt} &= k_1 n_1(e_1(0) - c_1) - k_{-1}c_1 - k_2 c_1 \\
\frac{dc_2}{dt} &= k_3 n_2(e_2(0) - c_2) - k_{-3}c_2 - k_4 c_2 \\
\frac{dc_3}{dt} &= k_5 n_3^2(e_3(0) - c_3) - k_{-5}c_3 - k_6 c_3 \\
\frac{dc_4}{dt} &= k_7 n_4(e_4(0) - c_4) - k_{-7}c_4 - k_8 c_4,
\end{aligned} \tag{2.5.2}$$

where $n_1 = [\mathrm{NO_3}]$, $n_2 = [\mathrm{NO_2}]$ etc. and $c_i = [C_i]$. We can then see that the following conservation of mass law holds,

$$n_1 + n_2 + n_3 + 2n_4 + 2n_5 + c_1 + c_2 + 2c_3 + 2c_4 = \text{const.}. \tag{2.5.3}$$

This law holds when considering the total amount of nitrogen in the system, which we assume must remain constant. We bear in mind that each molecule of nitrate, nitrite and nitric oxide includes just one element of nitrogen whereas nitrous oxide and dinitrogen have two.

Using Runge-Kutta we can find a numerical solution of this model to show the change in the concentration of all five compounds, this is shown in Figure 2.6a, below. We note that in this example all the rate constants have been chosen as equal. As a result of this none of the intermediary products are present in large quantities, because they are reduced as quickly as they are created. In particular this means that there is almost no build up of

nitrous oxide. It would be possible to create a build up of any of the products by choosing the rate constant for that chemicals reduction to be lower than the one before it. In the next section we consider an alternative potential reasoning for build up of products in the pathway.

It should also be noted that as we have solved the full system (2.5.2) rather than simplifying using the quasi-steady state hypothesis the fast reaction rates during the inner time-scale will also be included in our solution.

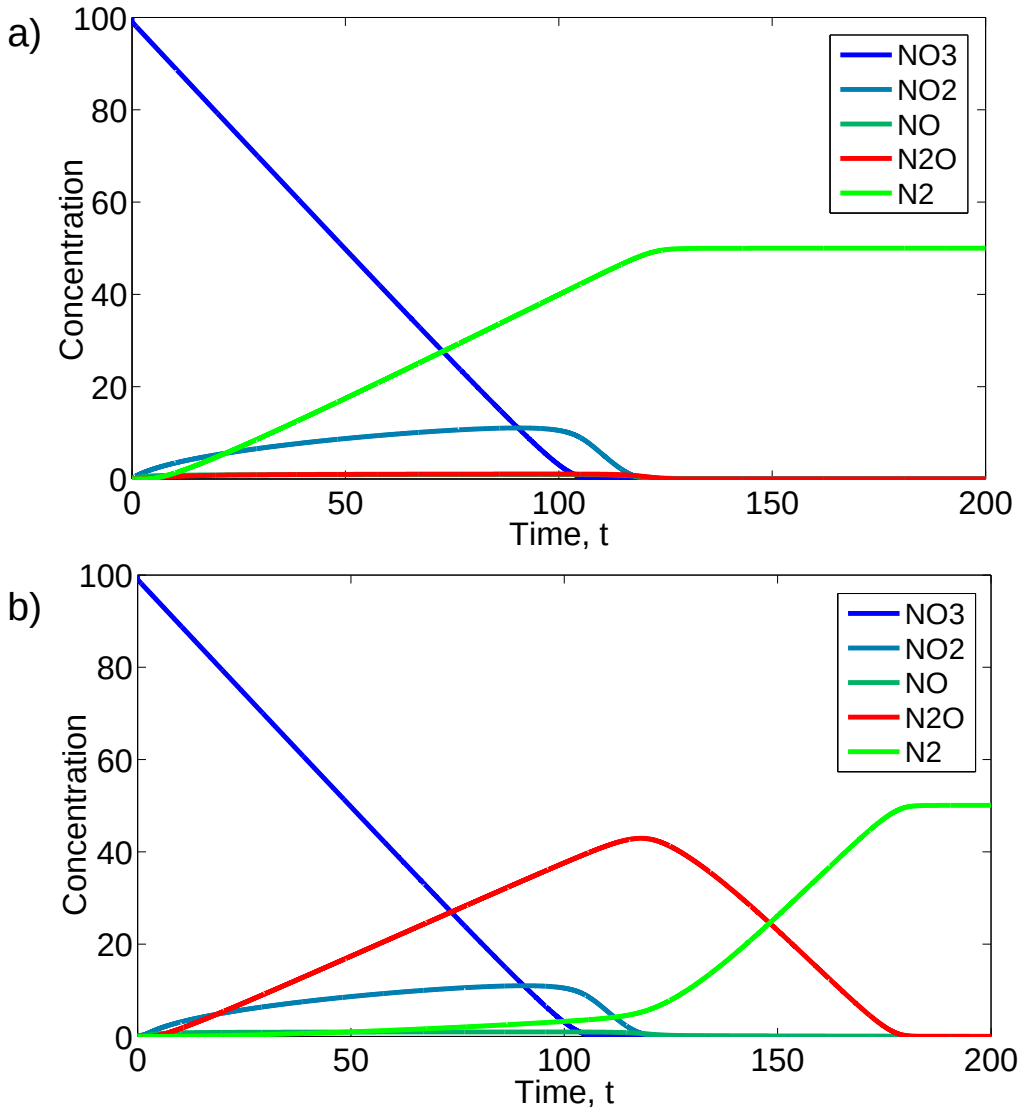

Figure 2.6: Solutions found using Runge-Kutta of:
a) (2.5.2) with $k_i = 1$ for $i = 1..8$ and $k_{-1} = k_{-3} = k_{-5} = k_{-7} = 0.1$
b) (2.6.2) with $k_i = 1$ for $i = 1..8$, $k_9 = 5$, and $k_{-1} = k_{-3} = k_{-5} = k_{-7} = k_{-9} = 0.1$

2.6 A Model With An Inhibitor

There are many examples in the literature of reports suggesting products in the denitrification pathway can behave as inhibitors to the reduction of others in the chain, such as [44],

[20] and [46]. In [44] Thomsen et al. discussed the use of the model by Betlach and Tiedje [6], described above. They found that this model could not be used to describe results seen in their experiments at acidic pH values as it did not include inhibitory effects. They used reaction rates determined using equations from [4] to model the denitrification pathway at acidic pH values, including the inhibitory effects, but this model again uses the steady-state hypothesis, and so is greatly simplified.

To briefly demonstrate how the inhibitory effects can affect our model we consider the possibility of inhibition of N_2O reduction by NO_2. This was investigated in [47], and linked to build up of free nitrous acid, which is dependent on nitrite concentration and pH. We can use a very simple model of inhibition as described in [8] to give,

$$\begin{aligned}
NO_3^- + E_1 &\underset{k_{-1}}{\overset{k_1}{\rightleftarrows}} C_1 \quad \overset{k_2}{\rightarrow} NO_2^- + E_1 \\
NO_2^- + E_2 &\underset{k_{-3}}{\overset{k_3}{\rightleftarrows}} C_2 \quad \overset{k_4}{\rightarrow} NO + E_2 \\
2\,NO + E_3 &\underset{k_{-5}}{\overset{k_5}{\rightleftarrows}} C_3 \quad \overset{k_6}{\rightarrow} N_2O + E_3 \\
N_2O + E_4 &\underset{k_{-7}}{\overset{k_7}{\rightleftarrows}} C_4 \quad \overset{k_8}{\rightarrow} N_2 + E_4 \\
NO_2 + E_4 &\underset{k_{-9}}{\overset{k_9}{\rightleftarrows}} C_5 \quad .
\end{aligned} \tag{2.6.1}$$

The addition of the extra reaction to (2.5.1), where nitrite reacts to form a new complex, C_5, creates the inhibitory effect. This is because the nitrite reacts with the same enzyme as the nitrous oxide meaning there is less enzyme available for the nitrous oxide reduction. Then, as the nitrous oxide reduction rate is proportional to the enzyme concentration, the rate is slowed. After adjusting the system (2.5.2), to include the new inhibitor, we have,

$$\begin{aligned}
\frac{dn_1}{dt} &= -k_1 n_1(e_1(0) - c_1) + k_{-1}c_1 \\
\frac{dn_2}{dt} &= -k_3 n_2(e_2(0) - c_2) + k_{-3}c_2 + k_2 c_1 - k_a n_2(e_4(0) - c_4 - c_5) + k_{-9}c_5 \\
\frac{dn_3}{dt} &= -2k_5 n_3^2(e_3(0) - c_3) + 2k_{-5}c_3 + k_4 c_2 \\
\frac{dn_4}{dt} &= -k_7 n_4(e_4(0) - c_4 - c_5) + k_{-7}c_4 + k_6 c_3 \\
\frac{dn_5}{dt} &= k_8 c_4 \\
\frac{dc_1}{dt} &= k_1 n_1(e_1(0) - c_1) - k_{-1}c_1 - k_2 c_1 \\
\frac{dc_2}{dt} &= k_3 n_2(e_2(0) - c_2) - k_{-3}c_2 - k_4 c_2 \\
\frac{dc_3}{dt} &= k_5 n_3^2(e_3(0) - c_3) - k_{-5}c_3 - k_6 c_3 \\
\frac{dc_4}{dt} &= k_7 n_4(e_4(0) - c_4 - c_5) - k_{-7}c_4 - k_8 c_4 \\
\frac{dc_5}{dt} &= k_9 n_2(e_4(0) - c_4 - c_5) - k_{-9}c_5.
\end{aligned} \tag{2.6.2}$$

With $k_9 > k_7$ the addition of this inhibitor greatly reduces the rate of the reduction of N_2O. Whilst the concentration of NO_2 is high the enzyme required for N_2O reduction is being used in the preferred reaction with NO_2. The rate of reduction of N_2O then increases only once the concentration of NO_2 has diminished, as shown in Figure 2.6b.

In Figures 2.6a and 2.6b , the difference in nitrous oxide concentrations is particularly important. Data collected by biologists working in labs here at UEA [18] has suggested build up similar to that shown in Figure 2.6b. Whilst the initial increase in the concentration of nitrous oxide is slow, later the build up is rapid, as shown in Figure (2.7). Therefore, our inhibitor model seems as though it could be particularly good at modelling the reaction pathway.

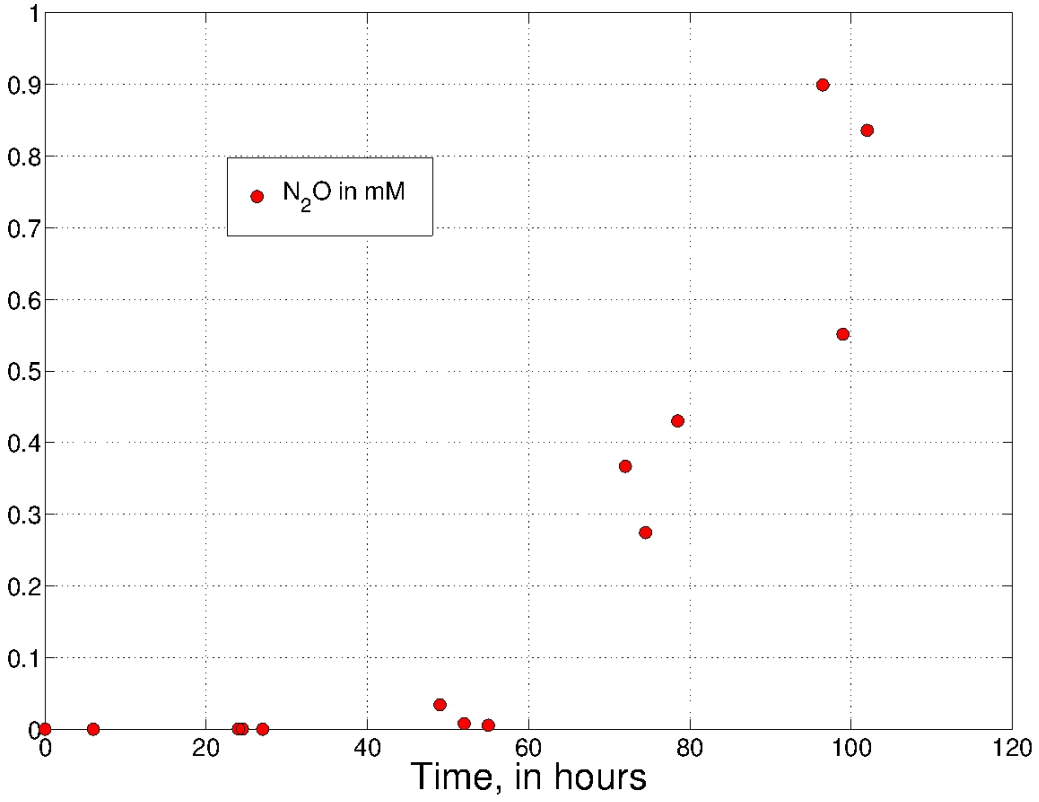

Figure 2.7: An example of experimental data collected at UEA [18].

2.7 Comparison With Experimental Results

In order to accurately compare the predicted reaction rates from our full model (2.5.2) to experimentally found results would require us to find the correct values for all fourteen of the rate constants. However, experimentally it is more common to find only the rate constants associated with a simplified Michaelis-Menten type model. In the paper by Woolfenden, Gates, Bocking, Blyth, Richardson and Moulton [45], the values of these parameters were found and reactions rates were calculated using a Michaelis-Menten version of a model very similar to those in this thesis. The model used in [45] included the factor of two related to the stoichiometry of the reactions that was first noticed in

this thesis and also feed and dilution rates to incorporate the flow from the chemostat, similar to the feed term discussion earlier in this chapter. It was found that the model was good at predicting reaction rates and levels of build up of the various chemicals in the denitrification pathway.

The modelling of the chemical reaction pathway mathematically allows for further insight into the experimental results as it highlights effects that may not have otherwise have been noticed, for example, the inhibitory effects as discussed previously. From our work earlier in this chapter considering the time-scales of the reactions we also know to apply our model after some initial time period, so that the reaction is allowed to settle to the slower behaviour of the outer time-scale. This has also been included in the experiments reported in [45] as a period of roughly 20 hours is left at the beginning of each experiment for anaerobic conditions to develop within the chemostats. We can then have more confidence in using the quasi-steady state approximation in order to predict reactions rates in the outer time-scale.

Chapter 3

One Dimensional Oxygen Distribution Models

We now begin working towards creating models of oxygen distribution in soil. These models shall aim to identify anaerobic micro-sites within the soil where denitrification can take place. These anaerobic micro-sites are created by bacteria depleting the oxygen levels in the soil as they absorb the oxygen for use in respiration. When the anaerobic conditions are met the bacteria switch to denitrification, which is when the chemical reactions discussed in the previous chapter take place and nitrous oxide is produced as a bi-product.

In this chapter we first consider some preliminary models of oxygen distribution which are all one-dimensional in order to keep the calculations simple. We shall show that by modelling using variations of Poisson's equation we can predict oxygen levels compared to depth, which then imply directly where in the soil bacteria have the potential to denitrify.

None of the models within this chapter have been non-dimensionalised. Each of the models are considered just briefly and as they each consist of only one basic partial differential equation it seems clearer to keep the original parameters.

3.1 Absorption-Diffusion Equation

There are several examples in the literature, such as [24], [25], [35], [37], where oxygen distribution in soil is modelled using the equation:

$$\frac{\partial \varphi}{\partial t} = D\frac{\partial^2 \varphi}{\partial x^2} - \lambda^2. \tag{3.1.1}$$

In this model oxygen concentration, given by φ, diffuses throughout the depth, x, of a one-dimensional domain of soil with constant diffusivity, D, and is absorbed throughout the soil at a constant rate λ^2. In [24], Kanwar uses the boundary conditions

$$\begin{aligned} \varphi(0,t) &= \mu \\ \varphi_x(\infty,t) &= 0. \end{aligned} \tag{3.1.2}$$

The first of these, where depth is zero, represents the boundary between the air and the soil. We approximate that the concentration of oxygen in the air is a constant, μ. The second boundary condition says that the flux of oxygen tends to zero as depth increases. This can be related to there being an impermeable layer of rock at large depth. Kanwar then finds solutions for two initial conditions,

$$\varphi(x,0) = \varphi_1 \tag{3.1.3}$$

$$\varphi(x,0) = \varphi_1 - ax \tag{3.1.4}$$

where $\varphi_1 < \mu$, and a is a constant. In this thesis we use neither of these initial conditions as they do not agree with the boundary condition at $x = 0$. At $t = 0$, we have $\varphi = \mu$ from the boundary condition and $\varphi = \varphi_1 < \mu$ from the initial condition. Therefore, it seems φ_t is singular at $t = 0$ since φ jumps from φ_1 to μ instantaneously. Also, for large enough depth (3.1.4) gives a negative oxygen concentration which is unrealistic. Therefore, we suggest using

$$\varphi(x,0) = \mu e^{-\kappa x}. \tag{3.1.5}$$

This initial condition matches with both boundary conditions (3.1.2) and remains positive over the whole domain. As in [24], we now solve (3.1.1), with (3.1.2) and (3.1.5) using the Laplace transform from [9],

$$\mathcal{L}(\varphi) = \bar{\varphi} = \int_0^\infty e^{-pt}\varphi(x,t)dt. \tag{3.1.6}$$

This Laplace transform has various important properties which make it useful for solving partial differential equations, as described in [9]. Using three of these properties we can write,

$$\mathcal{L}\left(\frac{\partial\varphi}{\partial t}\right) = p\bar{\varphi} - \varphi(x,0), \qquad \mathcal{L}\left(\frac{\partial^2\varphi}{\partial x^2}\right) = \frac{\partial^2\bar{\varphi}}{\partial x^2}, \qquad \mathcal{L}(\lambda^2) = \frac{\lambda^2}{p}. \tag{3.1.7}$$

Therefore the transformed version of (3.1.1) using (3.1.6) is,

$$p\bar{\varphi} - \mu e^{-\kappa x} = D\bar{\varphi}_{xx} - \frac{\lambda^2}{p}, \tag{3.1.8}$$

and the boundary conditions (3.1.2) become,

$$\begin{aligned} \bar{\varphi}(0,p) &= \frac{\mu}{p} \\ \bar{\varphi}_x(\infty,p) &= 0. \end{aligned} \tag{3.1.9}$$

This problem now only involves partial derivatives in the depth variable, x, and can therefore be solved using standard methods. It can be shown that,

$$\bar{\varphi} = \left[\frac{\mu}{p} + \frac{\lambda^2}{p^2} - \frac{\mu}{p - D\kappa^2}\right]e^{-\sqrt{\frac{p}{D}}x} + \frac{\mu}{p - D\kappa^2}e^{-\kappa x} - \frac{\lambda^2}{p^2}. \tag{3.1.10}$$

This expression for $\bar{\varphi}$ can then be transformed back to the original variables. All of the terms in (3.1.10) can be manipulated into forms that each can be found in Laplace transform tables, such as the one in [9]. Using these tables it is a simple matter to re-transform the solution. We find that,

$$\begin{aligned}\varphi(x,t) &= \mu\,\mathrm{erfc}\left(\frac{x}{2\sqrt{Dt}}\right) + \lambda^2\left(t+\frac{x^2}{2D}\right)\mathrm{erfc}\left(\frac{x}{2\sqrt{Dt}}\right)\\ &\quad -\frac{\mu}{2}e^{D\kappa^2 t}\left[e^{-\kappa x}\mathrm{erfc}\left(\frac{x}{2\sqrt{Dt}}-\sqrt{D\kappa^2 t}\right)+e^{\kappa x}\mathrm{erfc}\left(\frac{x}{2\sqrt{Dt}}+\sqrt{D\kappa^2 t}\right)\right]\\ &\quad -\lambda^2 x\left(\frac{t}{\pi D}\right)^{\frac{1}{2}}e^{-x^2/4Dt}-\lambda^2 t+\mu e^{-\kappa x}e^{tD\kappa^2}. \end{aligned} \tag{3.1.11}$$

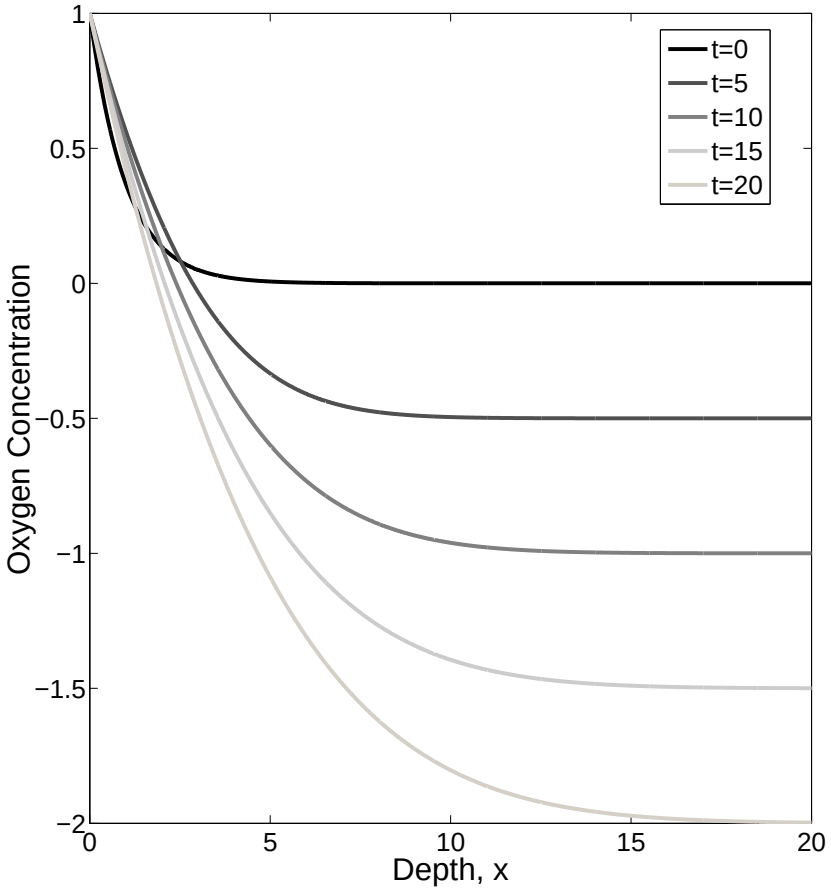

Figure 3.1: Concentration of oxygen given by (3.1.11) for various t. $\lambda^2 = 0.1, D = 1, \kappa = 0.5$

Upon inspection of the solution (3.1.11) it seems that this is a bad model, as for large enough x and/or t oxygen concentration will be negative, which is unrealistic. A plot of the solution for some example parameters, as shown in Figure 3.1, highlights this problem. To create a model which does not have this property we must change the original equation (3.1.1).

Alternatively, the results from this model could be interpreted as a way to approximate a critical depth below which all the soil is considered anaerobic. In the anaerobic depths the bacteria within the soil would denitrify instead of respire. We can define these anaerobic

conditions mathematically as being when the oxygen concentration in the soil is below some threshold value, call it T, where $T < \mu$. Therefore, in this model we could say that for all depths where $\varphi(x) < T$ denitrification will take place. This will be considered in more detail in our later chapters when we extend our models to properly consider the possibility of anaerobic areas in the soil.

3.2 Proportional Absorption

In order to avoid negative oxygen concentrations we now consider a modified version of (3.1.1) given by,

$$\frac{\partial \varphi}{\partial t} = D\frac{\partial^2 \varphi}{\partial x^2} - \lambda^2 \varphi. \tag{3.2.1}$$

We keep the same initial and boundary conditions as above, as we believe them to be acceptable biologically,

$$\begin{aligned} \varphi(0,t) &= \mu \\ \varphi_x(\infty,t) &= 0 \\ \varphi(x,0) &= \mu e^{-\kappa x}. \end{aligned} \tag{3.2.2}$$

In (3.2.1) the absorption term is proportional to the local oxygen concentration (rather than constant, as in (3.1.1)) and so the oxygen concentration cannot become negative, which we consider to be more realistic. Although oxygen absorption due to bacterial respiration is usually considered to be constant in the literature, modelling it as proportional to local oxygen concentration appears similar to the way we calculated reactions rates earlier in the thesis. In [37] there is mention of modelling the respiration using Michaelis-Menten techniques, but a solution to the problem is not found.

In order to solve (3.2.1) we once again apply the Laplace transform (3.1.6), the transformed version of (3.2.1) is,

$$(p + \lambda^2)\bar{\varphi} - D\bar{\varphi}_{xx} = \mu e^{-\kappa x}. \tag{3.2.3}$$

This can be solved for $\bar{\varphi}$ using the normal methods for second order differential equations of one variable. After applying the transformed boundary conditions we find that the transformed variable can be written as,

$$\bar{\varphi}(x,p) = \frac{(D\kappa^2 - \lambda^2)\mu}{p(D\kappa^2 - \lambda^2 - p)} e^{-\sqrt{\frac{p+\lambda^2}{D}}x} - \frac{\mu e^{-\kappa x}}{D\kappa^2 - \lambda^2 - p}. \tag{3.2.4}$$

The second term in (3.2.4) can be transformed back easily and can be found in many Laplace transform tables such as those found in [9]. The first term is more complicated, and does not appear in the tables. In order to compute the inverse transform we consider the Bromwich integral,

$$\varphi = \frac{1}{2\pi i} \lim_{R\to\infty} \int_{\gamma - iR}^{\gamma + iR} e^{pt}\bar{\varphi} dp \tag{3.2.5}$$

where γ must be chosen to be a constant large enough that all the poles of the integrand in (3.2.5) lie to the left of the line of integration. For our problem we need to find the value of,

$$\frac{(D\kappa^2 - \lambda^2)\mu}{2\pi i} \lim_{R\to\infty} \int_{\gamma-iR}^{\gamma+iR} \frac{e^{pt} e^{-\sqrt{\frac{p+\lambda^2}{D}}x}}{p(D\kappa^2 - \lambda^2 - p)} dp. \tag{3.2.6}$$

In order to evaluate this integral we first integrate around a semi-circular contour with a branch cut, we call it Γ, as shown in Figure 3.2. This contour has been chosen so that the poles of (3.2.6) lie within it whilst also cutting out the branch along the real axis up to the branch point at $p = -\lambda^2$. We take the radius of C_ϵ to be ϵ, which we wish to tend to zero as R tends to infinity. As Γ is a closed curve we can evaluate using Cauchy's residue theorem and then subtract the integrals around the parts of Γ that we do not require for (3.2.6).

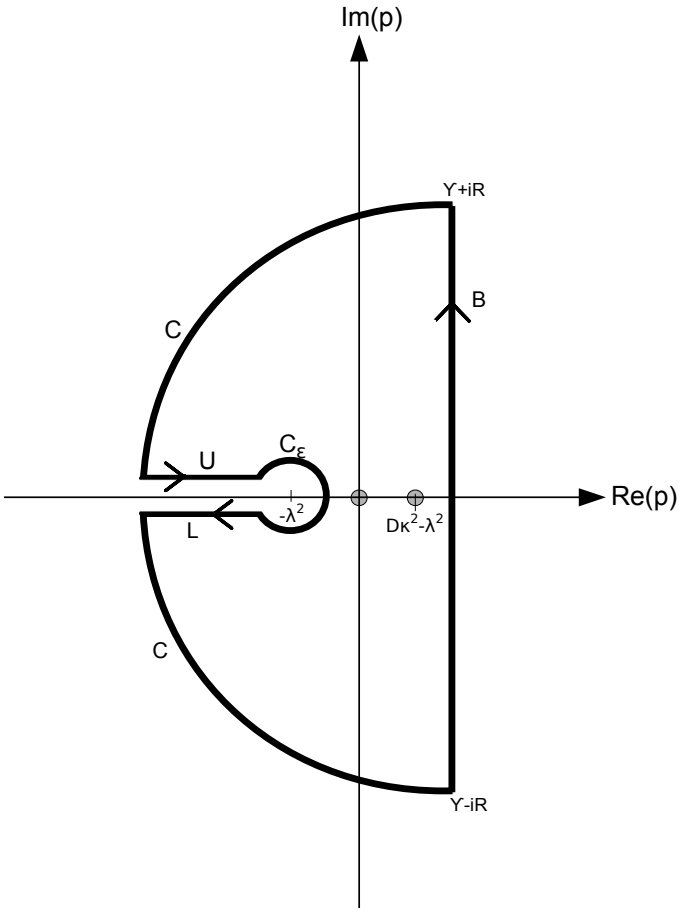

Figure 3.2: Contour used to integrate (3.2.6), $\Gamma = B + C + U + C_\epsilon + L$

Assuming that $D\kappa^2 \neq \lambda^2$, there are simple poles in (3.2.6) at $p = 0$, with residue $\mu e^{-\sqrt{\frac{\lambda^2}{D}}x}$, and $p = D\kappa^2 - \lambda^2$, with residue $-\mu e^{(D\kappa^2-\lambda^2)t-\kappa x}$. By Cauchy's residue theorem,

$$\frac{(D\kappa^2 - \lambda^2)\mu}{2\pi i} \int_\Gamma \frac{e^{pt} e^{-\sqrt{\frac{p+\lambda^2}{D}}x}}{p(D\kappa^2 - \lambda^2 - p)} dp = \mu\left(e^{-\sqrt{\frac{\lambda^2}{D}}x} - e^{(D\kappa^2-\lambda^2)t-\kappa x}\right) \tag{3.2.7}$$

The contribution from the curved section of the contour, C, is zero in the limit $R \to \infty$, and the contribution from the other curved section, C_ϵ, is zero in the limit $\epsilon \to 0$. On U, $p = re^{i\pi}$, whilst on L, $p = re^{-i\pi}$, for $\lambda^2 \leq r \leq \infty$. The sum of the integrals over U and L can then be rearranged to,

$$\frac{(D\kappa^2 - \lambda^2)\mu}{\pi} \int_{\lambda^2}^{\infty} \frac{e^{-rt} \sin\left(\sqrt{\frac{r-\lambda^2}{D}}x\right)}{r(-r - D\kappa^2 + \lambda^2)} dr, \tag{3.2.8}$$

which we will compute numerically. We can now re-transform (3.2.4) by using (3.2.7) and (3.2.8), we find that,

$$\varphi(x,t) = \mu e^{-\sqrt{\frac{\lambda^2}{D}}x} - \frac{(D\kappa^2 - \lambda^2)\mu}{\pi} \int_{\lambda^2}^{\infty} \frac{e^{-rt} \sin\left(\sqrt{\frac{r-\lambda^2}{D}}x\right)}{r(r + D\kappa^2 - \lambda^2)} dr. \tag{3.2.9}$$

We can now evaluate (3.2.9) using the trapezium rule. A comparison with a finite-difference solution of (3.2.1) is shown in Figure 3.3. The finite difference solution was found by rewriting (3.2.1) as

$$\frac{\varphi_{i,k+1} - \varphi_{i,k}}{\Delta t} = D\frac{\varphi_{i+1,k} - 2\varphi_{i,k} + \varphi_{i-1,k}}{(\Delta x)^2} - \lambda^2 \varphi_{i,k} \tag{3.2.10}$$

where $\varphi_{i,k} = \varphi(x_i, t_k)$, $x_i = (i-1)\Delta x$ and $t_k = (k-1)\Delta t$. This can then be solved with the appropriate forms of the initial and boundary conditions. Generally the finite difference solution matches well with the Laplace transform solution (3.2.9). For larger values of t the integrand in (3.2.9) tends to zero, and we approach the steady state,

$$\varphi(x) = \mu e^{-\sqrt{\frac{\lambda^2}{D}}x}. \tag{3.2.11}$$

For small values of t, the integrand in (3.2.9) gives a more significant contribution and as we are approximating the bounds to be finite in our computation of the trapezium method, it is expected that (3.2.9) will give a less accurate solution.

This model appears to be suitable for modelling soil when it is assumed respiration throughout remains proportional to local oxygen concentration. However, in the literature, it is generally assumed that oxygen absorption due to respiration is constant until the level of oxygen decreases to some critical level when denitrification switches on. Also it is known that within a soil there are areas of higher bacterial activity where much higher levels of respiration occur, such as around decomposing leaves, and the soil respiration levels should generally not be modelled as uniform throughout. We therefore move on to thinking about a soil where only a finite area or volume is absorbing oxygen.

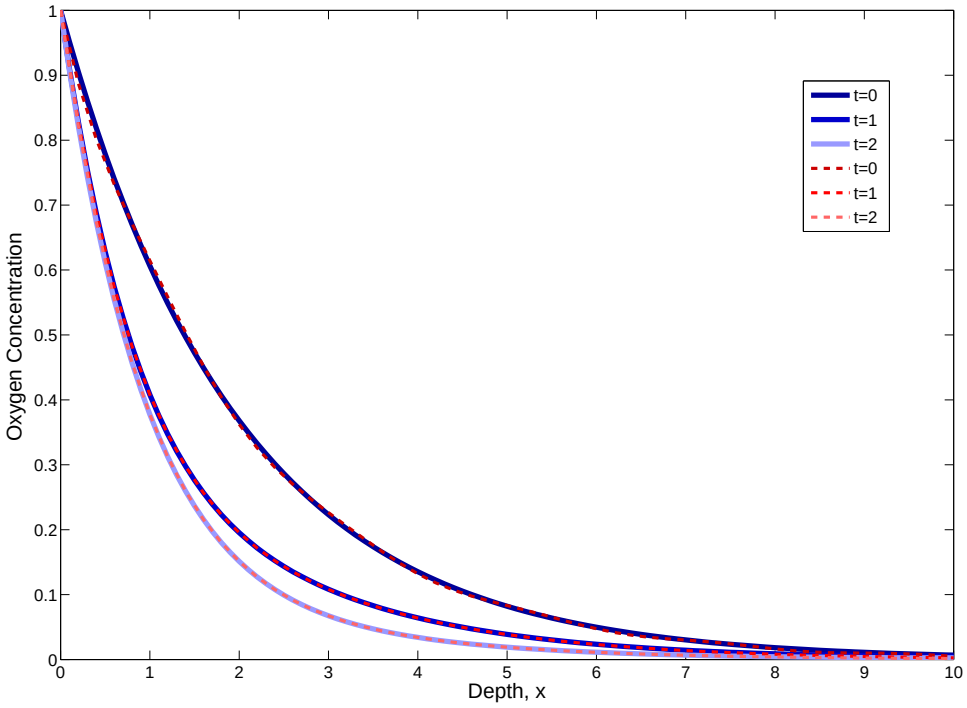

Figure 3.3: Oxygen concentration modelled by (3.2.1) solved using a finite difference method (in blue) and a Laplace transform method (in red). Using parameters: $\mu = 1, D = 1, \lambda^2 = 1, \kappa = 0.5$

3.3 Time Dependent Point Sink Model

We now modify (3.1.1), to include only a single point of oxygen absorption at $x = x_a$. This could represent a single soil bacterium respiring at some depth below ground surrounded by other soil that is not absorbing oxygen. We write,

$$\varphi_t = D\varphi_{xx} - \lambda^2 \delta(x - x_a) \tag{3.3.1}$$

where δ is the standard Dirac delta function, with the conditions,

$$\begin{aligned} \varphi(x, 0) &= \mu e^{-\kappa x} \\ \varphi(0, t) &= \mu \\ \varphi_x(\infty, t) &= 0. \end{aligned} \tag{3.3.2}$$

We once again solve for φ using the Laplace transform (3.1.6). The transformed version of (3.3.1) is,

$$p\bar{\varphi} - \mu e^{-\kappa x} = D\bar{\varphi}_{xx} - \frac{\lambda^2}{p}\delta(x - x_a) \tag{3.3.3}$$

and the boundary conditions become,

$$\begin{aligned} \bar{\varphi}(0, t) &= \frac{\mu}{p} \\ \bar{\varphi}_x(\infty, t) &= 0. \end{aligned} \tag{3.3.4}$$

We now split the problem into two parts, for $x < x_a$ and $x > x_a$, to remove the delta function from (3.3.3). This allows us to write,

$$D\bar{\varphi}_{xx} - p\bar{\varphi} = \mu e^{-\kappa x}, \quad x \neq x_a, \tag{3.3.5}$$

to which the general solution is

$$\bar{\varphi} = Ae^{\sqrt{\frac{p}{D}}x} + Be^{-\sqrt{\frac{p}{D}}x} - \left(\frac{\mu}{\kappa^2 D - p}\right)e^{-\kappa x}. \tag{3.3.6}$$

In (3.3.6) A and B are different constants for each of the two parts. To find the values of A and B we enforce the relevant boundary condition from (3.3.4) for each part, along with the condition that at $x = x_a$,

$$\bar{\varphi}(x_a^+) = \bar{\varphi}(x_a^-), \tag{3.3.7}$$

for continuity, and a kink condition

$$D\left[\bar{\varphi}_x(x_a^+) - \bar{\varphi}_x(x_a^-)\right] = \frac{\lambda^2}{p}. \tag{3.3.8}$$

This kink condition has been derived by integrating (3.3.3), between $x_a - dx$ and $x_a + dx$, in the limit as $dx \to 0$. We find that for $x < x_a$,

$$\bar{\varphi} = \left(\frac{\mu\kappa^2 D}{p(\kappa^2 D - p)} + \frac{\lambda^2}{p^{\frac{3}{2}}D^{\frac{1}{2}}}e^{-\sqrt{\frac{p}{D}}x_a}\right)e^{-\sqrt{\frac{p}{D}}x} - \frac{\lambda^2}{2p^{\frac{3}{2}}D^{\frac{1}{2}}}e^{\sqrt{\frac{p}{D}}(x-x_a)} - \left(\frac{\mu}{\kappa^2 D - p}\right)e^{\kappa x}, \tag{3.3.9}$$

and for $x > x_a$,

$$\bar{\varphi} = \left(\frac{\mu\kappa^2 D}{p(\kappa^2 D - p)} - \frac{\lambda^2}{p^{\frac{3}{2}}D^{\frac{1}{2}}}\sinh\sqrt{\frac{p}{D}}x_a\right)e^{-\sqrt{\frac{p}{D}}x} - \left(\frac{\mu}{\kappa^2 D - p}\right)e^{-\kappa x}. \tag{3.3.10}$$

All of the terms in (3.3.9) and (3.3.10) have a known inverse transform, which can be found in a table such as in [9] and so we can write for $x < x_a$,

$$\begin{aligned}\varphi(x,t) \quad = \quad & \frac{-\lambda^2 x}{D} + \frac{\lambda^2(x - x_a)}{2D}\mathrm{erf}\left(\frac{-x + x_a}{2\sqrt{Dt}}\right) + \frac{\lambda^2(x + x_a)}{2D}\mathrm{erf}\left(\frac{x + x_a}{2\sqrt{Dt}}\right) \\ & + \frac{\lambda^2 t^{\frac{1}{2}}}{(D\pi)^{\frac{1}{2}}}\left(e^{-\frac{(x+x_a)^2}{4Dt}} - e^{-\frac{(x-x_a)^2}{4Dt}}\right) + \mu e^{-\kappa x + \kappa^2 Dt} + \mu\mathrm{erfc}\left(\frac{x}{2\sqrt{Dt}}\right) \\ & - \frac{\mu e^{\kappa^2 Dt}}{2}\left(e^{-\kappa x}\mathrm{erfc}\left(\frac{x}{2\sqrt{Dt}} - \kappa\sqrt{Dt}\right) + e^{\kappa x}\mathrm{erfc}\left(\frac{x}{2\sqrt{Dt}} + \kappa\sqrt{Dt}\right)\right).\end{aligned} \tag{3.3.11}$$

And for $x > x_a$,

$$\begin{aligned}\varphi(x,t) &= \frac{-\lambda^2 x_a}{D} - \frac{\lambda^2(x-x_a)}{2D}\mathrm{erf}\left(\frac{x-x_a}{2\sqrt{Dt}}\right) + \frac{\lambda^2(x+x_a)}{2D}\mathrm{erf}\left(\frac{x+x_a}{2\sqrt{Dt}}\right) \\ &+ \frac{\lambda^2 t^{\frac{1}{2}}}{(D\pi)^{\frac{1}{2}}}\left(e^{-\frac{(x+x_a)^2}{4Dt}} - e^{-\frac{(x-x_a)^2}{4Dt}}\right) + \mu e^{-\kappa x+\kappa^2 Dt} + \mu\mathrm{erfc}\left(\frac{x}{2\sqrt{Dt}}\right) \\ &- \frac{\mu e^{\kappa^2 Dt}}{2}\left(e^{-\kappa x}\mathrm{erfc}\left(\frac{x}{2\sqrt{Dt}} - \kappa\sqrt{Dt}\right) + e^{\kappa x}\mathrm{erfc}\left(\frac{x}{2\sqrt{Dt}} + \kappa\sqrt{Dt}\right)\right). \quad (3.3.12)\end{aligned}$$

By taking the limit $t \to \infty$ in either (3.3.11) or (3.3.12), it is clear that for the concentration of oxygen to remain positive absorption must be less than a constant given by,

$$\lambda^2 < \frac{\mu D}{x_a}. \quad (3.3.13)$$

This is an interesting feature of the model as it could be used as a way of relating these parameters to denitrification levels. This inequality implies that if oxygen absorption from the bacterium is large, then the bacterium must be close to the surface and/or the diffusivity within the soil around it must be high, in order to prevent a shortage of oxygen and denitrification starting. This can also be seen from inspection of the steady state, which can be found by setting $\frac{\partial\varphi}{\partial t} = 0$ in (3.3.1),

$$\begin{aligned}\varphi &= \mu - \frac{\lambda^2 x}{D} \qquad \text{for} \quad 0 \le x < x_a \\ \varphi &= \mu - \frac{\lambda^2 x_a}{D} \qquad \text{for} \quad x_a < x. \quad (3.3.14)\end{aligned}$$

3.4 Proportional Absorption At A Point

We now consider proportional oxygen absorption at a single point in our domain. This can be thought of as an individual bacterium respiring within an area of soil with no microbial activity, where the rate of respiration is dependent on the concentration of oxygen around the bacterium. As we saw earlier, this will stop our model from predicting negative oxygen concentrations. We add a delta function to (3.2.1), so that

$$\frac{\partial\varphi}{\partial t} = D\frac{\partial^2\varphi}{\partial x^2} - \lambda^2\delta(x-x_a)\varphi, \quad (3.4.1)$$

with the same conditions as above,

$$\begin{aligned}\varphi(0,t) &= \mu \\ \varphi_x(\infty,t) &= 0 \\ \varphi(x,0) &= \mu e^{-\kappa x}. \quad (3.4.2)\end{aligned}$$

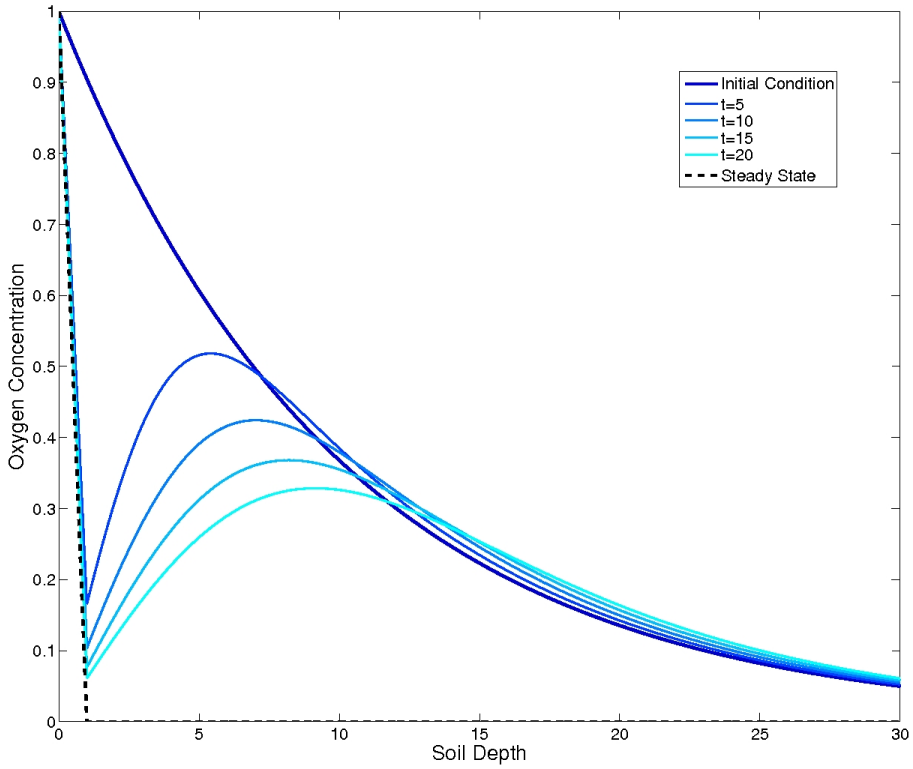

Figure 3.4: Concentration of oxygen with a point of constant absorption, given by (3.3.11) and (3.3.12), with conditions (3.3.2). $x_a = 1$, $\lambda^2 = 1$, $D = 1$, $\kappa = 0.1$

The working involved with solving this problem is very similar to that used in the previous section, using the same Laplace transform. We once again split the problem into $0 \leq x < x_a$ and $x > x_a$, with the same continuity condition and a kink condition, which is now,

$$D\left[\bar{\varphi}_x(x_a^+) - \bar{\varphi}_x(x_a^-)\right] = \lambda^2 \bar{\varphi}(x_a). \tag{3.4.3}$$

After solving we find that, for $0 \leq x < x_a$,

$$\begin{aligned}\bar{\varphi} \quad = \quad & \left[\frac{\frac{\mu\lambda^2 e^{-\kappa x_a}}{D(\kappa^2 D - p)} - \left(\frac{\lambda^2}{D} + 2\sqrt{\frac{p}{D}}\right)\frac{\mu\kappa^2 D}{p(\kappa^2 D - p)} e^{\sqrt{\frac{p}{D}}x_a}}{\left(\frac{\lambda^2}{D} + 2\sqrt{\frac{p}{D}}\right)e^{\sqrt{\frac{p}{D}}x_a} - \frac{\lambda^2}{D}e^{-\sqrt{\frac{p}{D}}x_a}} + \frac{\kappa^2 D\mu}{p(\kappa^2 D - p)}\right] e^{\sqrt{\frac{p}{D}}x} \\ & - \left[\frac{\frac{\mu\lambda^2 e^{-\kappa x_a}}{D(\kappa^2 D - p)} - \left(\frac{\lambda^2}{D} + 2\sqrt{\frac{p}{D}}\right)\frac{\mu\kappa^2 D}{p(\kappa^2 D - p)} e^{\sqrt{\frac{p}{D}}x_a}}{\left(\frac{\lambda^2}{D} + 2\sqrt{\frac{p}{D}}\right)e^{\sqrt{\frac{p}{D}}x_a} - \frac{\lambda^2}{D}e^{-\sqrt{\frac{p}{D}}x_a}}\right] e^{-\sqrt{\frac{p}{D}}x} - \frac{\mu e^{-\kappa x}}{\kappa^2 D - p},\end{aligned} \tag{3.4.4}$$

and for $x > x_a$,

$$\begin{aligned}\bar{\varphi} &= \left[\frac{\frac{\mu\lambda^2 e^{-\kappa x_a}}{D(\kappa^2 D-p)} - \left(\frac{\lambda^2}{D}+2\sqrt{\frac{p}{D}}\right)\frac{\mu\kappa^2 D}{p(\kappa^2 D-p)}e^{\sqrt{\frac{p}{D}}x_a}}{\left(\frac{\lambda^2}{D}+2\sqrt{\frac{p}{D}}\right)e^{\sqrt{\frac{p}{D}}x_a} - \frac{\lambda^2}{D}e^{-\sqrt{\frac{p}{D}}x_a}} + \frac{\kappa^2 D\mu}{p(\kappa^2 D-p)}\right]e^{\sqrt{\frac{p}{D}}(2x_a-x)} \\ &\quad - \left[\frac{\frac{\mu\lambda^2 e^{-\kappa x_a}}{D(\kappa^2 D-p)} - \left(\frac{\lambda^2}{D}+2\sqrt{\frac{p}{D}}\right)\frac{\mu\kappa^2 D}{p(\kappa^2 D-p)}e^{\sqrt{\frac{p}{D}}x_a}}{\left(\frac{\lambda^2}{D}+2\sqrt{\frac{p}{D}}\right)e^{\sqrt{\frac{p}{D}}x_a} - \frac{\lambda^2}{D}e^{-\sqrt{\frac{p}{D}}x_a}}\right]e^{-\sqrt{\frac{p}{D}}x} - \frac{\mu e^{-\kappa x}}{\kappa^2 D-p}. \qquad (3.4.5)\end{aligned}$$

Rather than attempt to find the inversion of this Laplace transform analytically we use the substitution $p = \gamma + ir$ in the inversion formula so that,

$$\varphi(x,t) = \frac{1}{2\pi}\int_{-\infty}^{\infty} e^{(\gamma+ir)t}\bar{\varphi}(r,x)dr, \qquad (3.4.6)$$

from which a solution can be computed numerically via the trapezium rule.

We can also solve (3.4.1) directly using a finite difference equation. We will use the Crank-Nicholson method and compute solutions using the Thomas Algorithm. Unfortunately, in order to use this method we must enforce our lower boundary condition at a finite position, $x = x_{max}$, instead of at infinity, however we can set x_{max} as large as is needed so that the effect on the area around the respiring bacteria is minimal. We once again split the problem into two sections where for $0 \le x < x_a$, $\varphi^k_{1,i}$ denotes the value of $\varphi(x,t)$ at time-step k ($k = 0, 1, 2..$ and $t = k\Delta t$), with position, $i = 1, 2, ..., N$ where $N = \frac{x_a}{\Delta x}$ and Δx is the gap between points. So for $0 \le x < x_a$, (3.4.1) becomes,

$$\varphi^{k+1}_{1,i} = \frac{D\Delta t}{2(\Delta x)^2}\left(\varphi^{k+1}_{1,i+1} - 2\varphi^{k+1}_{1,i} + \varphi^{k+1}_{1,i-1} + \varphi^{k}_{1,i+1} - 2\varphi^{k}_{1,i} + \varphi^{k}_{1,i-1}\right) + \varphi^{k}_{1,i} + O((\Delta x)^2). \quad (3.4.7)$$

Similarly for $x_a < x < x_{max}$, where $j = 1, 2, ...M$ and $M = \frac{x_{max}-x_a}{h}$ we write,

$$\varphi^{k+1}_{2,j} = \frac{D\Delta t}{2(\Delta x)^2}\left(\varphi^{k+1}_{2,j+1} - 2\varphi^{k+1}_{2,j} + \varphi^{k+1}_{2,j-1} + \varphi^{k}_{2,j+1} - 2\varphi^{k}_{2,j} + \varphi^{k}_{2,j-1}\right) + \varphi^{k}_{2,j} + O((\Delta x)^2). \quad (3.4.8)$$

Our boundary conditions can now be written as $\varphi^k_{1,1} = \mu$, for the air/soil boundary and $\varphi^k_{2,M+1} = \varphi^k_{2,M-1}$ derived from the no-flux condition at $x = x_{max}$. Our initial condition remains as $\varphi^k_{1,i} = \mu e^{-\kappa x_i}$ and $\varphi^k_{2,j} = \mu e^{-\kappa x_j}$. We must also apply the continuity condition,

$$\varphi^k_{1,N} = \varphi^k_{2,1}, \qquad (3.4.9)$$

and the kink condition, which must be rewritten using appropriate forward and backward difference equations, as in [23], so that

$$\left(\frac{2\Delta x\lambda^2}{D}+6\right)\varphi^k_{1,N} = 4\varphi^k_{2,2} - \varphi^k_{2,3} - \varphi^k_{1,N-2} + 4\varphi^k_{1,N-1}. \qquad (3.4.10)$$

Due to the unknown value at the kink, and the no-flux boundary condition, we must also apply a Newton iteration method. We start by guessing the value of $\varphi^k_{1,N}$ at the current

time-step, evaluate φ over the whole domain and then use the kink condition to improve our guessed value for $\varphi^k_{1,N}$.

When solutions of (3.4.1) are computed using the two methods above, it is found that there is good agreement for small values of t. For larger values of t (roughly $t > 5$), the two methods give less good agreement. This is due to the exponential term in (3.4.6). In order to find solutions via the trapezium rule it was necessary to use finite limits, and for the increased values of t, much larger values of these limits must be used to find an accurate solution.

Observing solutions for large values of t (which can be found via the finite difference method) the oxygen concentration appears to approach a steady state, as shown in Figure 3.5. The steady state solution can be found by setting,

$$\frac{\partial \varphi}{\partial t} = 0, \tag{3.4.11}$$

in (3.4.1), solving and then applying the boundary conditions (3.4.2). We find that at steady state,

$$\begin{aligned} \varphi &= \mu - \frac{\lambda^2 \mu x}{D + \lambda^2 x_a} \quad \text{for} \quad 0 \le x < x_a \\ \varphi &= \frac{\mu D}{D + \lambda^2 x_a} \quad \text{for} \quad x_a < x \end{aligned} \tag{3.4.12}$$

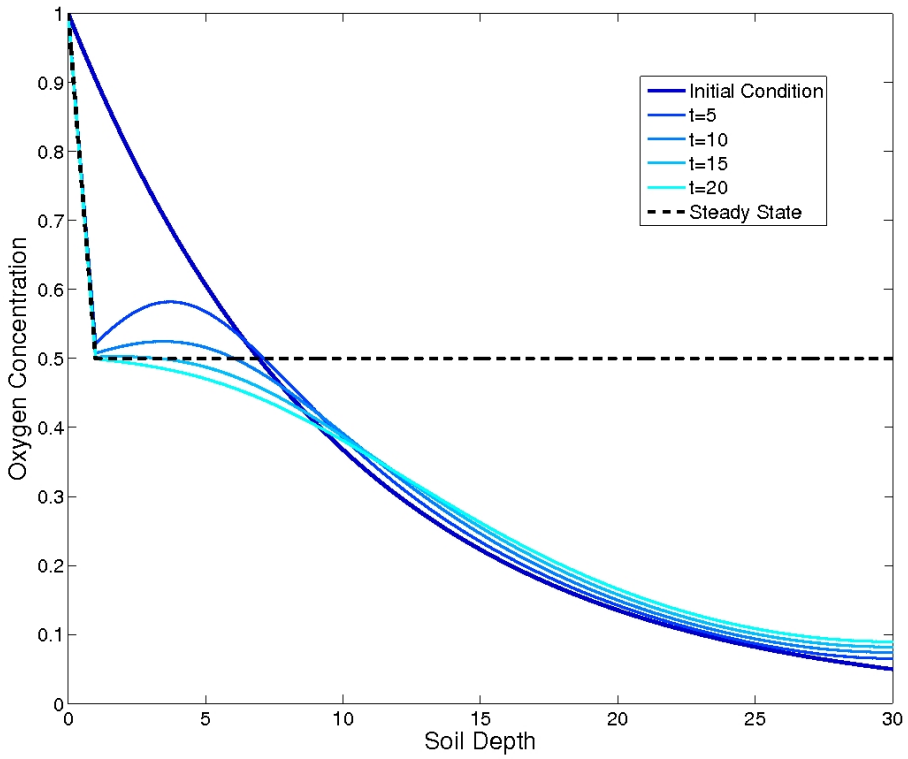

Figure 3.5: Concentration of oxygen with a point of proportional absorption, given by (3.4.1), with conditions (3.4.2). $x_a = 1$, $\lambda^2 = 1$, $D = 1$, $\kappa = 0.1$. Found by the Finite Difference Method

The models described in the previous two sections, given by (3.3.1) and (3.4.1) show

oxygen distribution as you would expect for a domain with a single point sink. Oxygen concentration decreases from the constant value in the air and reaches its minimum at the point of absorption. The constant oxygen absorption model is more closely related to what is described in the literature, but it can predict negative oxygen concentrations which is unrealistic. Therefore, we must adapt these models to include switching between respiration and denitrification when the oxygen level decreases to some critical value.

3.5 Point Absorption With A Switch

We now consider that an individual bacterium within the soil can switch-on or switch-off absorption of oxygen based on the concentration of oxygen around it. When the oxygen concentration drops below a particular value, $\hat{\varphi}$, the bacterium will stop respiring and start denitrifying. The model below of bacteria that constantly absorb oxygen during respiration until anaerobic conditions are reached is our most biologically realistic so far.

We use an approximation to the Heaviside step function as the mathematical switch,

$$H(\varphi - \hat{\varphi}) \approx \frac{1 + \tanh(s(\varphi - \hat{\varphi}))}{2}, \tag{3.5.1}$$

where s is a constant chosen to be large. The larger the value of s the more the function resembles the Heaviside step function as for increasing s, it tends towards an instantaneous jump at $\varphi = \hat{\varphi}$. For smaller values of s the function becomes a smoother curve, and thus our switch would have an intermediate half-on/half-off stage when φ was close to $\hat{\varphi}$. When $\varphi = \hat{\varphi}$ our Heavside approximation will be equal to 0.5.

We can insert this switch into either the proportional or constant absorption models, and solve numerically using the same finite difference method as above. For the constant absorption model we modify (3.3.1), so that,

$$\frac{\partial \varphi}{\partial t} = D\frac{\partial^2 \varphi}{\partial x^2} - \lambda^2 \left(\frac{1 + \tanh(s(\varphi - \hat{\varphi}))}{2} \right) \delta(x - x_a). \tag{3.5.2}$$

The boundary and initial conditions are still given by (3.3.2), the continuity condition still holds, but the kink condition is now,

$$D\left[\varphi_x(x_a^+) - \varphi_x(x_a^-)\right] = \left(\frac{\lambda^2 + \lambda^2 \tanh(s(\varphi(x_a) - \hat{\varphi}))}{2} \right). \tag{3.5.3}$$

Similarly for the proportional absorption model we modify (3.4.1), so that,

$$\frac{\partial \varphi}{\partial t} = D\frac{\partial^2 \varphi}{\partial x^2} - \lambda^2 \left(\frac{1 + \tanh(s(\varphi - \hat{\varphi}))}{2} \right) \delta(x - x_a)\varphi. \tag{3.5.4}$$

Again the boundary, initial, and continuity conditions from earlier still hold, but the kink condition is now,

$$D\left[\varphi_x(x_a^+) - \varphi_x(x_a^-)\right] = \left(\frac{\lambda^2 + \lambda^2 \tanh(s(\varphi(x_a) - \hat{\varphi}))}{2} \right) \varphi(x_a). \tag{3.5.5}$$

In both models for the steady state, there are three possibilities which depend on the value of $\hat{\varphi}$. If $\hat{\varphi} \ll \varphi(x_a)$, the bacterium never turns on (i.e. it is not respiring), and the value of φ at steady state is $\varphi = \mu$, throughout the domain. If $\hat{\varphi} \gg \varphi(x_a)$, the bacterium is always on (i.e. it is continuously respiring), which means we have the same models as we had in the previous sections and the steady state is again given by (3.3.14) for constant absorption and (3.4.12) for proportional absorption. All other steady states fall between the two of these, and when $\hat{\varphi}$ is very close to $\varphi(x_a)$, for constant absorption,

$$\varphi(x_a) = \mu - \frac{\lambda^2 x_a}{2D} \tag{3.5.6}$$

and for proportional absorption,

$$\varphi(x_a) = \frac{2\mu D}{2D + \lambda^2 x_a}. \tag{3.5.7}$$

This would also be true if we had chosen s, in the switch (3.5.1), to be small. If s is chosen to be large enough, it must be true in both models that the minimum possible value of $\varphi(x_a)$ is equal to $\hat{\varphi}$. This is because as soon as the oxygen concentration reaches this threshold value the bacterium will stop absorbing oxygen. As we are modelling the bacterium as only a single point, we cannot say much more about how much denitrification would be now occurring. We must improve our model to include an area of soil with uniformly distributed bacteria within it. Then it will be possible to find results where some of the soil can be respiring whilst some denitrifies.

3.6 Multiple Points Of Absorption

Using the work in the previous sections, it is possible to construct a model with, $n \in \mathbb{N}$, bacteria absorbing at n individual points, $x_{a,1}, x_{a,2}, ..., x_{a,n}$. By taking the finite difference equation method used above, we can split the problem into $n + 1$ sections, and then work exactly as before. For the steady state, when $x < x_{a,1}$, $\varphi = Ax + \mu$, when $x > x_{a,n}$, $\varphi = B$, and for every section in-between, $\varphi = S_i x + T_i$, for constants A, B, S_i, T_i which can be found using the conditions as before. An example of a multiple respiring bacteria model, with switches for all the bacteria, is shown in Figure 3.6.

This type of model is good for observing the shape of oxygen distribution throughout the depth of a soil with points of high oxygen absorption. Constant absorption of oxygen due to respiration and then a switch to denitrification at some threshold value of oxygen concentration, matches the behaviour of bacteria as described in the literature very well. However, in order to know how much denitrification is going to occur in such a system we must extend to at least a two dimensional model, where we can include patches of soil, or soil aggregates, of finite area where microbial respiration occurs throughout.

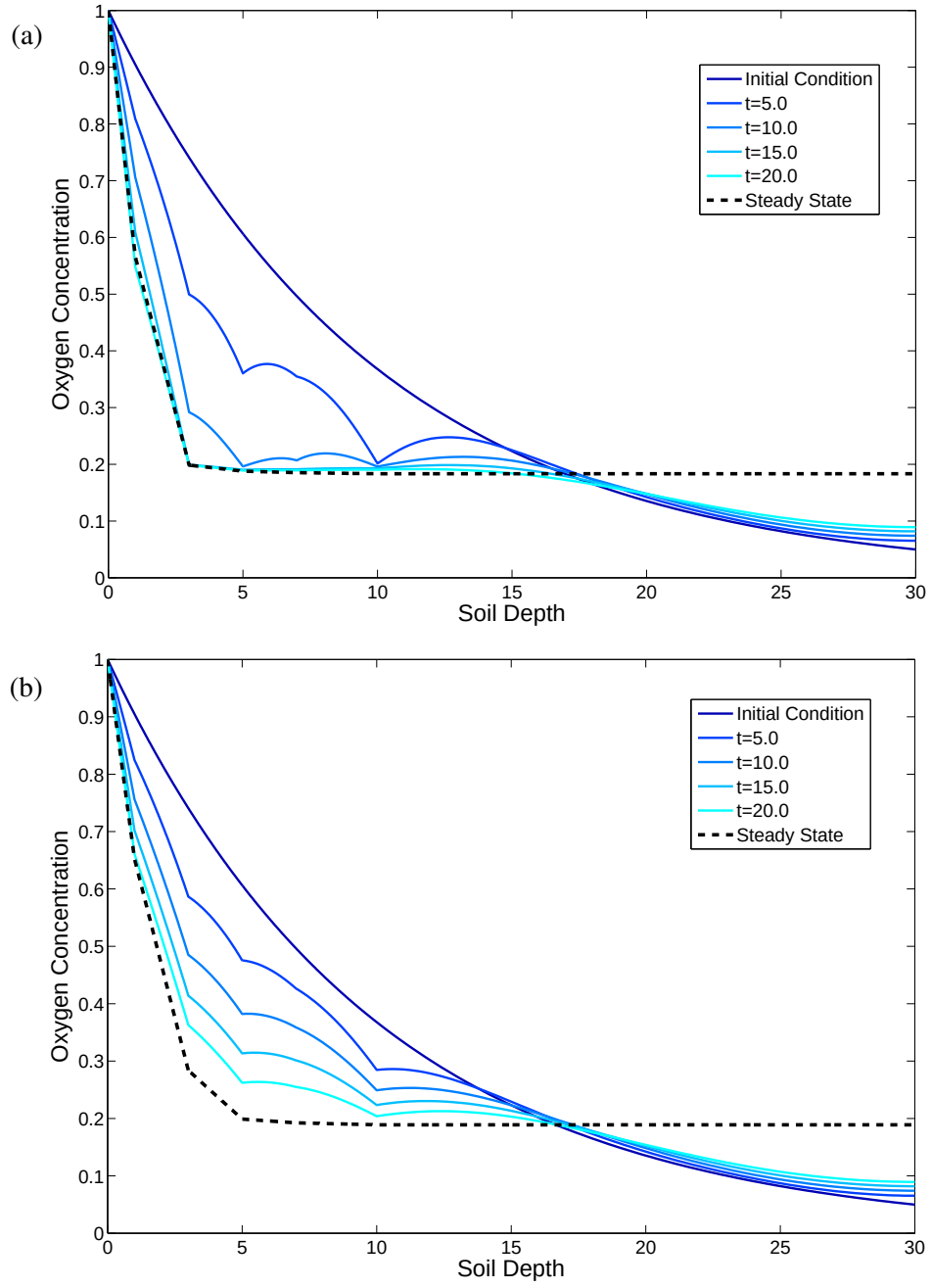

Figure 3.6: An example of a 1D oxygen distribution model with multiple points of absorption and switches. a) Constant absorption, b) Proportional absorption. $\hat{\varphi} = 0.2$, $\kappa = 0.1$, $D = 1$. $x_{a,1} = 1$, $x_{a,2} = 3$, $x_{a,3} = 5$, $x_{a,4} = 7$, $x_{a,5} = 10$. $\lambda_1^2 = 0.25$, $\lambda_2^2 = 0.5$, $\lambda_3^2 = 0.5$, $\lambda_4^2 = 0.25$, $\lambda_5^2 = 0.5$

Chapter 4

Two Dimensional Oxygen Distribution Models

In this chapter a two-dimensional model of oxygen distribution in soil is developed. The main benefit of the models created throughout the chapter is that a finite sized area of soil with respiring bacteria within it can be included. We shall see that from a constant supply of oxygen in the air, oxygen levels decrease with increasing soil depth, as the oxygen diffuses into the area of absorption. Later in the chapter the first models with areas of bacteria that are denitrifying rather than respiring are found. Essentially these are models of the anaerobic areas of the soil, created entirely because of respiring bacteria. These areas are defined as anaerobic whenever the oxygen has been depleted to a critical level. In anaerobic soil the bacteria are forced to denitrify rather than respire in order to create energy. From these models we can then imply the fraction of the soil which is anaerobic, and thus the amount of bacteria that are denitrifying, in order to predict the levels of nitrous oxide that could be released into the atmosphere.

4.1 Soil With No Absorption

We start by looking at the simplest two-dimensional model, where oxygen concentration, φ, diffuses throughout the half-plane $y \leq 0$, according to $\nabla^2\varphi = 0$. We specify that the oxygen concentration is constant at the soil surface, $\varphi(x, 0) = \mu$, which represents the concentration of oxygen in normal air. We also impose a no-flux condition at infinite depth in the soil, which represents an impermeable layer of rock deep below the soil. A diagram of the domain is shown below in Figure 4.1.

It is clear that there is a solution that does not depend upon x, so we may simply solve

$$\frac{d^2\varphi}{dy^2} = 0, \tag{4.1.1}$$

which, after applying the boundary conditions gives

$$\varphi(y) = \mu. \tag{4.1.2}$$

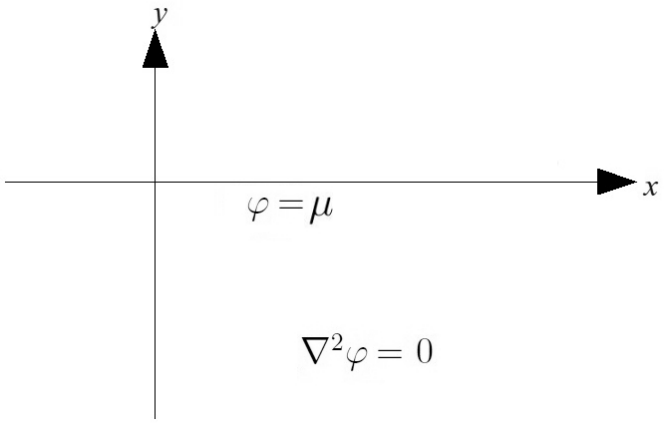

Figure 4.1: The zero absorption model

This solution is expected from the definition of the model. There is no oxygen absorption within the domain so oxygen concentration remains constant throughout, as specified on the x-axis as the concentration in the air. Clearly we require at least one respiring bacterium in the soil to remove the oxygen and give a more interesting solution.

4.2 A Conformal Mapping Model

In this model a single circle of oxygen-absorbing soil, with boundary B, of radius r_B, is positioned with centre $(0, c)$, where $c < 0$, below a boundary representing ground level at $y = 0$. The boundary at $y = 0$ represents where the soil is open to the air, so here oxygen concentration will be assumed to be a constant, μ_1. Oxygen diffuses at the same rate throughout the soil outside B, and we specify constant concentration μ_2, where $\mu_2 < \mu_1$, on B. This should create a model where oxygen diffuses into the soil from the air down a concentration gradient that decreases to the minimum value μ_2 on the edge of the area of oxygen absorbing soil. We assume nothing about the behaviour of the oxygen within B, but from the way the model has been set up there must be some oxygen absorption. The domain and boundary conditions are shown in Figure 4.2.

To make progress with this model we use a conformal mapping, as in [2]. We set $z = x + iy$ and then define,

$$w(x, y) = \frac{z + ai}{z - ai}, \tag{4.2.1}$$

where $a = \sqrt{c^2 - r_B^2}$. Using this mapping the soil surface $y = 0$ gives,

$$w = \frac{x^2 - a^2 + 2axi}{x^2 + a^2}. \tag{4.2.2}$$

Taking the absolute value of (4.2.2) shows that $|w| = 1$, therefore in the mapped plane this is a circle, of radius one, centred at the origin.

In the unmapped plane, the boundary, B, is given by $x^2 + (y - c)^2 = r_B^2$. So we can also

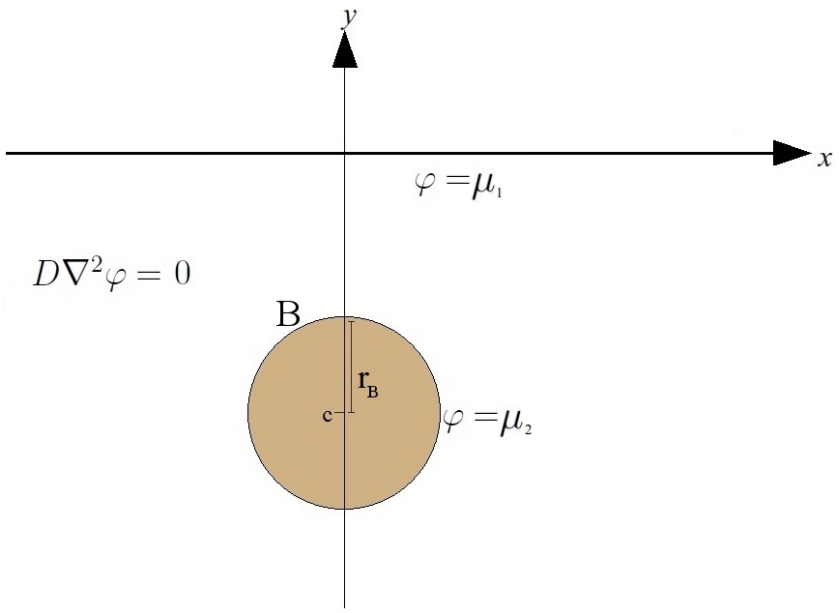

Figure 4.2: The oxygen distribution model used in the conformal mapping method

describe B as

$$z = ic + r_B e^{i\theta}, \tag{4.2.3}$$

which we use to find the correct expression for w that describes B in the mapped plane. We note that from (4.2.3),

$$\begin{aligned} z\bar{z} &= c^2 + r_B^2 + ic\left(r_B e^{-i\theta} - r_B e^{i\theta}\right) \\ z - \bar{z} &= 2ic + r_B e^{i\theta} - r_B e^{-i\theta}. \end{aligned} \tag{4.2.4}$$

Combining the properties in (4.2.4) we can show that,

$$z\bar{z} + ic(z - \bar{z}) + a^2 = 0. \tag{4.2.5}$$

Now we rearrange (4.2.1) to give an expression for z in terms of w,

$$z = \frac{ai(1 + w)}{w - 1}, \tag{4.2.6}$$

and we can show that the complex conjugate can be written as,

$$\bar{z} = \frac{-ai(1 + \bar{w})}{\bar{w} - 1}. \tag{4.2.7}$$

Then by substituting (4.2.6) and (4.2.7) into (4.2.5), after rearranging we can show that,

$$w\bar{w} = \frac{r_B^2}{(c - a)^2}. \tag{4.2.8}$$

So we have that $|w| = \delta$, where δ^2 is equal to the constant on the RHS of (4.2.8). Therefore, B also maps to a circle centred at the origin. From the definition of a, it can be seen that

$\delta < 1$, so we have now mapped to two concentric circles, as shown in Figure 4.3, from which it is easier to solve Laplace's equation.

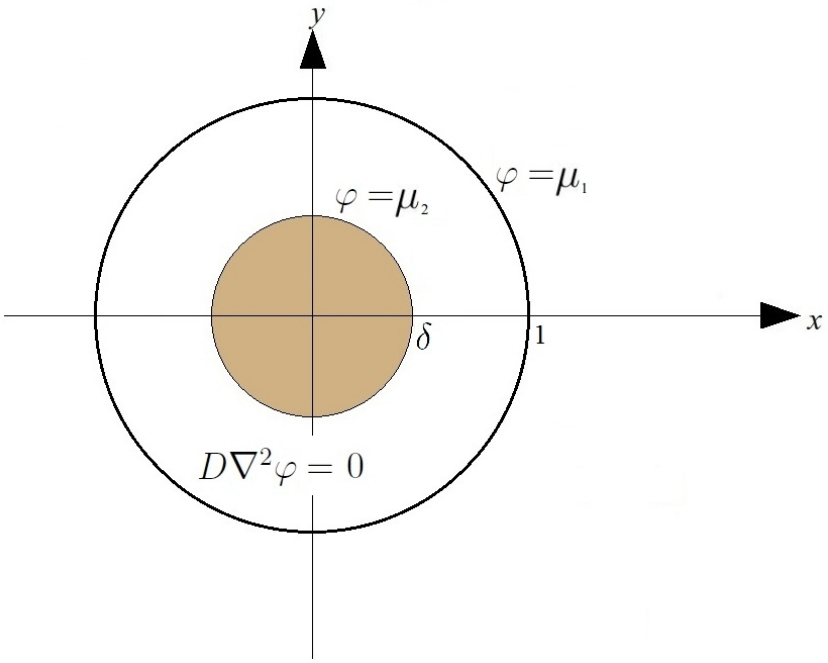

Figure 4.3: The domain shown in Figure 4.2 after it has been mapped

To find the concentration of oxygen, φ, in the mapped domain, we solve using polar coordinates. However, we can see immediately that in our problem there is no need to include angular dependence as the problem is axially symmetric. Therefore, we solve,

$$\nabla^2\varphi(r) = \frac{1}{r}\frac{\partial}{\partial r}\left(r\frac{\partial\varphi(r)}{\partial r}\right) = 0, \tag{4.2.9}$$

where r is radial distance, from the centre of the mapped region of oxygen absorbing soil. The boundary conditions are $\varphi(1) = \mu_1$ and $\varphi(\delta) = \mu_2$. We find that,

$$\varphi(r) = \mu_1 + (\mu_2 - \mu_1)\frac{\ln(r)}{\ln(\delta)}, \tag{4.2.10}$$

which when written in the original variables is

$$\varphi(x, y) = \mu_1 + \frac{(\mu_2 - \mu_1)}{\ln(\delta)}\ln\left(\frac{\sqrt{(x^2 + y^2 - a^2)^2 + (2ax)^2}}{x^2 + (y - a)^2}\right) \tag{4.2.11}$$

In Figure 4.4, $\varphi(x, y)$ as given in (4.2.11) has been plotted to observe oxygen concentration throughout the soil. The region outside of the oxygen absorbing soil in this model shows oxygen concentration decreasing as it gets closer to B. As oxygen diffuses down the concentration gradient, this means that oxygen is moving into B as if oxygen is being absorbed inside, which is realistic. However, inside B, oxygen concentration becomes infinitely negative at the point $(0, a)$, which is obviously unrealistic. This can be seen from (4.2.11), by substituting in $x = 0$, $y = a$.

Another problem with this model is that we have insisted that the concentration of oxygen on B is constant. With the air/soil line boundary above B it would make more physical sense for the concentration of oxygen to be less on the lower side of B.

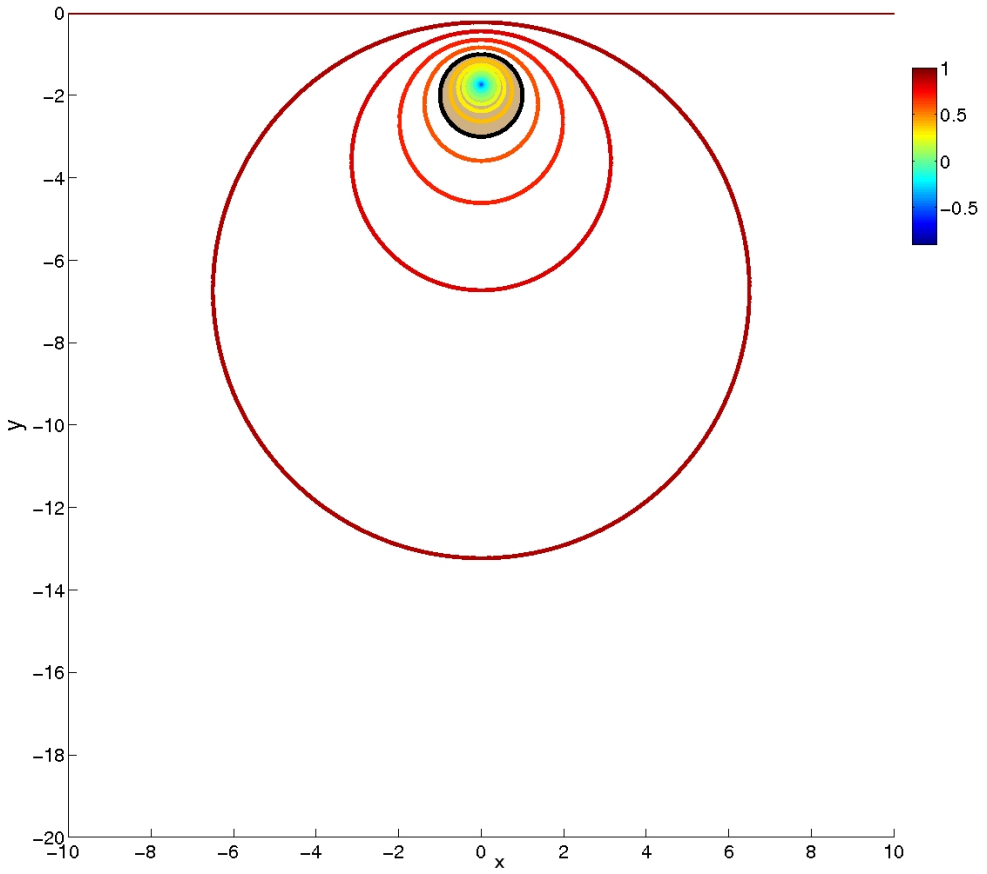

Figure 4.4: A contour plot of the concentration of oxygen, modelled using (4.2.11), with $r_B = 1$, $c = -2, \mu_1 = 1, \mu_2 = 0.5$

4.3 A Model With Multiple Point Sinks

Our next idea is to find a solution to Laplace's equation where a constant flux of oxygen into the soil along the x-axis is completely absorbed by one row of point sinks. This should mean oxygen concentration tends to zero as depth increases. The point sinks could be thought of as individual respiring bacterium in the soil.

4.3.1 Neumann Boundary Condition

We begin with an infinite array of point sinks of strength m, a positive constant, as shown in Figure 4.5. The sinks are in pairs such that for each sink at (na, b) there is a partner on the opposite side of the y-axis at $(na, -b)$. This use of the method of images creates a boundary at $y = 0$, as described in [29]. As we have chosen pairs of sinks, the boundary condition created at $y = 0$ will be that of zero flux.

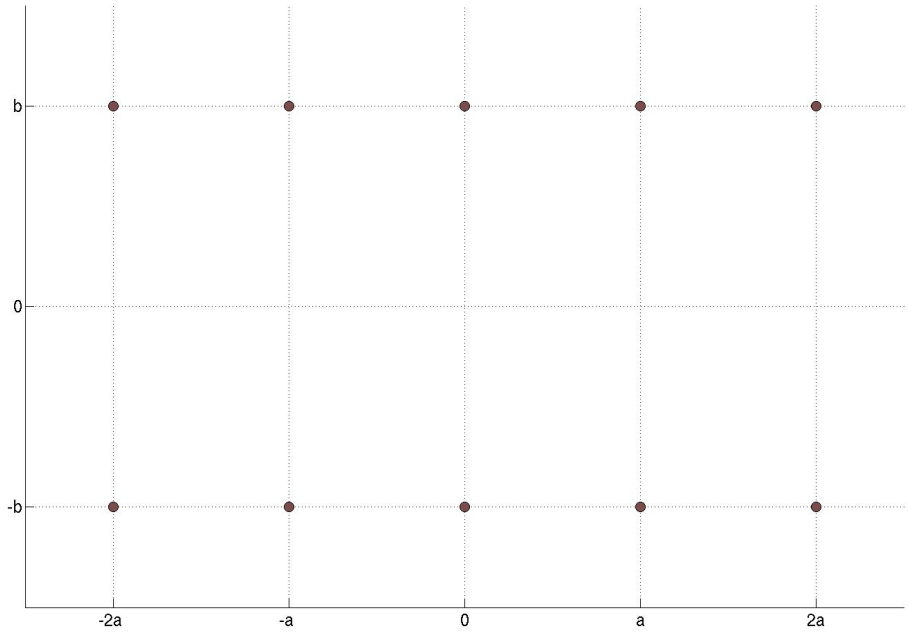

Figure 4.5: Position of soil particles modelled as point sinks, with strength m.

The complex potential of each pair of sinks is given by,

$$\omega_n = m\log(z - ib - na) + m\log(z + ib - na), \tag{4.3.1}$$

where $n \in \mathbb{Z}$. The sum of all the sinks can then be written as

$$\omega = \sum_{n=-\infty}^{\infty} m\log\left(z - ib - na\right) + \sum_{n=-\infty}^{\infty} m\log\left(z + ib - na\right), \tag{4.3.2}$$

which can also be written as,

$$\omega = m\log\left[(z - ib)\prod_{n=1}^{\infty}\left(1 - \left(\frac{z - ib}{na}\right)^2\right)\right] + m\log\left[(z + ib)\prod_{n=1}^{\infty}\left(1 - \left(\frac{z + ib}{na}\right)^2\right)\right]. \tag{4.3.3}$$

Where we have first divided the arguments of the log terms in (4.3.2 by na, which is allowable as this is equivalent only to adding a constant to the complex potential. We can then use an identity found in [3] to re-write the products in the square brackets in terms of sine functions. So we can simplify the complex potential to,

$$\omega = m\log\left[\sin\left(\frac{(z - ib)\pi}{a}\right)\sin\left(\frac{(z + ib)\pi}{a}\right)\right]. \tag{4.3.4}$$

This can be separated into real and imaginary parts,

$$\begin{aligned}
\mathrm{Re}(\omega) &= \frac{m}{2}\log\left(\frac{1}{4}\left[\cosh(\alpha b) - \cos(\alpha x)\cosh(\alpha y)\right]^2 + \frac{1}{4}\sin^2(\alpha x)\sinh^2(\alpha y)\right) \\
\mathrm{Im}(\omega) &= m\arctan\left[\frac{\sin(\alpha x)\sinh(\alpha y)}{\cosh(\alpha b) - \cos(\alpha x)\cosh(\alpha y)}\right],
\end{aligned} \tag{4.3.5}$$

where $\alpha = \frac{2\pi}{a}$. We take $\hat{\varphi} = \mathrm{Re}(\omega)$, and check the properties of this function. Firstly,

$$\lim_{y\to-\infty} \hat{\varphi} = \frac{m}{2}\log\left[\frac{1}{4}e^{-2\alpha y}\right] = -\alpha m y - m\log(4). \tag{4.3.6}$$

So as depth becomes large so does $\hat{\varphi}$, which is not acceptable for our oxygen distribution model. We also need to know about the flux of oxygen along $y = 0$. Differentiating the complex potential, ω, with respect to z gives

$$\frac{d\omega}{dz} = \alpha m\left[\frac{\sin(\alpha z)}{\cos(\alpha b i) - \cos(\alpha z)}\right] \tag{4.3.7}$$

We know from the Cauchy-Riemann equations that $\mathrm{Im}\left(\frac{d\omega}{dz}\right) = -\hat{\varphi}_y$. Thus, by separating (4.3.7) into real and imaginary parts, it can be shown that

$$\hat{\varphi}_y = \alpha m\left[\frac{\cos(\alpha x)\sinh(\alpha y)\cosh(\alpha b) - \cosh(\alpha y)\sinh(\alpha y)}{[\cosh(\alpha b) - \cos(\alpha x)\cosh(\alpha y)]^2 + \sin^2(\alpha x)\sinh^2(\alpha y)}\right]. \tag{4.3.8}$$

From (4.3.8) we can see that,

$$\hat{\varphi}_y = 0 \quad \text{on} \quad y = 0, \tag{4.3.9}$$

as expected. We can now combine this solution with two others in order to find one function that satisfies all the properties we require.

In order to counter the property that $\hat{\varphi} \to -\infty$ as $y \to -\infty$, shown in (4.3.6), we look to add to $\hat{\varphi}(x, y)$ a solution, $\bar{\varphi}(x, y)$, that satisfies Laplace's equation and where $\bar{\varphi}_y(x, 0) = 1$ and $\lim_{y\to-\infty} \bar{\varphi} = y$. By Fick's law, oxygen moves down a concentration gradient, so the first condition implies oxygen moving into the soil. An obvious solution is $\bar{\varphi}(x, y) = y$. We now choose the strength of our sink to be $m = \frac{1}{\alpha}$, so that

$$\lim_{y\to-\infty} (\bar{\varphi} + \hat{\varphi}) = -\frac{1}{\alpha}\log(4). \tag{4.3.10}$$

Lastly we add another solution of Laplace's equation, $\breve{\varphi} = \frac{1}{\alpha}\log(4)$, to cancel the remaining constant in (4.3.10). The complete solution, where all the required properties hold is given by

$$\begin{aligned} \varphi &= \hat{\varphi} + \bar{\varphi} + \breve{\varphi} \\ &= y + \frac{1}{2\alpha}\log\left(4[\cosh(\alpha b) - \cos(\alpha x)\cosh(\alpha y)]^2 + 4\sin^2(\alpha x)\sinh^2(\alpha y)\right) \end{aligned} \tag{4.3.11}$$

By taking the limit $y \to -\infty$ of (4.3.11) we can show that all oxygen that enters the soil through $y = 0$ is absorbed into the sinks, so that there is no oxygen found at infinite depth. The amount of oxygen entering the soil remains constant $\varphi_y(x, 0) = 1$ and the sink has strength $m = \frac{a}{2\pi}$. This can be seen in Figure 4.6, below. One problem with this solution is that upon approaching the point sinks concentration becomes infinitely negative. The concentration gradient shows that oxygen is moving towards the sink, but in order to find a

solution that makes physical sense, it seems we will need a model where oxygen absorption occurs within a region of a finite area.

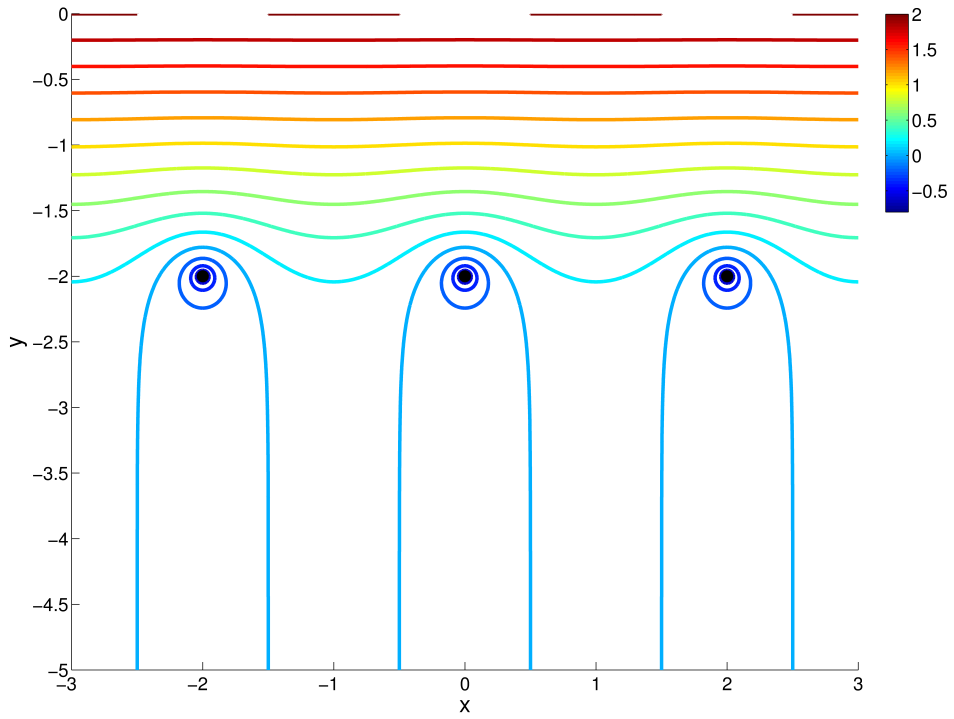

Figure 4.6: Concentration of oxygen using the array of point sinks model, with Neumann boundary condition. $a = b = 2$ and $m = \frac{a}{2\pi}$. Note that the oxygen concentration is not constant on the air/soil boundary at $y = 0$.

4.3.2 Dirichlet Boundary Condition

For this type of model to include the air/soil boundary we desire, i.e. $\varphi|_{y=0} = \text{const.}$, we must use one row of point sinks mirrored by a row of point sources. Effectively this just changes a plus sign to a minus sign in the complex potential (4.3.1). We now have,

$$\omega_n = -m \log(z - ib - na) + m \log(z + ib - na), \tag{4.3.12}$$

for each pair. Using the same identity as for the Neumann case, we arrive at,

$$\omega = -m \log\left[\sin\left(\frac{(z - ib)\pi}{a}\right)\right] + m \log\left[\sin\left(\frac{(z + ib)\pi}{a}\right)\right] \tag{4.3.13}$$

And we choose to take the real part for our function so that,

$$\hat{\varphi} = -\frac{m}{2} \log\left[\cosh^2\left(\frac{(y - b)\pi}{a}\right) - \cos^2\left(\frac{\pi x}{a}\right)\right] + \frac{m}{2} \log\left[\cosh^2\left(\frac{(y + b)\pi}{a}\right) - \cos^2\left(\frac{\pi x}{a}\right)\right] \tag{4.3.14}$$

We can choose a constant to add to our solution in order to find the desired boundary condition at $y = 0$. We add to our solution,

$$\breve{\varphi} = \mu. \tag{4.3.15}$$

Then,

$$\varphi = \hat{\varphi} + \breve{\varphi} = \mu - \frac{m}{2} \log \left[\frac{\cosh^2\left(\frac{(y-b)\pi}{a}\right) - \cos^2\left(\frac{\pi x}{a}\right)}{\cosh^2\left(\frac{(y+b)\pi}{a}\right) - \cos^2\left(\frac{\pi x}{a}\right)} \right] \tag{4.3.16}$$

As $y \to -\infty$,

$$\varphi \to \mu + m \log \left[\frac{\cosh \frac{\pi b}{a} - \sinh \frac{\pi b}{a}}{\cosh \frac{\pi b}{a} + \sinh \frac{\pi b}{a}} \right], \tag{4.3.17}$$

which is acceptable as we now have that,

$$\begin{aligned} \varphi|_{y=0} &= \mu \\ \lim_{y \to -\infty} \varphi_y &= 0. \end{aligned} \tag{4.3.18}$$

These boundary conditions are the same as those we would hope to include in a biologically realistic model. However, we still have the problem of infinitely negative oxygen concentration at the point sinks. In the next section we shall develop our model to include an area of oxygen absorbing bacteria, instead of individual points. The current model however still gives an indication to how the concentration gradients will look in later models and shows clearly how oxygen concentration changes with increasing depth into the soil.

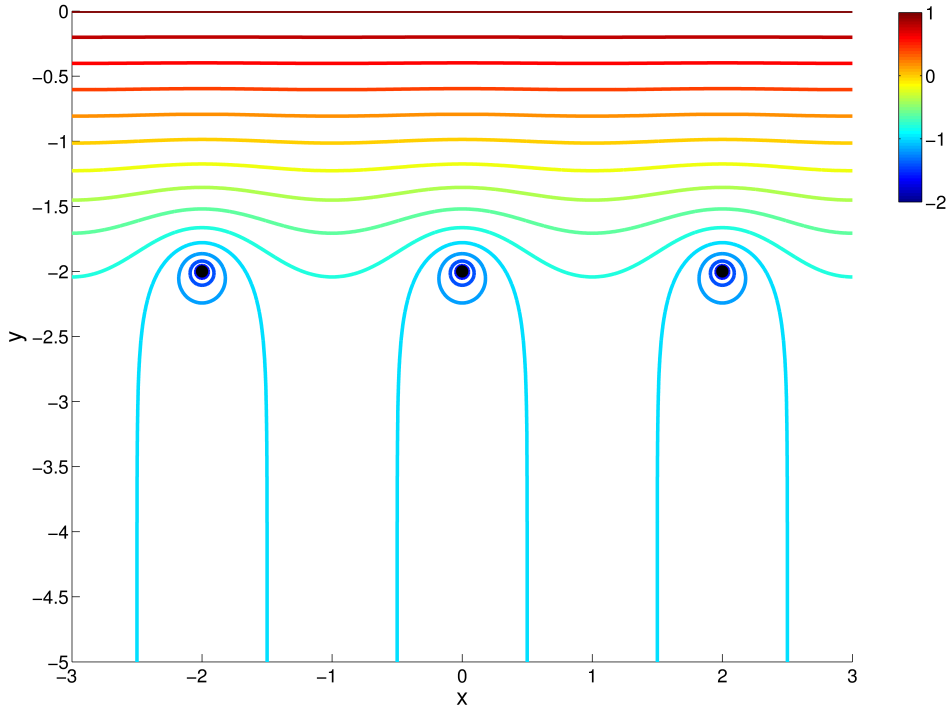

Figure 4.7: Concentration of oxygen using the array of point sinks model, with Dirichlet boundary condition. $a = b = 2$ and $m = \frac{a}{2\pi}$. Note that the oxygen concentration is constant on the air/soil boundary at $y = 0$.

4.4 Further Development Of A Two-Dimensional Model

As discussed in the introduction, throughout the literature there are models of oxygen distribution in soil used to predict the anaerobic area or volume of the soil where bacteria can denitrify. Several models use a spherical soil aggregate (a round lump of soil) to show that when bacteria in this soil respire quick enough a central anaerobic core within the aggregate will develop. Within this core the oxygen level has dipped below a threshold value meaning that the bacteria can no longer respire, and so absorption of oxygen stops. Most of these models consider this single sphere of soil with oxygen concentration assumed to be constant on the outer edge, such as [21] and [42]. We wish to create a model where the oxygen concentration does not have to be constant on the edge of the aggregate and the anaerobic core need not be central or circular.

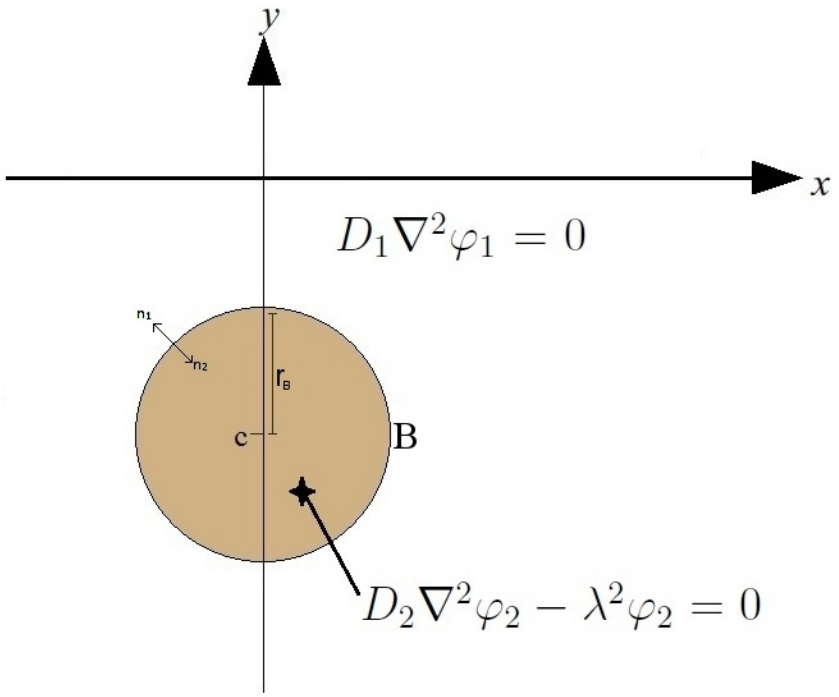

Figure 4.8: The 2D non-symmetric oxygen distribution model with proportional absorption

In order to create a model of oxygen distribution where we can find the anaerobic area within a circle of oxygen absorbing soil, we shall again consider a two dimensional model. We shall start our development of the model by investigating the model shown in Figure 4.8. In this model the area of oxygen absorbing soil is placed below the air/soil boundary at $y = 0$ and as such the problem is non-symmetric. We initially do not include an anaerobic area within the soil in order to keep the calculations simpler. Later once we have found a solution for this problem, we shall develop the model further to also include a core of anaerobic soil within B, where we shall assume the bacteria are denitrifying.

We split the domain of Figure 4.8 into two sections, region 1 and region 2. We call the oxygen concentration in these two sections φ_1 and φ_2 respectively.

In the main body of the soil, region 1, oxygen can diffuse via Laplace's equation

$D_1\nabla^2\varphi_1 = 0$ and absorption is negligible.

Region 2 is the circular area representing soil that is absorbing oxygen. This circle with boundary, B, has radius r_B, and oxygen behaves according to the Helmholtz equation $D_2\nabla^2\varphi_2 - \lambda^2\varphi_2 = 0$. The oxygen absorption is therefore proportional to the local oxygen concentration, so our model will never predict negative concentrations.

We also have the boundary conditions of constant oxygen concentration at $y = 0$ (as we assume oxygen levels to be constant in the air) and a no-flux condition at infinite depth representing an impermeable layer of rock,

$$\begin{aligned} \varphi_1(x, 0) &= \mu \\ \frac{\partial\varphi_1}{\partial y}(x, -\infty) &= 0. \end{aligned} \tag{4.4.1}$$

The conditions on the boundary, B, between the two regions (i.e. between the edge of the oxygen absorbing aggregate and the rest of the soil) are those of continuity and equal flux,

$$\begin{aligned} \varphi_1 &= \varphi_2 \\ D_1\mathbf{n}_1 \cdot \nabla\varphi_1 &= -D_2\mathbf{n}_2 \cdot \nabla\varphi_2. \end{aligned} \tag{4.4.2}$$

With these boundary conditions we can see that the oxygen concentration need not be constant on B as in previous models. This seems to be an improvement on previous models, as we assume that oxygen levels will be at their maximum value at $y = 0$, and around the edge of B oxygen levels will be lower for increasing depth due to the absorption within B.

To find a solution for this model we are going to use the Boundary Element Method, as described in the introduction. In order to do this we must first choose appropriate Green's functions.

For region 1 we shall choose to use a modified free space Green's function, we call it G_1. This Green's function will satisfy,

$$\nabla^2 G_1(\mathbf{x}, \mathbf{x_0}) + \delta(\mathbf{x} - \mathbf{x_0}) = 0, \tag{4.4.3}$$

as usual, but will also have the property that it becomes zero at $y = 0$. Therefore our chosen Green's function is,

$$G_1(\mathbf{x}, \mathbf{x_0}) = \frac{1}{2\pi}\left[\log r - \log \tilde{r}\right], \tag{4.4.4}$$

where $r = \sqrt{(x - x_0)^2 + (y - y_0)^2}$ and $\tilde{r} = \sqrt{(x - x_0)^2 + (y + y_0)^2}$. It can also be shown that,

$$\lim_{y\to-\infty} \frac{\partial G_1}{\partial y} = 0. \tag{4.4.5}$$

Also in region 1, we shall define

$$\hat{\varphi}_1(x, y) = \varphi_1(x, y) - \mu, \tag{4.4.6}$$

so that on $y = 0$, $\hat{\varphi}_1$ is also equal to zero. From the generic boundary integral equation

(1.7.5), we can then derive the equation relevant to region 1. From all the properties of G_1 and $\hat{\varphi}_1$ mentioned above, the region 1 boundary integral equation will only involve integrals that are non-zero on B. Our boundary integral equation in region 1 is therefore,

$$\hat{\varphi}_1(\mathbf{x_0}) = -\int_B G_1 \mathbf{n}_1 \cdot \nabla\hat{\varphi}_1 dl + \int_B \hat{\varphi}_1 \mathbf{n}_1 \cdot \nabla G_1 dl. \tag{4.4.7}$$

In the oxygen-absorbing part of the soil, region 2, we need a Green's function that satisfies

$$\nabla^2 G_2(\mathbf{x}, \mathbf{x_0}) - \frac{\lambda^2}{D_2} G_2(\mathbf{x}, \mathbf{x_0}) + \delta(\mathbf{x} - \mathbf{x_0}) = 0, \tag{4.4.8}$$

so we use the modified Bessel function,

$$G_2(\mathbf{x}, \mathbf{x_0}) = \frac{1}{2\pi} K_0(mr), \tag{4.4.9}$$

where $m = \frac{\lambda}{\sqrt{D_2}}$, as given in [36]. Setting $G = G_2(\mathbf{x}, \mathbf{x_0})$ in (1.7.4) gives for region 2,

$$\varphi_2(\mathbf{x_0}) = -\int_B G_2 \mathbf{n}_2 \cdot \nabla\varphi_2 dl + \int_B \varphi_2 \mathbf{n}_2 \cdot \nabla G_2 dl. \tag{4.4.10}$$

We are now in a position to be able to find first the solution on the boundary, and then throughout the domain. Following the method described in the introduction, we shall discretize the boundary B into N straight elements, along each of which we assume $\hat{\varphi}_1$, φ_2 and their derivatives are constant. Then by positioning $\mathbf{x_0}$ at the midpoint of each element, and evaluating at each of these there will be $2N$ integral equations with $4N$ unknowns. We reduce the number of unknowns to $2N$ by use of the boundary conditions, which means we are then left with a solvable matrix equation.

Our system of integral equations for when $\mathbf{x_0}$ is on the boundary is created as discussed in the introduction. The only difference from those that apply if $\mathbf{x_0}$ is chosen to be an interior point being that the integrals are multiplied by a factor of a half. So for an $\mathbf{x_0}$ on B, we have in region 1,

$$\begin{aligned}\hat{\varphi}_1(\mathbf{x_0}) &= \frac{1}{2\pi}\int_B \log\left[\frac{(x-x_0)^2+(y-y_0)^2}{(x-x_0)^2+(y+y_0)^2}\right]\mathbf{n}_1 \cdot \nabla\hat{\varphi}_1(\mathbf{x}) dl(\mathbf{x}) \\ &\quad -\frac{1}{2\pi}\int_B^{PV} \hat{\varphi}_1 \mathbf{n}_1 \cdot \nabla\left[\log\sqrt{\frac{(x-x_0)^2+(y-y_0)^2}{(x-x_0)^2+(y+y_0)^2}}\right] dl(\mathbf{x}).\end{aligned} \tag{4.4.11}$$

And in region 2 we have,

$$\begin{aligned}\varphi_2(\mathbf{x_0}) &= \frac{1}{\pi}\int_B K_0\left(m\sqrt{(x-x_0)^2+(y-y_0)^2}\right)\mathbf{n}_2 \cdot \nabla\varphi_2(\mathbf{x}) dl(\mathbf{x}) \\ &\quad -\frac{1}{\pi}\int_B^{PV} \varphi_2(\mathbf{x})\mathbf{n}_2 \cdot \nabla K_0\left(m\sqrt{(x-x_0)^2+(y-y_0)^2}\right) dl(\mathbf{x}).\end{aligned} \tag{4.4.12}$$

As we have assumed $\hat{\varphi}_1$, φ_2 and their derivatives are constant on each boundary element

we can write (4.4.11) and (4.4.12) as,

$$\frac{1}{2}\hat{\varphi}_1(\mathbf{x_0}) = \sum_{i=1}^{N} \alpha_i(\mathbf{x_0})\,(\mathbf{n}_1 \cdot \nabla\hat{\varphi}_1)_i + \sum_{i=1}^{N} \beta_i(\mathbf{x_0})\hat{\varphi}_{1,i} \tag{4.4.13}$$

$$\frac{1}{2}\varphi_2(\mathbf{x_0}) = \sum_{i=1}^{N} a_i(\mathbf{x_0})\,(\mathbf{n}_2 \cdot \nabla\varphi_2)_i + \sum_{i=1}^{N} b_i(\mathbf{x_0})\varphi_{2,i}, \tag{4.4.14}$$

where the integrals in (4.4.11) and (4.4.12) have been discretized into N straight elements and $\alpha,\ \beta,\ a,\ b$ are the influence matrices

Integration along each non-singular element can be done using Gauss-Legendre quadrature. For the singular elements, i.e. when $\mathbf{x_0}$ lies on that element, we separate out the singularity so that we can integrate analytically. For example, the first integral in (4.4.12), for a straight element that has a singularity at $\mathbf{x_0}$. From [3], $K_0(z) \approx -\ln(z)$ as $z \to 0$ so we subtract $\frac{-1}{2\pi}\ln(mr)$, to remove the singularity and we can then integrate using Gauss-Legendre quadrature. This leaves us with the singular integral,

$$\frac{-1}{2\pi}\int_{E_i} \log\left(m[(x-x_0)^2 + (y-y_0)^2]^{\frac{1}{2}}\right) dl, \tag{4.4.15}$$

which can be rewritten as,

$$\frac{-1}{2\pi}\int_{l_i}^{l_{i+1}} \log\left(m|l-l_0|\right) dl = \frac{1}{\pi}\left(l_{i+1} - l_0 - (l_{i+1}-l_0)\log[m(l_{i+1}-l_0)]\right). \tag{4.4.16}$$

This method is in explained in detail by Pozrikidis, in [36].

By applying the equations (4.4.13) and (4.4.14) at each of the $\mathbf{x_0}$ on the elements around B we arrive at $2N$ integral equations consisting of $4N$ unknowns. From our boundary conditions (4.4.2) we know that,

$$\begin{aligned} \hat{\varphi}_1 &= \varphi_2 - \mu \\ D_1\mathbf{n}_1 \cdot \nabla\hat{\varphi}_1 &= -D_2\mathbf{n}_2 \cdot \nabla\varphi_2. \end{aligned} \tag{4.4.17}$$

We can use (4.4.17) to substitute $\hat{\varphi}_1$ into (4.4.14) so that the system of equations now consists of only $2N$ unknowns. This allows us to write the $2N$ integral equations in the form of a solvable matrix system. We define,

$$\mathbf{F} = \begin{pmatrix} \hat{\varphi}_{1,1} \\ \vdots \\ \hat{\varphi}_{1,N} \\ (\mathbf{n}_1 \cdot \nabla\hat{\varphi}_1)_1 \\ \vdots \\ (\mathbf{n}_1 \cdot \nabla\hat{\varphi}_1)_N \end{pmatrix}, \tag{4.4.18}$$

$$\mathbf{A} = \begin{pmatrix} \beta_1(\mathbf{x_0}_{,1}) & \cdots & \beta_N(\mathbf{x_0}_{,1}) & \alpha_1(\mathbf{x_0}_{,1}) & \cdots & \alpha_N(\mathbf{x_0}_{,1}) \\ \vdots & \vdots & \vdots & \vdots & \vdots & \vdots \\ \beta_1(\mathbf{x_0}_{,N}) & \cdots & \beta_N(\mathbf{x_0}_{,N}) & \alpha_1(\mathbf{x_0}_{,N}) & \cdots & \alpha_N(\mathbf{x_0}_{,N}) \\ b_1(\mathbf{x_0}_{,1}) & \cdots & b_N(\mathbf{x_0}_{,1}) & -\frac{D_1}{D_2}a_1(\mathbf{x_0}_{,1}) & \cdots & -\frac{D_1}{D_2}a_N(\mathbf{x_0}_{,1}) \\ \vdots & \vdots & \vdots & \vdots & \vdots & \vdots \\ b_1(\mathbf{x_0}_{,N}) & \cdots & b_N(\mathbf{x_0}_{,N}) & -\frac{D_1}{D_2}a_1(\mathbf{x_0}_{,N}) & \cdots & -\frac{D_1}{D_2}a_N(\mathbf{x_0}_{,N}) \end{pmatrix}, \tag{4.4.19}$$

and,

$$\mathbf{K} = \begin{pmatrix} \mathbf{0}_{N,1} \\ \mu \sum_{i=1}^{N} b_i(\mathbf{x_0}_{,1}) \\ \vdots \\ \mu \sum_{i=1}^{N} b_i(\mathbf{x_0}_{,N}) \end{pmatrix}, \tag{4.4.20}$$

where $\mathbf{0}_{N,1}$ is a zero column vector of length N. We therefore have defined all the unknowns to be grouped together in $\mathbf{F}$. We can then write the matrix equation in order to find $\mathbf{F}$ as,

$$\frac{1}{2}\begin{pmatrix} \mathbf{I}_N & \mathbf{0}_N \\ \mathbf{I}_N & \mathbf{0}_N \end{pmatrix}\mathbf{F} + \frac{\mu}{2}\begin{pmatrix} \mathbf{0}_{N,1} \\ \mathbf{1}_{N,1} \end{pmatrix} = \mathbf{A}\mathbf{F} + \mathbf{K} \tag{4.4.21}$$

where $\mathbf{I}_N$ is the N by N identity matrix, $\mathbf{0}_N$ is the N by N zero matrix and $\mathbf{1}_{N,1}$ is a column vector of length N with entries of all ones.

Solving the matrix system (4.4.21) gives a solution for $\mathbf{F}$, which tells us the concentration and flux of oxygen on the boundary B. A solution for an example set of parameters is shown in Figure 4.9, below.

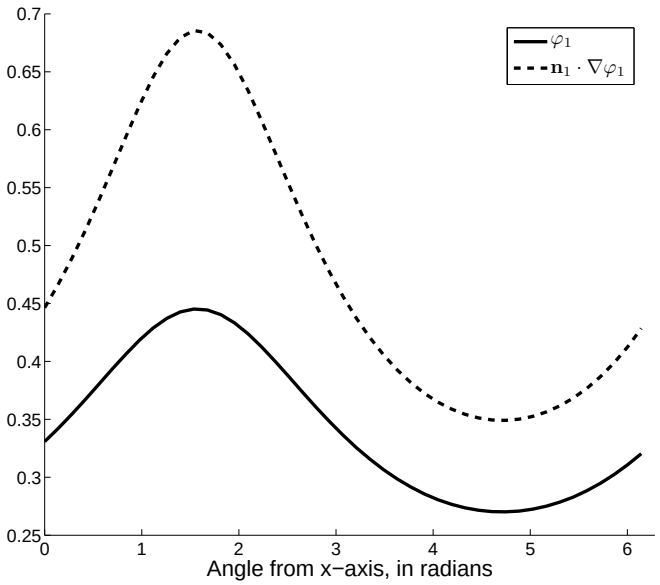

Figure 4.9: Oxygen concentration on the boundary, B. Found using the boundary element method. B was split into 45 straight elements. $r_B = 1$, $c = -2$, $\mu = 1$ $D_1 = D_2 = 1$, $\lambda = 2$

We now know the values of φ_1 and φ_2 and their normal derivatives on all the boundaries within our domain. We can therefore use these to find oxygen concentration at any point,

x, via the system,

$$\hat{\varphi}_1(\mathbf{x_0}) = \sum_{i=1}^{N} \alpha_i(\mathbf{x_0})\,(\mathbf{n}\cdot\nabla\hat{\varphi}_1)_i + \sum_{i=1}^{N} \beta_i(\mathbf{x_0})\hat{\varphi}_{1,i} \tag{4.4.22}$$

$$\varphi_2(\mathbf{x_0}) = \sum_{i=1}^{N} a_i(\mathbf{x_0})\,(\mathbf{n}\cdot\nabla\varphi_2)_i + \sum_{i=1}^{N} b_i(\mathbf{x_0})\varphi_{2,i}. \tag{4.4.23}$$

A solution showing oxygen concentration throughout the domain is plotted in Figure 4.10 for the same set of parameters and thus the same boundary values as in Figure 4.9.

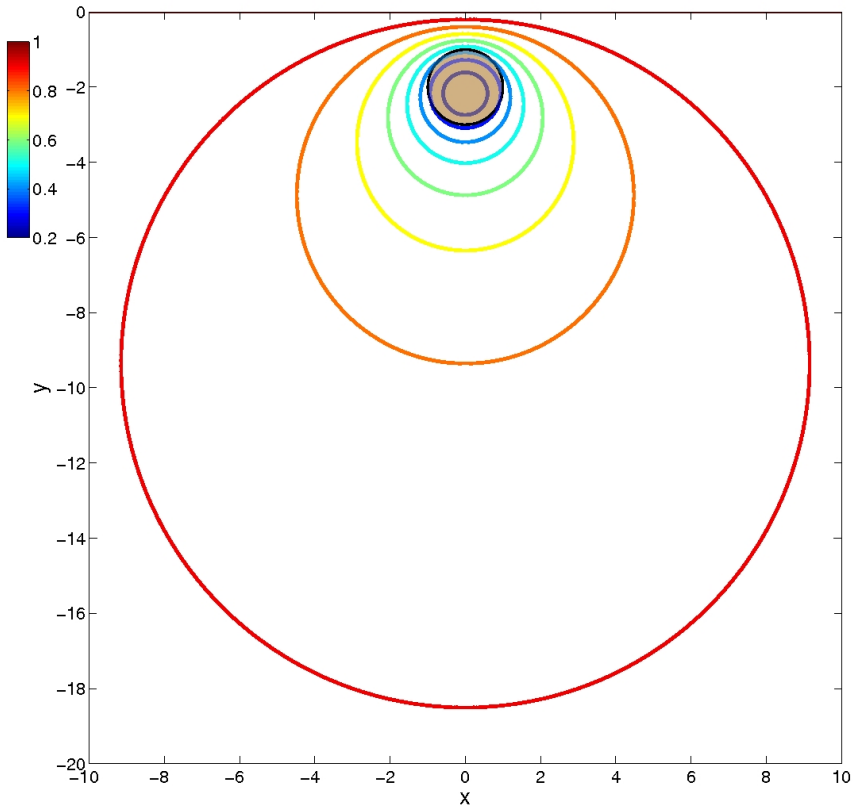

Figure 4.10: Oxygen concentration found throughout the domain using the boundary values found previously and shown in Figure 4.9. $r_B = 1$, $c = -2$, $\mu = 1$ $D_1 = D_2 = 1$, $\lambda = 2$

For our current example, Figure 4.11 shows the minimum oxygen concentration is not in the exact centre of region 2. The centre of region 2 is at $(0, -2)$ and the minimum oxygen concentration is found at roughly $(0, -2.15)$. This is of course due to the non-symmetric properties of the model, and is as we were expecting. On the upper edge of B oxygen concentration is higher than on the lower edge, because the oxygen is diffusing into the soil from its maximum concentration in the air at $y = 0$. As the oxygen is absorbed in region 2 the concentration decreases until its minimum point. In Figure 4.11, we have looked at how the position of the point of minimum oxygen concentration moves as the depth of region 2 increases. The further away region 2 is from the air/soil boundary the less effect the air will have on region 2 and thus the minimum point becomes more central.

As we have chosen to use a proportional absorption model, the minimum oxygen

concentration will always be positive. For the bacteria within the soil to stop respiring and start denitrifying, the oxygen concentration must dip below a certain threshold value, known to be close to zero. In the next section we hope to show exactly which areas of the soil have reached this threshold value. For those models we shall consider both proportional and constant absorption of oxygen. This is because in those models the oxygen absorption will switch off when the concentration reaches a certain point, which will stop the model from predicting negative concentrations. As the current model does not incorporate this feature, we shall not investigate constant oxygen absorption.

We also note that as distance from B is increased the oxygen concentration returns to the background level, this can be clearly seen in Figure 4.10. The background oxygen level in this model is μ due to the boundary at $y = 0$. This will always be true for models with a finite area of oxygen absorbing soil in an infinitely large domain.

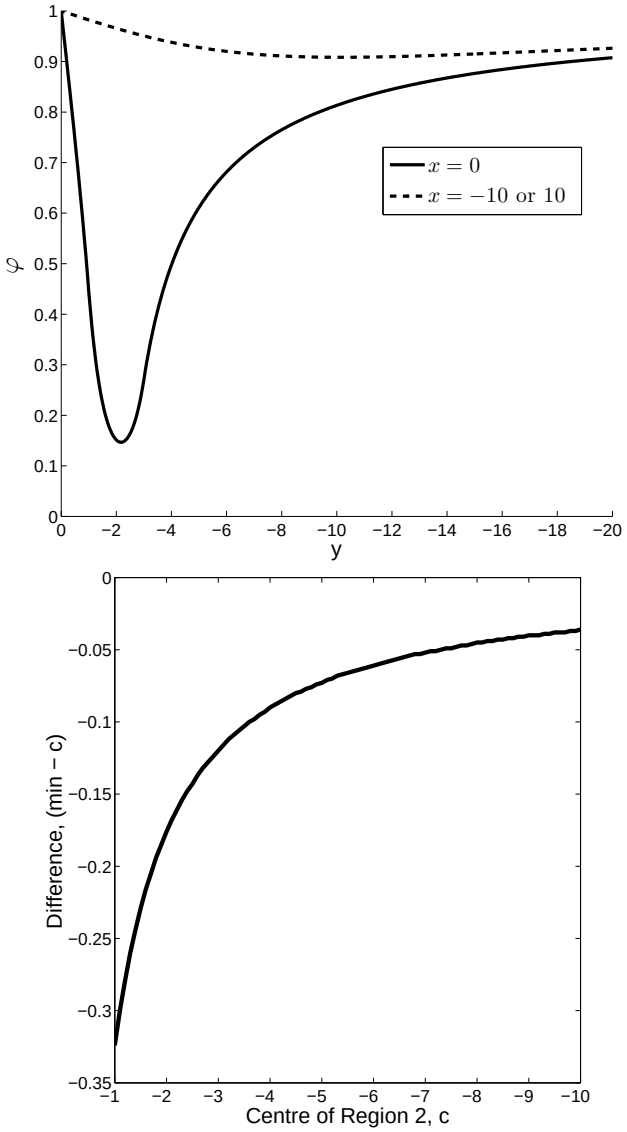

Figure 4.11: Showing that the minimum value of oxygen concentration does not coincide with the centre of region 2. The second graph is a plot of the difference between the depth of the point of minimum oxygen concentration and the centre of region 2. $r_B = 1, \mu = 1$ $D_1 = D_2 = 1, \lambda = 2$

4.5 The Anaerobic Core Model

We wish to refine our model to include a core within the circle of soil with microbial activity, B, where oxygen is no longer absorbed through respiration and instead denitrification will be taking place.

4.5.1 Concentric Circles Model, with Proportional Absorption

Our first model of this type, shown in Figure 4.12, is based on concentric circles, comparable to the three-dimensional spherical models mentioned above. The benefit of starting with this simplified model is that we can find an analytic solution as the problem is axi-symmetric.

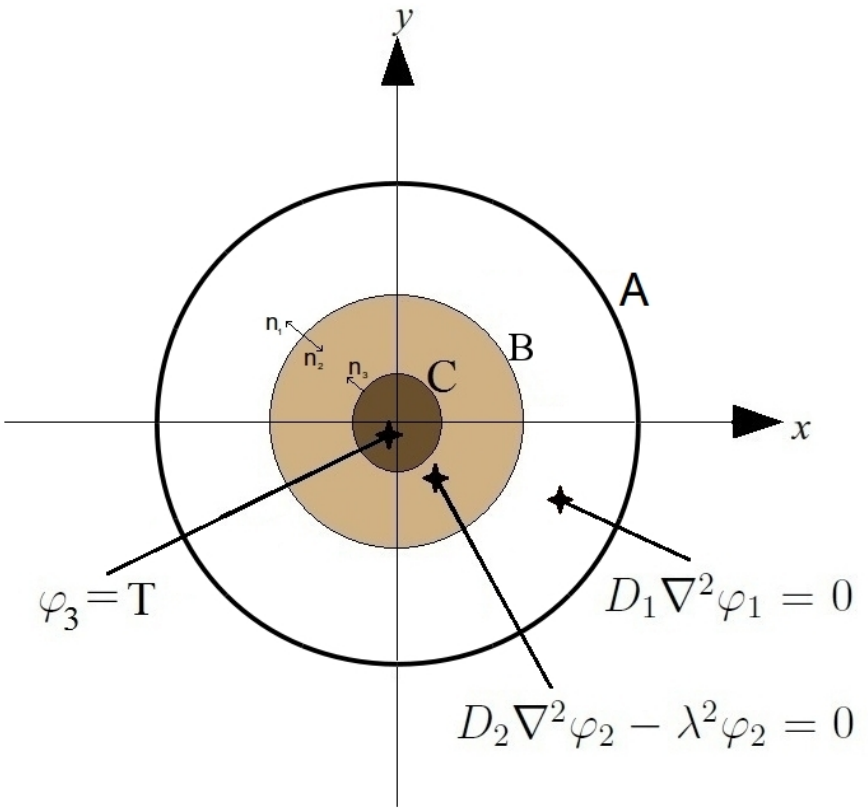

Figure 4.12: The Concentric Circle Anaerobic Core Model

In this model the area of soil with microbial activity (i.e. where the bacteria are either respiring or denitrifying) has boundary B and is once again denoted as region 2. Region 1 is the area between B and the air/soil boundary where $\varphi_1 = \mu$ which is now the outer circle A, of radius r_A. The anaerobic core, with surface C, is the innermost circle, with unknown radius, r_C. We know the value of oxygen concentration on C as this is just the given threshold value below which respiration stops. We also know there exists a no-flux condition on C, $\frac{\partial \varphi}{\partial r} = 0$. This therefore means that the concentration of oxygen throughout the core is constant at the threshold value, so $\varphi_3 = T$. The only new unknowns compared to the previous model are the position of the elements on the anaerobic core boundary.

As we know the solution is going to be axi-symmetric, φ_1 and φ_2 are constant for any given radius. Therefore we can solve Laplace's and Helmholtz's equations, for regions 1 and 2 respectively, to show,

$$\begin{aligned}
\varphi_1(r) &= a\log r + b && (4.5.1)\\
\varphi_1'(r) &= \frac{a}{r} && (4.5.2)\\
\varphi_2(r) &= \alpha I_0(mr) + \beta K_0(mr) && (4.5.3)\\
\varphi_2'(r) &= \alpha m I_1(mr) - \beta m K_1(mr), && (4.5.4)
\end{aligned}$$

where $m = \frac{\lambda}{\sqrt{D_2}}$. We can then use (4.5.1) to (4.5.4) with the boundary conditions,

$$\begin{aligned}
\varphi_1(r_A) &= \mu\\
\varphi_1(r_B) &= \varphi_2(r_B)\\
D_1\varphi_1'(r_B) &= D_2\varphi_2'(r_B)\\
\varphi_2(r_C) &= T, && (4.5.5)
\end{aligned}$$

to show,

$$\begin{pmatrix} I_0(mr_C) & K_0(mr_C) & 0 & 0\\ 0 & 0 & \log(r_A) & 1\\ -I_0(mr_B) & -K_0(mr_B) & \log(r_B) & 1\\ -mD_2I_1(mr_B) & mD_2K_1(mr_B) & \frac{D_1}{r_B} & 0 \end{pmatrix}\begin{pmatrix} \alpha\\ \beta\\ a\\ b \end{pmatrix} = \begin{pmatrix} T\\ \mu\\ 0\\ 0 \end{pmatrix}. \qquad (4.5.6)$$

We can then solve this system using a bisection method to find r_C, the radius of the anaerobic core, such that $\varphi_2'(r_C) = 0$. Alternatively, we can find expressions for a, b, α, β in terms of only r_C analytically. Using the identity, from [3],

$$I_\nu(z)K_{\nu+1}(z) + I_{\nu+1}(z)K_\nu(z) = \frac{1}{z}, \qquad (4.5.7)$$

it can be shown that,

$$\begin{aligned}
a(r_C) &= \frac{mr_BD_2T}{D_1}\left[mr_CK_1(mr_C)I_1(mr_B) - \left(\frac{1 - mr_CK_1(mr_C)I_0(mr_C)}{K_0(mr_C)}\right)K_1(mr_B)\right]\\
b(r_C) &= \mu - a(r_C)\log(r_A) && (4.5.8)
\end{aligned}$$

and,

$$\begin{aligned}
\alpha(r_C) &= mr_CTK_1(mr_C)\\
\beta(r_C) &= \frac{T - mr_CTK_1(mr_C)I_0(mr_C)}{K_0(mr_C)} && (4.5.9)
\end{aligned}$$

We then use the remaining boundary condition to show,

$$a\log(r_B) + b - \alpha I_0(mr_B) - \beta K_0(mr_B) = 0 \qquad (4.5.10)$$

from which we can find r_C, using a bisection method.

We can find the same result using the boundary element method coupled with a Newton iteration scheme to find the position of the anaerobic core. For this model we use a new Green's function for region 1. As oxygen diffuses according to Laplace's equation in this region we choose a Green's function that once again satisfies $\nabla^2 G(\mathbf{x}, \mathbf{x_0}) = -\delta(\mathbf{x} - \mathbf{x_0})$. We also again require the Green's function to have the property that $G_1(\mathbf{x}, \mathbf{x}_0) = 0$ for $\mathbf{x}$ on the air/soil boundary, A. However, as this boundary is now circular, with radius r_A, we choose,

$$G_1(\mathbf{x}, \mathbf{x}_0) = \frac{-1}{2\pi} \ln\left(\frac{r_A|\mathbf{x} - \mathbf{x}_0|}{|\mathbf{x}_0||\mathbf{x} - \frac{r_A^2}{|\mathbf{x}_0|^2}\mathbf{x}_0|} \right). \tag{4.5.11}$$

By using $\hat{\varphi}_1(x, y) = \varphi_1(x, y) - \mu$ in region 1, the integrals carried out around the boundary A will both equal zero. After applying the relevant boundary conditions from (4.5.5) our system of boundary integral equations is, for $\mathbf{x}_0$ on B,

$$\hat{\varphi_1} = -2\int_B G_1 \mathbf{n}_1 \cdot \nabla\hat{\varphi}_1 dl + 2\int_B^{PV} \hat{\varphi}_1 \mathbf{n}_1 \cdot \nabla G_1 dl \tag{4.5.12}$$

$$\begin{aligned} \hat{\varphi}_1 + \mu = {} & \frac{2D_1}{D_2}\int_B G_2 \mathbf{n}_1 \cdot \nabla\hat{\varphi}_1 dl + 2\int_B^{PV} (\hat{\varphi}_1 + \mu)\mathbf{n}_2 \cdot \nabla G_2 dl \\ & -2\int_C G_2 \mathbf{n}_3 \cdot \nabla\varphi_2 dl + 2T\int_C \mathbf{n}_3 \cdot \nabla G_2 dl, \end{aligned} \tag{4.5.13}$$

and for $\mathbf{x}_0$ on C,

$$\begin{aligned} T = {} & \frac{2D_1}{D_2}\int_B G_2 \mathbf{n}_1 \cdot \nabla\hat{\varphi}_1 dl + 2\int_B (\hat{\varphi}_1 + \mu)\mathbf{n}_2 \cdot \nabla G_2 dl \\ & -2\int_C G_2 \mathbf{n}_3 \cdot \nabla\varphi_2 dl + 2T\int_C^{PV} \mathbf{n}_3 \cdot \nabla G_2 dl. \end{aligned} \tag{4.5.14}$$

If B and C are discretized into N and M straight boundary elements respectively and we place $\mathbf{x}_0$ once in the centre of each element we will have $2N + M$ boundary integral equations. We can evaluate these integrals in the same way as in previous sections. For our Newton iteration scheme we first guess the position of the elements on the anaerobic core, C. We are then left with the unknowns $\hat{\varphi}_{1,i}$ and $(\mathbf{n}_1 \cdot \nabla\hat{\varphi}_1)_i$ for $i = 1, ..., N$, which correspond to the $\mathbf{x}_0$'s on the boundary B, and $(\mathbf{n}_3 \cdot \nabla\varphi_2)_j$ for $j = 1, ..., M$, which correspond to the $\mathbf{x}_0$'s on the guessed boundary C. We then iterate to find where $\mathbf{n}_3 \cdot \nabla\varphi_2 = 0$ by moving the end points of each anaerobic core boundary element in the outward normal direction by an amount determined by,

$$\mathbf{P}_{k+1} = \mathbf{P}_k - \mathbf{J}_k^{-1} \mathbf{n}_3 \cdot \nabla\varphi_{2,k}, \tag{4.5.15}$$

where k represents the current iteration, and $\mathbf{J}$ is the relevant Jacobian. We stop iterating when $\mathbf{n}_3 \cdot \nabla\varphi_2 = 0$, to a desired accuracy. For this concentric circles model $\mathbf{n}_3$ is always in the radial direction, and the movement of the end points is also in the radial direction. However, for our later models this is not the case, which means $\mathbf{n}_3$ and the direction of movement will be found individually for each element at each iteration.

Once the anaerobic core boundary position has been found and the boundary values have been calculated it is a simple task to find oxygen concentration at any point in the domain. Using the found boundary values all that remains is to evaluate the relevant integral equations, for $\mathbf{x}_0$ in region 1,

$$\hat{\varphi_1} = -\int_B G_1 \mathbf{n}_1 \cdot \nabla\hat{\varphi}_1 dl + \int_B \hat{\varphi}_1 \mathbf{n}_1 \cdot \nabla G_1 dl \tag{4.5.16}$$

for $\mathbf{x}_0$ in region 2,

$$\begin{aligned} \varphi_2 \quad = \quad & \frac{D_1}{D_2}\int_B G_2 \mathbf{n}_1 \cdot \nabla\hat{\varphi}_1 dl + \int_B (\hat{\varphi}_1 + \mu)\mathbf{n}_2 \cdot \nabla G_2 dl \\ & - \int_C G_2 \mathbf{n}_3 \cdot \nabla\varphi_2 dl + T\int_C \mathbf{n}_3 \cdot \nabla G_2 dl. \end{aligned} \tag{4.5.17}$$

In Figure 4.13, oxygen concentration has been plotted against radius for a set of example parameters. The figure shows that both the boundary element method and the analytical solution predict the same size of anaerobic core and the same oxygen concentration throughout the rest of the domain.

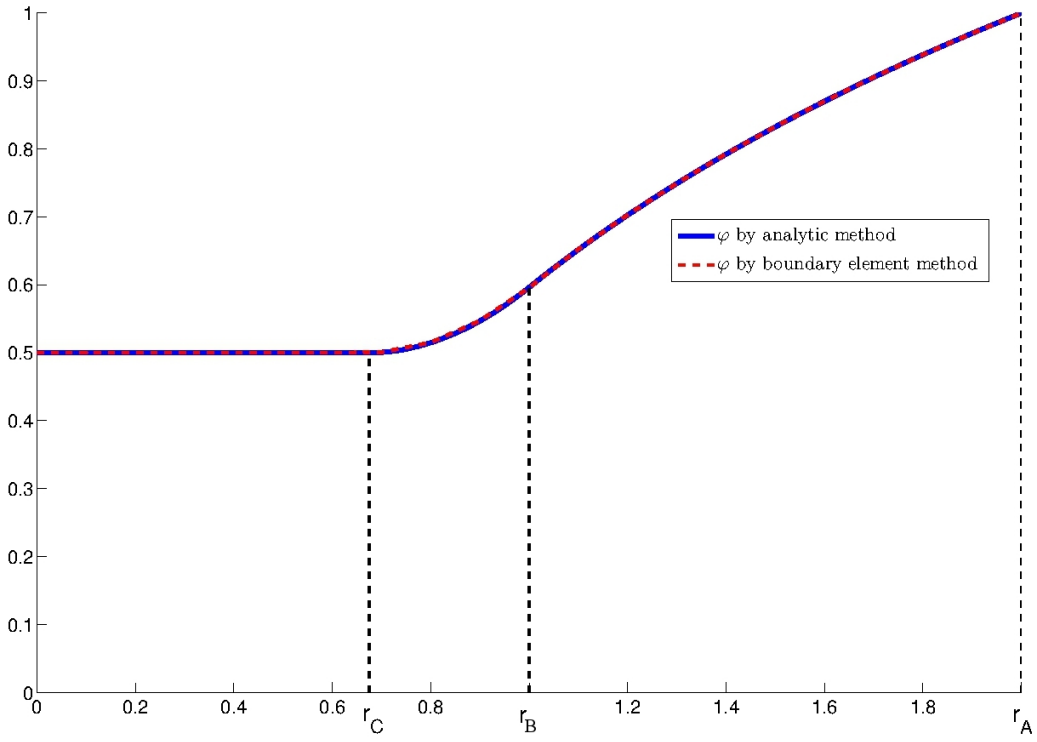

Figure 4.13: Oxygen concentration, φ, throughout the domain of the concentric circles model with proportional absorption. With $r_B = 1, \lambda = 2, D_1 = D_2 = 1$ and a threshold value of $T = 0.5$, it was found that $r_C = 0.67$.

4.5.2 Line Boundary Model, with Proportional Absorption

We now move on to the slightly more complicated model shown in Figure 4.14. The model is no longer axi-symmetric and the anaerobic core, with boundary C, will not be circular or share a centre with the outer boundary B. In order to find the solution to this problem we shall use the same boundary element method coupled with a Newton-iteration scheme as in the previous section.

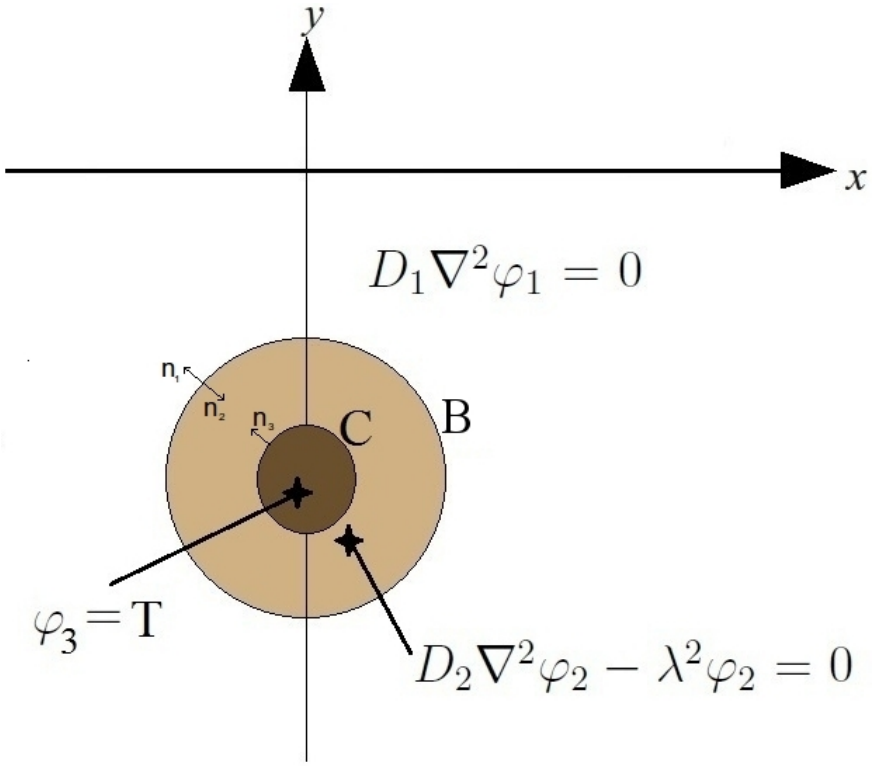

Figure 4.14: The Anaerobic Core Model with Proportional Absorption

The boundary integral equations we need to solve, after applying the relevant boundary conditions, are exactly the same as in the concentric circle case, but we now use our original Green's functions (4.4.4) and (4.4.9). First we evaluate (4.5.12) to (4.5.14) and use the Newton iteration scheme to find the boundary values and the position of the anaerobic core. Upon calculation it is seen that the anaerobic core is not centrally positioned within region 2, as predicted, and is not perfectly circular. We then can find the oxygen concentration anywhere in the domain using the integral equations (4.5.16) and (4.5.17), as shown in Figure 4.15.

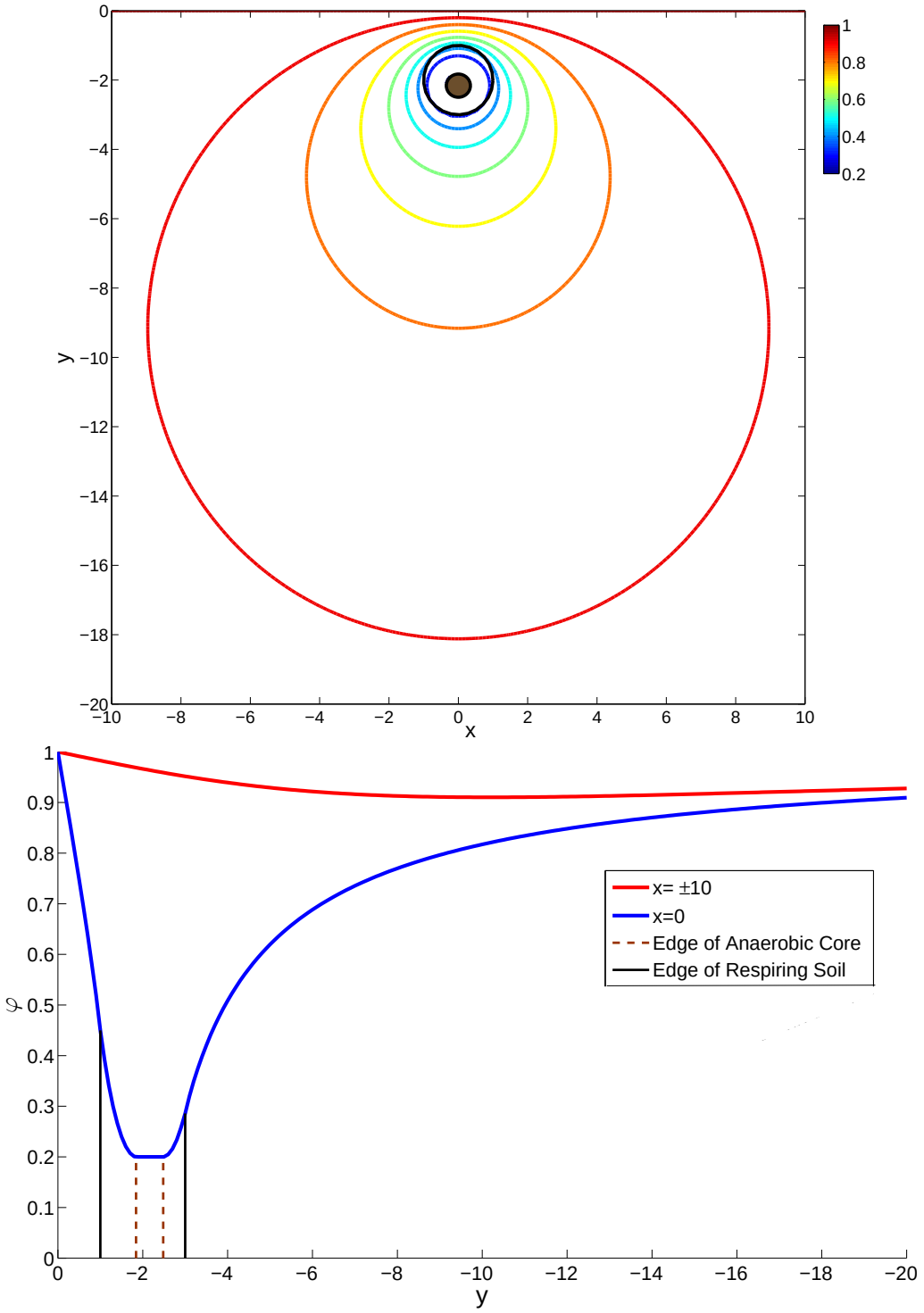

Figure 4.15: Oxygen concentration found using the proportional absorption anaerobic core model. $r_B = 1, \lambda = 2, D_1 = D_2 = 1, T = 0.2, \mu = 1$

4.5.3 Concentric Circles Model, with Constant Absorption

Now that we have a model that includes an anaerobic core we can go back to modelling using constant absorption of oxygen without the possibility of predicting negative concentrations. As mentioned previously constant absorption of oxygen is used in many papers, such as [14], to model the respiration of bacteria uniformly distributed through a sphere of solid soil. We first work with the concentric circles model, and solve the system,

$$\begin{aligned} D_1\nabla^2\varphi_1(r) = 0 \quad &\text{for} \quad r_B < r < r_A \\ D_2\nabla^2\varphi_2(r) = \lambda^2 \quad &\text{for} \quad r_C < r < r_B \\ \varphi_3 = T \quad &\text{for} \quad 0 < r < r_C. \end{aligned} \tag{4.5.18}$$

As the problem is axially symmetric we can easily solve analytically, we find that,

$$\begin{aligned} \varphi_1 &= a\log r + b \\ \varphi_1' &= \frac{a}{r} \\ \varphi_2 &= \frac{m^2r^2}{4} + \alpha\log r + \beta \\ \varphi_2' &= \frac{m^2r}{2} + \frac{\alpha}{r}, \end{aligned} \tag{4.5.19}$$

where $m^2 = \frac{\lambda^2}{D_2}$. We then apply the same boundary conditions as were used previously (4.5.5) to find the constants a, b, α, β. We can either use the matrix system,

$$\begin{pmatrix} \frac{D_1}{r_B} & 0 & \frac{-D_2}{r_B} & 0 \\ 0 & 0 & \log r_C & 1 \\ \log r_A & 1 & 0 & 0 \\ \log r_B & 1 & -\log r_B & -1 \end{pmatrix} \begin{pmatrix} \alpha \\ \beta \\ a \\ b \end{pmatrix} = \begin{pmatrix} \frac{\lambda^2 r_B}{2} \\ T - \frac{\lambda^2 r_C^2}{4D_2} \\ \mu \\ \frac{\lambda^2 r_B^2}{4D_2} \end{pmatrix}, \tag{4.5.20}$$

and then apply $\varphi_2'(r_C) = 0$ with a bisection method to find r_C, or we can work by hand to show,

$$\begin{aligned} a(r_C) &= \frac{m^2 r_B^2 D}{2} + \alpha D \\ b(r_C) &= \mu - \left(\frac{m^2 r_B^2 D}{2} + \alpha D\right)\log r_A \\ \alpha(r_C) &= \left[D\log\frac{r_B}{r_A} + \log\frac{r_C}{r_B}\right]^{-1}\left[\frac{m^2}{4}\left(r_B^2 - r_C^2\right) - \frac{m^2 r_B^2 D}{2}\log\frac{r_B}{r_A} + T - \mu\right] \\ \beta(r_C) &= T - \frac{m^2 r_C^2}{4} - \alpha\log r_C, \end{aligned} \tag{4.5.21}$$

where $D = \frac{D_2}{D_1}$. By then using $\varphi_2'(r_C) = 0$ we obtain an expression from which we can find the value of r_C,

$$0 = \frac{m^2}{2}\left(D\log\frac{r_B}{r_A} + \log\frac{r_C}{r_B} - \frac{1}{2}\right)r_C^2 + \frac{m^2 r_B^2}{4}\left(1 + 2D\log\frac{r_A}{r_B}\right) + T - \mu. \tag{4.5.22}$$

As the first term in (4.5.22) is always negative we can see from inspection that a necessary condition for the existence of an anaerobic core is,

$$T > \mu - \frac{m^2 r_B^2}{4}\left(1 + 2D\log\frac{r_A}{r_B}\right). \tag{4.5.23}$$

Therefore, our model will break down if we choose the threshold value, T, to be too low. As T represents the value of oxygen concentration below which bacteria stop respiring this value is actually a predefined constant. So instead we consider the condition (4.5.23) as a way of describing how large an area of oxygen absorbing soil must be in order for anaerobic conditions to occur within it.

To apply the boundary integral method to this problem we are going to need to find a new integral equation for inside region 2, where the governing diffusion equation is the Poisson equation, $D_2\nabla^2\varphi_2 = \lambda^2$. In order to find this new integral equation we must derive it from Green's second identity similarly to in the introduction for our previous boundary integral equations. By integrating Green's second identity over the domain we find (1.7.4). We then set $G = G_2(\mathbf{x}, \mathbf{x_0})$, where we choose G_2 to be the free space Green's function,

$$G_2(\mathbf{x}, \mathbf{x_0}) = -\frac{1}{4\pi}\log((x - x_0)^2 + (y - y_0)^2). \tag{4.5.24}$$

We then have,

$$\frac{\lambda^2}{D_2}\iint G_2 dA + \varphi_2(\mathbf{x_0}) = -\int_{B,C} G_2\mathbf{n}\cdot\nabla\varphi_2 dl + \int_{B,C}\varphi_2\mathbf{n}\cdot\nabla G_2 dl. \tag{4.5.25}$$

To deal with the new area integral on the left hand side of (4.5.25), we use Green's theorem in the plane,

$$\oint_{D'}(Ldx + Mdy) = \iint_D\left(\frac{\partial M}{\partial x} - \frac{\partial L}{\partial y}\right)dx\,dy. \tag{4.5.26}$$

So by inspection we choose,

$$\begin{aligned} M &= \frac{1}{8\pi}(-2\hat{x}\log r + \hat{x}) \\ L &= \frac{1}{8\pi}(2\hat{y}\log r - \hat{y}), \end{aligned} \tag{4.5.27}$$

where $\hat{\mathbf{x}} = \mathbf{x} - \mathbf{x}_0$ and $r = |\hat{\mathbf{x}}|$. Then we can write, using (4.5.26),

$$\begin{aligned} \iint G_2 dA &= \frac{1}{8\pi}\oint_B (2\hat{y}\log r - \hat{y})\,dx + (-2\hat{x}\log r + \hat{x})\,dy \\ &\quad -\frac{1}{8\pi}\oint_C (2\hat{y}\log r - \hat{y})\,dx + (-2\hat{x}\log r + \hat{x})\,dy. \end{aligned} \tag{4.5.28}$$

This can also be written as,

$$\iint G_2 dA = \oint_B \mathbf{a} \cdot \mathbf{t} dl - \oint_C \mathbf{a} \cdot \mathbf{t} dl, \tag{4.5.29}$$

where $\mathbf{a} = \frac{1}{8\pi}(2\hat{y}\log r - \hat{y}, -2\hat{x}\log r + \hat{x})$, and $\mathbf{t}$ is a unit vector tangent to each boundary. This can then be integrated using Gauss-Legendre quadrature, in the same way as the other boundary integrals for this model. It can be shown from (4.5.25) that for $\mathbf{x}_0$ on B,

$$\hat{\varphi_1} = -2\int_B G_1 \mathbf{n}_1 \cdot \nabla\hat{\varphi}_1 dl + 2\int_B^{PV} \hat{\varphi}_1 \mathbf{n}_1 \cdot \nabla G_1 dl \tag{4.5.30}$$

$$\begin{aligned}\hat{\varphi}_1 + \mu = {} & \frac{2}{D}\int_B G_2 \mathbf{n}_1 \cdot \nabla\hat{\varphi}_1 dl + 2\int_B^{PV} (\hat{\varphi}_1 + \mu)\mathbf{n}_2 \cdot \nabla G_2 dl - 2m^2 \oint_B \mathbf{a} \cdot \mathbf{t} dl \\ & -2\int_C G_2 \mathbf{n}_3 \cdot \nabla\varphi_2 dl + 2T\int_C \mathbf{n}_3 \cdot \nabla G_2 dl + 2m^2 \oint_C \mathbf{a} \cdot \mathbf{t} dl,\end{aligned} \tag{4.5.31}$$

and for $\mathbf{x}_0$ on C,

$$\begin{aligned}T = {} & \frac{2}{D}\int_B G_2 \mathbf{n}_1 \cdot \nabla\hat{\varphi}_1 dl + 2\int_B (\hat{\varphi}_1 + \mu)\mathbf{n}_2 \cdot \nabla G_2 dl - 2m^2 \oint_B \mathbf{a}.\mathbf{t} dl \\ & -2\int_C G_2 \mathbf{n}_3 \cdot \nabla\varphi_2 dl + 2T\int_C^{PV} \mathbf{n}_3 \cdot \nabla G_2 dl + 2m^2 \oint_C \mathbf{a}.\mathbf{t} dl,\end{aligned} \tag{4.5.32}$$

where G_1 is given by (4.5.11). As with the proportional absorption model we also need to use a Newton iteration scheme in order to find the position of the boundary, C. Once the position of C is known, and the boundary values have been calculated we can find the oxygen concentration at any point in the domain. For $\mathbf{x}_0$ in region 1,

$$\hat{\varphi_1} = -\int_B G_1 \mathbf{n}_1 \cdot \nabla\hat{\varphi}_1 dl + \int_B \hat{\varphi}_1 \mathbf{n}_1 \cdot \nabla G_1 dl \tag{4.5.33}$$

and for $\mathbf{x}_0$ in region 2,

$$\begin{aligned}\varphi_2 = {} & \frac{1}{D}\int_B G_2 \mathbf{n}_1 \cdot \nabla\hat{\varphi}_1 dl + \int_B (\hat{\varphi}_1 + \mu)\mathbf{n}_2 \cdot \nabla G_2 dl - m^2 \oint_B \mathbf{a}.\mathbf{t} dl \\ & -\int_C G_2 \mathbf{n}_3 \cdot \nabla\varphi_2 dl + T\int_C \mathbf{n}_3 \cdot \nabla G_2 dl + m^2 \oint_C \mathbf{a}.\mathbf{t} dl,\end{aligned} \tag{4.5.34}$$

We can then compare the solution of this to the exact solution found above, as shown in Figure 4.16.

We can also compare the solution of the constant absorption model to that of the proportional absorption model. The most important difference is the change in area of the anaerobic core, as this is directly related to the amount of denitrification that can take place within the soil. Modelling using proportional absorption of oxygen predicts an anaerobic core of smaller area than in the constant absorption model. As should be clear, if λ is chosen to have the same value in both models then the amount of oxygen absorption is greater in the constant absorption model when oxygen concentration is less than one.

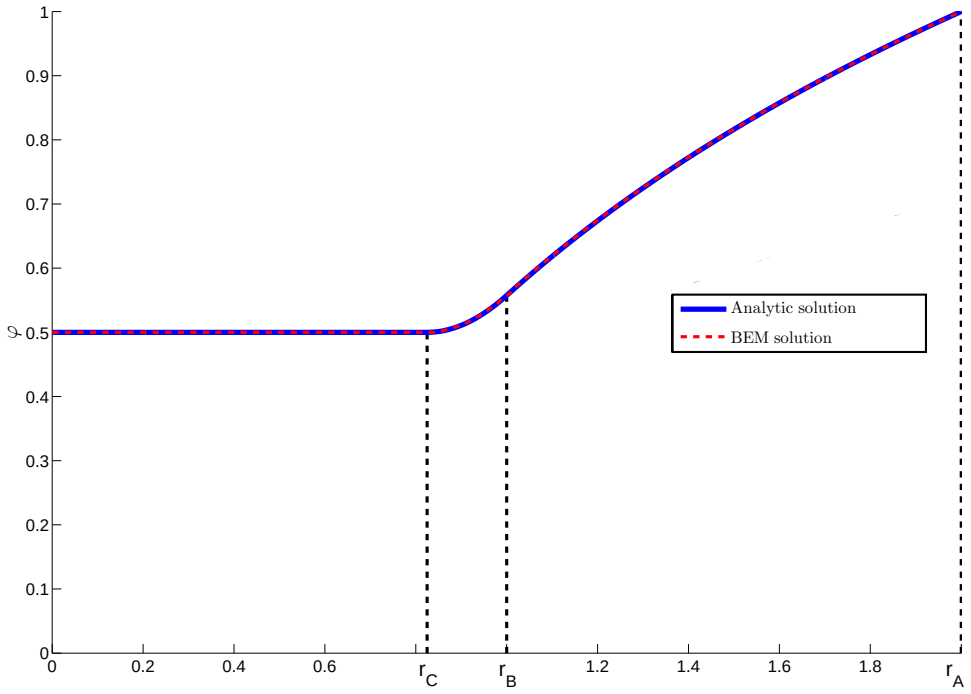

Figure 4.16: Oxygen concentration, φ, throughout the domain of the concentric circle model with constant absorption. With $r_B = 1, \lambda = 2, D_1 = D_2 = 1$ and a threshold value of $T = 0.5$, it was found that $r_C = 0.82$.

4.5.4 Line Boundary Model, with Constant Absorption

We now move on to our most realistic model so far. In this model an area of soil is positioned below a boundary representing the ground at $y = 0$. In this area of soil oxygen is absorbed at a constant rate until anaerobic conditions are reached. As in the similar proportional absorption model, once again as the model is not axi-symmetric the anaerobic core will not be positioned centrally in region 2, and it will not be perfectly circular. This model is first discussed in the introduction and is shown in Figure 1.5.

We compute solutions for this model using boundary integral equations which are the same as those used in the concentric circles version of the model, (4.5.30) to (4.5.32). However, we now use our original Green's function G_1, given by (4.4.4), which gives $G_1 = 0$ on $y = 0$. As before we evaluate the relevant integral equations and apply a Newton iteration scheme to find the position of the boundary elements on the edge of the anaerobic core.

The overall result shows similar oxygen distribution throughout the domain as seen above for the proportional absorption model. The plots in Figure 4.17 show the decrease in oxygen around the area of absorption and a return to the background level as distance from region 2 is increased. This is because we still have only included a finite area of oxygen absorption in an infinitely wide domain.

Figure 4.18 shows a comparison of the size and shape of the anaerobic cores found from the constant and proportional absorption models for the same set of parameters. As mentioned earlier as we have $\varphi \leq 1$ throughout the domain oxygen absorption is greater

for the constant absorption model which means a larger anaerobic core.

As discussed in the introduction we consider the inclusion of the air/soil boundary at $y = 0$ to be more realistic than previous models found in the literature, where an aggregate of soil has a constant level of oxygen surrounding it. Such a model would only predict central circular anaerobic cores as it would be axi-symmetric. A solution of this type is additionally plotted in Figure 4.18. On the boundary B oxygen concentration is taken to be constant and equal to the level in the air. The oxygen inside B then diffuses and is absorbed according to the same Poisson equation as in the constant absorption model above. We notice that the anaerobic core found is central and circular and much smaller than those found using our new models. Our results nicely illustrate how our model predicts the centre of the anaerobic core to be lower than the centre of region 2. This is even more evident if region 2 is positioned closer to the boundary A. Anaerobic core shape and size differences for increasing depth are considered in more detail for biologically realistic parameters in the results section of this thesis. For now we note that it appears the area of the anaerobic core is going to increase with depth until it reaches a finite limit.

The model we have developed here could be thought of as representing a single soil aggregate at a depth below ground. However, this would then imply that region 1 consists solely of air, and therefore the model would not be so realistic. In order to realistically model an aggregated soil it would be important to include many soil aggregates in order to properly represent the ground. This will be considered in a later chapter.

For our current model region 2 should be considered as an area of high microbial activity within an area of solid (i.e. non-aggregated) soil with much lower microbial activity. Therefore everywhere below $y = 0$ would be solid soil but oxygen absorption shall only occur inside B. A likely cause for the development of such an area could be a region of decomposing organic matter. The results shown in the various figures here then show the oxygen concentration throughout a large area of soil, and the fraction that is denitrifying can be found. If considering the model in this manner, we would always choose $D_1 = D_2$, as the diffusion of oxygen would be the same in regions 1 and 2. If we were to consider region 1 to be air, we would have $D_2 \ll D_1$ as oxygen diffusion is much faster through air than through soil. This is discussed in detail and expanded upon in the following section.

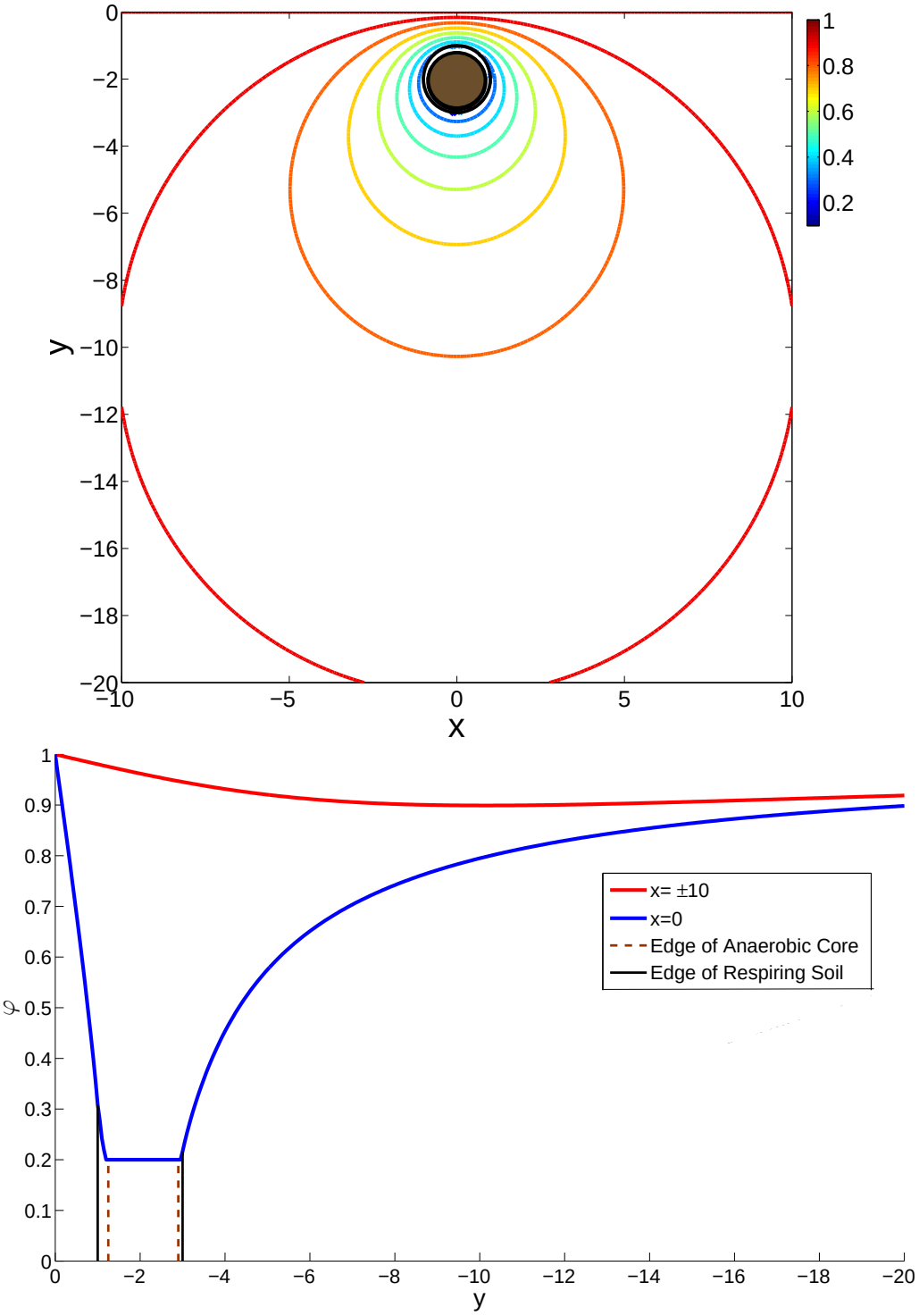

Figure 4.17: Oxygen concentration found using the constant absorption anaerobic core model. $r_B = 1$, $\lambda = 2$, $D_1 = D_2 = 1$, $T = 0.2$, $\mu = 1$

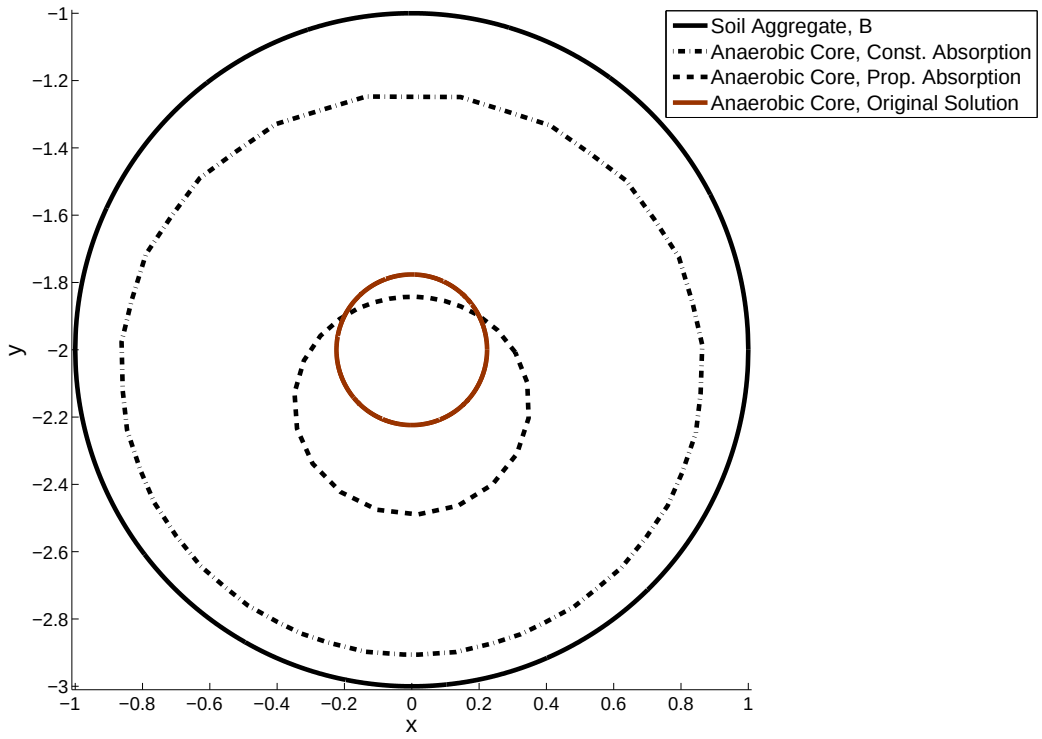

Figure 4.18: Comparing anaerobic core sizes created by the different oxygen-absorption definitions, for $T = 0.2, \lambda = 2, \mu = 1, D_1 = D_2 = 1$.

4.6 An Asymptotic Expansion Method

Eventually in this thesis we shall construct a model of an aggregated soil. This model will resemble a cross section of the ground with an infinite array of circular oxygen-absorbing soil aggregates surrounded by air or water. Within each of these aggregates the diffusion of oxygen will be much slower than in the air or water around them. This is discussed in the introduction, and in [14] and [38] among others. Therefore, the model of aggregated soil will have the property that,

$$\frac{D_2}{D_1} = \epsilon \ll 1. \tag{4.6.1}$$

This small parameter then allows us to perform some asymptotic analysis.

We shall initially work with models that consist of only a single soil aggregate, similar to those previously developed. In this chapter each problem will be split into two parts, the region 1 problem with oxygen concentration φ and the region 2 problem where absorption occurs with oxygen concentration ψ. Whilst a single aggregate of soil surrounded by fast diffusing air may seem similar to the three-dimensional model mentioned in the introduction, we shall still work to include the boundary at $y = 0$ where the oxygen concentration is kept constant. This will mean that the models with this line boundary will once again include anaerobic cores that are not axi-symmetric.

We begin the asymptotic work by writing,

$$\varphi = \varphi_0 + \epsilon\varphi_1 \tag{4.6.2}$$

$$\psi = \psi_0 + \epsilon\psi_1 \tag{4.6.3}$$

$$\text{and} \quad r_C = r_{C,0} + \epsilon r_{C,1}. \tag{4.6.4}$$

Note that we only expand the radius of the anaerobic core boundary, C, as this is unknown, whereas the other two boundaries are set in the definition of the model. We choose $r_{C,0}$ to be constant and allow slight variations in r_C by setting $r_{C,1}$ to be a function of θ. Once again, the value of the anaerobic core radius, r_C, is the most important value to find as it can be used to give a direct indication of how much denitrification is occurring within the soil.

4.6.1 Concentric Circles Model, with Constant Absorption

We start by considering the simpler concentric circles model, as this makes the problem axi-symmetric, and r_C will be constant. The constant absorption concentric circles model is shown in Figure 4.19.

The $O(1)$ problem for region 1 is shown on the left of Figure 4.20. From inspection it is clear that the only possible solution is

$$\varphi_0 = \mu \tag{4.6.5}$$

everywhere in the region 1.

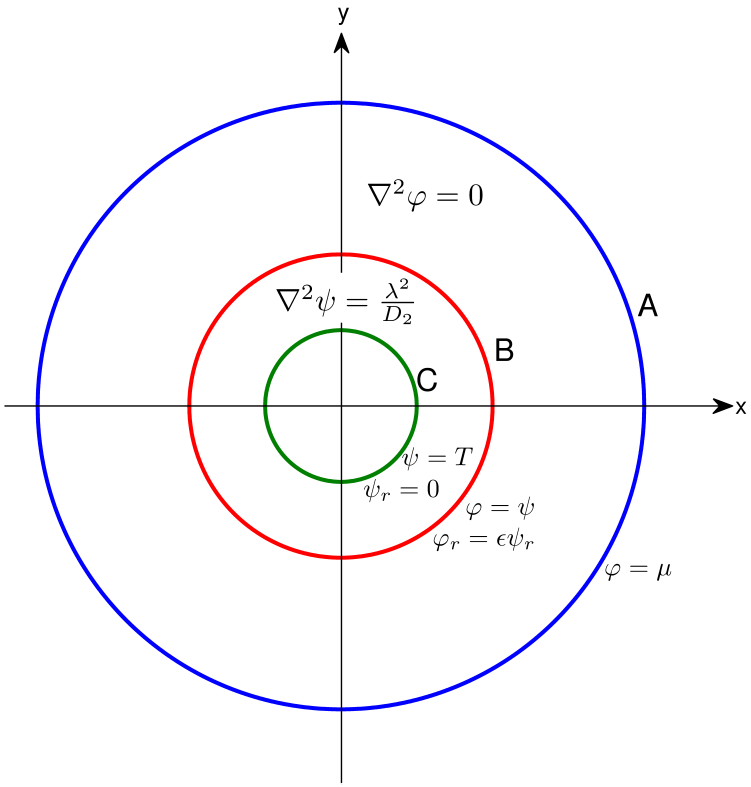

Figure 4.19: The concentric circle constant absorption model

For region 2, we now have the problem shown on the right of Figure 4.20. The boundary condition on B is straightforward and follows from finding $\varphi_0 = \mu$ everywhere, so $\psi_0(r_B) = \mu$. This condition is equivalent to that used in the aforementioned three-dimensional models from the literature. Due to this boundary condition we shall find the same solution within region 2 for the $O(1)$ part of the problem in both the concentric circles and line boundary models. Clearly the full solution more closely matches the $O(1)$ solution as $\epsilon \to 0$. We assume that $D_2 \neq 0$ and so $\epsilon \to 0$ would require $D_1 \to \infty$. If this was the case the oxygen in region 1 would be diffusing infinitely fast so that oxygen would be evenly distributed around the boundary B, and therefore the effect of the boundary at $y = 0$ would be completely nullified.

For the boundary conditions on C, we expand our original two conditions,

$$\psi(r_C) = T \tag{4.6.6}$$

$$\psi_r(r_C) = 0, \tag{4.6.7}$$

to show that,

$$\psi_0(r_{C,0}) + \epsilon[\psi_1(r_{C,0}) + r_{C,1}\psi_0'(r_{C,0})] = T \tag{4.6.8}$$

$$\psi_0'(r_{C,0}) + \epsilon[\psi_1'(r_{C,0}) + r_{C,1}\psi_0''(r_{C,0})] = 0, \tag{4.6.9}$$

so that in the $O(1)$ problem we have

$$\psi_0(r_{C,0}) = T \tag{4.6.10}$$

$$\psi_0'(r_{C,0}) = 0. \tag{4.6.11}$$

Inside region 2 the governing diffusion equation is $\nabla^2\psi_0 = \frac{\lambda^2}{D_2}$, which can be easily integrated as the problem depends only on the radial variable, r. We solve,

$$\frac{1}{r}\frac{d}{dr}\left(r\frac{d\psi_0}{dr}\right) = \frac{\lambda^2}{D_2}, \tag{4.6.12}$$

and apply the boundary condition on C (4.6.10), and the continuity condition on B, to show that,

$$\psi_0 = \frac{m^2}{4}\left(r^2 - r_B^2\right) + \mu + \left[\frac{T - \frac{m^2}{4}\left(r_{C,0}^2 - r_B^2\right) - \mu}{\log\left(\frac{r_{C,0}}{r_B}\right)}\right]\log\left(\frac{r}{r_B}\right), \tag{4.6.13}$$

where we have set $m^2 = \frac{\lambda^2}{D_2}$. This leaves $r_{C,0}$, the $O(1)$ part of the radius of the anaerobic core, as the only unknown in the $O(1)$ problem. To find $r_{C,0}$ we apply the last boundary condition on C (4.6.11), to (4.6.13), which gives,

$$0 = m^2 r_{C,0}^2 \log\left(\frac{r_{C,0}}{r_B}\right) + 2\left(T - \mu\right) - \frac{m^2}{2}\left(r_{C,0}^2 - r_B^2\right), \tag{4.6.14}$$

which we can solve for $r_{C,0}$ using a bisection method. Note that in the full solution to the concentric circles model found earlier we can arrive at the same equation for r_C by setting $D = 0$ in (4.5.22). This is a good check to confirm our current asymptotic solution is correct. We also note that a biologically realistic solution for $r_{C,0}$ requires that,

$$0 < r_{C,0} < r_B. \tag{4.6.15}$$

By then considering these limits in (4.6.14) we see that in for an anaerobic core to exist,

$$\lambda^2 > \frac{4D_2(\mu - T)}{r_B^2}. \tag{4.6.16}$$

We also see that the aggregate will only be entirely anaerobic if $T = \mu$, which will not be true for biologically realistic parameters.

For the $O(\epsilon)$ problem in region 1, which is shown on the left of Figure 4.21, we will substitute in the $O(1)$ solution into the flux continuity condition on B. We can then integrate $\nabla^2\varphi_1 = 0$, and apply the boundary conditions on A and B to show that,

$$\varphi_1 = \left[\frac{m^2 r_B^2}{2} + \frac{T - \frac{m^2}{4}\left(r_{C,0}^2 - r_B^2\right) - \mu}{\log\left(\frac{r_{C,0}}{r_B}\right)}\right]\log\left(\frac{r}{r_A}\right) \tag{4.6.17}$$

For the $O(\epsilon)$ problem in region 2, which is shown on the right of Figure 4.21, we use the boundary conditions $\psi_1(r_B) = \varphi_1(r_B)$, from continuity on B and $\psi_1(r_{C,0}) = 0$ on C. The

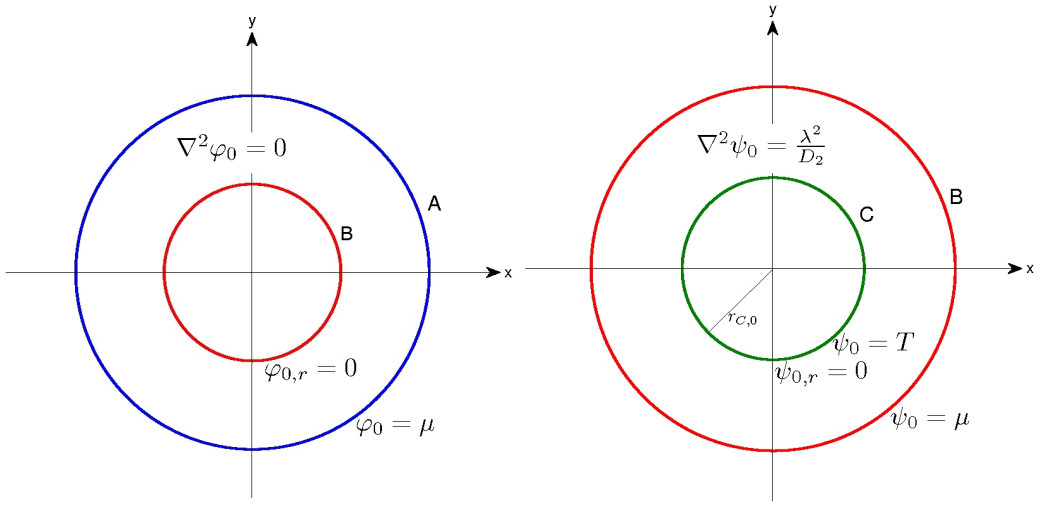

Figure 4.20: The concentric circle constant absorption $O(1)$ problem.
Left: Region 1. Right: Region 2.

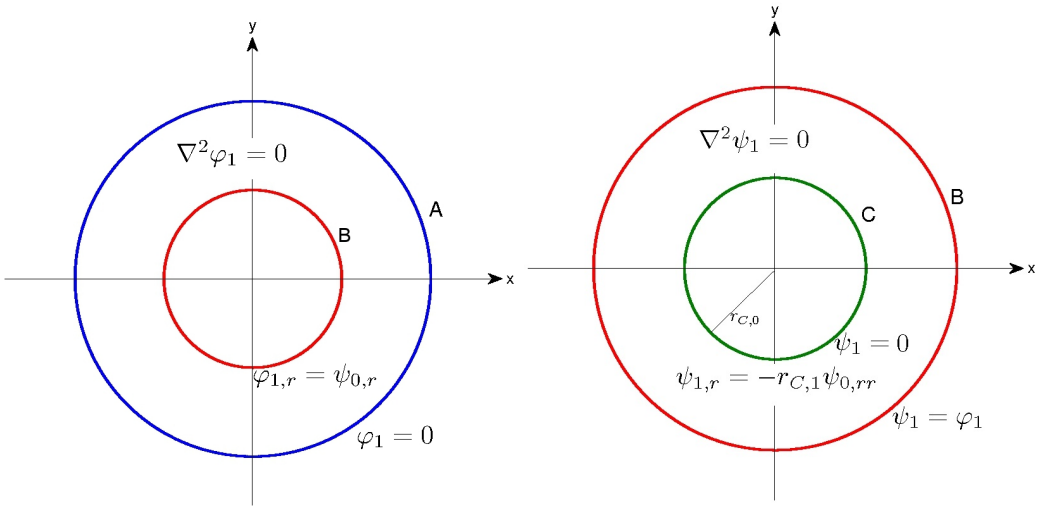

Figure 4.21: The concentric circle constant absorption $O(\epsilon)$ problem.
Left: Region 1. Right: Region 2.

latter is true because we know from (4.6.8), that

$$\psi_1(r_{C,0}) + r_{C,1}\psi_0'(r_{C,0}) = 0, \tag{4.6.18}$$

and it is already known that, $\psi_0'(r_{C,0}) = 0$, from (4.6.9). Therefore, we can integrate $\nabla^2\psi_1 = 0$ and show,

$$\psi_1(r) = \left[\frac{m^2 r_B^2}{2} + \frac{T - \frac{m^2}{4}\left(r_{C,0}^2 - r_B^2\right) - \mu}{\log\left(\frac{r_{C,0}}{r_B}\right)}\right]\left(\frac{\log r_A}{\log r_{C,0}}\right)\log\left(\frac{r}{r_{C,0}}\right). \tag{4.6.19}$$

We can find the value of $r_{C,1}$, using the $O(\epsilon)$ terms of (4.6.9),

$$\psi_1'(r_{C,0}) + r_{C,1}\psi_0''(r_{C,0}) = 0. \tag{4.6.20}$$

We can solve this analytically, and after rearranging show that,

$$r_{C,1} = \left(\frac{m^2 r_B^2}{2} + \frac{\left(T - \frac{m^2}{4}\left(r_{C,0}^2 - r_B^2\right) - \mu\right) \log r_A}{r_{C,0} \log r_{C,0} \log\left(\frac{r_{C,0}}{r_B}\right)} \right) \left(\frac{m^2}{2} - \left[\frac{T - \frac{m^2}{4}\left(r_{C,0}^2 - r_B^2\right) - \mu}{\log\left(\frac{r_{C,0}}{r_B}\right)} \right] \right)^{-1} \tag{4.6.21}$$

4.6.2 Concentric Circles Model, with Proportional Absorption

We shall now also conduct asymptotic analysis on the proportional absorption concentric circles model, shown in Figure 4.22. We can then compare anaerobic core size with the constant absorption version of the model.

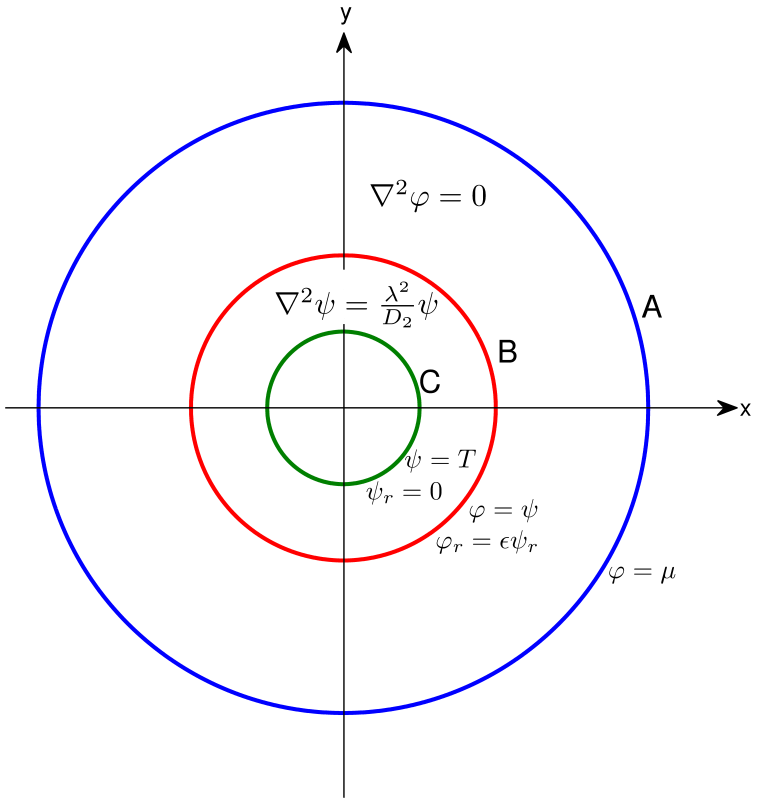

Figure 4.22: The concentric circle proportional absorption model

The derivation of the solutions is very similar to the method used in the constant absorption model. In region 1, we can once again find φ_0 by inspection.

$$\varphi_0(r) = \mu. \tag{4.6.22}$$

In region 2, we have

$$\nabla^2\psi_0 = \frac{\lambda^2}{D_2}\psi_0, \tag{4.6.23}$$

where as ψ_0 depends only on r we can rearrange to the modified Bessel equation,

$$r\frac{d^2\psi_0}{dr^2} + \frac{d\psi_0}{dr} - m^2 r\psi_0 = 0, \tag{4.6.24}$$

with $m^2 = \frac{\lambda^2}{D_2}$. The solution is therefore in the form of modified Bessel functions and by applying the relevant boundary conditions we find,

$$\psi_0(r) = \alpha_0 I_0(mr) + \beta_0 K_0(mr), \tag{4.6.25}$$

where,

$$\begin{aligned} \alpha_0 &= \frac{\mu K_0(mr_{C,0}) - T K_0(mr_B)}{I_0(mr_B)K_0(mr_{C,0}) - I_0(mr_{C,0})K_0(mr_B)} \\ \beta_0 &= \frac{T - \alpha_0 I_0(mr_{C,0})}{K_0(mr_{C,0})}. \end{aligned} \tag{4.6.26}$$

As above, we use the remaining $O(1)$ boundary condition to find an equation from which we can find $r_{C,0}$ using a bisection method. The $r_{C,0}$ equation is,

$$0 = m\alpha_0 I_1(mr_{C,0}) - m\beta_0 K_1(mr_{C,0}). \tag{4.6.27}$$

The $O(\epsilon)$ region 1 problem is solved straightforwardly by integrating $\nabla^2\varphi_1 = 0$ and applying the flux continuity condition, similarly to in the constant absorption model equivalent, we find that,

$$\varphi_1(r) = (mr_B\alpha_0 I_1(mr_B) - mr_B\beta_0 K_1(mr_B)) \log\left(\frac{r}{r_A}\right). \tag{4.6.28}$$

For the region 2 $O(\epsilon)$ problem, we must solve, $\nabla^2\psi_1 = m^2\psi_1$, and so we will once again arrive at a modified Bessel equation, to which we can find the solution,

$$\psi_1(r) = \alpha_1 I_0(mr) + \beta_1 K_0(mr). \tag{4.6.29}$$

Using the continuity condition on B and $\psi_1(r_{C,0}) = 0$, as shown earlier, we can find the values of the constants to be,

$$\begin{aligned} \alpha_1 &= \frac{-\beta_1 K_0(mr_{C,0})}{I_0(mr_{C,0})} \\ \beta_1 &= \frac{I_0(mr_{C,0})\left[mr_B\alpha_0 I_1(mr_B) - mr_B\beta_0 K_1(mr_B)\right]\log\left(\frac{r_B}{r_A}\right)}{I_0(mr_{C,0})K_0(mr_B) - I_0(mr_B)K_0(mr_{C,0})}. \end{aligned} \tag{4.6.30}$$

The $O(\epsilon)$ anaerobic core radius term can be found from the remaining boundary condition. It can be shown that,

$$r_{C,1} = \frac{-m\alpha_1 I_1(mr_{C,0}) + m\beta_1 K_1(mr_{C,0})}{\frac{\alpha_0 m^2}{2}\left(I_0(mr_{C,0}) + I_2(mr_{C,0})\right) + \frac{\beta_0 m^2}{2}\left(K_0(mr_{C,0}) + K_2(mr_{C,0})\right)}. \tag{4.6.31}$$

We now have all the elements of the solutions of both the proportional absorption and constant absorption concentric circles models, up to and including $O(\epsilon)$ terms. Solutions for a set of example parameters are shown in (4.23), which can be used to compare the differences between the two models.

Upon plotting the oxygen concentration against radius, as in (4.23), we see that there is only a small decrease in oxygen levels in region 1. However, there is a sharp decrease in oxygen concentration upon entering region 2 at the outer edge of the soil aggregates. This is clearly due to the high diffusion coefficient outside of the aggregate, which allows for oxygen to move quickly from the air at A to the edge of the aggregate at B. Once the oxygen enters the aggregate it diffuses much slower and is absorbed until it reaches the threshold value. We find again that whilst $\psi < 1$, there will be more absorption in the constant absorption model and therefore a larger anaerobic core.

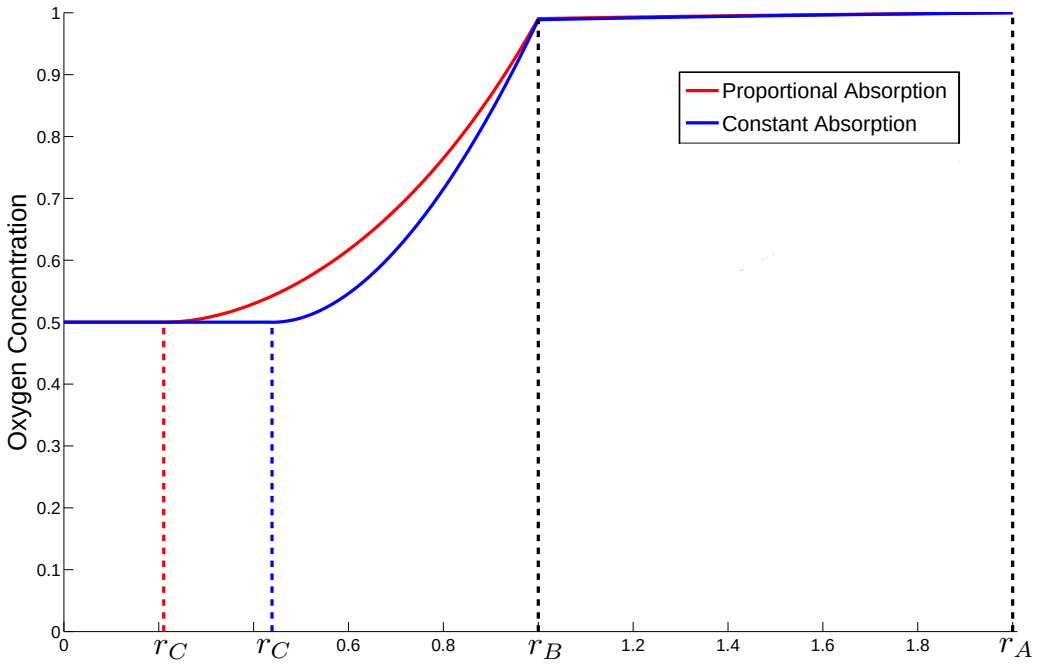

Figure 4.23: Comparing oxygen distribution throughout the concentric circles models. $D_1 = 100$, $D_2 = 1$, $\lambda = 2$ and the threshold, $T = 0.5$

4.6.3 Line Boundary Model, with Constant Absorption

For the more realistic models, with the air/soil boundary at $y = 0$, it is possible to do very similar asymptotic analysis. The main difference between the two types of model is that $r_{C,1}$ must now be a function of both r and θ, as the straight line boundary at $y = 0$ will make the anaerobic core no longer axi-symmetric. As will be shown below, the difference in core shape will not be apparent in the $O(1)$ problem, and will only be realised at the $O(\epsilon)$ level.

Firstly we work with the constant oxygen absorption version of the model, as shown in Figure 4.24.

For the $O(1)$ problem, shown on the left in Figure 4.25, it is clear from inspection that the only possible solution is

$$\varphi_0 = \mu \tag{4.6.32}$$

everywhere in region 1.

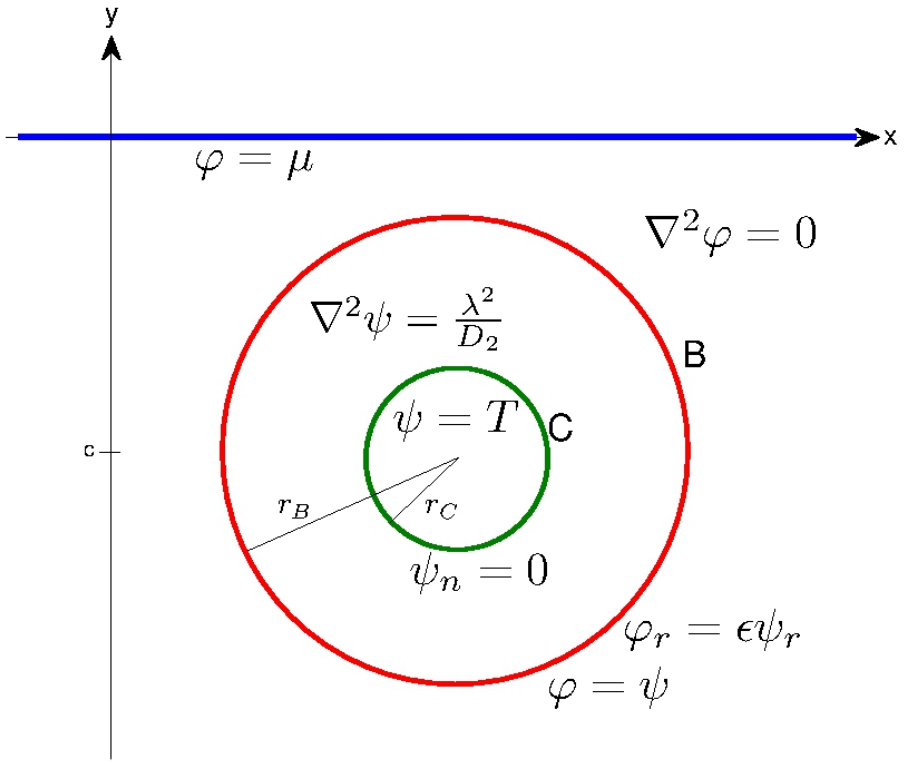

Figure 4.24: The line boundary constant absorption model

In region 2 we have the problem shown in the picture on the right of Figure 4.25. The boundary condition on B is straightforward and follows from finding $\varphi_0 = \mu$ everywhere, so $\psi_0(r_B, \theta) = \mu$. For the boundary conditions on C, we must expand our original two conditions,

$$\psi(r_C) = T \tag{4.6.33}$$

$$\psi_n(r_C) = 0. \tag{4.6.34}$$

This is exactly the same as in the concentric circles model, but we now must use the normal derivative instead of the derivative in the radial direction, as the anaerobic core might not be circular. We treat the normal derivative with care by noting that on C,

$$\mathbf{n} = \frac{\nabla(r - r_C)}{|\nabla(r - r_C)|} = \frac{1}{M}\left(1, \frac{-r'_C}{r}\right), \tag{4.6.35}$$

where,

$$M = \left(1 + \frac{r'^2_C}{r^2}\right)^{\frac{1}{2}} = 1 + O(\epsilon^2), \tag{4.6.36}$$

because, $r'_C = \epsilon r'_{C,1}$, as $r_{C,0}$ is a constant. Then using the definition of the normal (4.6.35), we can write the normal derivative as,

$$\psi_{\mathbf{n}} = \mathbf{n}.\nabla\psi = \psi_r - \frac{r'_C}{r^2}\psi_\theta = \psi_{0,r} + \epsilon\psi_{1,r} + O(\epsilon^2), \tag{4.6.37}$$

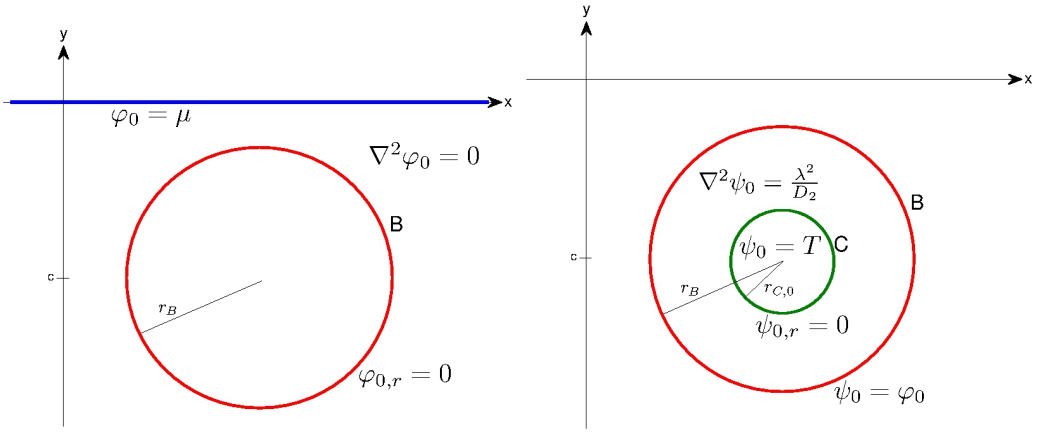

Figure 4.25: The line boundary constant absorption $O(1)$ problem.
Left: Outer problem. Right: Inner problem.

which uses the fact that we know ψ_0 will be a function of r only. We have therefore shown that for our asymptotic approximation, if we do not include $O(\epsilon^2)$ terms, the normal derivative on the anaerobic core boundary is actually only radially dependent. This makes it the same as the concentric circles model. Therefore if we use the normal derivative as given in (4.6.37), we find the same expansion of the boundary conditions (4.6.34), which gives,

$$\psi_0(r_{C,0}) + \epsilon[\psi_1(r_{C,0}) + r_{C,1}\psi_{0,r}(r_{C,0})] = T \tag{4.6.38}$$

$$\psi_{0,r}(r_{C,0}) + \epsilon[\psi_{1,r}(r_{C,0}) + r_{C,1}\psi_{0,rr}(r_{C,0})] = 0. \tag{4.6.39}$$

We can then infer from (4.6.38) and (4.6.39) the same anaerobic core boundary conditions as above,

$$\psi_0(r_{C,0}) = T \tag{4.6.40}$$

$$\psi_0'(r_{C,0}) = 0. \tag{4.6.41}$$

This means when we solve the $O(1)$ problem in region 2 we find the same solution as when we solved for the concentric circles model. We find that,

$$\psi_0 = \frac{m^2}{4}\left(r^2 - r_B^2\right) + \mu + \left[\frac{T - \frac{m^2}{4}\left(r_{C,0}^2 - r_B^2\right) - \mu}{\log\left(\frac{r_{C,0}}{r_B}\right)}\right]\log\left(\frac{r}{r_B}\right), \tag{4.6.42}$$

where we have set $m^2 = \frac{\lambda^2}{D_2}$. This leaves $r_{C,0}$ as the only unknown in the $O(1)$ problem, to find it we apply the last boundary condition on C (4.6.41), to (4.6.42), which gives,

$$0 = m^2 r_{C,0}^2 \log\left(\frac{r_{C,0}}{r_B}\right) + 2\left(T - \mu\right) - \frac{m^2}{2}\left(r_{C,0}^2 - r_B^2\right), \tag{4.6.43}$$

which we can solve for $r_{C,0}$ using a bisection method.

As the above solution is the same as for the related concentric circles model we have

now proven that for the $O(1)$ problem, or when $\epsilon = 0$ in the full problem, the line boundary at $y = 0$ has no effect on the size or shape of the anaerobic core.

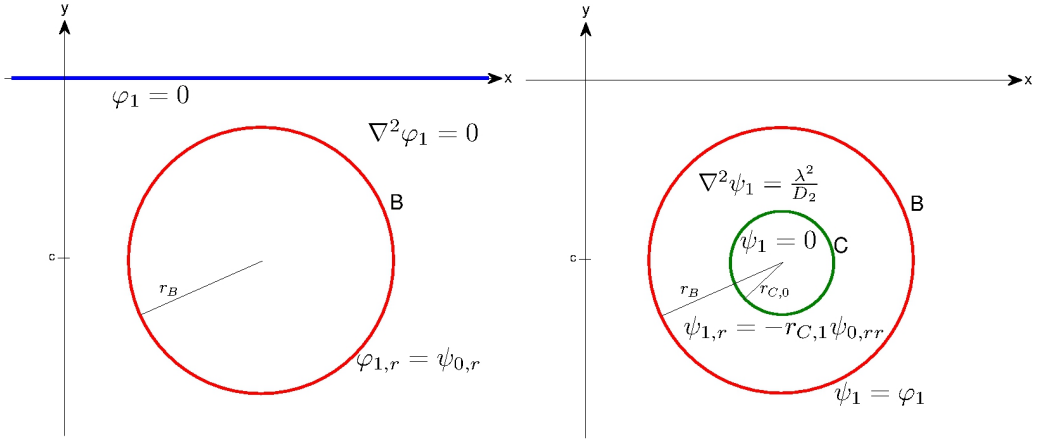

Figure 4.26: The line boundary constant absorption $O(\epsilon)$ problem.
Left: Region 1. Right: Region 2.

The first differences between the line boundary model and the concentric circles model appear now in the $O(\epsilon)$ problem in region 1, which is shown on the left of Figure 4.26. In order to find a solution in region 1 we use bipolar coordinates, similar to those used by [10], to solve a problem involving two cylinders. We define,

$$\begin{aligned} x &= \frac{r_B \sinh\eta_1 \sin\xi}{\cosh\eta - \cos\xi} \\ y &= \frac{-r_B \sinh\eta_1 \sinh\eta}{\cosh\eta - \cos\xi}, \end{aligned} \tag{4.6.44}$$

where η_1, is some constant such that $\varphi(\eta_1, \xi)$, gives the edge of the soil aggregate. The clearest way to understand how this coordinate system works is to keep η constant and vary ξ from 0 to 2π, as shown in Figure 4.27.

Using the defined bipolar coordinate system $\xi = 0$ and $\xi = \pi$ give opposite points on any of the circles in Figure 4.27. Therefore from the definition of y in terms of our bipolar coordinates (4.6.44) we can write, for when $\eta = \eta_1$,

$$2c = -\frac{r_B \sinh^2\eta_1}{\cosh\eta_1 - 1} - \frac{r_B \sinh^2\eta_1}{\cosh\eta_1 + 1}. \tag{4.6.45}$$

And then from (4.6.45) it can be shown that,

$$\cosh\eta_1 = \frac{-c}{r_B}, \tag{4.6.46}$$

which we can use to find the value of η_1.

To find φ_1, in region 1, we solve in terms of η and ξ. In order to derive the relevant diffusion equation we must first find the scale factors h_ξ and h_η, which are defined as,

$$h_\eta = \left|\frac{\partial \mathbf{r}}{\partial \eta}\right|, \qquad h_\xi = \left|\frac{\partial \mathbf{r}}{\partial \xi}\right| \tag{4.6.47}$$

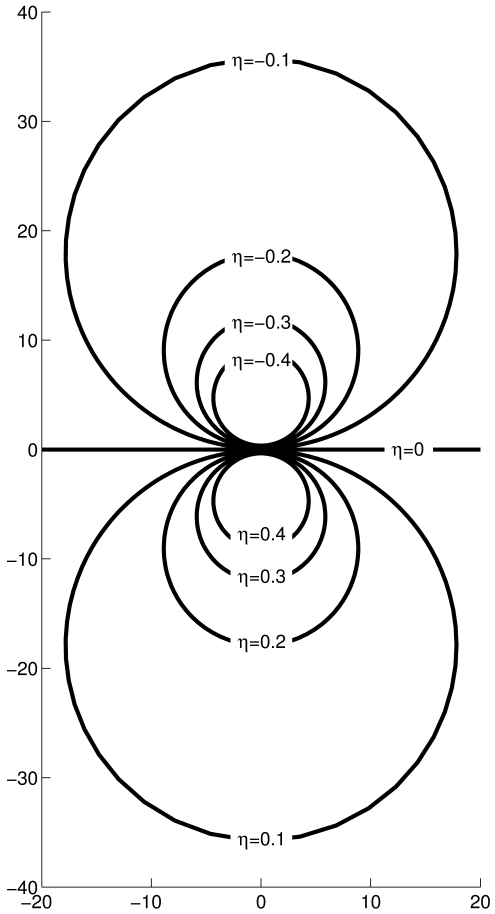

Figure 4.27: The bipolar coordinate system, as defined by (4.6.44), for circles of constant η where $0 \leq \xi < 2\pi$

where,

$$\frac{\partial \mathbf{r}}{\partial \eta} = (x_\eta, y_\eta), \qquad \frac{\partial \mathbf{r}}{\partial \xi} = (x_\xi, y_\xi). \tag{4.6.48}$$

Using the definitions (4.6.44) it can be shown, after some manipulation, that,

$$h_\eta = h_\xi = \frac{r_B \sinh \eta_1}{\cosh \eta - \cos \xi}. \tag{4.6.49}$$

Thus it can be shown that the Laplace operator in our bipolar system is given by,

$$\nabla^2 \varphi_1 = \frac{(\cosh \eta - \cos \xi)^2}{r_B^2 \sinh^2 \eta_1} \left(\varphi_{1,\eta\eta} + \varphi_{1,\xi\xi} \right). \tag{4.6.50}$$

Therefore, the diffusion equation we need to solve simplifies to,

$$\varphi_{1,\eta\eta} + \varphi_{1,\xi\xi} = 0, \tag{4.6.51}$$

which can be solved via the method of separation of variables. The solution must be

2π-periodic in ξ, and must satisfy the boundary condition on A,

$$\varphi_1\Big|_{\eta=0} = 0, \tag{4.6.52}$$

as $y = 0$ requires $\sinh(\eta) = 0$. We can write the general solution as,

$$\varphi_1(\eta, \xi) = a_0\eta + 2\sum_{n=1}^{\infty}(a_n \cos n\xi + b_n \sin n\xi)\sinh n\eta, \tag{4.6.53}$$

where the a_i's and b_i's are to be found from Fourier series by using the flux continuity condition on B. This condition has to be adapted for the bipolar coordinates in region 1 by using the scale factor h_η, thus the equal flux condition on the boundary B is re-written as,

$$\frac{\partial\varphi_1}{\partial\eta}\bigg|_{\eta_1} = \left(\frac{-r_B \sinh\eta_1}{\cosh\eta - \cos\xi}\right)\frac{\partial\psi_0}{\partial r}\bigg|_{r_B}, \tag{4.6.54}$$

which is the equation we can use to find the values of the a_i's and b_i's.

For the inner $O(\epsilon)$ problem, shown on the right of Figure 4.26, we switch back to using polar coordinates and solve,

$$\nabla^2\psi_1 = 0. \tag{4.6.55}$$

The general solution is,

$$\psi_1 = k_{0,a} + k_{0,b}\ln r + \sum_{n=1}^{\infty} A_n \cos nt\,(k_n r^{-n} + r^n) \tag{4.6.56}$$

where $t = \theta + \frac{\pi}{2}$ as we know the solution will be even about $t = 0$. We define,

$$A_n^* = \left(k_n r_B^{-n} + r_B^n\right)A_n, \tag{4.6.57}$$

then use the continuity condition on B,

$$\psi_1(r_B, t) = \varphi_1(r_B, t), \tag{4.6.58}$$

to show,

$$k_{0,a} + k_{0,b}\ln r_B = a_0\eta_1 \tag{4.6.59}$$

$$\sum_{n=1}^{\infty} A_n^* \cos nt = 2\sum_{n=1}^{\infty}(a_n \cos n\xi + b_n \sin n\xi)\sinh n\eta_1. \tag{4.6.60}$$

We define the right hand side of (4.6.60) to be equal to a new function $f(\xi)$, then we can find the constants A_n^* using Fourier series via,

$$A_n^* = \frac{1}{\pi}\int_0^{2\pi} f(\xi)\cos(nt)dt. \tag{4.6.61}$$

In order to compute this integral we need to change variables from t to ξ remembering that

$r = r_B$ and so $\eta = \eta_1$. From polar coordinates, we can convert to cartesians in the usual way,

$$\begin{aligned} x &= r_B \sin t \\ y &= -c + r_B \cos t. \end{aligned} \tag{4.6.62}$$

Then by substituting in our bipolar coordinates definition (4.6.44) into (4.6.62) we find the relationships required for the change of variables,

$$\sin t = \frac{\sinh \eta_1 \sin \xi}{\cosh \eta_1 - \cos \xi} \tag{4.6.63}$$

$$\cos t = \frac{1 - \cosh \eta_1 \cos \xi}{\cosh \eta_1 - \cos \xi}. \tag{4.6.64}$$

We also note that,

$$\cos(nt) = \frac{1}{2}(\cos t + i \sin t)^n + \frac{1}{2}(\cos t - i \sin t)^n, \tag{4.6.65}$$

and that differentiating (4.6.64) with respect to ξ leads to,

$$\frac{dt}{d\xi} = \frac{-\sinh \eta_1}{\cosh \eta_1 - \cos \xi}. \tag{4.6.66}$$

So by using the change of variables given by (4.6.63) and (4.6.64), and the substitutions (4.6.65) and (4.6.66), we arrive at an integrable expression for A_n^*,

$$\begin{aligned} A_n^* = \; & \frac{-1}{2\pi} \int_0^{2\pi} f(\xi) \left(\frac{1 - \cosh \eta_1 \cos \xi - i \sinh \eta_1 \sin \xi}{\cosh \eta_1 - \cos \xi} \right)^n \frac{\sinh \eta_1}{\cosh \eta_1 - \cos \xi} d\xi \\ & - \frac{1}{2\pi} \int_0^{2\pi} f(\xi) \left(\frac{1 - \cosh \eta_1 \cos \xi + i \sinh \eta_1 \sin \xi}{\cosh \eta_1 - \cos \xi} \right)^n \frac{\sinh \eta_1}{\cosh \eta_1 - \cos \xi} d\xi. \end{aligned} \tag{4.6.67}$$

This can be integrated numerically via a method such as the trapezium rule, as was used in this thesis.

From the expanded boundary condition on C (4.6.38), we know that,

$$\psi_1(r_{C,0}) = -r_{C,1} \psi_{0,r}(r_{C,0}) = 0. \tag{4.6.68}$$

We can apply this to the general solution (4.6.56) to find,

$$k_{0,a} + k_{0,b} \ln r_{C,0} = 0 \tag{4.6.69}$$

$$k_n = -r_{C,0}^{2n}. \tag{4.6.70}$$

So now the only remaining unknown is $r_{C,1}$, the $O(\epsilon)$ term of the anaerobic core radius. As we know that the anaerobic core radius will be an even function about $t = 0$ we define,

$$r_{C,1} = \sum_{n=0}^{\infty} \gamma_n \cos nt. \tag{4.6.71}$$

We know from inspection of the other expanded boundary condition on C (4.6.39) that,

$$\psi_{1,r}(r_{C,0}) = -r_{C,1}\psi_{0,rr}(r_{C,0}). \tag{4.6.72}$$

Substituting (4.6.71) into (4.6.72), and rearranging using (4.6.43) gives,

$$\gamma_0 = \frac{-k_{0,b}}{m^2 r_{C,0}} \tag{4.6.73}$$

$$\gamma_n = \frac{-A_n}{m^2}\left(-k_n n r_{C,0}^{-n-1} + n r_{C,0}^{n-1}\right), \tag{4.6.74}$$

in which all the terms on the right hand sides have already been found.

We now have a complete asymptotic approximation of the single aggregate constant absorption model. Using this we can find the size and shape of the anaerobic core and plot oxygen concentration throughout the domain. The result is shown in Figure 4.28 for a set of example parameters. As can be seen from the figure the most significant changes at the $O(\epsilon)$ level are around the lower edge of the soil aggregate. This clearly shows the deviation from the axi-symmetric solution created by the inclusion of the boundary at $y = 0$. As the largest decrease in oxygen concentration comes deeper in the soil aggregate, the anaerobic core will be positioned below the centre of the aggregate. The $O(\epsilon)$ result also shows how the anaerobic core will be of larger area than would be predicted using the previous models from the literature, even when oxygen is diffusing quickly around the aggregate.

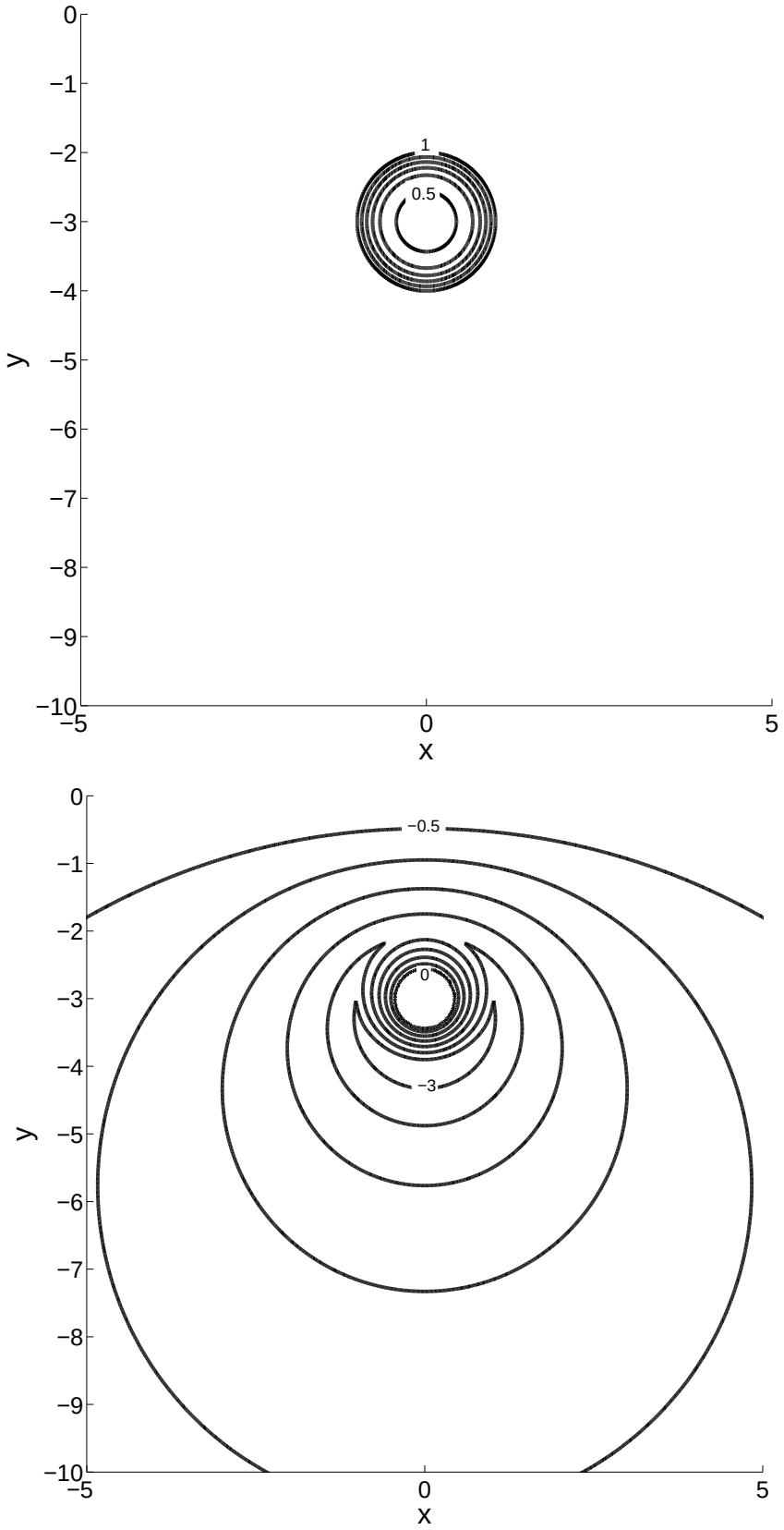

Figure 4.28: The individual parts of the constant absorption asymptotic solution, where $\epsilon = 0.01$, $c = -3$, $m = 2$, $r_B = 1$, and $T = 0.5$. Top: $O(1)$, contours at gaps of 0.1. Bottom: $O(\epsilon)$, contours at gaps of 0.5.

4.6.4 Line Boundary Model, with Proportional Absorption

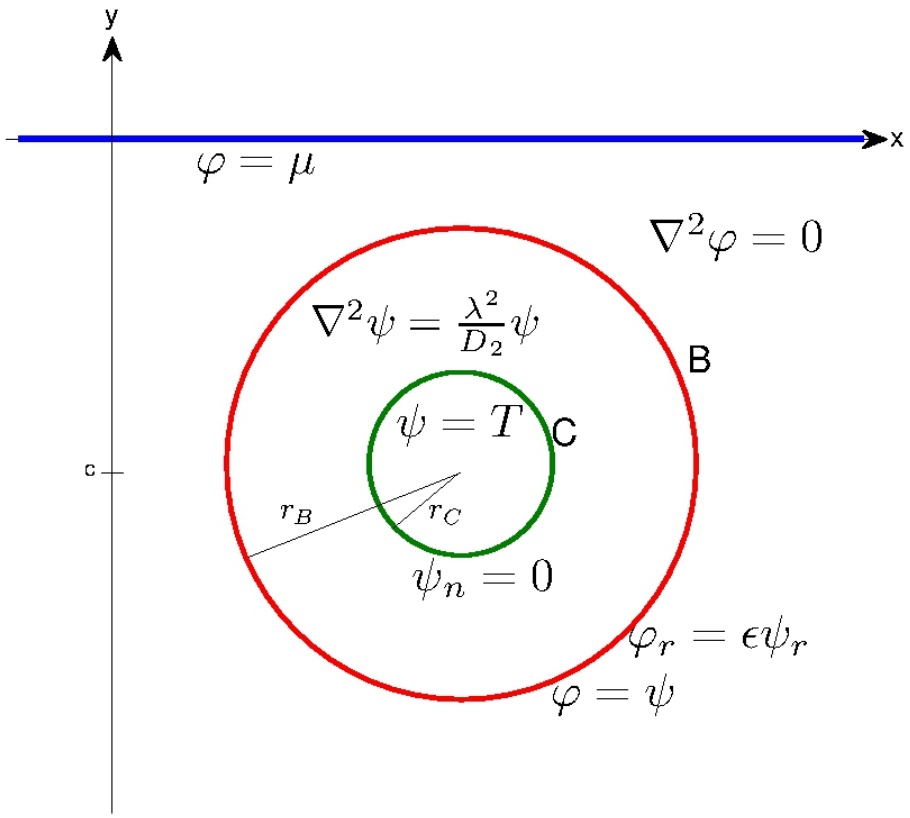

Figure 4.29: The line boundary proportional absorption model

For completeness we shall now also find solutions for the proportional absorption model shown in Figure 4.29, the methods used to find the solutions are all taken from the similar parts of the previous models.

The solution of the $O(1)$ problem is the same as in the proportional absorption concentric circles model. For the two regions these solutions are,

$$\begin{aligned} \varphi_0(r) &= \mu & (4.6.75)\\ \psi_0(r) &= \alpha I_0(mr) + \beta K_0(mr), & (4.6.76) \end{aligned}$$

where α and β are constants that can be found subject to the boundary conditions

$$\begin{aligned} \psi_0(r_{C,0}) &= T \\ \psi_0(r_B) &= \mu. \end{aligned} \qquad (4.6.77)$$

We find that,

$$\begin{aligned} \beta &= \frac{\mu I_0(mr_{C,0}) - T I_0(mr_B)}{K_0(mr_B)I_0(mr_{C,0}) - K_0(mr_{C,0})I_0(mr_B)} \\ \alpha &= \frac{T - \beta K_0(mr_{C,0})}{I_0(mr_{C,0})} \end{aligned} \qquad (4.6.78)$$

We can then find the value of $r_{C,0}$, using a bisection method on the remaining boundary condition,

$$\psi_{0,r}(r_{C,0}) = 0. \tag{4.6.79}$$

For the $O(\epsilon)$ problem, we once again solve using bipolar coordinates, as described in (4.6.44) and (4.6.46). In region 1 we find the same general solution as in the constant absorption model (4.6.53),

$$\varphi_1(\eta, \xi) = a_0\eta + 2\sum_{n=1}^{\infty}(a_n \cos n\xi + b_n \sin n\xi)\sinh n\eta, \tag{4.6.80}$$

where the a_i's and b_i's are to be found from Fourier series by using the flux continuity condition on B,

$$\left.\frac{\partial\varphi_1}{\partial\eta}\right|_{\eta_1} = \left(\frac{-r_B \sinh\eta_1}{\cosh\eta - \cos\xi}\right)\left.\frac{\partial\psi_0}{\partial r}\right|_{r_B}. \tag{4.6.81}$$

For the $O(\epsilon)$ region 2 problem, we switch back to using polar coordinates, and solve,

$$\nabla^2\psi_1 - m^2\psi_1 = 0, \tag{4.6.82}$$

using separation of variables. We find the general solution,

$$\psi_1 = \sum_{n=0}^{\infty}\left[A_n \cos n\theta + B_n \sin n\theta\right]\left[I_n(mr) + C_n K_n(mr)\right], \tag{4.6.83}$$

where the A_i's, and B_i's can be found from the continuity condition,

$$\psi_1(r_B, \theta) = \varphi_1(\eta_1, \xi). \tag{4.6.84}$$

Again we will use Fourier series. We define, $t = \theta + \frac{\pi}{2}$, and

$$A_n^* = A_n\left[I_n(mr_B) + C_n K_n(mr_B)\right]. \tag{4.6.85}$$

As we know that ψ_1 will be even about $t = 0$ we can write,

$$\psi_1(r_B, t) = \sum_{n=0}^{\infty} A_n^* \cos nt, \tag{4.6.86}$$

where, from the continuity condition (4.6.84),

$$A_0^* = a_0\eta_1 \tag{4.6.87}$$

$$\sum_{n=0}^{\infty} A_n^* \cos nt = 2\sum_{n=1}^{\infty}(a_n \cos n\xi + b_n \sin n\xi)\sinh n\eta. \tag{4.6.88}$$

We set the right hand side of (4.6.88) to be equal to the new function $f(\xi)$, similarly to

before, and then we can find the constants A_n^* using the Fourier series,

$$A_n^* = \frac{1}{\pi}\int_0^{2\pi} f(\xi)\cos(nt)dt. \tag{4.6.89}$$

This is the exact same integral as (4.6.61), and may be solved using the method outlined earlier.

Once we have evaluated (4.6.89) we must still find the individual constants that make up A_n^*. We can find the value of the C_i's from one of the boundary conditions on the anaerobic centre,

$$\psi_1(r_{C,0}) = -r_{C,1}\psi_{0,r}(r_{C,0}) = 0, \tag{4.6.90}$$

so that,

$$C_n = \frac{-I_n(mr_{C,0})}{K_n(mr_{C,0})}, \tag{4.6.91}$$

and then a simple rearrangement of (4.6.85) gives,

$$A_n = \frac{A_n^*}{I_n(mr_B) + C_n K_n(mr_B)}. \tag{4.6.92}$$

The only unknown left is the $O(\epsilon)$ anaerobic core radius term, $r_{C,1}$. We can find this using the remaining boundary condition,

$$\psi_{1,r}(r_{C,0}) = -r_{C,1}\psi_{0,r,r}(r_{C,0}). \tag{4.6.93}$$

As $r_{C,1}$ depends on θ and we know it will be even about $\theta = \frac{-\pi}{2}$ we shall write it in terms of $t = \theta + \frac{\pi}{2}$, in the form,

$$r_{C,1} = \sum_{n=0}^{\infty} \gamma_n \cos nt. \tag{4.6.94}$$

Substituting into (4.6.93) and rearranging gives,

$$\gamma_n = \frac{A_n\left[I_{n-1}(mr_{C,0}) + I_{n+1}(mr_{C,0}) - C_n K_{n-1}(mr_{C,0}) - C_n K_{n+1}(mr_{C,0})\right]}{-m\left[\alpha I_0(mr_{C,0}) + \alpha I_2(mr_{C,0}) + \beta K_0(mr_{C,0}) + \beta K_2(mr_{C,0})\right]}. \tag{4.6.95}$$

We now have all expressions required to describe the entire proportional absorption line boundary model. A solution for an example set of parameters is shown in Figure 4.30, and its similarity to the constant absorption solution should be noted.

Comparing the constant absorption model to the proportional absorption model once again shows a smaller anaerobic core for the proportional case, as shown in Figure 4.31.

This is the last model that will have the property of oxygen absorption being proportional to the local oxygen concentration. In the following chapters we only consider constant absorption as it is widely regarded in the literature that the absorption should be approximated as constant.

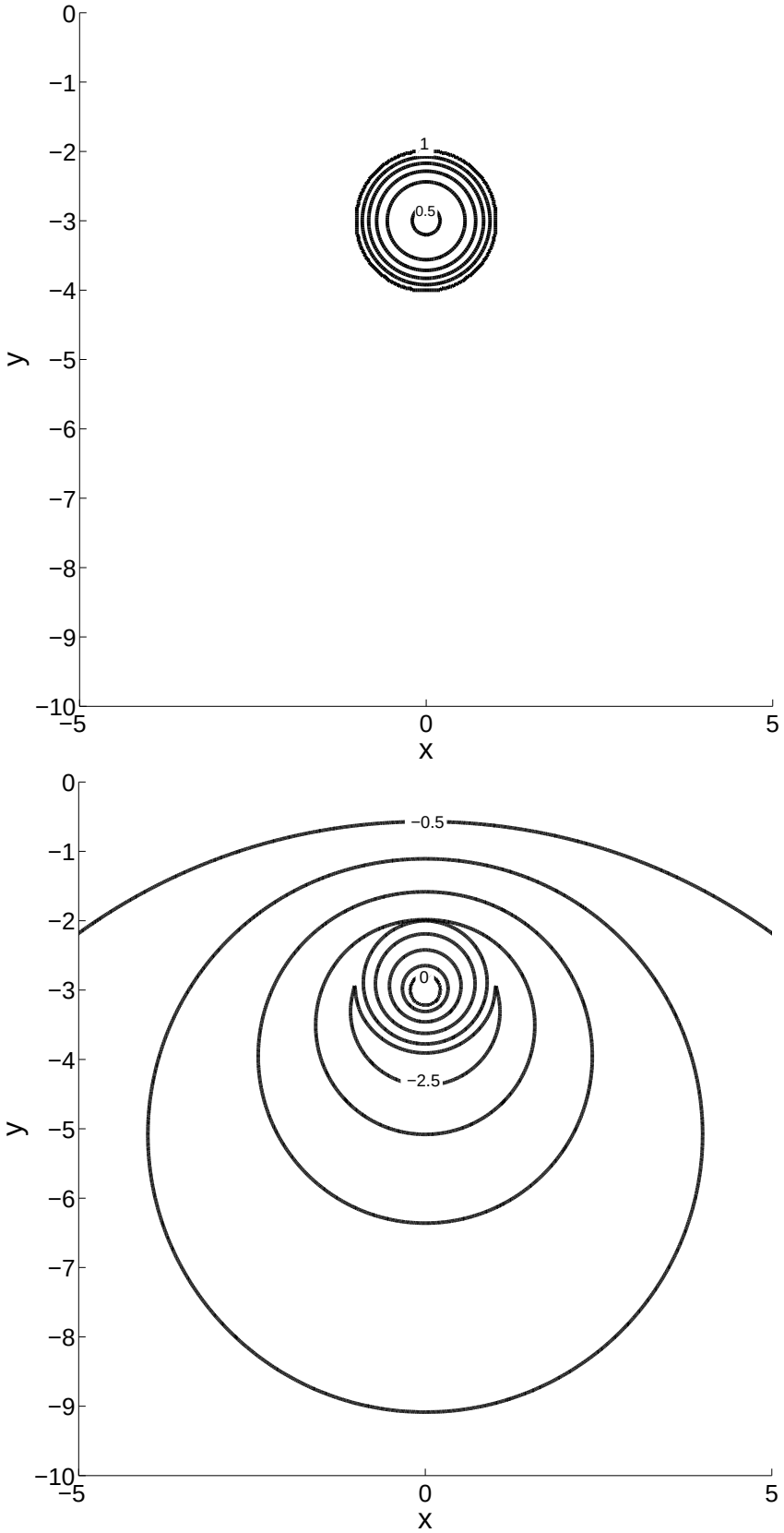

Figure 4.30: The individual parts of the proportional absorption asymptotic solution, where $\epsilon = 0.01$, $c = -3$, $m = 2$, $r_B = 1$, and $T = 0.5$. Top: $O(1)$, contours at gaps of 0.1. Bottom: $O(\epsilon)$, contours at gaps of 0.5.

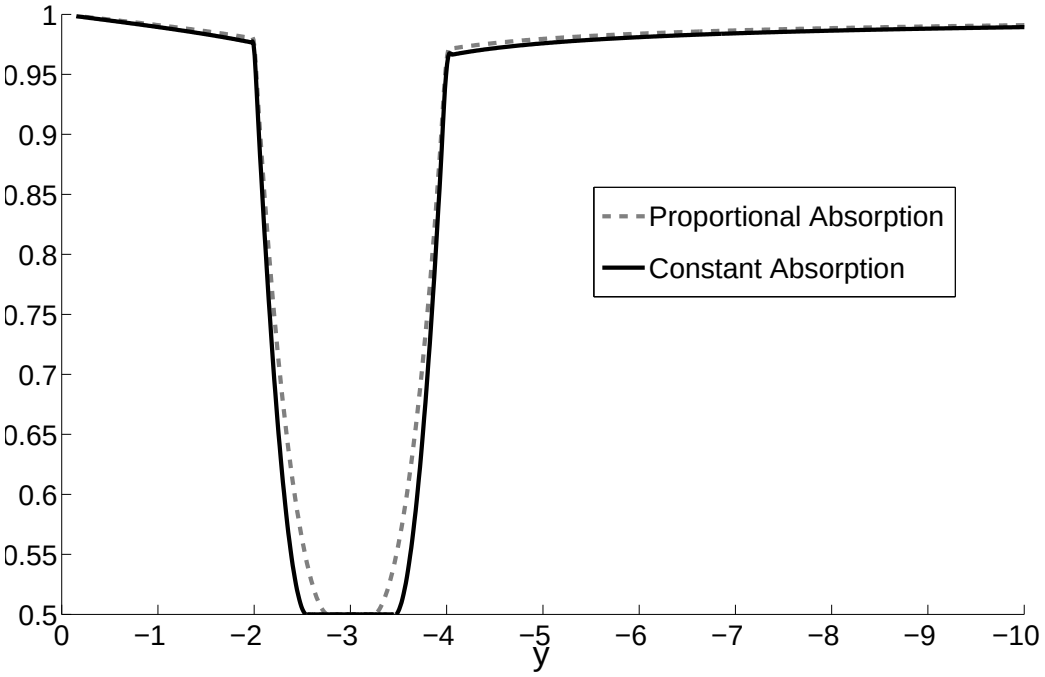

Figure 4.31: Oxygen concentration for the line boundary model when $x = 0$, found using the asymptotic approximation with terms up to $O(\epsilon)$ included. Showing a comparison between proportional absorption and constant absorption of oxygen within the aggregate. Where $\epsilon = 0.01$, $c = -3$, $m = 2$ and $r_B = 1$, $T = 0.5$.

4.6.5 Asymptotic Method Summary

The four models above with solutions found using the asymptotic method all consist of a single soil aggregate surrounded by air or water. Clearly this is not representative of what would be seen in a natural environment, such as a ploughed field. In reality an aggregated soil would consist of many individual closely packed aggregates. Therefore, these asymptotic models should be considered as important building blocks on the way to creating a more realistic model that shall include multiple soil aggregates. However, even though only one soil aggregate is included, the $O(\epsilon)$ solution shows clearly the effect of including the air/soil boundary at $y = 0$. The oxygen level around the aggregate has clearly been depleted in a non-uniform way and by looking at the $O(\epsilon)$ solution separately we can more clearly see this behaviour than had we used a full boundary element method. As the inclusion of this boundary is an important development on previous models in the literature we shall continue to plot and consider the individual parts of the asymptotic method solution throughout this thesis.

Another important benefit of the asymptotic method is that it uses much simpler calculations than our previous numerical method would in order to solve the same problem. In the previous method it was required to solve the interior-exterior problem simultaneously via a system of boundary integrals. We now have a solution valid for when $D_1 \gg D_2$, which can be expressed in a straightforward manner that only requires numerical integration to find the values of the constants.

We consider the constant absorption line boundary model to be our most realistic model so far as this matches the requirements discussed previously. It includes fast diffusing oxygen below ground level, and a single soil aggregate within which oxygen diffuses more slowly and is absorbed until it is depleted to a level defined as being the threshold between aerobic and anaerobic conditions. For this model our solution can now be written as, for region 1,

$$\varphi = \mu + \epsilon\left(a_0\eta + 2\sum_{n=1}^{\infty}(a_n\cos n\xi + b_n\sin n\xi)\sinh n\eta\right) \tag{4.6.96}$$

and for region 2,

$$\begin{aligned}\psi &= \frac{m^2}{4}\left(r^2 - r_B^2\right) + \mu + \left[\frac{T - \frac{m^2}{4}\left(r_{C,0}^2 - r_B^2\right) - \mu}{\log\left(\frac{r_{C,0}}{r_B}\right)}\right]\log\left(\frac{r}{r_B}\right) \\ &\quad + \epsilon\left(k_{0,a} + k_{0,b}\ln r + \sum_{n=1}^{\infty}A_n\cos nt\left(k_n r^{-n} + r^n\right)\right).\end{aligned} \tag{4.6.97}$$

Another advantage over the previous method is that the anaerobic core radius, $r_C = r_{C,0} + \epsilon r_{C,1}$, can now be calculated directly via,

$$\begin{aligned}0 &= m^2 r_{C,0}^2\log\left(\frac{r_{C,0}}{r_B}\right) + 2\left(T - \mu\right) - \frac{m^2}{2}\left(r_{C,0}^2 - r_B^2\right), \\ r_{C,1}(t) &= \frac{-k_{0,b}}{m^2 r_{C,0}} + \sum_{n=1}^{\infty}\frac{-A_n}{m^2}\left(-k_n n r_{C,0}^{-n-1} + n r_{C,0}^{n-1}\right)\cos nt.\end{aligned} \tag{4.6.98}$$

In the solutions found using the boundary element method it was required to discretize the anaerobic core boundary and then find the position of boundary elements using the Newton iteration scheme.

The asymptotic solutions can be compared to those found using the boundary element method in order to confirm the accuracy. Generally, it has been noted that a much higher level of computational power is required in order to process the boundary method than the asymptotic method.

Chapter 5

Multiple Areas Of Oxygen-Absorbing Soil

In this chapter we shall work to extend our previous models in order to include multiple areas of oxygen-absorbing soil. The development of these models has been carried out in the previous chapters and the various extensions outlined below do not require too much additional work. We shall be building upon the existing constant absorption line boundary models, looking at both the asymptotic and boundary element methods.

Both of these methods have useful features, as discussed previously, and by extending both we shall gain a better understanding of the solutions. The boundary element method can be used to calculate solutions for all the models described in the results section of this thesis. However, we continue to investigate the asymptotic method, as it provides simpler calculations which allow us to gain a better insight into what is happening in the problems. Also we shall be able to validate some of our solutions by comparing the results found from the two methods.

5.1 Extending The Boundary Element Method

We begin this chapter by considering the boundary element method. This method presents the clearest opportunity to straightforwardly add more regions of oxygen-absorbing soil as this will only require the addition of extra boundary integrals. Below we have created a model that includes two regions of oxygen-absorption, a similar method should be followed if more regions are required.

The model shown in Figure 5.1 represents two circular regions of oxygen-absorbing soil with boundaries B_1 and B_2. The boundary conditions are the same as for previous models. Oxygen concentration is kept constant at $y = 0$, there is a no-flux condition at infinite depth, and the conditions of continuity and equal flux on both B_1 and B_2 are required. As with all the boundary element method models the oxygen-absorbing regions can be positioned anywhere within the domain, and can be of different shapes as long as the boundaries can still be discretized into straight elements.

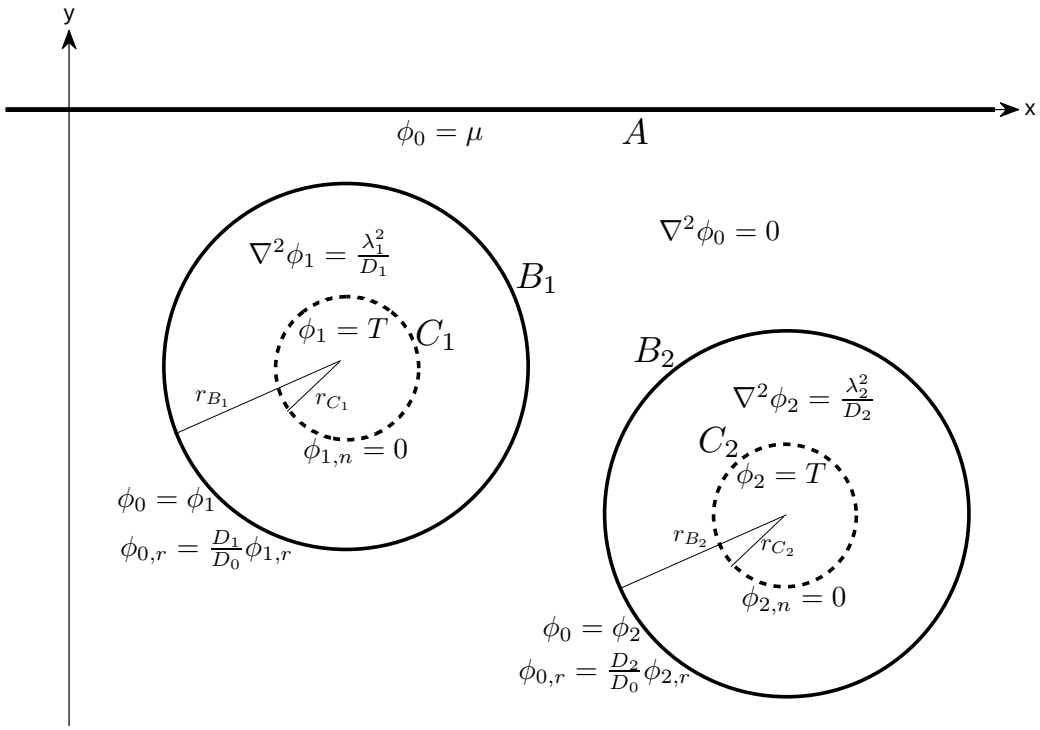

Figure 5.1: A model with two circular regions of oxygen absorbing soil, below an air/soil boundary at $y = 0$

5.1.1 Anaerobic Cores Excluded

We shall first consider the problem without the anaerobic cores, C_1 and C_2, as this significantly reduces the complexity of the problem. This model then represents the scenario where the oxygen is diffusing quickly enough from the air into the soil that there are no anaerobic conditions created. Thus the bacteria in the soil continue to respire and no denitrification will take place.

The formulation of the boundary integral equations is exactly the same as in the previous chapters. In this version of the model we denote oxygen concentration in the outer region as ϕ_0, and inside the two oxygen-absorbing regions as ϕ_1 and ϕ_2, as shown in Figure 5.1. For everywhere outside the oxygen-absorbing regions, we once again define,

$$\hat{\phi}_0(x, y) = \phi_0(x, y) - \mu, \tag{5.1.1}$$

so that $\hat{\phi}_0(x, 0) = 0$. We shall also use the same Green's functions as previously. For the outer region, we use the modified free space Green's function (4.4.4), which satisfies $\nabla^2 G_1(\mathbf{x}, \mathbf{x_0}) + \delta(\mathbf{x} - \mathbf{x_0}) = 0$, so that our boundary integral equation for the outer region will only involve integrals that are non-zero on B_1 and B_2. The boundary integral equation is then, for x_0 on B_1 or B_2, with the normal $\mathbf{n}$ pointing into the outer region,

$$\hat{\phi}_0 = -2\int_{B_1} G_1 \mathbf{n}\cdot\nabla\hat{\phi}_0 dl + 2\int_{B_1}^{PV} \hat{\phi}_0 \mathbf{n}\cdot\nabla G_1 dl - 2\int_{B_2} G_1 \mathbf{n}\cdot\nabla\hat{\phi}_0 dl + 2\int_{B_2}^{PV} \hat{\phi}_0 \mathbf{n}\cdot\nabla G_1 dl. \tag{5.1.2}$$

For both the inner regions we choose G_2 to once again be the free space Green's function

(4.5.24), which satisfies $\nabla^2 G_2(\mathbf{x}, \mathbf{x_0}) + \delta(\mathbf{x} - \mathbf{x_0}) = 0$. The boundary integral equation for the inner regions is then, for x_0 on B_1 with $\mathbf{n}$ pointing inside B_1,

$$\hat{\phi}_0 + \mu = \frac{2D_0}{D_1} \int_{B_1} G_2 \mathbf{n} \cdot \nabla \hat{\phi}_0 dl + 2 \int_{B_1}^{PV} (\hat{\phi}_0 + \mu) \mathbf{n} \cdot \nabla G_2 dl - 2m_1^2 \oint_{B_1} \mathbf{a}.\mathbf{t} dl, \tag{5.1.3}$$

and for x_0 on B_2 with $\mathbf{n}$ pointing inside B_2,

$$\hat{\phi}_0 + \mu = \frac{2D_0}{D_2} \int_{B_2} G_2 \mathbf{n} \cdot \nabla \hat{\phi}_0 dl + 2 \int_{B_2}^{PV} (\hat{\phi}_0 + \mu) \mathbf{n} \cdot \nabla G_2 dl - 2m_2^2 \oint_{B_2} \mathbf{a}.\mathbf{t} dl, \tag{5.1.4}$$

where $m_1^2 = \frac{\lambda_1^2}{D_1}$ and $m_2^2 = \frac{\lambda_2^2}{D_2}$. The last integrals in (5.1.3) and (5.1.4) are found using Green's theorem in the plane as derived previously. It was defined that $\hat{\mathbf{x}} = \mathbf{x} - \mathbf{x}_0$, , $\mathbf{a} = \frac{1}{8\pi}(2\hat{y}\log r - \hat{y}, -2\hat{x}\log r + \hat{x})$, and $\mathbf{t}$ is a unit vector tangent to each boundary.

The oxygen distribution can be found first on the boundaries using the equations above, and then throughout the rest of the domain using similar boundary integral equations, similarly to in previous sections. This model does allow negative oxygen concentrations because oxygen-absorption is constant with no threshold value to switch to anaerobic conditions where the bacteria would stop respiring. However, it is interesting to note the position of the minimum values of the oxygen concentration and see the effect that the two regions of oxygen-absorption are having on each other. The minimum point in each region will be positioned away from centre and closer to the other region. If these points are known they can be used in the following anaerobic core model in order to predict the position of the anaerobic core. This is quite useful as when we find the correct position of the anaerobic core we can choose a more accurate initial guess in the Newton iteration scheme.

5.1.2 Anaerobic Cores Included

We now extend our model to include anaerobic cores in both of the oxygen-absorbing regions, as shown in Figure 5.1. Our boundary integral system is now, for x_0 on B_1 or B_2, with the normal $\mathbf{n}$ pointing into the outer region,

$$\hat{\phi}_0 = -2 \int_{B_1}^{PV} G_1 \mathbf{n} \cdot \nabla \hat{\phi}_0 dl + 2 \int_{B_1} \hat{\phi}_0 \mathbf{n} \cdot \nabla G_1 dl - 2 \int_{B_2}^{PV} G_1 \mathbf{n} \cdot \nabla \hat{\phi}_0 dl + 2 \int_{B_2} \hat{\phi}_0 \mathbf{n} \cdot \nabla G_1 dl, \tag{5.1.5}$$

and on B_i, where $i = 1, 2$, with $\mathbf{n}$ pointing into the oxygen-absorbing regions,

$$\begin{aligned} \hat{\phi}_0 + \mu \quad = \quad & \frac{2D_0}{D_i} \int_{B_i} G_2 \mathbf{n} \cdot \nabla \hat{\phi}_0 dl + 2 \int_{B_i}^{PV} (\hat{\phi}_0 + \mu) \mathbf{n} \cdot \nabla G_2 dl - 2m_i^2 \oint_{B_i} \mathbf{a}.\mathbf{t} dl \\ & -2 \int_{C_i} G_2 \mathbf{n} \cdot \nabla \phi_i dl + 2T_i \int_{C_i} \mathbf{n} \cdot \nabla G_2 dl - 2m_i^2 \oint_{C_i} \mathbf{a}.\mathbf{t} dl, \end{aligned} \tag{5.1.6}$$

and on C_i with $\mathbf{n}$ pointing into the oxygen-absorbing regions,

$$\begin{aligned} T &= \frac{2D_0}{D_i}\int_{B_i} G_2\mathbf{n}\cdot\nabla\hat{\phi}_0 dl + 2\int_{B_i}(\hat{\phi}_0+\mu)\mathbf{n}\cdot\nabla G_2 dl - 2m_i^2\oint_{B_i}\mathbf{a}.\mathbf{t}dl \\ &\quad -2\int_{C_i} G_2\mathbf{n}\cdot\nabla\phi_i dl + 2T_i\int_{C_i}^{PV}\mathbf{n}\cdot\nabla G_2 dl - 2m_i^2\oint_{C_i}\mathbf{a}.\mathbf{t}dl, \end{aligned} \tag{5.1.7}$$

As with the previous boundary element method models that included an anaerobic core we first guess the position of the boundary elements and then move them according to a Newton iteration scheme until we find the point where $\mathbf{n}\cdot\nabla\phi_i = 0$. Once this has been established we can find the oxygen concentration on all the boundaries and then calculate oxygen concentration at any point in the domain via the relevant boundary integral equations.

The best feature of this method is its flexibility. It can accept any set of parameter values and any shape of the regions. However, there is quite a large amount of computation required in order to evaluate the boundary integrals along each boundary element, solve the simultaneous inner/outer system, and run the Newton iteration scheme.

This model with two oxygen-absorbing regions best describes a solid or non-aggregated soil where there are two regions of high microbial activity. As discussed previously, this could occur where a soil has some decomposing organic matter within it, perhaps two dead leaves in this instance. This would lead us to choose $D_0 = D_1 = D_2$ as everywhere below $y = 0$ is solid soil and thus the diffusion coefficient would be the same throughout. We shall use the method described above to find solutions and discuss the results found when modelling this scenario in the next chapter.

5.2 Extending the Asymptotic Method

When considering models where the diffusivity of oxygen in the outer region is much faster than in the inner regions we can use the asymptotic expansion method, as described previously. These type of models represent air surrounding individual solid soil aggregates where oxygen-absorption is taking place. We previously found a solution for the model shown in Figure 4.24. From inspection of the previous solution it becomes clear that in order to extend the model to include multiple soil aggregates we need only change the method for solving the $O(\epsilon)$ outer region problem. In all the other parts of the solution the exact same method will still work whether there is one, two, or many soil aggregates.

The $O(\epsilon)$ outer region problem is shown again below in Figure 5.2. Previously we used a bipolar coordinate method to solve this problem. Unfortunately this method cannot easily be extended to multiple aggregates. Therefore we now consider a method used by Crowdy, Surana and Yick in [13], which can be extended to multiple aggregates using the Shottky-Klein prime function as described by Crowdy in [11].

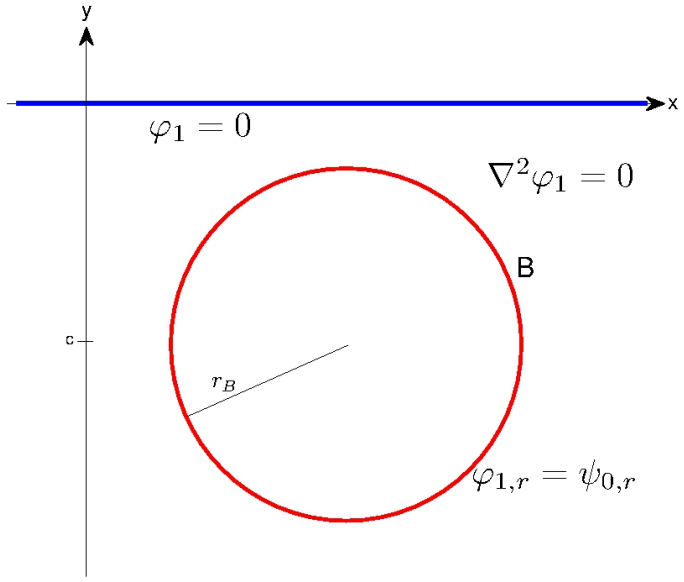

Figure 5.2: The outer region, $O(\epsilon)$ problem

We first reconsider the problem of modelling a single soil aggregate, but now use the method of images to create the air/soil boundary at $y = 0$, as shown in Figure 5.3. This allows us to redefine our model as a doubly connected domain which can be mapped to an annulus, from which we can then apply the integral equations described by Crowdy [11], as discussed in the introduction.

We already know that $\psi_{0,r} = C$ on the edge of our soil aggregate B, where C is a constant. We therefore add a reflection of B in $y = 0$, with the opposite boundary condition. This ensures that the air/soil boundary condition $\varphi_1(x, 0) = 0$ holds, without us having to

explicitly include it in further calculations. Thus, we now have the boundary conditions,

$$\begin{aligned} \varphi_{1,n} &= C \qquad \text{on } B \\ \varphi_{1,n} &= -C \qquad \text{on } B^R, \end{aligned} \tag{5.2.1}$$

around which oxygen can diffuse according to Laplace's equation, as shown in Figure 5.3.

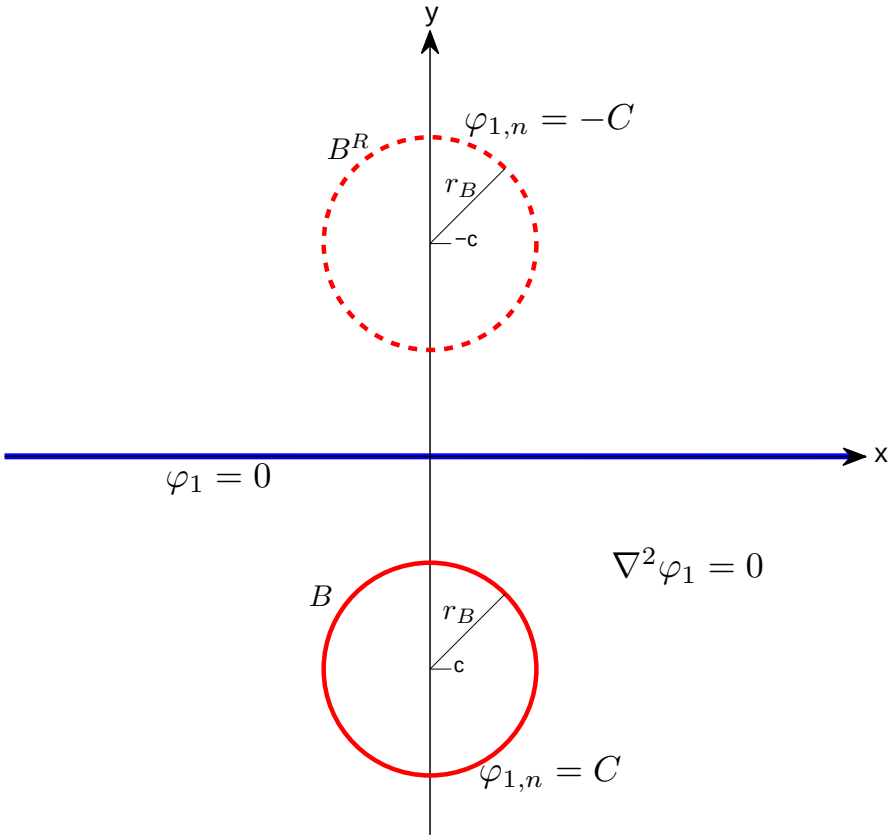

Figure 5.3: The outer region $O(\epsilon)$ problem using method of images, in the complex z-plane

We progress by using a conformal mapping to map the domain in Figure 5.3 to an annulus, as shown in Figure 5.4. The mapping is given by,

$$\zeta = a\left(\frac{-z + Ai}{z + Ai}\right), \qquad A^2 = -c^2 - r_B^2, \qquad \rho = \frac{ci - A}{ci + A}, \qquad a = \sqrt{\rho}. \tag{5.2.2}$$

Note that c is a purely imaginary number as it has been taken from the complex z-plane where $z = x + iy$. The outer boundary of the annulus, B_M, has unit radius and corresponds to the original soil aggregate B. The inner boundary of the annulus, B_M^R, has radius ρ and corresponds to the mirror image of the aggregrate B^R.

In order to use the integral equations described by Crowdy [11] we need to switch our boundary conditions from Neumann to Dirichlet and adapt our problem to get it into a suitable form. We therefore consider our problem in the form of a complex potential, so that,

$$\Omega(z) = \varphi_1 + if. \tag{5.2.3}$$

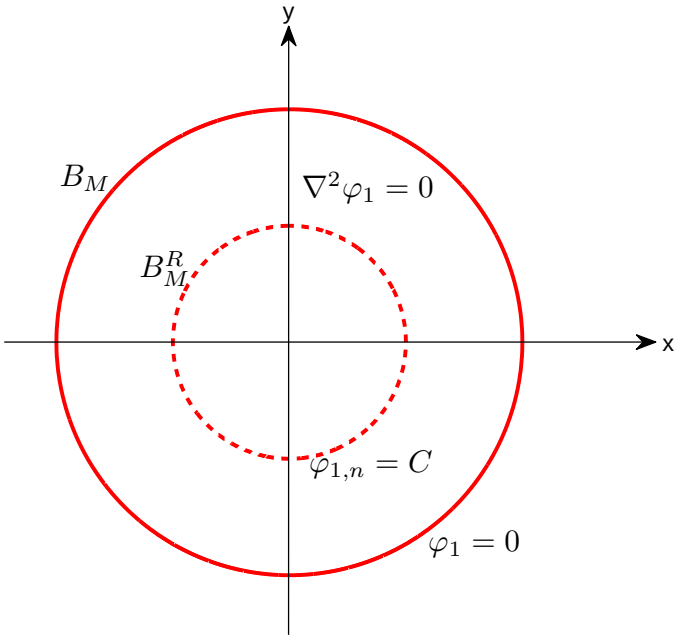

Figure 5.4: The outer region $O(\epsilon)$ problem in the ζ-plane

We can then use the Cauchy-Riemann equations to rewrite the boundary conditions (5.2.1) as

$$\begin{aligned} f_s &= C \qquad \text{on } B \\ f_s &= -C \qquad \text{on } B^R \end{aligned} \tag{5.2.4}$$

where the subscript s refers to the arc-length around each circle. This allows us to then integrate (5.2.4) with respect to arc length, so that we arrive at a problem with Dirichlet boundary conditions,

$$\begin{aligned} f &= Cs + d_1 \qquad \text{on } B \\ f &= -Cs + d_2 \qquad \text{on } B^R. \end{aligned} \tag{5.2.5}$$

Thus we now try to find $-i\Omega(z)$, so that we have $\text{Re}(-i\Omega) = f$, where f satisfies (5.2.5). Once we have found f we can then deduce φ_1. However, first we must decompose our solution into two parts, as there is a jump in the boundary conditions. For increasing arc-length around B, at $s = 2\pi r_B$, there is a jump of $-2\pi r_B C$ and on B^R there is a jump of $2\pi r_B C$. We therefore define a new function, in the ζ plane as,

$$W(\zeta) = -r_B C \log\left(\frac{\zeta}{a}\right) + g(\zeta), \tag{5.2.6}$$

such that $\Omega(z) = W(\zeta)$. The extra log term includes a jump equivalent to the one in the previous boundary conditions therefore the new function, g, will be continuous. This

decomposition is acceptable because,

$$-\log\left(\frac{\zeta}{a}\right) = -\log\left(\frac{-z+Ai}{z+Ai}\right) = \log(z+Ai) - \log(z-Ai) - i\pi, \tag{5.2.7}$$

which corresponds to a source and a sink located in the z-plane at Ai and $-Ai$ respectively, so our boundary conditions hold. Due to the fact that,

$$\frac{c}{i} < -A < \frac{c}{i} + r_B, \tag{5.2.8}$$

from (5.2.2), the source and sink fall within our soil aggregates and the new log term added in (5.2.6) accounts for the jump in the boundary conditions (5.2.5). So we have now arrived at the problem of finding the new function $g(\zeta)$ from (5.2.6), where the boundary conditions (5.2.5) have now become,

$$\begin{aligned} \mathrm{Re}(-ig) &= \mathrm{Re}\left[-ir_BC\log\left(\frac{\zeta}{a}\right)\right] - Cs + d_1 \qquad \text{on } B_M \\ \mathrm{Re}(-ig) &= \mathrm{Re}\left[-ir_BC\log\left(\frac{\zeta}{a}\right)\right] - Cs + d_2 \qquad \text{on } B_M^R. \end{aligned} \tag{5.2.9}$$

Note that the penultimate term on B_M now includes a minus sign. This is because when mapping B into the ζ-plane, increasing the arc-length, s, in the anti-clockwise direction in the z-plane corresponds to clockwise movement around B_M in the ζ-plane. This is not the case for B_M^R.

As we can write $\zeta = e^{i\theta}$ on B_M and $\zeta = \rho e^{i\theta}$ on B_M^R, we can write (5.2.9) as,

$$\begin{aligned} \mathrm{Re}(-ig) &= r_BC\theta - Cs + d_1 \qquad \text{on } B_M \\ \mathrm{Re}(-ig) &= r_BC\theta - Cs + d_2 \qquad \text{on } B_M^R. \end{aligned} \tag{5.2.10}$$

Our soil aggregate problem is now in a form suitable to be solved via the Villat formula as described in the introduction of this thesis, and as used in [13]. We have that

$$-ig(\zeta) = I_+(\zeta) - I_-(\zeta) + I_c \tag{5.2.11}$$

Note that the additional imaginary constant seen in the generic Villat formula in [13] is set to zero here, as it was included when we decomposed $g(\zeta)$ in (5.2.9), in order to satisfy the boundary condition at $y = 0$. The integrals we need to compute are,

$$I_+ = \frac{1}{2\pi i}\oint_{|\zeta'|=1} \frac{d\zeta'}{\zeta'} K\left(\zeta/\zeta'\right)\left(r_BC\theta - Cs + d_1\right), \tag{5.2.12}$$

$$I_- = \frac{1}{2\pi i}\oint_{|\zeta'|=\rho} \frac{d\zeta'}{\zeta'} K\left(\zeta/\zeta'\right)\left(r_BC\theta - Cs + d_2\right) \tag{5.2.13}$$

and

$$I_c = -\frac{1}{2\pi i}\oint_{|\zeta'|=\rho} \frac{d\zeta'}{\zeta'}\left(r_BC\theta - Cs + d_2\right). \tag{5.2.14}$$

The function, $K(\zeta)$, in these integrals is given by,

$$K(\zeta) = 1 - 2\zeta \frac{P'(\zeta)}{P(\zeta)} \tag{5.2.15}$$

where,

$$P(\zeta) = (1-\zeta)\prod_{k=1}^{\infty}(1-\rho^{2k}\zeta)(1-\rho^{2k}\zeta^{-1}). \tag{5.2.16}$$

In order to compute the integrals in (5.2.11) we will find ζ and arc-length s, in terms of θ and integrate via the trapezium rule. We note that, on B_M,

$$ds = |dz| = |z'(\zeta)d\zeta|. \tag{5.2.17}$$

We can rearrange our mapping to show that,

$$z = Ai\left(\frac{a-\zeta}{a+\zeta}\right), \tag{5.2.18}$$

it is then clear that,

$$z'(\zeta) = \frac{-2Aai}{(a+\zeta)^2}. \tag{5.2.19}$$

Substituting (5.2.19) into (5.2.17) and by using $\zeta = e^{i\theta}$ on B_M, we then have for ζ on B_M,

$$ds = \frac{2Aa}{\rho + 2a\cos\theta + 1}d\theta \tag{5.2.20}$$

On B_M^R we know that $\zeta = \rho e^{i\theta}$, and

$$ds = \rho|z'(\zeta)|d\theta, \tag{5.2.21}$$

so on B_M^R, it can be shown that ds is also given by (5.2.20).

There is also a solvability condition, as defined in [13], which our problem must satisfy. It states that,

$$\oint_{|\zeta|=1}\frac{d\zeta}{\zeta}\left(r_B C\theta - Cs + d_1\right) = \oint_{|\zeta|=\rho}\frac{d\zeta}{\zeta}\left(r_B C\theta - Cs + d_2\right), \tag{5.2.22}$$

must hold for there to be a solution via the Villat formula. This can be re-written as,

$$\int_0^{2\pi}\left(r_B C\theta - Cs + d_1\right)d\theta = \int_0^{2\pi}\left(r_B C\theta - Cs + d_2\right)d\theta, \tag{5.2.23}$$

which leads us to choose $d_1 = d_2 = 0$.

Using all of the above we arrive at first a solution for $g(\zeta)$, from which we can find $W(\zeta)$, $\Omega(z)$, and finally φ_1 via

$$\varphi_1 = \mathrm{Re}(\Omega). \tag{5.2.24}$$

This method of finding the $O(\epsilon)$ region 1 problem is in many ways neater than our previous bipolar solution. For any point in the domain, all that is required for the solution is the

numerical integration of the relevant integrals above, there is no Fourier series to find as there was in the bipolar method. As results have already been shown for a single aggregate with $D_1 \gg D_2$ they shall not be repeated here, but it should be noted that results from this method match well with the bipolar solution and have been further verified using the boundary element method.

The full asymptotic method using the above is also still clearly much simpler than a boundary element method solution would be for the same problem. In the boundary element method we must solve the inner and outer problems simultaneously via large matrix equations created by integrating along the individual boundary elements. Using this method oxygen concentration is found at any point in the domain via computation of integrals involving known terms.

The most important feature of the new $O(\epsilon)$ region 1 method is that it can be readily extended to multiple soil aggregates. This can be achieved by replacing the Villat formula with the full version of the integral equation (1.8.25), originally described by Crowdy in [11]. This integral equation simply requires more integrals for each soil aggregate we wish to add, as they can all be mapped to circles within the annulus. For the current problem, involving just one aggregate we have,

$$\begin{aligned} -ig(\alpha) = \frac{1}{2\pi i}\oint_{B_M} [r_B C\theta - Cs]\left[d\log\omega(z,\alpha) + d\log\bar{\omega}(z^{-1},\alpha^{-1})\right] \\ -\frac{1}{2\pi i}\oint_{B_M^R} [r_B C\theta - Cs]\left[d\log\omega(z,\alpha) + d\log\bar{\omega}(\rho^2\bar{z}^{-1},\alpha^{-1})\right] \end{aligned} \tag{5.2.25}$$

Either of the integral equations, (5.2.25) or (5.2.11), will give the same solution for φ_1.

The boundary element method to find the solution of the outer region $O(\epsilon)$ problem, for N soil aggregates in each period, with $i = 1, ..., N$, gives the following integral equation for anywhere in the outer region,

$$\varphi_1 = \sum_{i=1}^{N}\left[-\int_{B_i} G_1\mathbf{n}\cdot\nabla\varphi_1 dl + \int_{B_i}\varphi_1\mathbf{n}\cdot\nabla G_1 dl\right]. \tag{5.2.26}$$

This boundary integral equation is much simpler than for the full problem, it only includes the outer boundaries which are pre-defined, and the $\mathbf{n}\cdot\nabla\varphi_1$ for each element are already known. These would have been found using the $O(1)$ parts of the problem. We therefore only have to solve a single matrix equation to find φ_1.

Whether there is one soil aggregate or more, the methods to find the remaining parts of the asymptotic solution are the same as described earlier in the thesis, so we now have a complete solution for N soil aggregates surrounded by air. However, this model will still only ever have a finite amount of oxygen-absorbing soil within it but an infinite supply of oxygen. Therefore, as distance is increased away from the aggregates the level of oxygen will return to a background level equal that in the air. We can see this clearly in the outer region $O(\epsilon)$ solution, which has been calculated for a set of example parameters in Figure 5.5. In order to create a domain resembling a large area of the ground where oxygen levels decrease with depth we need to repeat the aggregates periodically in the x-direction. This

is described in the following section.

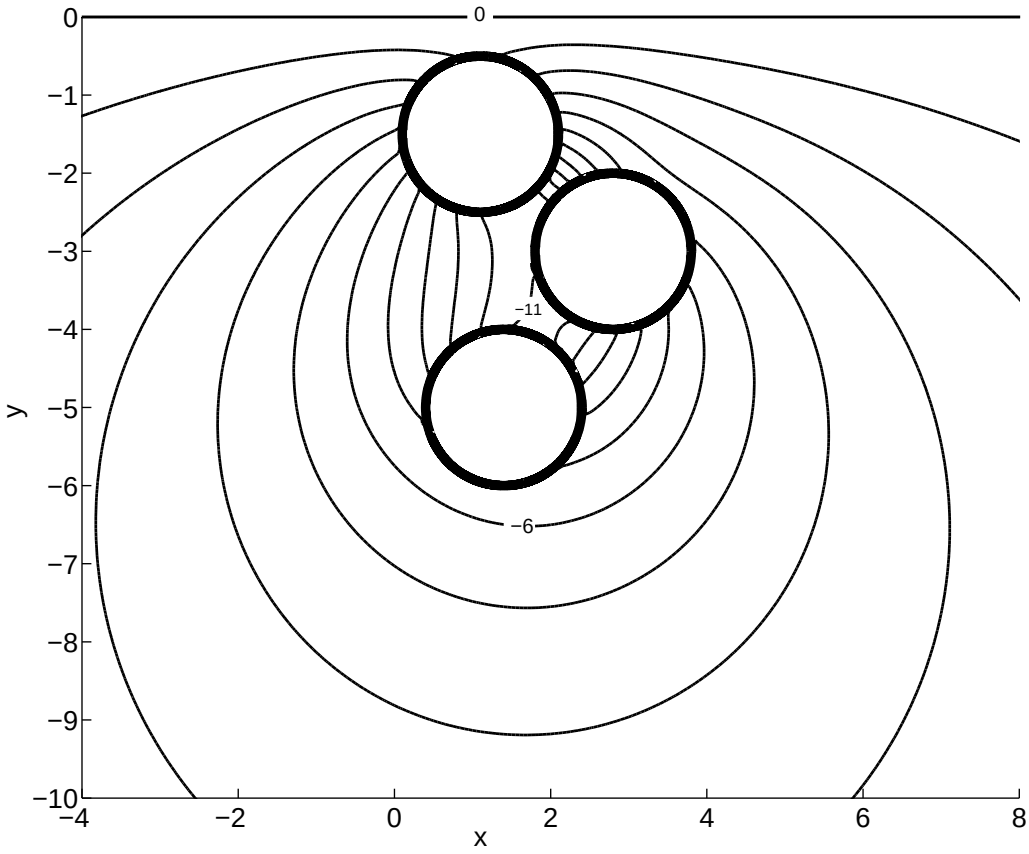

Figure 5.5: A contour plot of φ_1 from the outer region $O(\epsilon)$ problem. which shows the oxygen concentration decreasing around the soil aggregates but returning to the background level with increased depth. Each contour represents a level step of 1, decreasing towards a minimum in the area between the aggregates. $r_B = 1$, $m = 2$, $\epsilon = 0.01$, $T = 0.5$

5.3 An Infinite Array of Soil Aggregates

We now construct our final model, which is that of an aggregated soil where round soil aggregates are aligned periodically the whole way along the x-axis. This will give an infinite total area of oxygen-absorbing soil so that for any x, the concentration of oxygen in the soil should decrease with depth.

In order to construct a periodic solution we shall once again work with the boundary element method as this is easily extendible to a periodic solution via the use of a relevant Green's function. There are then two options. Either we can solve the full problem using the periodic boundary element method, or we can use the asymptotic method above using the boundary element method to solve only the outer $O(\epsilon)$ problem.

If we were to find the solution using the full boundary element method, we could choose any values of the diffusion coefficients D_1 and D_2. However, this is perhaps less relevant as we are attempting to model an aggregated soil where we know that $D_1 \gg D_2$. The asymptotic method then seems preferable as the boundary element method part of

the solution would be much simpler than for the full problem. To solve the outer $O(\epsilon)$ problem using the boundary element method would require integral equations for only one region where all the boundary positions would already be known. However, it must be remembered that the asymptotic solution is only an approximation as we have only expanded up to and including $O(\epsilon)$ terms. Therefore, in this thesis, both methods were used. The asymptotic solution can then be used as a guide in order to check the full boundary element method solution.

In order to construct a periodic boundary element method solution for either the full problem or the outer region $O(\epsilon)$ problem we shall require a periodic Green's function. The main difficulty is that this Green's function must also have all the same properties as in our previous boundary element methods. In order to construct such a Green's function we first consider the complex potential created by an array of point sinks, reflected by point sources. Note that this derivation is similar to the work carried out earlier when considering an array of points sinks. For our current problem one sink is needed for each $\mathbf{x_0}$ around the soil aggregate boundaries. We then repeat the sinks along the x-axis spaced apart by a gap of L in the x-direction. The complex potential of each sink/source pair is given by,

$$\omega_n = -\frac{1}{2\pi}\log(z - iy_0 - x_0 + nL) + \frac{1}{2\pi}\log(z + iy_0 - x_0 + nL), \tag{5.3.1}$$

where $n \in \mathbb{Z}$. We then take the sum of all the sinks and sources, and recast our complex potential as,

$$\begin{aligned}\omega &= -\frac{1}{2\pi}\log\left[(z - iy_0 - x_0)\prod_{n=1}^{\infty}\left(1 - \left(\frac{z - iy_0 - x_0}{nL}\right)^2\right)\right] \\ &\quad + \frac{1}{2\pi}\log\left[(z + iy_0 - x_0)\prod_{n=1}^{\infty}\left(1 - \left(\frac{z + iy_0 - x_0}{nL}\right)^2\right)\right].\end{aligned} \tag{5.3.2}$$

As with the point sink model earlier, we use an identity from [3] to rewrite (5.3.2) in terms of sine functions and arrive at,

$$\omega = -\frac{1}{2\pi}\log\left(\sin\left[\frac{\pi}{L}(z - iy_0 - x_0)\right]\right) + \frac{1}{2\pi}\log\left(\sin\left[\frac{\pi}{L}(z + iy_0 - x_0)\right]\right). \tag{5.3.3}$$

We now wish to take the real part of (5.3.3) to be our new Green's function, G_3. We can find this by first using the sine angle addition rule, and then by noting that

$$\log(re^{i\theta}) = \log r + i\theta. \tag{5.3.4}$$

Therefore, we can show that,

$$\begin{aligned}G_3 = &-\frac{1}{4\pi}\log\left[\sin^2\left(\frac{\pi(x - x_0)}{L}\right)\cosh^2\left(\frac{\pi(y - y_0)}{L}\right) + \cos^2\left(\frac{\pi(x - x_0)}{L}\right)\sinh^2\left(\frac{\pi(y - y_0)}{L}\right)\right] \\ &+\frac{1}{4\pi}\log\left[\sin^2\left(\frac{\pi(x - x_0)}{L}\right)\cosh^2\left(\frac{\pi(y + y_0)}{L}\right) + \cos^2\left(\frac{\pi(x - x_0)}{L}\right)\sinh^2\left(\frac{\pi(y + y_0)}{L}\right)\right]\end{aligned} \tag{5.3.5}$$

then simplify to show that,

$$\begin{aligned} G_3 &= -\frac{1}{4\pi}\log\left[\cosh^2\left(\frac{\pi(y-y_0)}{L}\right)-\cos^2\left(\frac{\pi(x-x_0)}{L}\right)\right] \\ &\quad +\frac{1}{4\pi}\log\left[\cosh^2\left(\frac{\pi(y+y_0)}{L}\right)-\cos^2\left(\frac{\pi(x-x_0)}{L}\right)\right]. \end{aligned} \tag{5.3.6}$$

This choice of Green's function is then periodic and has two important properties, firstly that,

$$G_3\Big|_{y=0} = 0, \tag{5.3.7}$$

and secondly,

$$\lim_{y\to-\infty} G_3 = -\frac{1}{2\pi}\log\left[\frac{\cosh\frac{\pi y_0}{L}-\sinh\frac{\pi y_0}{L}}{\cosh\frac{\pi y_0}{L}+\sinh\frac{\pi y_0}{L}}\right], \tag{5.3.8}$$

which is a constant. As G_3 has these properties, when we derive our boundary integral equation from (1.7.4), we once again arrive at a system that only includes integrals on the aggregate boundaries.

In order to find the solution for the full periodic problem we can use a very similar system of boundary integrals to those seen previously. For N soil aggregates in each period, with $i = 1, ..., N$ we have, for x_0 on B_i, with the normal $\mathbf{n}$ pointing into the outer region,

$$\hat{\phi}_0 = \sum_{i=1}^{N}\left[-2\int_{B_i} G_3\mathbf{n}\cdot\nabla\hat{\phi}_0 dl + 2\int_{B_i}^{PV}\hat{\phi}_0\mathbf{n}\cdot\nabla G_3 dl\right] \tag{5.3.9}$$

and on B_i, with $\mathbf{n}$ pointing into the oxygen-absorbing regions,

$$\begin{aligned} \hat{\phi}_0+\mu &= \frac{2D_0}{D_i}\int_{B_i} G_2\mathbf{n}\cdot\nabla\hat{\phi}_0 dl + 2\int_{B_i}^{PV}(\hat{\phi}_0+\mu)\mathbf{n}\cdot\nabla G_2 dl - 2m_i^2\oint_{B_i}\mathbf{a}.\mathbf{t}dl \\ &\quad -2\int_{C_i} G_2\mathbf{n}\cdot\nabla\phi_i dl + 2T\int_{C_i}\mathbf{n}\cdot\nabla G_2 dl - 2m_i^2\oint_{C_i}\mathbf{a}.\mathbf{t}dl, \end{aligned} \tag{5.3.10}$$

and on C_i with $\mathbf{n}$ pointing into the oxygen-absorbing regions,

$$\begin{aligned} T &= \frac{2D_0}{D_i}\int_{B_i} G_2\mathbf{n}\cdot\nabla\hat{\phi}_0 dl + 2\int_{B_i}(\hat{\phi}_0+\mu)\mathbf{n}\cdot\nabla G_2 dl - 2m_i^2\oint_{B_i}\mathbf{a}.\mathbf{t}dl \\ &\quad -2\int_{C_i} G_2\mathbf{n}\cdot\nabla\phi_i dl + 2T\int_{C_i}^{PV}\mathbf{n}\cdot\nabla G_2 dl - 2m_i^2\oint_{C_i}\mathbf{a}.\mathbf{t}dl, \end{aligned} \tag{5.3.11}$$

Similarly to in our other boundary element method solutions, we first use these boundary integral equations with a Newton iteration scheme to find the unknown boundary values and the position of the anaerobic core in one period. Then we find oxygen concentration for any $\mathbf{x_0}$ in one period, using the similar relevant integral equations with the found boundary values. Once this is complete we simply repeat for all other periods. Results found using these equations for realistic parameters are shown in the following chapter.

In order to find the solution of the periodic outer region $O(\epsilon)$ problem we use the same equation as for the non-periodic version (5.2.26) but with G_3 replacing G_1. The results of

this are shown in Figure 5.6 for the same set of example parameters as were used in the non-periodic version of the model. In this diagram it is clear that the oxygen level has been reduced as it has diffused through the aggregates.

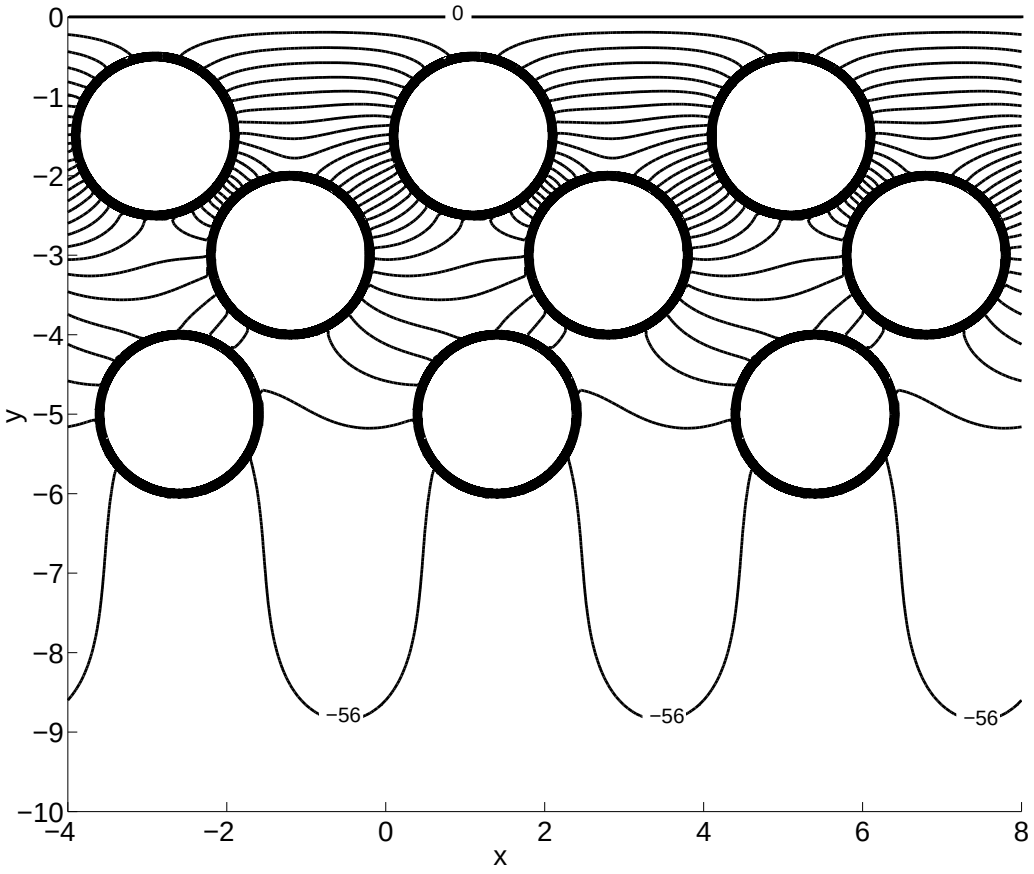

Figure 5.6: A contour plot of φ_1 from the outer region $O(\epsilon)$ periodic problem, which shows the oxygen concentration decreasing as depth into the soil is increasing. Each contour represents a level step of 2. $r_B = 1$, $m = 2$, $\epsilon = 0.01$, $T = 0.5$, $L = 4$

We can compare Figure 5.6 with Figure 5.5 directly to see the difference in overall oxygen levels in the system created by repeating the aggregates along the x-axis. As depth is increased in the periodic model oxygen concentration will not return to the background level, μ, as it did in the non-periodic version. This is clearly much more realistic as it describes what would be seen in a large section of soil.

If we were then to consider a three-dimensional version of the model we would have to include spherical soil aggregates aligned in a three-dimensional lattice. This lattice would extend into the page as well as along it. However, our current two-dimensional model actually represents a slice through a three-dimensional ground consisting of infinitely long cylindrical aggregates. To improve our model to three-dimensions, with spherical aggregates, is therefore a fundamentally different problem and is outside the scope of this thesis, but it is presumed a similar pattern of oxygen distribution would be observed.

5.4 Summary of Models Created

The models in this chapter are our most realistic and as such we shall evaluate them for biologically correct parameters in the following results chapter. We shall be investigating the two main model types we have developed, one for aggregated soil, and one for non-aggregated soil. These models and results have also been outlined in the paper by Bocking and Blyth [7].

In the non-aggregated soil model solutions, we shall consider a finite number of oxygen absorbing areas in a solid soil. We shall find solutions using the boundary element method described in section 5.1.2.

For the aggregated soil our most realistic model will be of circular regions of oxygen-absorbing positioned closely together and repeated periodically so that they resemble closely packed aggregates surrounded by air or water. We shall use the model described in section 5.3 and find solutions using the method discussed. We shall also consider further the model of a single aggregate surrounded by air or water, as this gives the clearest indication of how the air/soil boundary at $y = 0$ affects our solution. This is important as it shows the improvement over previous models in the literature where oxygen concentration was assumed constant around the edge of the aggregate. The main behaviour associated caused by this boundary can be seen the outer region $O(\epsilon)$ solution plotted above, where the deviation from the oxygen level in the air is shown.

Chapter 6

Oxygen Distribution Model Results

In this chapter we present results for both types of oxygen distribution model we have created, and attempt to predict the size of the anaerobic areas. First, we consider the ground (i.e. $y < 0$) to be comprising of air surrounding a network of soil aggregates, therefore representing an aggregated soil. In this case the oxygen diffusivity in the air (region 1) is much larger than inside one of aggregates (region 2) and so $\frac{D_2}{D_1} \ll 1$ as first considered in section 4.6. In the second viewpoint, we view the ground as being occupied by a non-aggregated soil. In this model a continuous distribution of soil with a uniform oxygen diffusivity contains one or more individual compact regions of respiring micro-organisms, where oxygen depletion takes place. This can be thought of as a solid soil with an area of much higher respiration due to, for example, decaying organic matter like dead leaves. In this case the ratio of oxygen diffusivities between region 1 and region 2 is of order unity. The first models created based on this were in section 4.5.

As mentioned in the introduction these models can be nondimensionalised using the region 2 radius, r_B, as the reference length and the ground oxygen level, μ, as the reference concentration. Repeated here for convenience the dimensionless parameters are,

$$\alpha = \frac{r_B^2 \lambda^2}{\mu D_2}, \qquad \delta = \frac{D_2}{D_1}, \qquad \tau = \frac{T}{\mu}, \qquad H = \frac{-c}{r_B}. \tag{6.0.1}$$

Note that all of these dimensionless parameters will be positive constants. As discussed, the oxygen level at which denitrification occurs is typically very small in comparison to the ambient oxygen concentration, so that $\tau \ll 1$. For computational purposes it is acceptable to simply set $\tau = 0$ and we do this throughout the remainder of this chapter. We shall also be able to set the values of D_1, D_2, μ and λ using biologically correct values found in the literature. This leaves the depth and size of region 2 as the most obvious parameters to vary in order to modify our model and investigate results.

6.1 Aggregated Soil

We first consider the parameters that make up the dimensionless parameter α. In a waterlogged soil, Radford & Greenwood [37], estimate oxygen absorption to be at a rate of $\lambda^2 = 8\times10^{-6}\,\mathrm{s}^{-1}$ and diffusion of oxygen to be at a rate of $D_2 = 1.05\times10^{-5}\,\mathrm{cm}^2\mathrm{s}^{-1}$. These values represent an average through a volume of waterlogged soil, therefore we take these to be good estimates of our parameters within the soil aggregates. The typical oxygen concentration in the atmosphere is $\mu \approx 21\%$, and the diffusivity of oxygen in air is widely reported (for example by Denny [16]) to be about $D_1 = 0.2\,\mathrm{cm}^2\mathrm{s}^{-1}$. Later we also consider lower values of D_1 which represents slower oxygen diffusion, as would be realistic if the soil was completely waterlogged and region 1 was filled with water instead of air. Taking an individual soil aggregate to be of size $r_B = 2$ cm as an initial choice, we then have $\alpha = 14.5$, and we will adopt this value throughout this section. Using the above values for D_1 and D_2, we have $\delta = 0.53\times10^{-5}$, which is small, raising confidence in the relevance of our asymptotic expansion method of section 4.6.

6.1.1 Single Aggregate Result

By using either the boundary element method described in section 4.5.4 or the asymptotic expansion method described in section 4.6.3 we can find oxygen concentration throughout a single aggregate domain. In this model we consider a single aggregate of soil surrounded by air, represented by a single circle positioned some depth, H, below $y = 0$. In Figures 6.1 and 6.2, the individual parts of the asymptotic method solution have been shown as they give the clearest indication of the variation in the oxygen distribution. Note that the anaerobic core is positioned slightly towards the bottom edge of the soil aggregate. However, for this single aggregate model, as δ is so small, the $O(1)$ terms dominate, and the soil aggregate almost has a constant level of oxygen around it. This makes the problem inside the aggregate close to being axi-symmetric, which would give the same results as for our previous concentric circles model and is similar to the tumour models found in the literature as mentioned in the introduction.

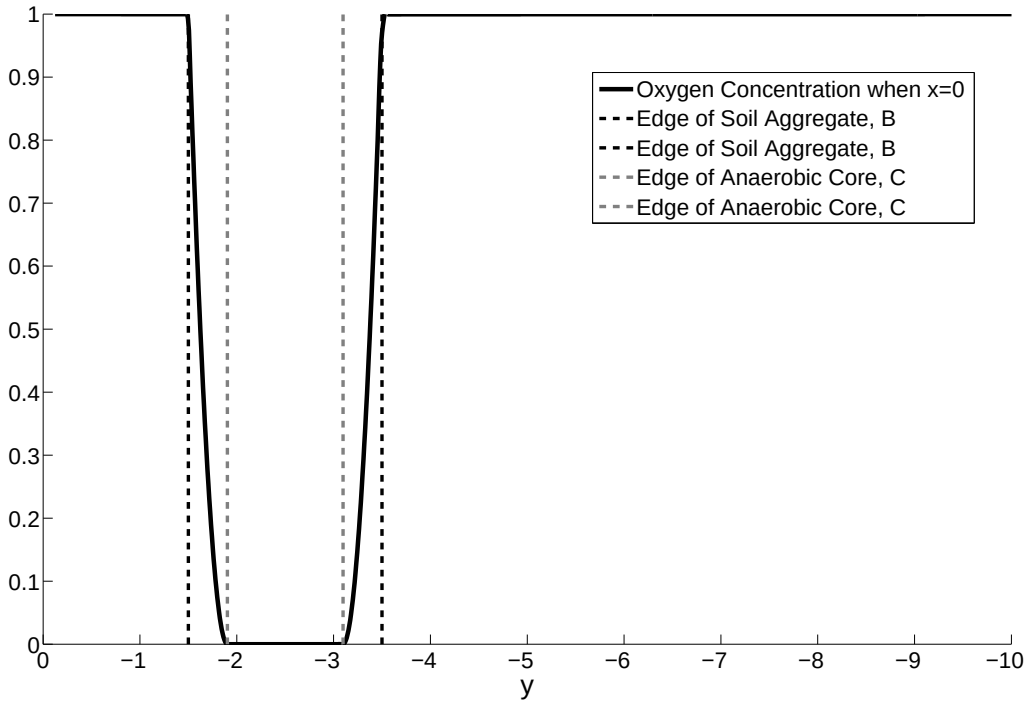

Figure 6.1: Oxygen concentration found using the non-dimensionalised line boundary model when $x = 0$. Found using the asymptotic approximation with terms up to $O(\epsilon)$ included. For an aggregate of depth $H = 2.5$ with $\alpha = 14.5$, $\delta = 0.53 \times 10^{-5}$, $\tau = 0$.

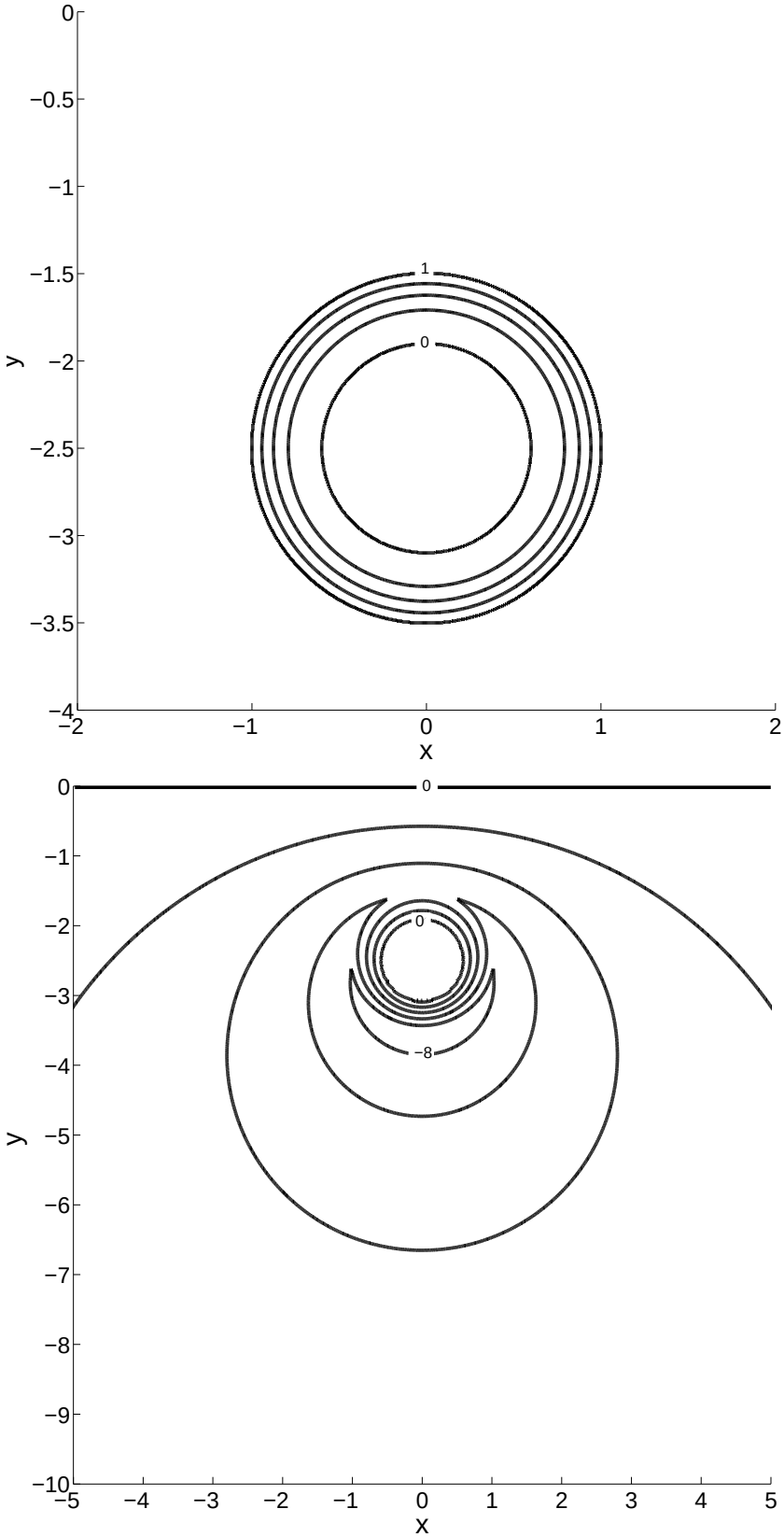

Figure 6.2: The individual parts of the single aggregate asymptotic solution. Top: $O(1)$, contours at gaps of 0.25. Bottom: $O(\epsilon)$, contours at gaps of 2. For an aggregate of depth $H = 2.5$ with $\alpha = 14.5$, $\delta = 0.53 \times 10^{-5}$, $\tau = 0$.

6.1.2 Multiple Aggregate Result

Using either of the periodic methods described previously in section 5.3 we can construct a model of an array of soil aggregates, which resemble an aggregated soil. In Figure 6.3 oxygen concentration is plotted for a representation of a top layer of soil, just two aggregates deep, but stretching the whole way along the x-axis. The first row of aggregates is positioned at depth $H_1 = 1.1$ and the second row at $H_2 = 3.2$, so that the aggregates are close together but not touching.

As the aggregates have been aligned into a grid the model solution is symmetric about the line $x = 0$. Once again we note that inside each aggregate the $O(1)$ solution is the same as the axi-symmetric problem, as the oxygen concentration in the outer region is constant. The effect of the boundary at $y = 0$ is then seen in the $O(\epsilon)$ solution. We note that the large values of oxygen concentration in the $O(\epsilon)$ problem (≈ -250) will give much slower convergence in our asymptotic expansion, however, as our value of δ is so small, this shouldn't be a problem.

The solution shows a decrease in oxygen levels as depth is increased into the soil, through the layers of aggregates, as we were expecting to observe. Starting from the maximum oxygen concentration at $y = 0$, each row of aggregates reduces the oxygen concentration level for all depths below, as can be seen in the $O(\epsilon)$ contour plot in Figure 6.3. This then means that deeper aggregates have larger anaerobic cores than those above them, as shown in Figure 6.4

We know from our boundary conditions that as depth approaches infinity oxygen concentration reaches a constant level. We can see from our solution that oxygen appears to be approaching a constant level soon after the lowest row of aggregates. Presumably, if we included an infinite number of rows of aggregates we would find that in the limit as depth increases to infinity the aggregates will become entirely anaerobic. Then the oxygen level outside the aggregates would be constant and equal to the threshold value T. This is in agreement with the literature which show soil approaching entirely anaerobic conditions as depth becomes large, such as [37] and [42]. This behaviour can be compared to the one-dimensional models in sections 3.5 and 3.6. In these models oxygen absorption occurs at individual points in the domain but can switch off when anaerobic conditions are met. As steady state conditions are approached, the result is for increasing soil depth, decreasing oxygen concentration until it reaches a minimum constant level.

The decrease in overall oxygen level would be more significant if there was slower diffusivity outside the aggregates. This could be the case if the gaps around the aggregates were filled with water instead of air. This would make the diffusion rate much slower, and of the same order of magnitude as the diffusion rate inside the aggregates. The diffusion of oxygen in water is approximately $2.1x10^{-5}\,\mathrm{cm^2 s^{-1}}$ [15] compared to $0.2\,\mathrm{cm^2 s^{-1}}$ in the air. We could infer from this that a completely waterlogged soil would have more anaerobic areas and therefore would produce more nitrous oxide through denitrification. This idea is in agreement with other reports in the literature, such as in [27], where it is reported that denitrification rates are significantly higher after rainfall events. Figure 6.5 shows how

slower diffusivity around the aggregates increases the anaerobic fraction of the soil.

Similarly, if the waterlogged soil inside the aggregates was to dry out then the average rate of oxygen diffusivity inside the aggregates, D_2, would slightly increase. Therefore this scenario would also lead to an increase in the diffusivity ratio, δ. However, increasing D_2 would also decrease the dimensionless absorption rate, α. Upon evaluating for increasing values of D_2 it can be shown that the overall effect is that the anaerobic core with actually decrease in size.

By spacing the aggregates further apart along the x-axis, via choosing a larger value of L, we see that the size of anaerobic cores decrease. The additional spacing allows for increased diffusion of oxygen around the aggregates, which can then aerate the deeper regions of the soil. This could indicate that a well ploughed field of soil will create less anaerobic conditions and therefore less denitrification than a compacted soil. A similar effect can be created by decreasing the radius of the aggregates whilst keeping their positions the same, as this will also increase the air to soil ratio. In Figure 6.6 the anaerobic area of each of the aggregates has been plotted against increasing aggregate radius, but with the distance between the aggregates kept constant. From this we can see how the diffusion of oxygen is more limited and as a result the anaerobic fraction of the soil has increased. Presumably there will be a finite limit to the size of the anaerobic area, which will be approached as the aggregate radius tends to infinity.

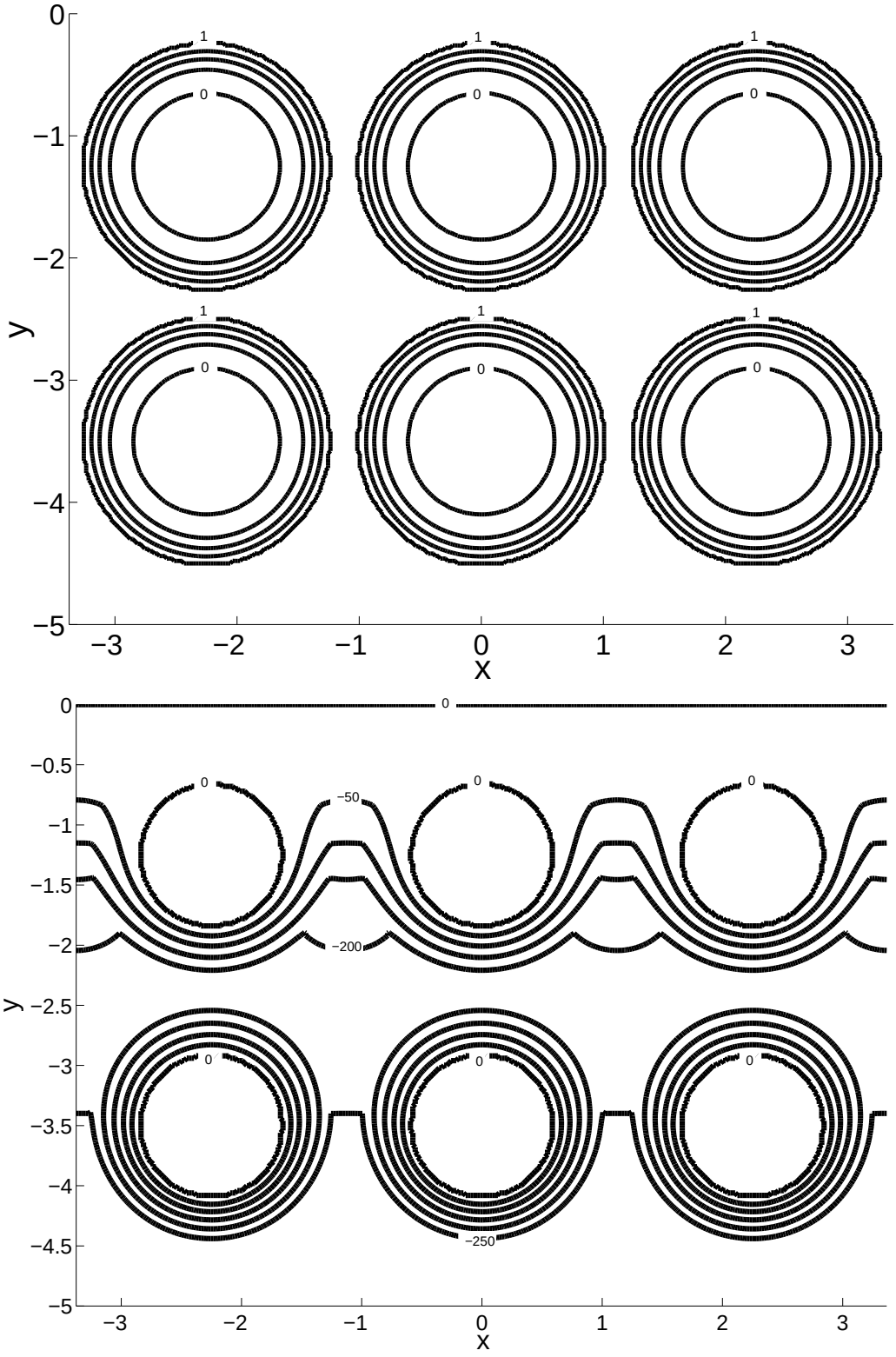

Figure 6.3: The individual parts of the periodic asymptotic solution, where there are two vertically aligned aggregates in each period. The aggregates are of depth $H_1 = 1.1$ and $H_1 = 3.2$ with $\alpha = 14.5$, $\delta = 0.53 \times 10^{-5}$, $\tau = 0$. Top: $O(1)$, contours at gaps of 0.25. Bottom: $O(\epsilon)$, contours at gaps of 50.

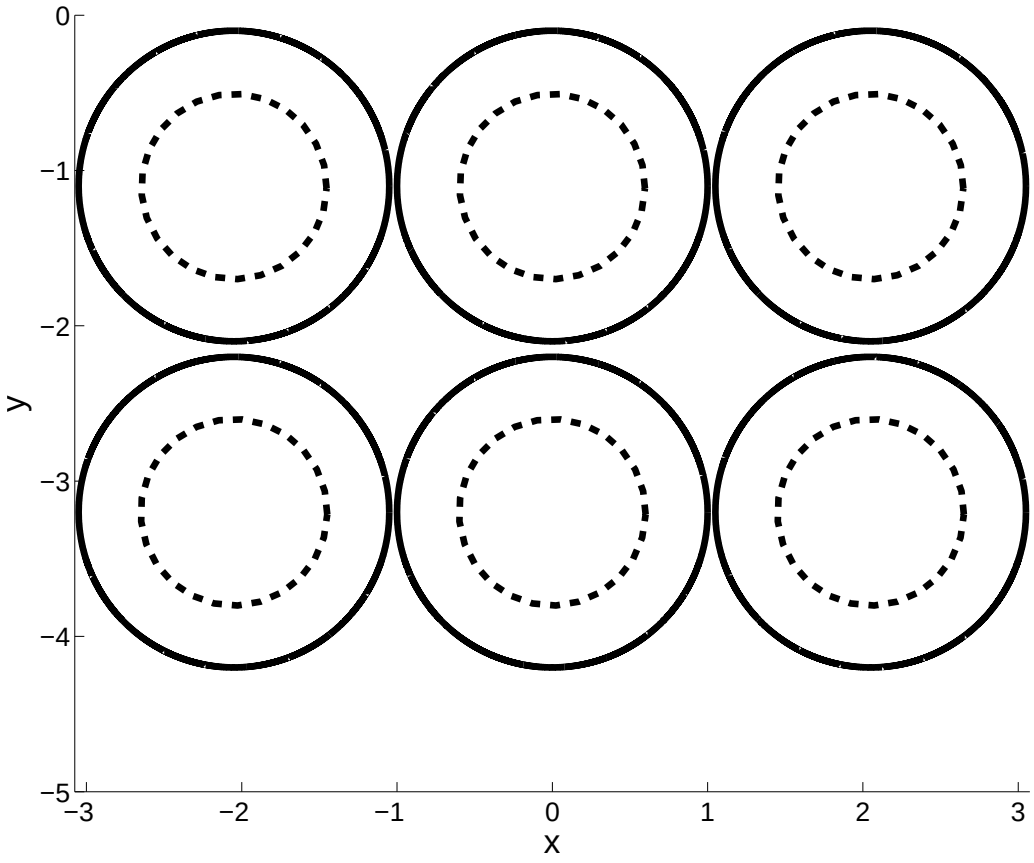

Figure 6.4: Showing the anaerobic cores (dotted lines) of the periodic model, found using the full boundary element method with the same parameter values as above.

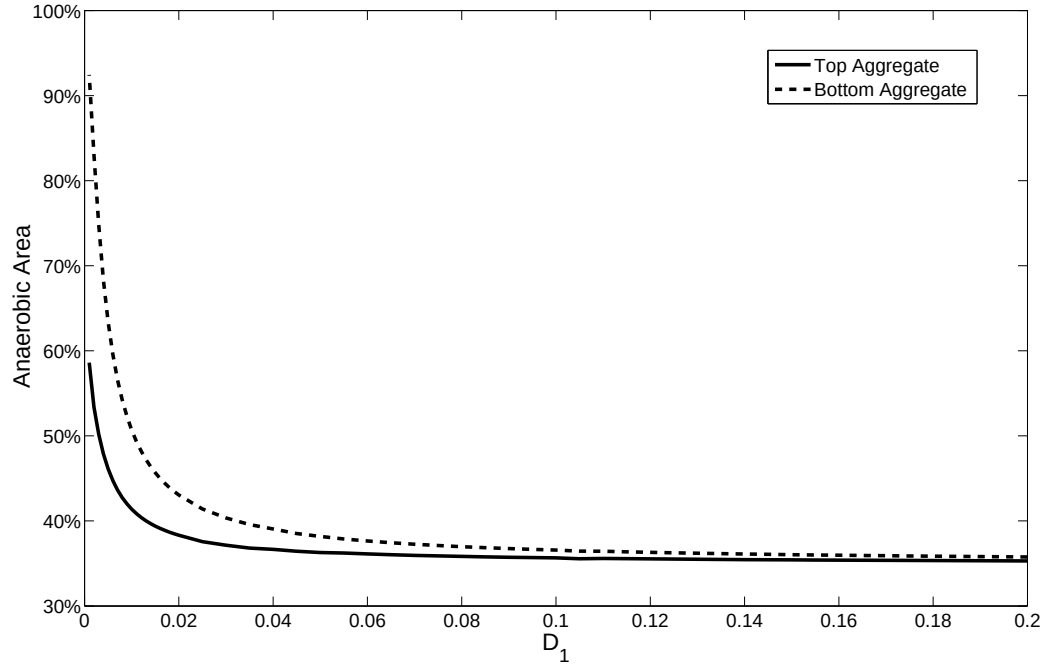

Figure 6.5: A plot of the areas of the anaerobic cores from the aggregated soil model for varying D_1. Keeping all the other parameter values the same as in previous results.

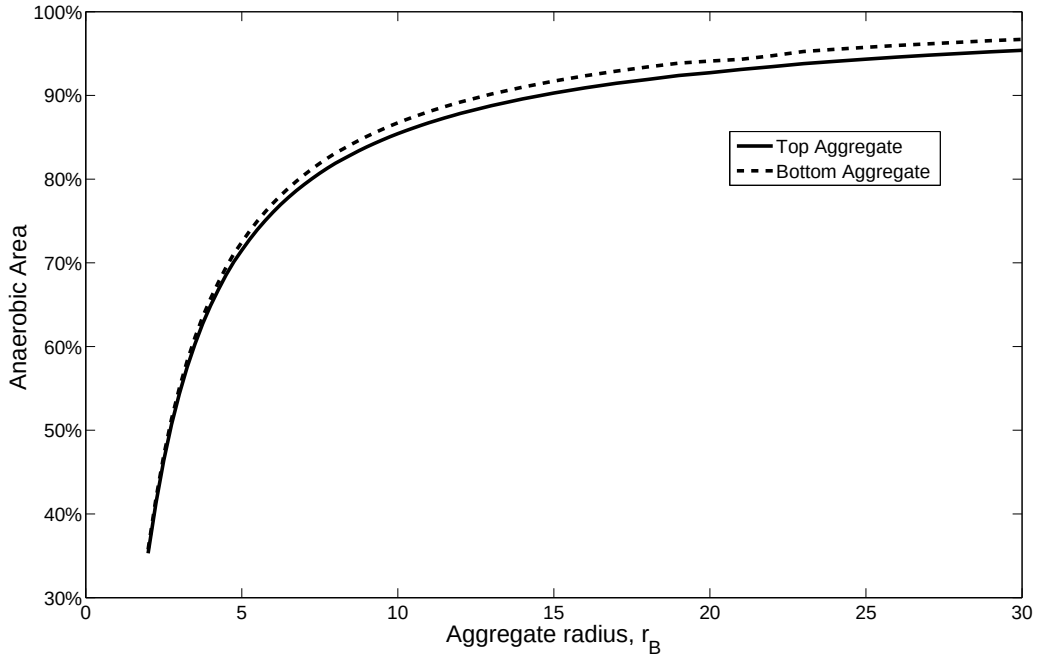

Figure 6.6: A plot of the area of the anaerobic cores from the aggregated soil model for increasing aggregate radius, r_B. With other parameter values kept constant, $\alpha = 14.5$, $\delta = 0.53 \times 10^{-5}$, $\tau = 0$.

6.2 Non-aggregated soil

In this section we consider the other type of model, that of a non-aggregated soil. Using this viewpoint the whole of the underground domain $y < 0$ is occupied with soil and oxygen depletion occurs in isolated areas occupied by micro-organisms of high microbial activity, containing for example, decaying plant matter. We shall consider these oxygen-absorbing micro-organisms to be small circular regions of radius, $r_B = 0.5$ cm. This will give a non-dimensional value of $\alpha = 0.91$. Choosing a small radius and relatively shallow depth for the patch could then represent part of a root or a leaf, that has been covered by the soil, started degrading and created high microbial activity in that area. To find solutions in this section, the relevant boundary element method will be used to find solutions, as described in sections 4.5.4 and 5.1.2, as by using these methods we can choose an arbitrary diffusion ratio δ.

6.2.1 A Single Region of Oxygen Absorption

We begin by considering results for a soil containing just one isolated micro-organism patch represented by a single circular area B as was first shown in Figure 1.5. As discussed, we work with the biologically realistic parameter values $\alpha = 0.91$, $\tau = 0$ and $\delta = 1$. In Figure 6.7, we show results for this solitary organism patch. Note that even though the size of microbial patch is small it has had a relatively large effect on the oxygen levels surrounding it, unlike in the aggregated models where the oxygen was diffusing much quicker and smoothing the overall distribution to more uniform values.

As shown in Figure 6.7, the anaerobic area in this instance is quite small, and thus the level of denitrification that can occur and the amount of nitrous oxide created as a result will be low. Increasing the radius of the oxygen-absorbing soil patch, increases the value of absorption, α, and decreases the depth, H. Thus for larger regions of oxygen absorbing soil, the effect of the boundary at $y = 0$ is greater and the anaerobic core larger.

Perhaps the most interesting results to observe are when the radius of the oxygen-absorbing region is kept constant and its depth is increased. As the depth of the patch increases the proportion of the soil that becomes anaerobic and thus starts denitrifying increases, which is shown in Figure 6.8. This figure appears to indicate that the anaerobic area is going to increase until it reaches a finite limit, as one would expect as the patch is of finite area. It is also apparent that the increase in depth reduces the effect of the air/soil boundary at $y = 0$ on the patch, which changes the shape and position of the anaerobic core, as shown in Figure 6.9. When the patch is placed close to the air/soil boundary the difference in oxygen concentration between the top and bottom edge is much more considerable. Hence, we see an anaerobic core that does not share a centre with the circular patch and is instead positioned towards the bottom.

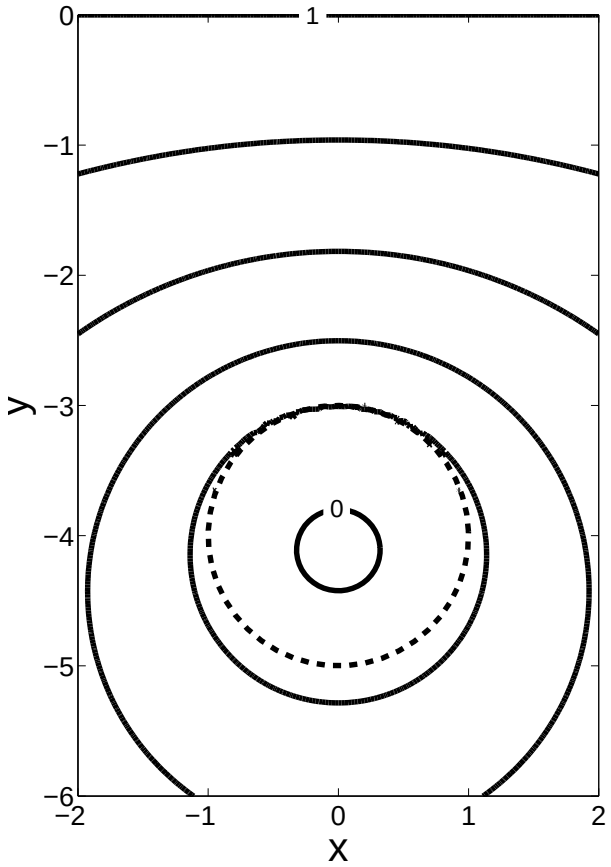

Figure 6.7: A contour plot showing oxygen distribution in a non-aggregated soil, where an area of high microbial activity at depth $H = 4$ has decreased the surrounding oxygen levels. The contour step size is 0.2. The dotted line represents the outside of the patch. $\alpha = 0.91$, $\delta = 1$, $\tau = 0$.

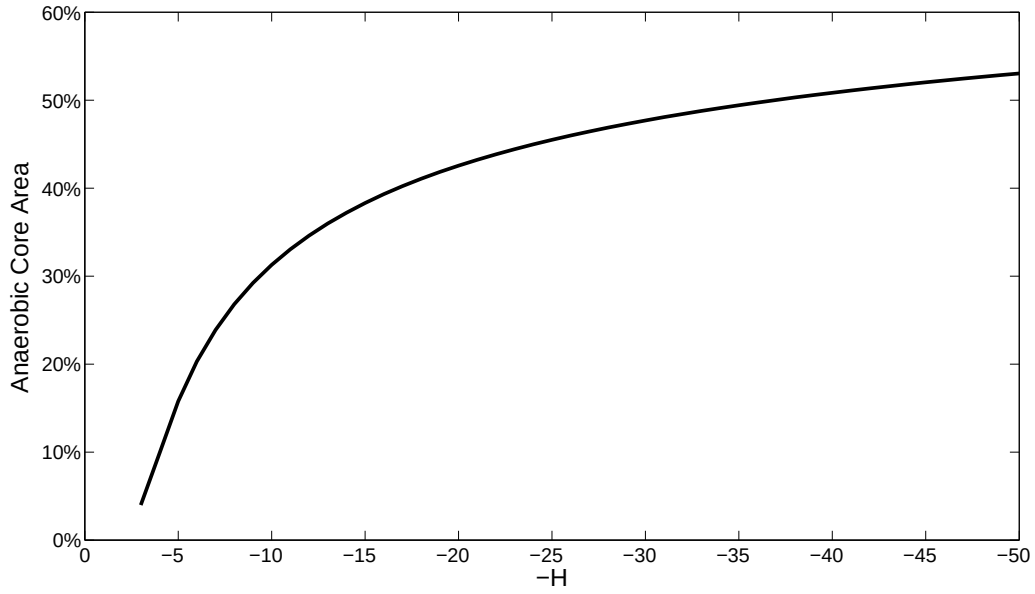

Figure 6.8: Anaerobic core area, as a percentage of the area of the high respiration patch, plotted against increasing depth.

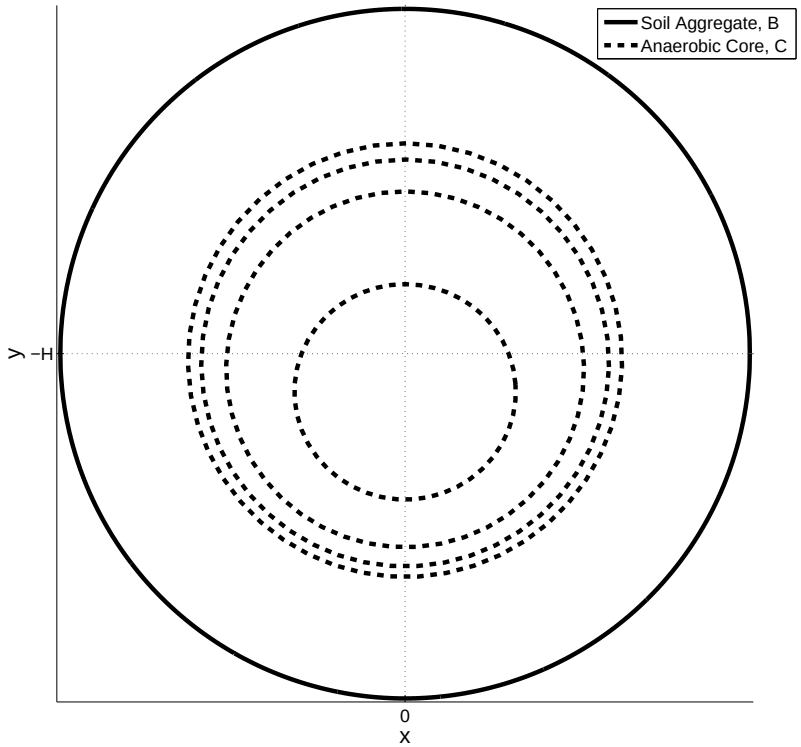

Figure 6.9: Comparing anaerobic cores for increasing depth, produced with a single circular high respiration patch within a non-aggregated soil. The most central dotted line represents the core when H=4, then moving outwards, H=8,12,16. $\alpha = 0.91$, $\delta = 1$, $\tau = 0$.

6.2.2 Two Regions of Oxygen Absorption

When considering two patches of higher microbial activity within solid soil we see that varying the patch positions results in different anaerobic cores, as shown in Figures 6.10 and 6.11. In both figures it is clear that the addition of a second area of high oxygen absorption has affected the position of the anaerobic cores. The area between the two patches will have lower values of oxygen concentration than in the areas away from them and as such, the anaerobic cores are positioned towards the other patch. In Figure 6.11 the deeper patch has a larger anaerobic core due to the patch above absorbing the oxygen from the air above it.

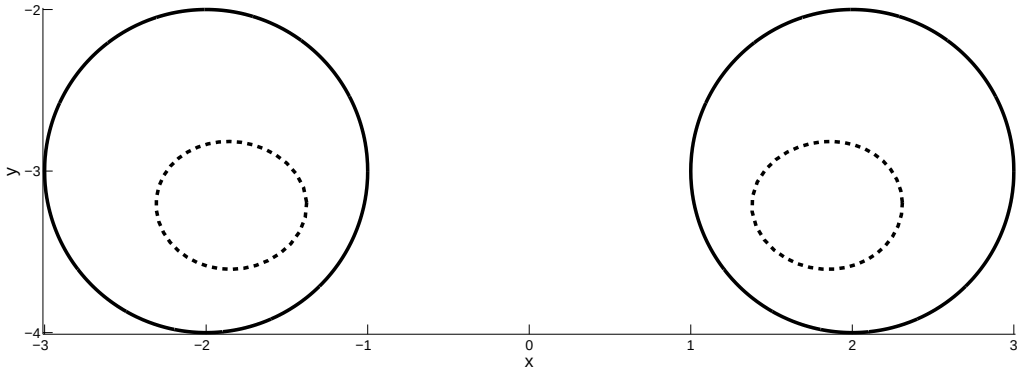

Figure 6.10: Comparing anaerobic cores, for a horizontal alignment of two high microbial activity patches.

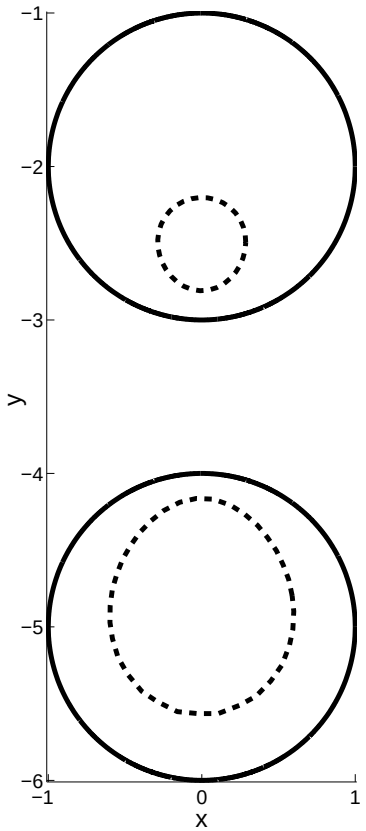

Figure 6.11: Comparing anaerobic cores, for a vertical alignment of two high microbial activity patches. The parameter values have been kept the same, $\alpha = 0.91$, $\delta = 1$, $\tau = 0$.

Chapter 7

Conclusions

7.1 Concluding Remarks

In this thesis several models relating to bacterial denitrification in soil have been developed. Each of these models have given an insight into the behaviour and properties of different aspects of the denitrification process. It is hoped these could help to predict nitrous oxide emissions from denitrification in future.

The initial models of the denitrification chemical pathway were based on *in vitro* experiments and showed how inhibitory effects from other competing chemicals can be highly significant. We have initially linked this to build-up of free nitrous acid, but there are many other possibilities. We have also highlighted the importance of considering a conservation of mass style equation, in order to ensure all the nitrogen in the system will be converted to products along the pathway.

When considering the oxygen distribution models we have included some important properties not previously discussed in the literature. The new boundary condition at ground level allows us to create a model of individual regions of oxygen absorbing bacteria where the oxygen level decreases with depth. This is an improvement on previous models in the literature where either oxygen absorption was considered constant throughout the soil, or aggregates were modelled separately with oxygen concentration considered constant on their surface. In our model even with only a single aggregate of soil considered we can see how the anaerobic region within it is affected by the ground level boundary. The two dimensional models can be used to predict the proportion of anaerobic soil, from which we can then infer directly the amount of denitrification that would occur.

7.2 Further Work

For the chemical pathway models, there are many other factors that could be included to help predict nitrous oxide emissions from the individual denitrifying bacteria. Some of the experiments and investigations have already been started based on the work in this thesis, such as in [45].

Further additions to this model, could initially include simply adding more regions of

oxygen absorption, which should be easily possible given enough computational power. This would allow us to show how in an aggregated soil the deepest soil aggregates will be the most anaerobic, and see whether they do in-fact become entirely anaerobic once a certain depth has been passed. It should also be possible to create a three-dimensional version of our model but this would require considerable amounts of further work.

Another useful future development would be to add time dependency and possibly a flow of water to our aggregated soil model. With this we would then be able to observe behaviour after rainfall events, where we should initially see a sizeable increase in denitrification, and then a slow decrease to the previous levels as the soil dries out.

Bibliography

[1] Nitrous oxide focus group, 2008. `http://www.nitrousoxide.org/overview.html`.

[2] M. J. Ablowitz and A. S. Fokas. *Complex Variables Introduction and Applications Second Edition*. Cambridge University Press, 2003.

[3] M. Abramowitz and I. A. Stegun. *Handbook of Mathematical Functions with Formulas, Graphs, and Mathematical Tables*. Dover, 1964.

[4] R. A. Alberty. The relationship between michaelis constants, maximum velocities and the equilibrium constant for an enzyme-catalyzed reaction. *The Journal of the American Chemical Society*, 75:1928–1932, 1953.

[5] P. W. Atkins. *Physical Chemistry*. Oxford University Press, 1998.

[6] M. R. Betlach and J. M. Tiedje. Kinetic explanation for accumulation of nitrite, nitric oxide, and nitrous oxide during bacterial denitrification. *Applied and Environmental Microbiology*, 42:1074–1084, 1981.

[7] C. Bocking and M. G. Blyth. Oxygen distribution in soils. *In Preparation*.

[8] N. F. Britton. *Essential Mathematical Biology*. Springer, 2003.

[9] H. S. Carslaw and J. C. Jaeger. *Conduction Of Heat In Solids*. Oxford University Press, 1959.

[10] W. Coenen and N. Riley. Oscillatory flow about a cylinder pair. *Quarterly Journal of Mechanics and Applied Maths*, 62:53–66, 2009.

[11] D. G. Crowdy. The schwarz problem in multiply connected domains and the schottky-klein prime function. *Complex Variables and Elliptic Functions*, 53:221–236, 2008.

[12] D. G. Crowdy and J. S. Marshall. Computing the schottky-klein prime function on the schottky double of planar domains. *Computational Methods and Function Theory*, 7(1):293–308, 2007.

[13] D. G. Crowdy, A. Surana, and K-Y. Yick. The irrotational motion generated by two planar stirrers in inviscid fluid. *Physics of Fluids*, 19, 2007.

[14] J. A . Currie. Gaseous diffusion in the aeration of aggregated soils. *Journal of Soil Science*, 16:279–289, 1965.

[15] E. L. Cussler. *Diffusion: Mass Transfer in Fluid Systems*. Cambridge University Press, 1997.

[16] M. W. Denny. *Air and Water: The Biology and Physics of Life's Media*. Princeton University Press, 1993.

[17] M. Van Dyke. *Perturbation Methods In Fluid Mechanics*. The Parabolic Press, 1975.

[18] H. Felgate. Private communications, 2010. University of East Anglia.

[19] P. Forster, V. Ramaswamy, P. Artaxo, T. Berntsen, R. Betts, D.W. Fahey, J. Haywood, J. Lean, D.C. Lowe, G. Myhre, J. Nganga, R. Prinn, G. Raga, M. Schulz, and R. Van Dorland. Changes in atmospheric constituents and in radiative forcing. *Climate Change 2007: The Physical Science Basis. Contribution of Working Group I to the Fourth Assessment Report of the Intergovernmental Panel on Climate Change [Solomon, S., D. Qin, M. Manning, Z. Chen, M. Marquis, K.B. Averyt, M.Tignor and H.L. Miller (eds.)].*

[20] P. Girsch and S. de Vries. Purification and initial kinetic and spectroscopic characterization of NO reductase from paracoccus denitrificans. *Biochimica et Biophysica Acta*, 1318:202–216, 1997.

[21] D. J. Greenwood. Nitrification and nitrate dissimilation in soil. *Plant and Soil*, 18:378–391, 1962.

[22] G. G. Hammes. *Principles of Chemical Kinetics*. Academic Press, 1978.

[23] J. D. Hoffman. *Numerical Methods For Engineers And Scientists*. McGraw-Hill, Inc., 1992.

[24] R. S. Kanwar. Analytical solutions of the transient state oxygen diffusion equation in soils with a production term. *Journal of Agronomy and Crop Science*, 156:101–109, 1986.

[25] P. Kowalik, C. J. Barnes, and D. E. Smiles. Oxidation of liquid animal wastes in soil. *Soil Science Society of America Journal*, 43:255–260, 1979.

[26] P. A. Leffelaar. Simulation of partial anaerobiosis in a model soil in respect to denitrification. *Soil Science*, 128:110–120, 1979.

[27] C. Li, S. Frolking, and T. A. Frolking. A model of nitrous oxide evolution from soil driven by rainfall events. 1. model structure and sensitivity. *Journal of Geophysical Research*, 97:9759–9776, 1992.

[28] C. C. Lin and L. A. Segel. *Mathematics Applied to Deterministic Problems in the Natural Sciences*. Society for Industrial and Applied Mathematics, 1988.

[29] L.M.Milne-Thomson. *Theoretical Hydrodynamics*. Macmillan and Company Limited, 1962.

[30] S. A. Montzka and P. J. Fraser. Controlled substances and other source gases. *Scientific Assessment of Ozone Depletion*, 2002. Chapter 1.

[31] J. D. Murray. *Mathematical Biology*. Springer-Verlag, 1989.

[32] D. D. Myrold and J. M. Tiedje. Diffusional constraints on denitrification in soil. *Soil Science Society of America Journal*, 49:651–657, 1985.

[33] J. Nicholas. *Chemical Kinetics A Modern Survey of Gas Reactions*. Harper and Row Ltd, 1976.

[34] Department of Energy and Climate Change. UK climate change sustainable development indicator: 2007 greenhouse gas emissions, final figures. February 2009.

[35] R. I. Papendick and J. R. Runkles. Transient-state oxygen diffusion in soil: I. the case when rate of oxygen consumption is constant. *Soil Science*, 100:251–261, 1965.

[36] C. Pozrikidis. *A Practical Guide to Boundary Element Methods*. Chapman and Hall/CRC, 2002.

[37] P. J. Radford and D. J. Greenwood. The simulation of gaseous diffusion in soils. *Journal of Soil Science*, 21:304–313, 1970.

[38] P. Renault and P. Stengel. Modeling oxygen diffusion in aggregated soils: I. anaerobiosis inside the aggregates. *Soil Science Society of America Journal*, 58:1017–1023, 1994.

[39] D. Richardson, H. Felgate, N. Watmough, A. Thomson, and E. Baggs. Mitigating release of the potent greenhouse gas N_2O from the nitrogen cycle - could enzymic regulation hold the key? *Trends in Biotechnology*, 27:388–397, 2009.

[40] S. I. Rubinow. *Introduction To Mathematical Biology*. John Wiley and Sons, 1975.

[41] L. A. Segel. *Mathematical Models In Molecular and Cellular Biology*. Cambridge University Press, 1980.

[42] K. A. Smith. A model of the extent of anaerobic zones in aggregated soils, and its potential application to estimates of denitrification. *Journal of Soil Science*, 31:263–277, 1980.

[43] K. A. Smith, T. Ball, F. Conen, K. E. Dobbie, J. Massheder, and A. Rey. Exchange of greenhouse gases between soil and atmosphere: interactions of soil physical factors and biological processes. *European Journal of Soil Science*, 54:779–791, 2003.

[44] J. K. Thomsen, T. Geest, and R. P. Cox. Mass spectrometric studies of the effect of ph on the accumulation of intermediates in denitrification by paracoccus denitrificans. *Applied and Environmental Microbiology*, 60:536–541, 1994.

[45] H. C. Woolfenden, A. J. Gates, C. Bocking, M. G. Blyth, D. J. Richardson, and V. Moulton. Modelling the effect of copper availability on bacterial denitrification. *Accepted by Microbiology Open*.

[46] B. Xu and S. Enfors. Modeling of nitrite accumulation by the denitrfiying bacterium pseudomonas stutzeri. *Journal of Fermentation and Bioengineering*, 82:56–60, 1996.

[47] Y. Zhou, M. Pijuan, R. J. Zeng, and Z. Yuan. Free nitrous acid inhibition on nitrous oxide reduction by a denitrifying-enhanced biological phosphorus removal sludge. *Environmental Science and Technology*, 42:8260–8265, 2008.